TECHNISCHE UNIVERSITÄT WIEN
Vienna University of Technology

DIPLOMARBEIT

Numerical Simulation of the Stationary Wigner Equation and Space–Based Acquisition, Pointing and Tracking Laser Systems

Ausgeführt am Institut für
Analysis und Scientific Computing
der Technischen Universität Wien

unter der Anleitung von
Ao. Univ. Prof. Dr. Ewa B. Weinmüller

von Jürgen Gschwindl, BSc.
Weichselgasse 36
2111 Harmannsdorf

February 9, 2016

Contents

1 Abstract

In this work, we address two different topics, which are discussed in the following main chapters.

The first part of the master thesis deals with the limits of validity of certain mathematical models from the area of space–based acquisition, pointing, and tracking (APT) laser systems, written as systems of ordinary differential equations (ODEs). The interest in the analysis and numerical solution of these models was strongly motivated from the international cooperation with Professor Jose Maria Gambi from the Charles III University of Madrid, Spain.
Our main goal was to demonstrate the considerable improvement that can be achieved by appropriately correcting the standard equations. This investigation was carried out for three different types of satellites and a number of different combinations of parameters. For the numerical solution of the respective model equations, the standard MATLAB code `ode45` was used.

In the second part of the work, we considered a discretisation of the stationary ε–dependent Wigner-Equation, which for $\varepsilon = 0$ turns out to be an Index-2 differential algebraic equation (DAE). This activity was developed within the cooperation with Professor Anton Arnold from the Vienna University of Technology, Vienna, Austria. Main aim here was to find information about the solutions behaviour, in the limit $\varepsilon \to 0$, to support the analysis of the original, continuous problem.
To numerically simulate this class of problems, we used a special version of the collocation method implemented in the MATLAB code `bvpsuite` and embedded into the least–squares minimization algorithm [26].

2 Space-Based Acquisition, Pointing, and Tracking Laser Systems

2.1 Introduction

The need of increasing the accuracy, particularly in space communications and surveillance, recognized in the last decade, made the implementation of increasingly accurate space inertial-guided APT laser systems a very relevant scientific issue [1]-[2]. Nowadays, systems with laser technology gain a lot of attention in other scenarios, such as in space debris removal, due to the fact that this technology has matured substantially in recent years [3]-[5].

In fact, some laser systems can already be designed to have sub-microradian divergences [6], which means that a laser system with an output beam diameter of one meter can readily have a 0.1 microradian beam divergence, expanding to only about 10 centimeters after traveling 1000 kilometres [7].

The post–Newtonian framework of the Earth surrounding space is the framework that meets the present needs in accurate space geodesy, positioning, and navigation. Thus, this is the framework presently used to synchronize the atomic clocks on board the GPS satellites, so as to determine the round–trip time taken by a laser beam in satellite–to–satellite laser ranging [8]-[12].

Likewise, it is within this framework where some latest geolocation models have been proposed to locate passive, i.e. non–cooperative, radio transmitters placed on the Earth surface or in the vicinity of the Earth [13]-[18].

However, this framework is not used yet in satellite–to–satellite laser communications, where increasing the accuracy of the present tracking procedures for systems endowed with very narrow laser beams is needed [19], nor in active space debris removal, where increasing the accuracy is even more necessary, taking into account that the average size of the near 17000 debris objects ranges between 1 cm to 10 cm, according to the catalogue of the US Space Surveillance Network (SSN) [20].

Now, since this fact is not due to the lack of accuracy of the modern APT hardware, we may conclude that this is due to the difficulty for the present procedures to account in real time for the variations of the tidal effects of the Earth between the orbital position of the destination object and that of the APT system. Or, in post–Newtonian terms, it may be due to the difficulty to account in real time for the variations of the curvature of the Earth surrounding space between the positions of the destination object and the positions of the system.

In summary, the sub–microradian divergences of accurate laser beams make us to face the challenge of pointing an APT system at a designated target, whether this is a communication satellite, a radio transmitter, or a piece of debris. Hence, the issue to track

the target is to accurately predict its position in order to know where to point the beam to reach the target at the desired instants.

The purpose of this work is twofold: (i) to numerically simulate the solutions of systems of post–Newtonian equations, linear and nonlinear, for the orbital relative motion, and (ii) to analyze the validity of these solutions by comparing them to the solutions of the respective Newtonian equations (directly and by means of the solutions of post–Newtonian equations for the Earth Centered Inertial (ECI) orbital motions of the APT system and the target). The equations have been derived by the group of the Gregorio Millan Institute of the Charles III University of Madrid, Spain, led by Professor Jose Maria Gambi, and are the resent development in a wide activity in this area [21]-[22].
In the analysis, we deal with the equations for ECI orbital and for relative motions divided in two groups. The first group contains the equations for the ECI orbital motion of the APT system, which will be denoted by S1, and those of the destination object, which will be denoted by S2. The essential assumptions are specified in the following way:

(i) The geometrical structure of the space–time around the Earth corresponds to the weak approximation to the exterior Schwarzschild field generated by the Earth, which in ECI coordinates (x^α, t), $\alpha=1,2,3$, is given by

$$\Phi_S = g_{ij}dx^i dx^j = \left[\left(\delta_{\alpha\beta} + \frac{2m x^\alpha x^\beta}{r^3} \right) dx^\alpha dx^\beta + \left(-1 + \frac{2m}{r} \right) dt^2 \right], \tag{1}$$

where m is the mass of the Earth and $r^2 = x^\alpha x^\alpha$, both measured in seconds.

(ii) The world–lines of S1 and S2 are time–like geodesics in the Schwarzschild field. As in (1), from now on, Latin indices range from 1 to 4.

The second group contains the equations of practical interest according to our aim, that is, the equations of the relative motion of S2 with respect to S1, which in the complete version are nonlinear. The equations in this group have been derived from Synge's equations for the geodesics corresponding to a Fermi frame that is co–moving with S1 [23]. They are written in local Cartesian coordinates X^α, $\alpha=1,2,3$.

The post–Newtonian equations for the ECI absolute motions derived according to (i) and (ii), appear to be natural generalizations of the Newtonian orbital equations, since the post–Newtonian terms can be considered as perturbations that produce small oscillations about the Newtonian motions, due to the geometrical structure about the Earth, see e.g. Figures in Section 2.3. The reason is that this structure corresponds to (1), so that, neglecting the second order terms in (1), we have

$$\Phi_C = \left[dx^\alpha dx^\alpha - dt^2 \right],$$

whose space part, as can be seen, is Euclidean.

Note that the Newtonian equations for the relative motion of S2 with respect to S1 are simply the difference of the ECI Newtonian orbital equations of S2 and S1. Therefore, one

should investigate whether the second post–Newtonian equations for the relative motion of S2 with respect to S1 produce predictions significantly different from those produced by the first group of equations, i.e., by taking the difference of the post–Newtonian ECI orbital motions of S1 and S2, as it is made within the Newtonian framework.

The justification for this analysis is that the structure of the space–time around S1 is given by [23],

$$
\begin{aligned}
\Phi_F = g_{(ij)} dX^{(i)} dX^{(j)} &= \left(\delta_{\alpha\beta} + 2h_{(\alpha_1\beta_1)} \right) dX^{(\alpha)} dX^{(\beta)} \\
&+ \left(-1 + 2h_{(4_14_1)} + 2h_{(4_14_2)} \right) dX^{(4)} dX^{(4)},
\end{aligned}
\tag{2}
$$

so that its principal part is

$$
\Phi_C = dX^{(\alpha)} dX^{(\alpha)} - dX^{(4)} dX^{(4)},
$$

which contains the structure of the Euclidean space in local Cartesian coordinates as viewed by S1. The terms $h_{(\alpha_1\beta_2)}$, $h_{(4_14_1)}$, and $h_{(4_14_2)}$ in (2) are given by

$$
h_{(\alpha_1\beta_2)} = \frac{3}{2} \sigma^{-3} X^{(\mu)} X^{(\nu)} \int_0^\sigma (\sigma - u) u S_{(\alpha\beta\mu\nu)} du,
$$

$$
h_{(4_14_1)} = \frac{3}{2} \sigma^{-3} X^{(\mu)} X^{(\nu)} \int_0^\sigma (\sigma - u)^2 S_{(44\mu\nu)} du,
$$

$$
h_{(4_14_2)} = \frac{3}{2} \sigma^{-3} X^{(\mu)} X^{(\nu)} \int_0^\sigma (\sigma - u) u S_{(44\mu\nu)} du,
$$

where $S_{(abcd)} = -\frac{1}{3} \left(R_{(acbd)} + R_{(adbc)} \right)$ and $R_{(abcd)}$ are the components of the Riemann tensor, R_{ijkm}, of the metric (1) with respect to the tetrads $\lambda^i_{(a)}$ Euclidean–parallel along the segment S1–S2 to the tetrad $\lambda^{i_1}_{(a)}$ that materializes the Fermi frame co–moving with S1. Hence, if s_1 is the proper time of S1, we have $R_{(abcd)} = R_{ijkm} \lambda^i_{(a)} \lambda^j_{(b)} \lambda^k_{(c)} \lambda^m_{(d)}$, where

$$
\lambda^{\mu_1}_{(\alpha)} = \delta^\mu_\alpha, \ \lambda^{4_1}_{(\alpha)} = v^{\alpha_1} = dx^{\alpha_1}/ds_1, \ \lambda^{\mu_1}_{(4)} = v^{\mu_1} = dx^{\mu_1}/ds_1, \ \frac{dt}{ds_1} = \lambda^{4_1}_{(4)} = 1 + \frac{m}{r} + \frac{1}{2}(v^{\alpha_1} v^{\alpha_1}),
$$

which in our case reduce to

$$
\lambda^{\mu_1}_{(\alpha)} = \delta^\mu_\alpha, \quad \lambda^{4_1}_{(\alpha)} = 0, \quad \lambda^{\mu_1}_{(4)} = 0, \quad \frac{dt}{ds_1} = \lambda^{4_1}_{(4)} = 1,
$$

so that the space components of $\lambda^{i_1}_{(a)}$ become the classical components of the inertial–guided reference frame co–moving with S1 that is parallel to the ECI reference frame.

To test the conjecture formulated above, we assume that S1 and S2 are in equatorial circular orbits around the Earth at typical distances from the Earth. This allows us to simplify the equations, as well as the notation, since we may consider systems of only two equations, so that the space ECI coordinates of S1 and S2 can be denoted by (x_1, y_1) and (x_2, y_2) respectively, and the coordinates of the relative position of S2 with respect to S1 for the second equations by (X, Y). In addition, the number of scenarios can be reduced to six, and the number of parameters needed to study the solutions for each scenario can be reduced to two.

The equations for the ECI post–Newtonian motions are

$$
\frac{d^2x}{dt^2} = \frac{-m}{((x)^2+(y)^2)^{3/2}}\left[1 - \frac{2m}{(x)^2+(y)^2} + \left(\frac{-3(x)^2}{(x)^2+(y)^2}+1\right)\left(\frac{dx}{dt}\right)^2\right.
$$

$$
\left. - \frac{6xy}{(x)^2+(y)^2}\frac{dx}{dt}\frac{dy}{dt} + \left(\frac{-3(y)^2}{(x)^2+(y)^2}+1\right)\left(\frac{dx}{dt}\right)^2\right]x,
$$

$$
\frac{d^2y}{dt^2} = \frac{-m}{((x)^2+(y)^2)^{3/2}}\left[1 - \frac{2m}{(x)^2+(y)^2} + \left(\frac{-3(x)^2}{(x)^2+(y)^2}+1\right)\left(\frac{dx}{dt}\right)^2\right.
$$

$$
\left. - \frac{6xy}{(x)^2+(y)^2}\frac{dx}{dt}\frac{dy}{dt} + \left(\frac{-3(y)^2}{(x)^2+(y)^2}+1\right)\left(\frac{dy}{dt}\right)^2\right]y.
$$

The equations for the linear approximation to the post–Newtonian relative motion are

$$
\frac{d^2X}{dt^2} =
$$

$$
mX\int_0^1\left(\frac{3(x_1)^2(1-u)^2+6x_1x_2(1-u)u+3(x_2)^2u^2}{\left[((x_1)^2+(y_1)^2)(1-u)^2+2(1-u)u(x_1x_2+y_1y_2)+((x_2)^2+(y_2)^2)u^2\right]^{5/2}}\right.
$$

$$
\left. - \frac{1}{\left[((x_1)^2+(y_1)^2)(1-u)^2+2(1-u)u(x_1x_2+y_1y_2)+((x_2)^2+(y_2)^2)u^2\right]^{3/2}}\right)\cdot
$$

$$
(1-2u+3u^2)du
$$

$$
+mY\int_0^1\left(\frac{3x_1y_1(1-u)^2+3(1-u)u(x_1y_2+y_1x_2)+3x_2y_2u^2}{\left[((x_1)^2+(y_1)^2)(1-u)^2+2(1-u)u(x_1x_2+y_1y_2)+((x_2)^2+(y_2)^2)u^2\right]^{5/2}}\right)\cdot
$$

$$
(1-2u+3u^2)du,
$$

$$\frac{d^2Y}{dt^2} =$$

$$mX \int_0^1 \left(\frac{3x_1 y_1 (1-u)^2 + 3(1-u)u \left(x_1 y_2 + y_1 x_2 \right) + 3x_2 y_2 u^2}{\left[\left((x_1)^2 + (y_1)^2 \right) (1-u)^2 + 2(1-u)u \left(x_1 x_2 + y_1 y_2 \right) + \left((x_2)^2 + (y_2)^2 \right) u^2 \right]^{5/2}} \right) \cdot$$

$$(1 - 2u + 3u^2) du$$

$$+ mY \int_0^1 \left(\frac{3(y_1)^2 (1-u)^2 + 6 y_1 y_2 (1-u) u + 3(y_2)^2 u^2}{\left[\left((x_1)^2 + (y_1)^2 \right) (1-u)^2 + 2(1-u)u \left(x_1 x_2 + y_1 y_2 \right) + \left((x_2)^2 + (y_2)^2 \right) u^2 \right]^{5/2}} \right.$$

$$\left. - \frac{1}{\left[\left((x_1)^2 + (y_1)^2 \right) (1-u)^2 + 2(1-u)u \left(x_1 x_2 + y_1 y_2 \right) + \left((x_2)^2 + (y_2)^2 \right) u^2 \right]^{3/2}} \right) \cdot$$

$$(1 - 2u + 3u^2) du,$$

and the nonlinear equations are

$$\frac{d^2X}{dt^2} =$$

$$mX \int_0^1 \left(\frac{3(x_1)^2(1-u)^2 + 6x_1x_2(1-u)u + 3(x_2)^2u^2}{\left[((x_1)^2 + (y_1)^2)(1-u)^2 + 2(1-u)u(x_1x_2 + y_1y_2) + ((x_2)^2 + (y_2)^2)u^2 \right]^{5/2}} \right.$$

$$\left. - \frac{1}{\left[((x_1)^2 + (y_1)^2)(1-u)^2 + 2(1-u)u(x_1x_2 + y_1y_2) + ((x_2)^2 + (y_2)^2)u^2 \right]^{3/2}} \right) \cdot$$

$$(1 - 2u + 3u^2)du$$

$$+ mY \int_0^1 \left(\frac{3x_1y_1(1-u)^2 + 3(1-u)u(x_1y_2 + y_1x_2) + 3x_2y_2u^2}{\left[((x_1)^2 + (y_1)^2)(1-u)^2 + 2(1-u)u(x_1x_2 + y_1y_2) + ((x_2)^2 + (y_2)^2)u^2 \right]^{5/2}} \right) \cdot$$

$$(1 - 2u + 3u^2)du$$

$$+ 3mX^2 \int_0^1 \left[\left(x_1(1-u) + x_2u \right) \cdot \right.$$

$$\left(\frac{5(x_1)^2(1-u)^2 + 10(1-u)ux_1x_2 + 5(x_2)^2u^2}{\left[((x_1)^2 + (y_1)^2)(1-u)^2 + 2(1-u)u(x_1x_2 + y_1y_2) + ((x_2)^2 + (y_2)^2)u^2 \right]^{7/2}} \right.$$

$$\left. \left. - \frac{3}{\left[((x_1)^2 + (y_1)^2)(1-u)^2 + 2(1-u)u(x_1x_2 + y_1y_2) + ((x_2)^2 + (y_2)^2)u^2 \right]^{5/2}} \right) \right] (1-u)u^2 du$$

$$+ 6mXY \int_0^1 \left[\left(y_1(1-u) + y_2u \right) \cdot \right.$$

$$\left(\frac{5(x_1)^2(1-u)^2 + 10(1-u)ux_1x_2 + 5(x_2)^2u^2}{\left[((x_1)^2 + (y_1)^2)(1-u)^2 + 2(1-u)u(x_1x_2 + y_1y_2) + ((x_2)^2 + (y_2)^2)u^2 \right]^{7/2}} \right.$$

$$\left. \left. - \frac{1}{\left[((x_1)^2 + (y_1)^2)(1-u)^2 + 2(1-u)u(x_1x_2 + y_1y_2) + ((x_2)^2 + (y_2)^2)u^2 \right]^{5/2}} \right) \right] (1-u)u^2 du$$

$$+ 3mY^2 \int_0^1 \left[\left(x_1(1-u) + x_2u \right) \cdot \right.$$

$$\left(\frac{5(y_1)^2(1-u)^2 + 10(1-u)uy_1y_2 + 5y_2^2u^2}{\left[((x_1)^2 + (y_1)^2)(1-u)^2 + 2(1-u)u(x_1x_2 + y_1y_2) + ((x_2)^2 + (y_2)^2)u^2 \right]^{7/2}} \right.$$

$$\left. \left. - \frac{1}{\left[((x_1)^2 + (y_1)^2)(1-u)^2 + 2(1-u)u(x_1x_2 + y_1y_2) + ((x_2)^2 + (y_2)^2)u^2 \right]^{5/2}} \right) \right] (1-u)u^2 du,$$

$$\frac{d^2Y}{dt^2} =$$

$$mX \int_0^1 \left(\frac{3x_1y_1(1-u)^2 + 3(1-u)u\left(x_1y_2 + y_1x_2\right) + 3x_2y_2u^2}{\left[\left((x_1)^2 + (y_1)^2\right)(1-u)^2 + 2(1-u)u\left(x_1x_2 + y_1y_2\right) + \left((x_2)^2 + (y_2)^2\right)u^2\right]^{5/2}} \right) \cdot$$

$$(1 - 2u + 3u^2)du$$

$$+mY \int_0^1 \left(\frac{3(y_1)^2(1-u)^2 + 6y_1y_2(1-u)u + 3(y_2)^2u^2}{\left[\left((x_1)^2 + (y_1)^2\right)(1-u)^2 + 2(1-u)u\left(x_1x_2 + y_1y_2\right) + \left((x_2)^2 + (y_2)^2\right)u^2\right]^{5/2}} \right.$$

$$\left. -\frac{1}{\left[\left((x_1)^2 + (y_1)^2\right)(1-u)^2 + 2(1-u)u\left(x_1x_2 + y_1y_2\right) + \left((x_2)^2 + (y_2)^2\right)u^2\right]^{3/2}} \right) \cdot$$

$$(1 - 2u + 3u^2)du$$

$$+3mX^2 \int_0^1 \left[\left(y_1(1-u) + y_2u\right) \cdot \right.$$

$$\left(\frac{5(x_1)^2(1-u)^2 + 10(1-u)ux_1x_2 + 5(x_2)^2u^2}{\left[\left((x_1)^2 + (y_1)^2\right)(1-u)^2 + 2(1-u)u\left(x_1x_2 + y_1y_2\right) + \left((x_2)^2 + (y_2)^2\right)u^2\right]^{7/2}} \right.$$

$$\left. \left. -\frac{1}{\left[\left((x_1)^2 + (y_1)^2\right)(1-u)^2 + 2(1-u)u\left(x_1x_2 + y_1y_2\right) + \left((x_2)^2 + (y_2)^2\right)u^2\right]^{5/2}} \right) \right] (1-u)u^2du$$

$$+6mXY \int_0^1 \left[\left(x_1(1-u) + x_2u\right) \cdot \right.$$

$$\left(\frac{5(y_1)^2(1-u)^2 + 10(1-u)uy_1y_2 + 5(y_2)^2u^2}{\left[\left((x_1)^2 + (y_1)^2\right)(1-u)^2 + 2(1-u)u\left(x_1x_2 + y_1y_2\right) + \left((x_2)^2 + (y_2)^2\right)u^2\right]^{7/2}} \right.$$

$$\left. \left. -\frac{1}{\left[\left((x_1)^2 + (y_1)^2\right)(1-u)^2 + 2(1-u)u\left(x_1x_2 + y_1y_2\right) + \left((x_2)^2 + (y_2)^2\right)u^2\right]^{5/2}} \right) \right] (1-u)u^2du$$

$$+3mY^2 \int_0^1 \left[\left(y_1(1-u) + y_2u\right) \cdot \right.$$

$$\left(\frac{5(y_1)^2(1-u)^2 + 10(1-u)uy_1y_2 + 5(y_2)^2u^2}{\left[\left((x_1)^2 + (y_1)^2\right)(1-u)^2 + 2(1-u)u\left(x_1x_2 + y_1y_2\right) + \left((x_2)^2 + (y_2)^2\right)u^2\right]^{7/2}} \right.$$

$$\left. \left. -\frac{3}{\left[\left((x_1)^2 + (y_1)^2\right)(1-u)^2 + 2(1-u)u\left(x_1x_2 + y_1y_2\right) + \left((x_2)^2 + (y_2)^2\right)u^2\right]^{5/2}} \right) \right] (1-u)u^2du.$$

2.2 Methodology

Before showing the results of the numerical simulations, let us first describe the methodology and all the different test cases we considered.

First of all, there were three different kind of satellites we simulated, they differ in the distance of their orbits to the Earth. First, we discussed the geostationary satellites, or in short, GEO satellites, which orbit the Earth at around 42.200 kilometres from the ECI center. The second type are the medium earth orbit (MEO) satellites, with distances to the ECI center ranging between 8.000 and 42.000 kilometres, and finally, we considered representatives of low earth orbit (LEO) satellites, which are typically of military use and for observation e.g. of other satellites and space debris, which orbit the earth at distances smaller than 8.000 kilometres.

For each of the above satellite types, we studied two situations. These are: S2 closer to the Earth than S1, and vice versa. The defining parameters for each of the test cases are the initial distance between S1 and S2, which is denoted by d, and the time interval for the integration, denoted by t.

The different parameter choices were motivated by trying to push the values for d and t as far as possible, while still staying in a realistic context, allowing to show how the Newtonian equations can be improved. Additionally, preliminary results are obtained for small values for d and t, just to show how the solutions behave.

The experiments correspond to three different parameter combinations for each of the satellites types. In order to draw valid conclusions, a variety of plots has been provided. Special focus is on figures where the distance between the Newtonian and post–Newtonian relative positions of S2 with respect to S1 are compared to the diameter of the spots of a laser beam with submicroradian divergence.

2.3 Results

2.3.1 GEO satellites with S2 being closer to the Earth than S1

2.3.1.1 Case 1

In this test, we display the solution for small parameter values, $d = 5$ kilometers and $t = 5$ days.
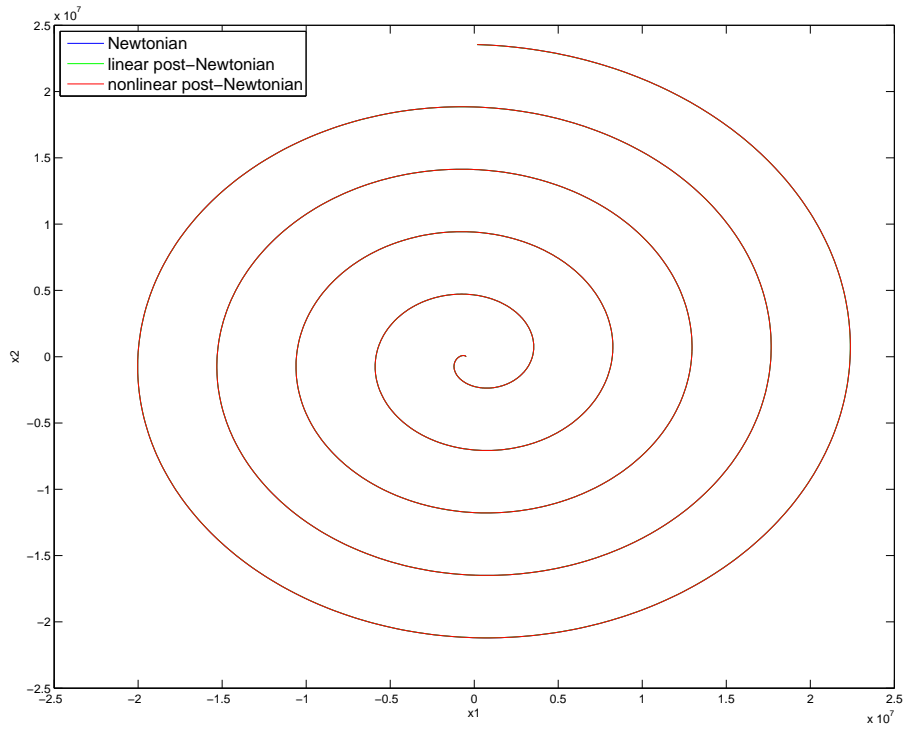
Figure 1: Case 1 for GEO satellites with S2 being closer to the earth than S1, $d = 5$ kilometres, $t = 5$ days: Relative motion of S2 with respect to S1.
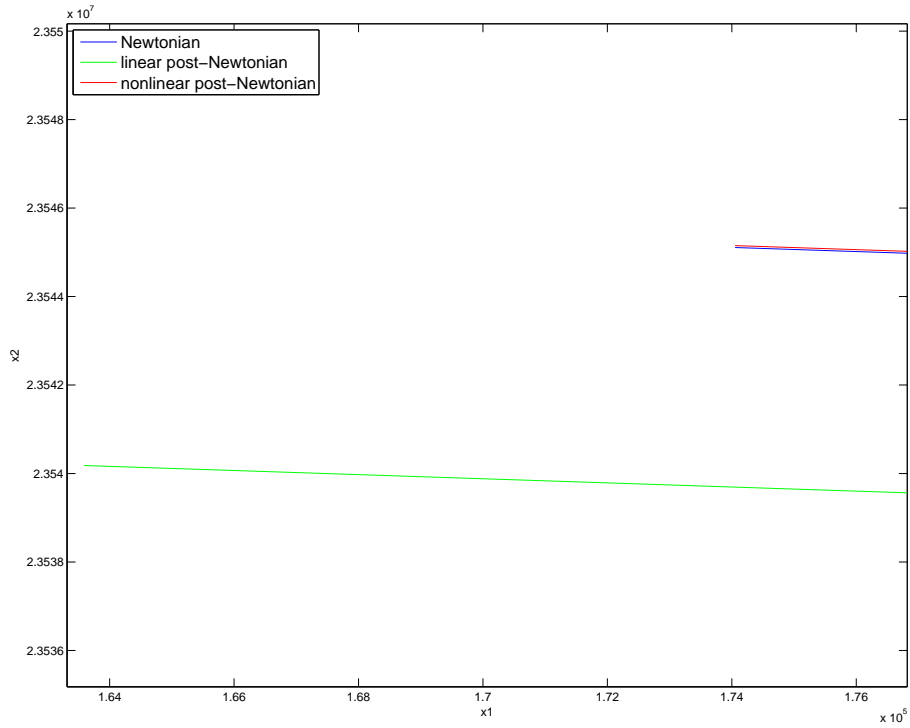
Figure 2: Case 1 for GEO satellites with S2 being closer to the earth than S1, $d = 5$ kilometres, $t = 5$ days: Zoomed in version of the previous plot. It is now possible to see the difference between solutions from different formulations.
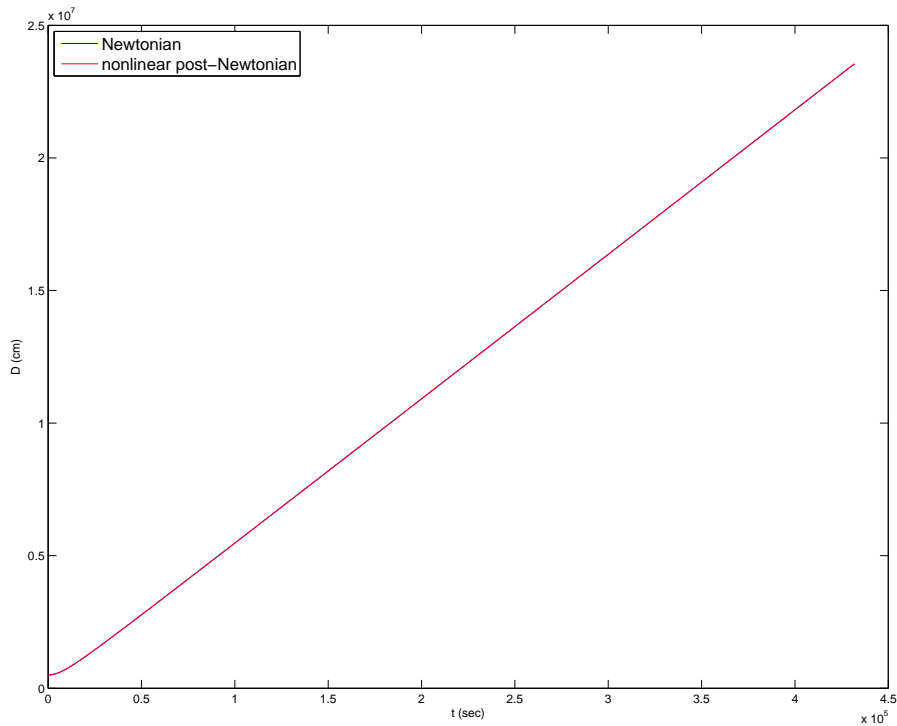

Figure 3: Case 1 for GEO satellites with S2 being closer to the earth than S1, $d = 5$ kilometres, $t = 5$ days: Absolute distance between S1 and S2.
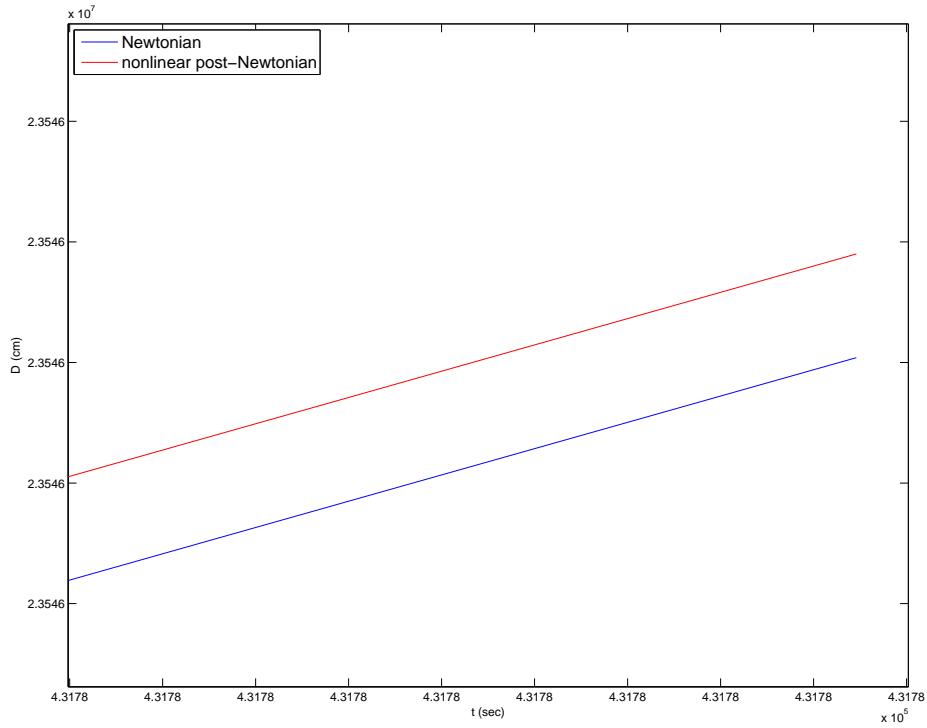
Figure 4: Case 1 for GEO satellites with S2 being closer to the earth than S1, $d = 5$ kilometres, $t = 5$ days: Zoomed in version of the previous plot. It is now possible to see differences between solutions from different formulations.
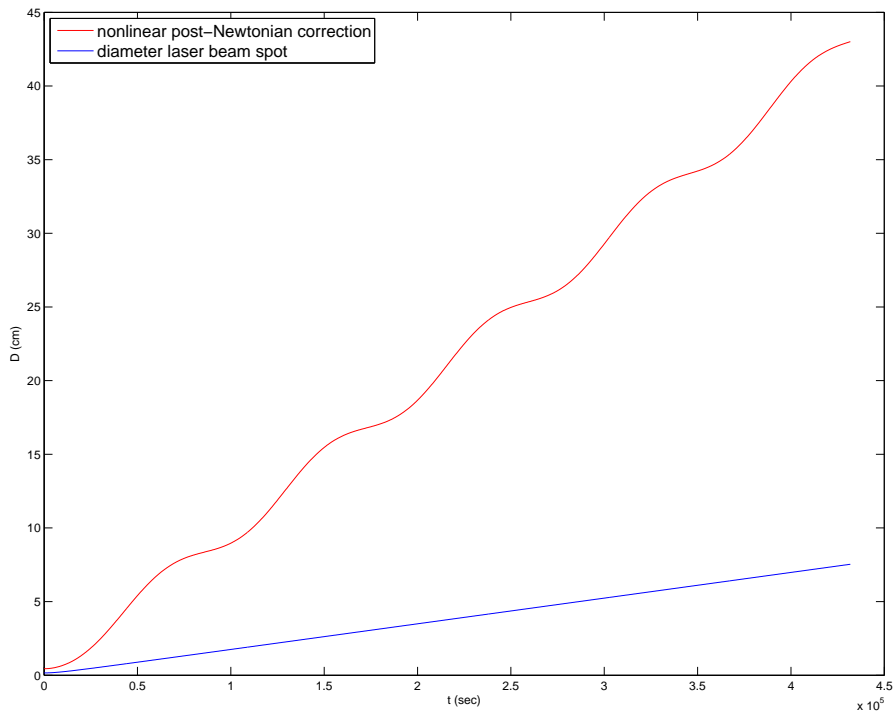
Figure 5: Case 1 for GEO satellites with S2 being closer to the earth than S1, $d = 5$ kilometres, $t = 5$ days: Correction provided from the nonlinear post–Newtonian equations compared to the laser beam.
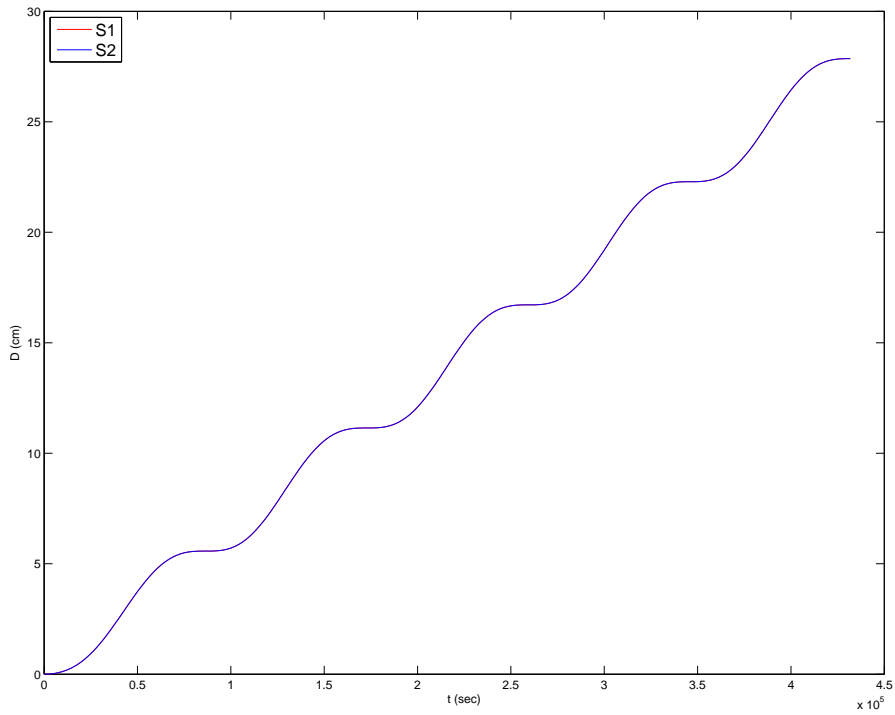
Figure 6: Case 1 for GEO satellites with S2 being closer to the earth than S1, $d = 5$ kilometres, $t = 5$ days: The distance between the ECI positions of the Newtonian and the nonlinear post–Newtonian solutions, both for S1 and S2, which almost completely overlap.
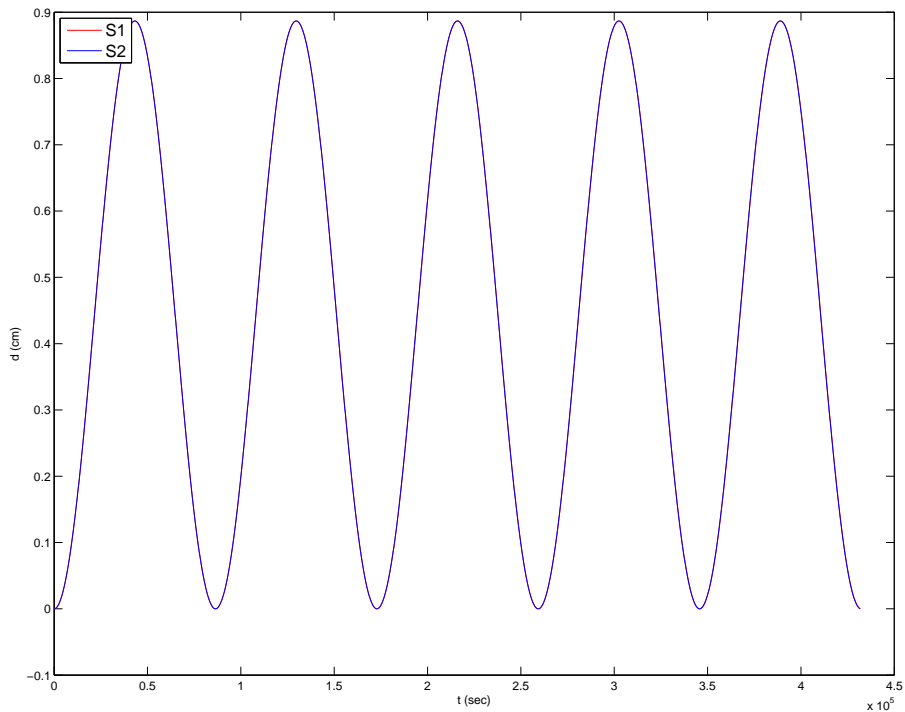
Figure 7: Case 1 for GEO satellites with S2 being closer to the earth than S1, $d = 5$ kilometres, $t = 5$ days: Difference in distances to the center of the Earth between Newtonian and nonlinear post–Newtonian.

13
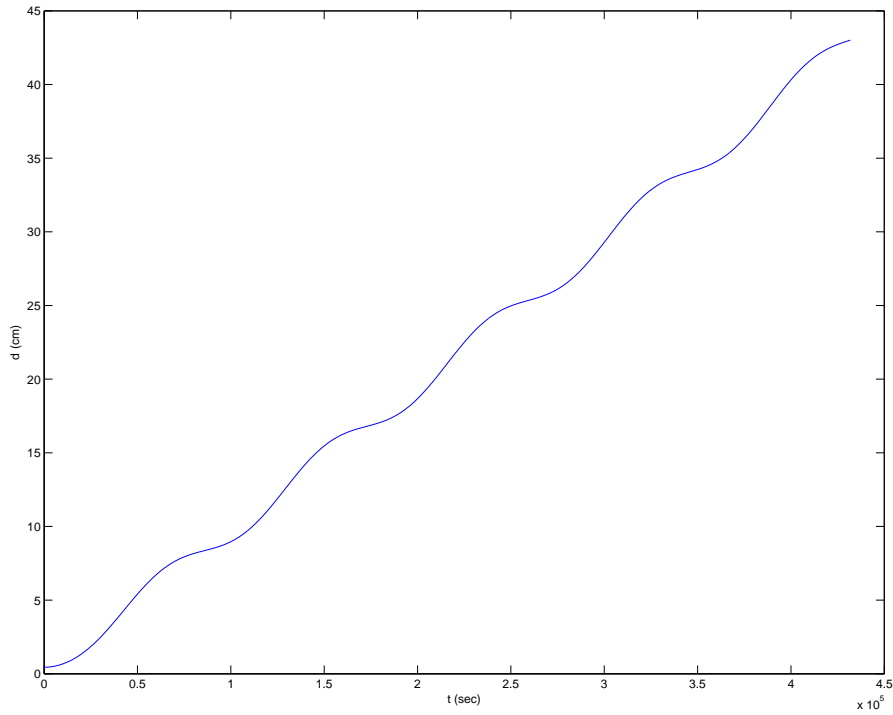
Figure 8: Case 1 for GEO satellites with S2 being closer to the earth than S1, $d = 5$ kilometres, $t = 5$ days, and nonlinear post–Newtonian formulation: Distance between ECI positions of S2 and S1 and the relative position of S2 with respect to S1.
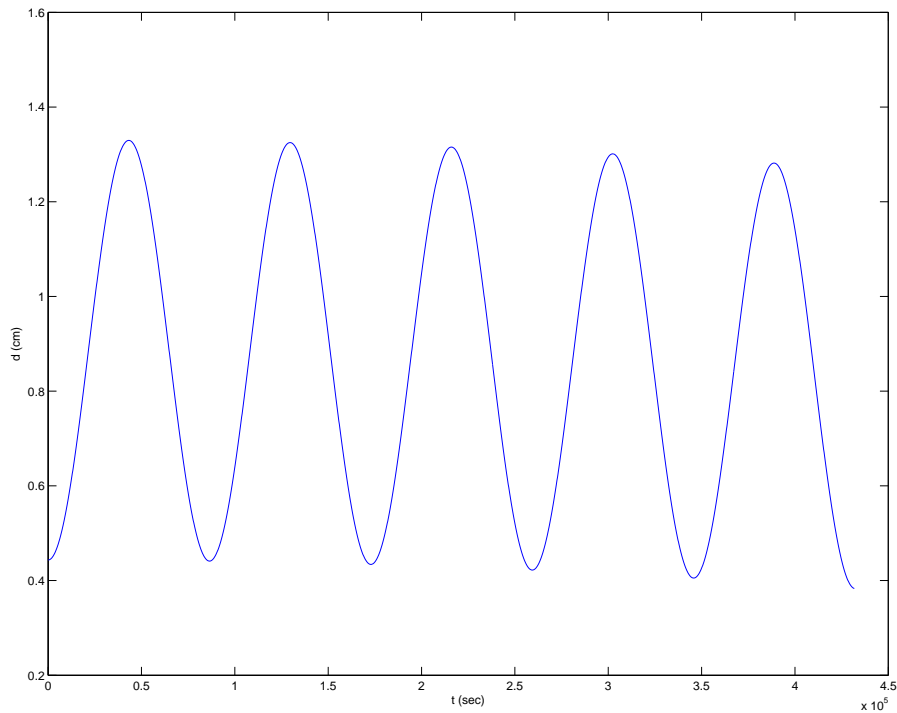
Figure 9: Case 1 for GEO satellites with S2 being closer to the earth than S1, $d = 5$ kilometres, $t = 5$ days, and nonlinear post–Newtonian formulation: This plot, similar to the above one, shows the difference in distances to the ECI center.

14

2.3.1.2 Case 2

In this experiment, the goal was to increase the value of d as much as possible. The parameters used for this test are $d = 25$ kilometres and $t = 5$ days.
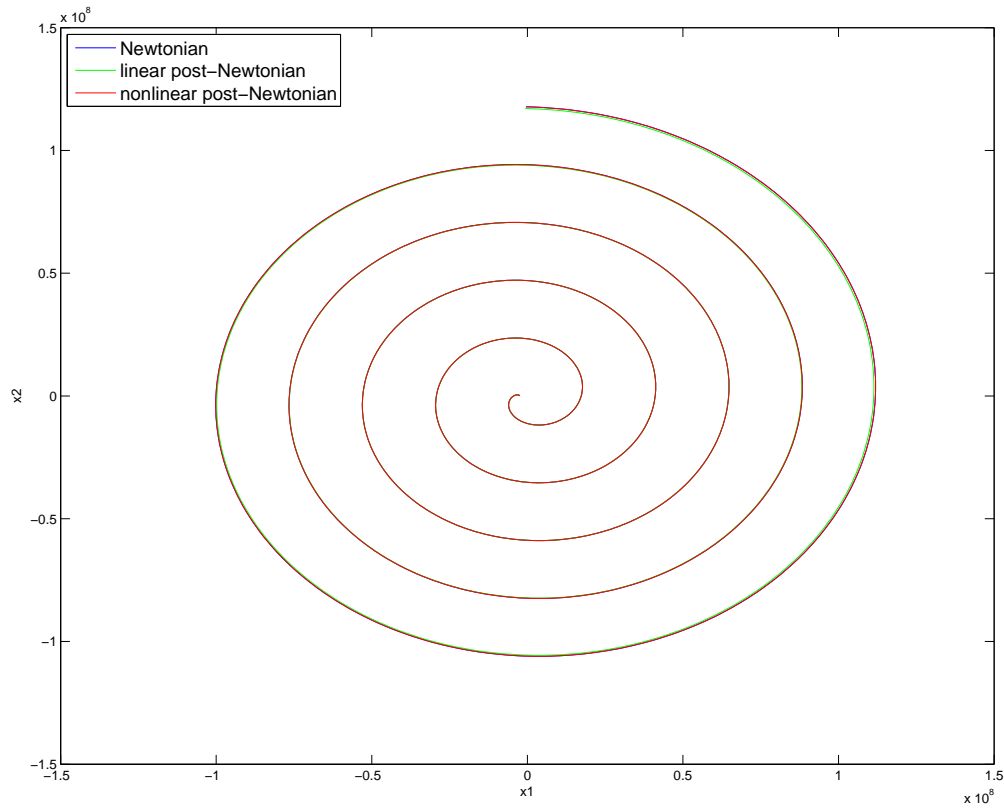
Figure 10: Case 2 for GEO satellites with S2 being closer to the earth than S1, $d = 25$ kilometres, $t = 5$ days: Relative motion of S2 with respect to S1.
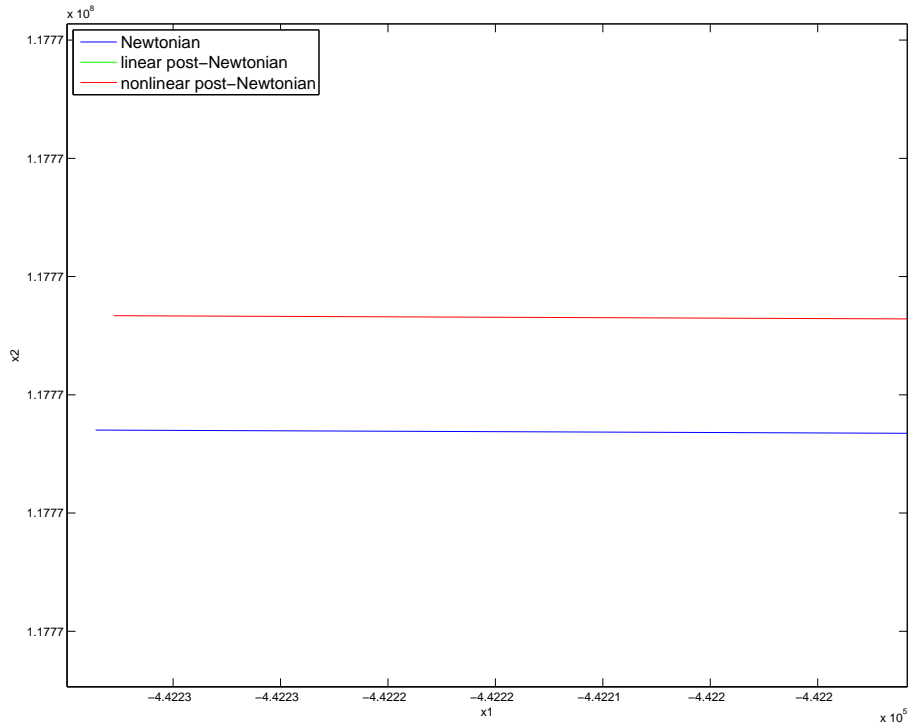
Figure 11: Case 2 for GEO satellites with S2 being closer to the earth than S1, $d = 25$ kilometres, $t = 5$ days: Zoomed in version of the previous plot. It is now possible to see the difference between solutions from different formulations.
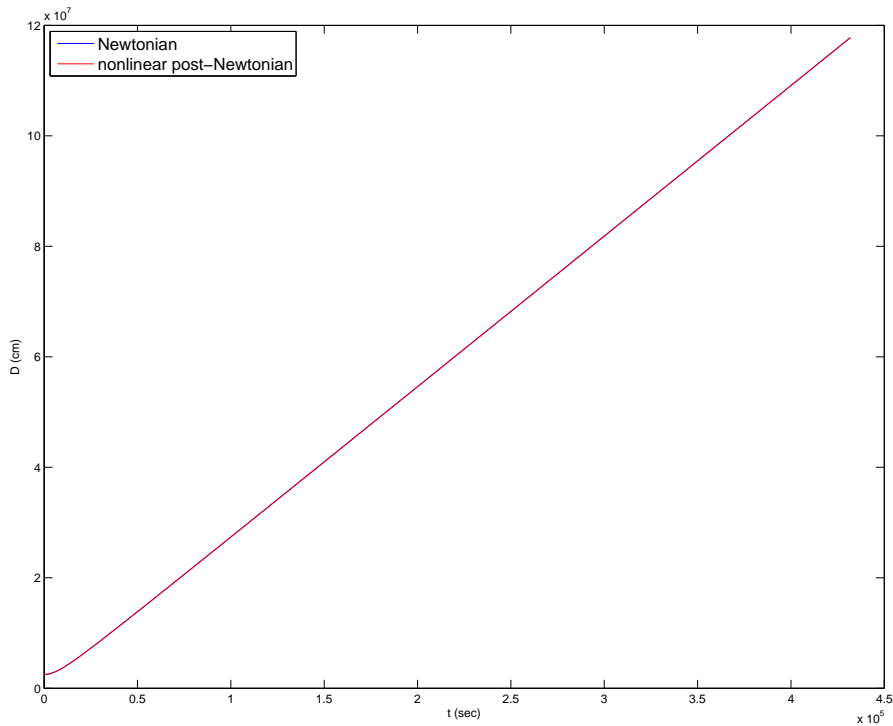
Figure 12: Case 2 for GEO satellites with S2 being closer to the earth than S1, $d = 25$ kilometres, $t = 5$ days: Absolute distance between S1 and S2.
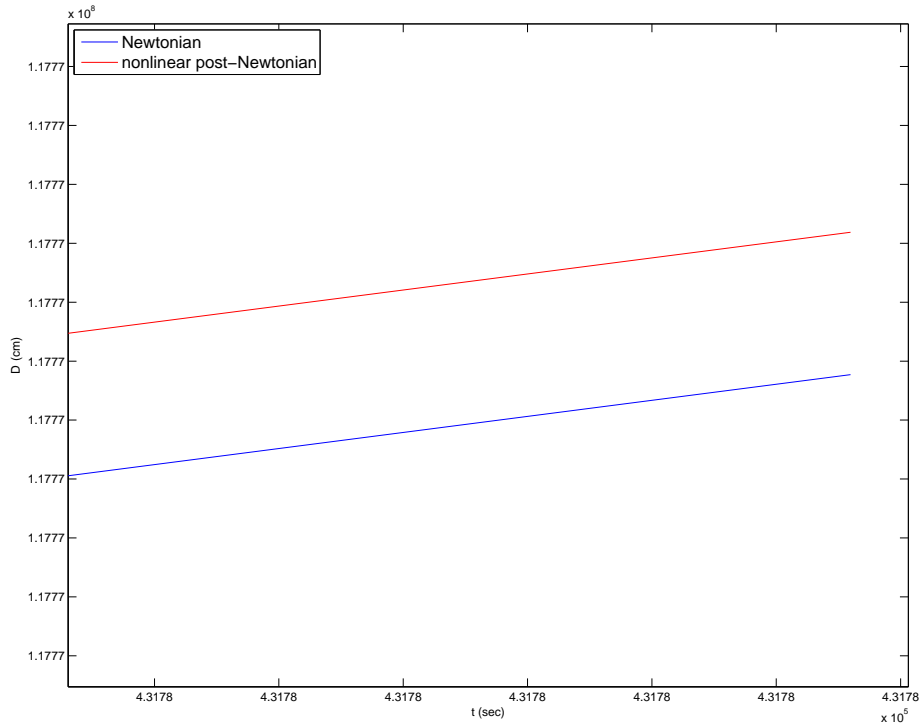
Figure 13: Case 2 for GEO satellites with S2 being closer to the earth than S1, $d = 25$ kilometres, $t = 5$ days: Zoomed in version of the previous plot. It is now possible to see differences between solutions from different formulations.
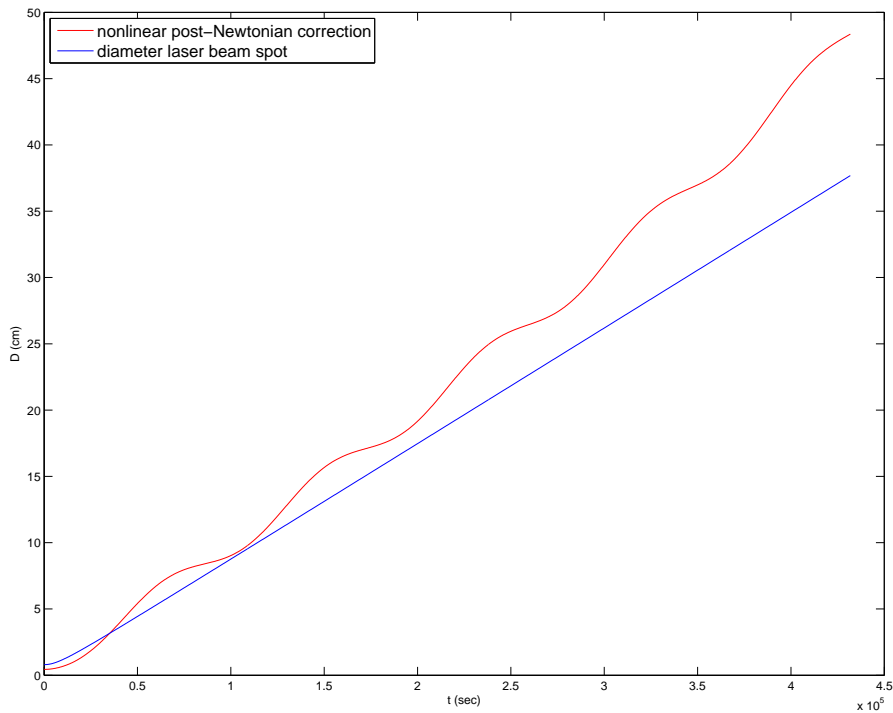
Figure 14: Case 2 for GEO satellites with S2 being closer to the earth than S1, $d = 25$ kilometres, $t = 5$ days: Correction provided from the nonlinear post–Newtonian equations compared to the laser beam.
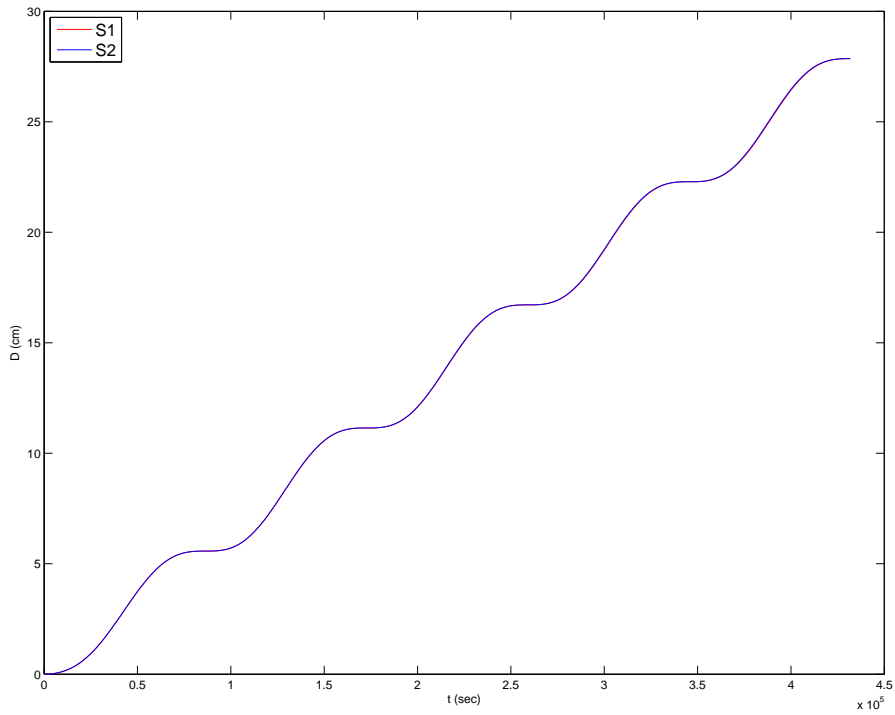
Figure 15: Case 2 for GEO satellites with S2 being closer to the earth than S1, $d = 25$ kilometres, $t = 5$ days: The distance between the ECI positions of the Newtonian and the nonlinear post–Newtonian solutions, both for S1 and S2, which almost completely overlap.
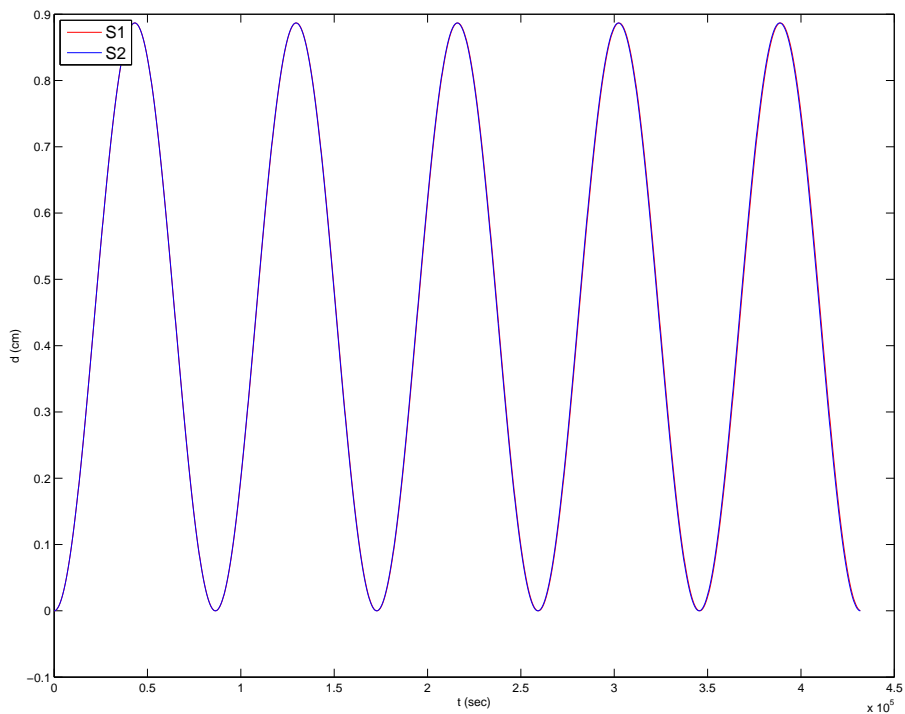

Figure 16: Case 2 for GEO satellites with S2 being closer to the earth than S1, $d = 25$ kilometres, $t = 5$ days: Difference in distances to the center of the Earth between Newtonian and nonlinear post–Newtonian.
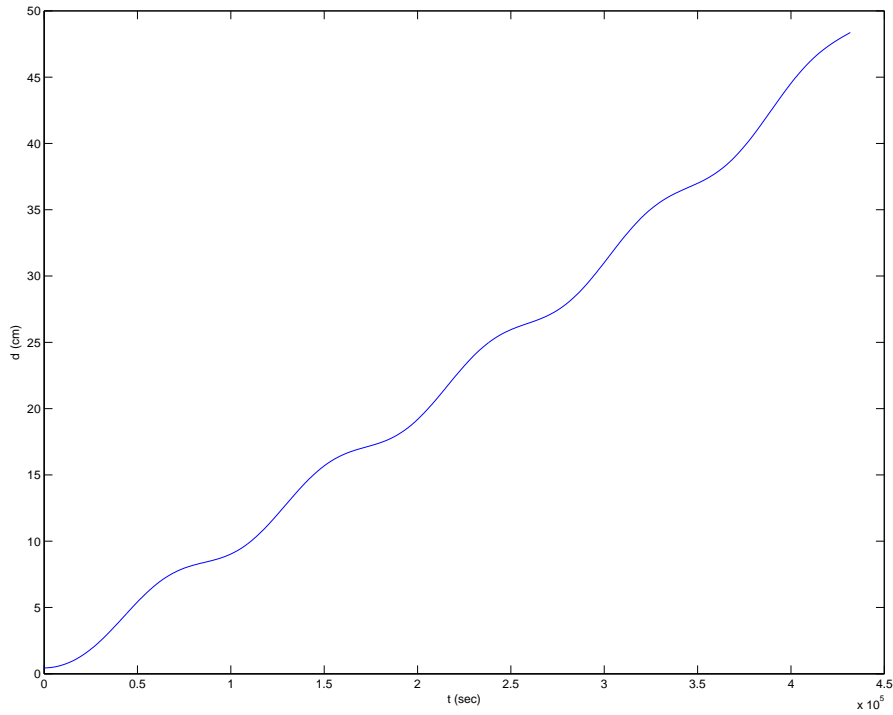
Figure 17: Case 2 for GEO satellites with S2 being closer to the earth than S1, $d = 25$ kilometres, $t = 5$ days, and nonlinear post–Newtonian formulation: Distance between ECI positions of S2 and S1 and the relative position of S2 with respect to S1.
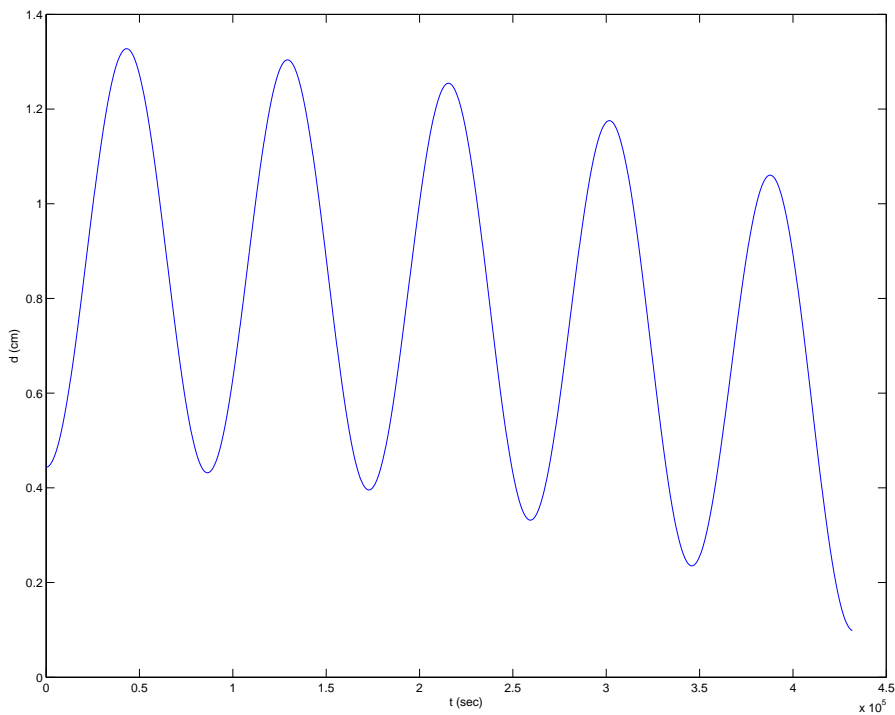

Figure 18: Case 2 for GEO satellites with S2 being closer to the earth than S1, $d = 25$ kilometres, $t = 5$ days, and nonlinear post–Newtonian formulation: This plot, similar to the above one, shows the difference in distances to the ECI center.

2.3.1.3 Case 3

For this test, the goal was to increase the value of t as much as possible. The parameters used for this test are $d = 5$ kilometres and $t = 20$ days.
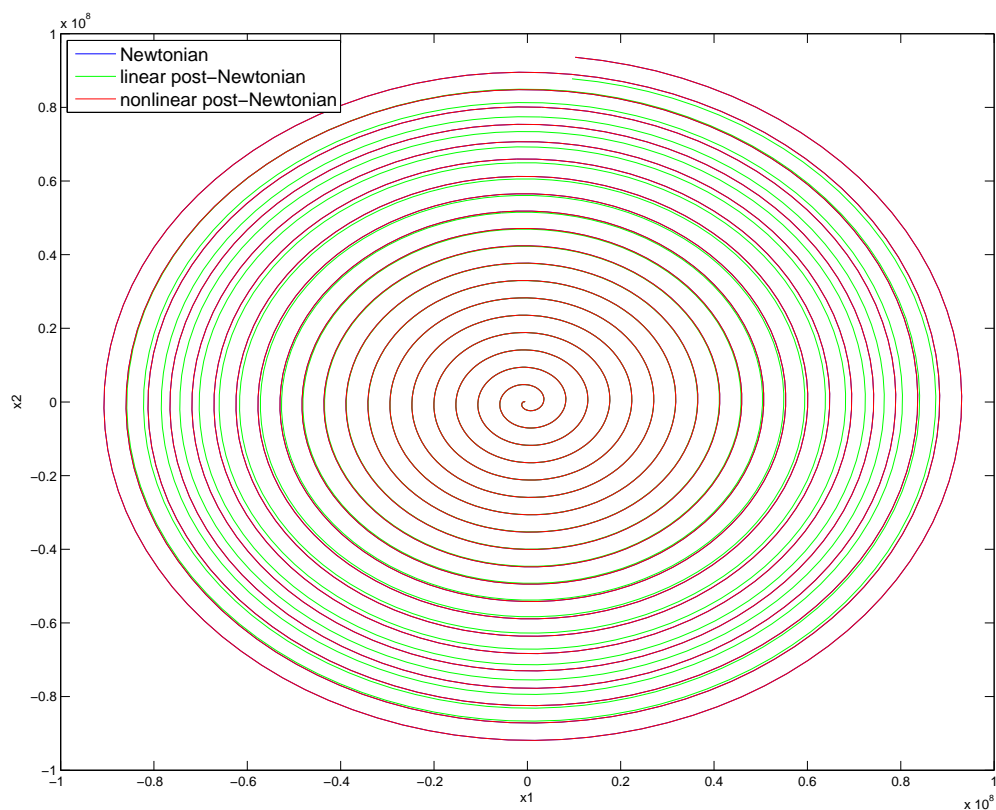
Figure 19: Case 3 for GEO satellites with S2 being closer to the earth than S1, $d = 5$ kilometres, $t = 20$ days: Relative motion of S2 with respect to S1.
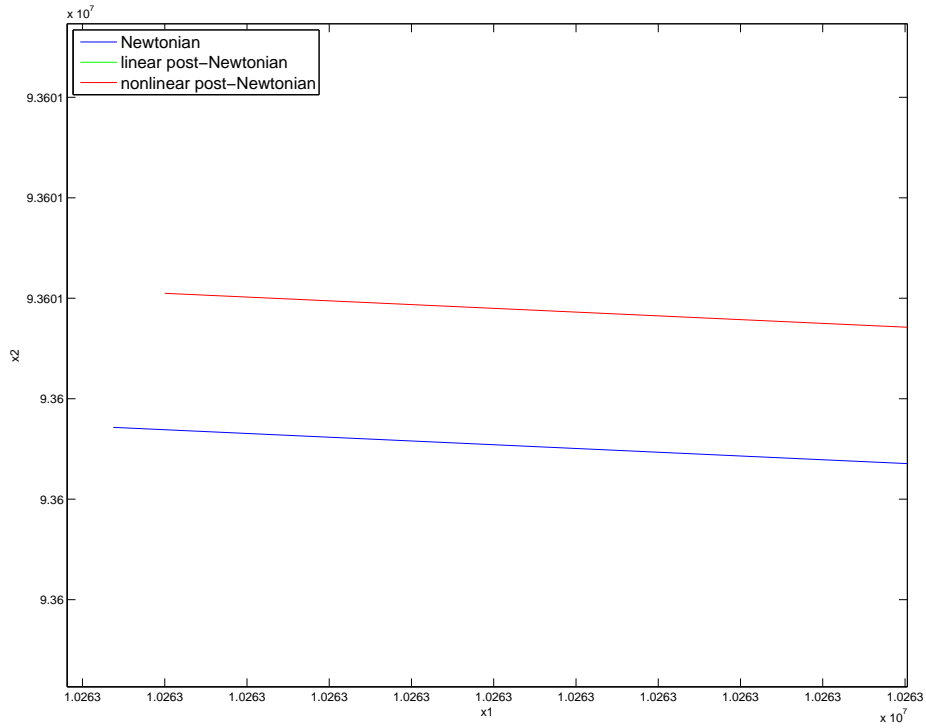
Figure 20: Case 3 for GEO satellites with S2 being closer to the earth than S1, $d = 5$ kilometres, $t = 20$ days: Zoomed in version of the previous plot. It is now possible to see the difference between solutions from different formulations.
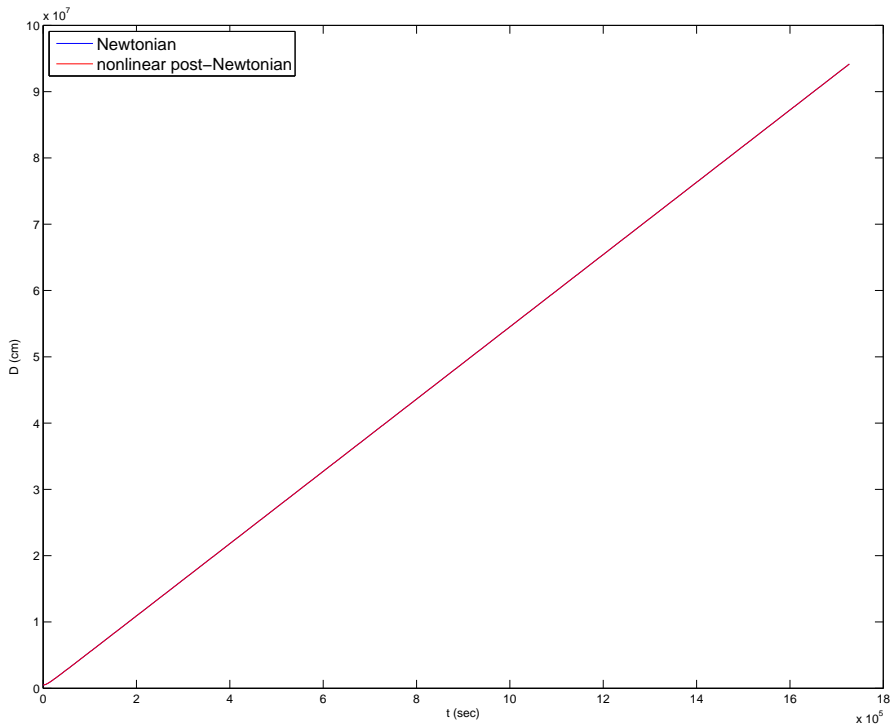

Figure 21: Case 3 for GEO satellites with S2 being closer to the earth than S1, $d = 5$ kilometres, $t = 20$ days: Absolute distance between S1 and S2.

21
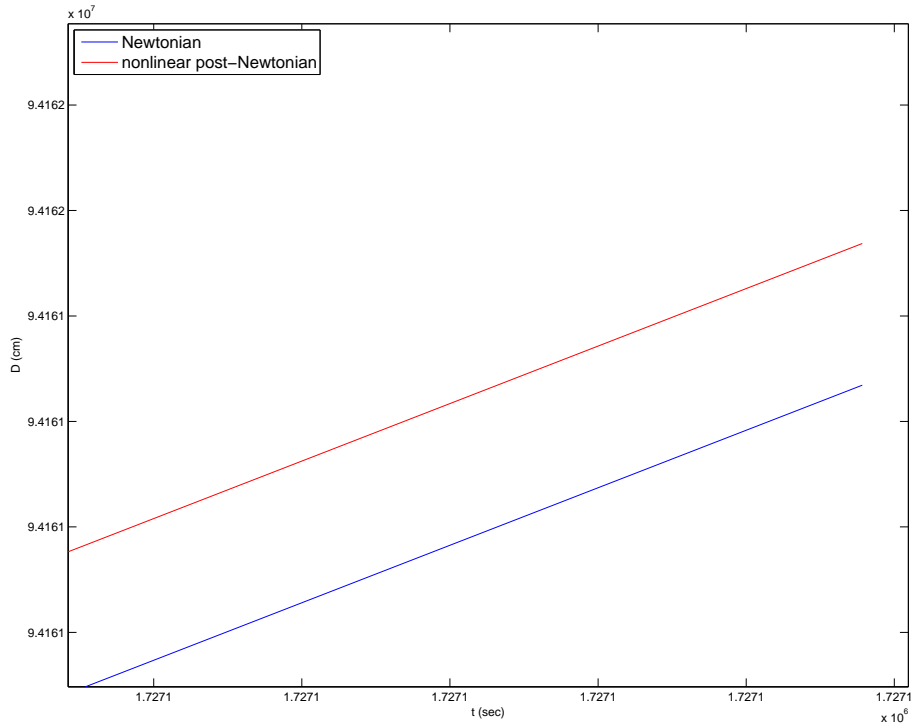
Figure 22: Case 3 for GEO satellites with S2 being closer to the earth than S1, $d = 5$ kilometres, $t = 20$ days: Zoomed in version of the previous plot. It is now possible to see differences between solutions from different formulations.
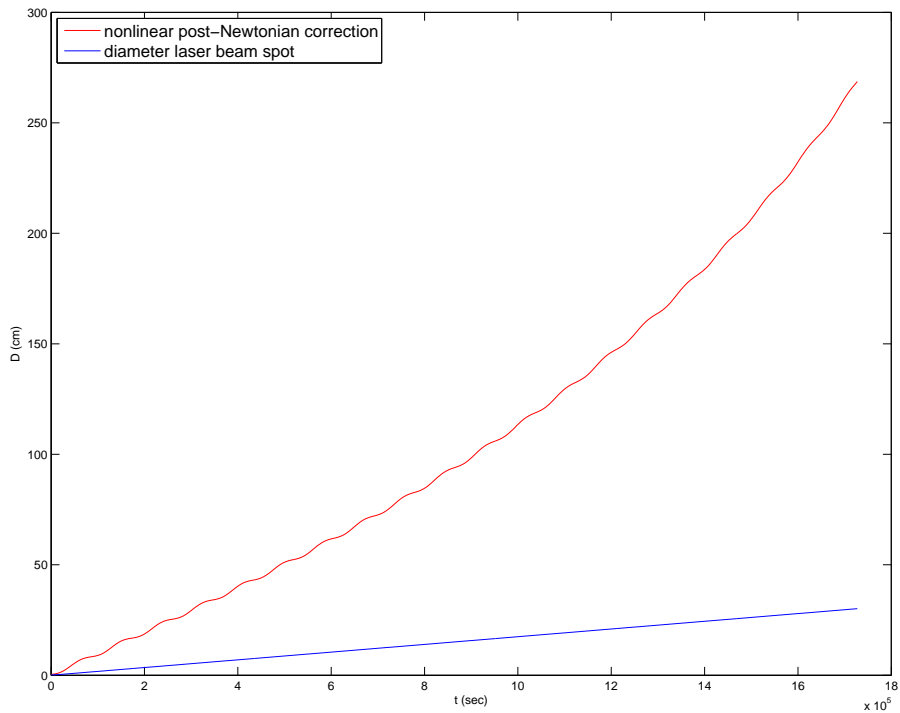

Figure 23: Case 3 for GEO satellites with S2 being closer to the earth than S1, $d = 5$ kilometres, $t = 20$ days: Correction provided from the nonlinear post–Newtonian equations compared to the laser beam.
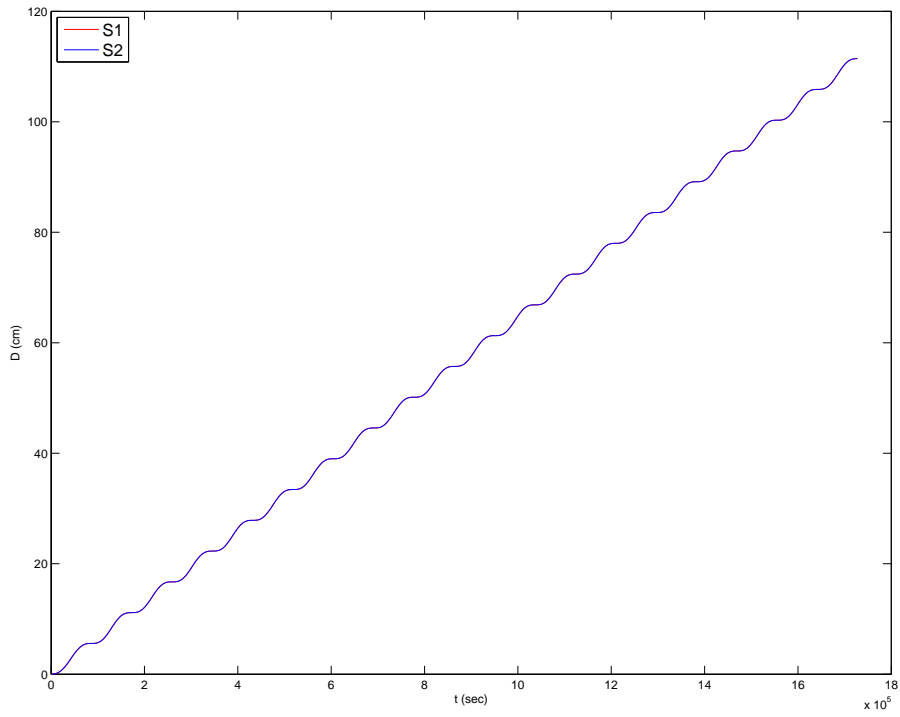
Figure 24: Case 3 for GEO satellites with S2 being closer to the earth than S1, $d = 5$ kilometres, $t = 20$ days: The distance between the ECI positions of the Newtonian and the nonlinear post–Newtonian solutions, both for S1 and S2, which almost completely overlap.
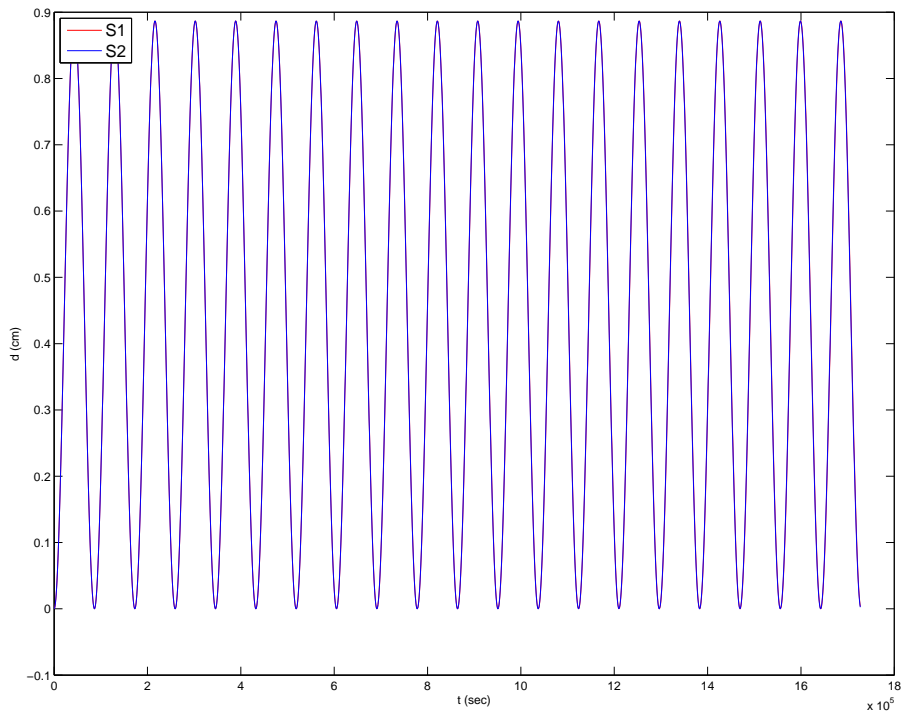

Figure 25: Case 3 for GEO satellites with S2 being closer to the earth than S1, $d = 5$ kilometres, $t = 20$ days: Difference in distances to the center of the Earth between Newtonian and nonlinear post–Newtonian.
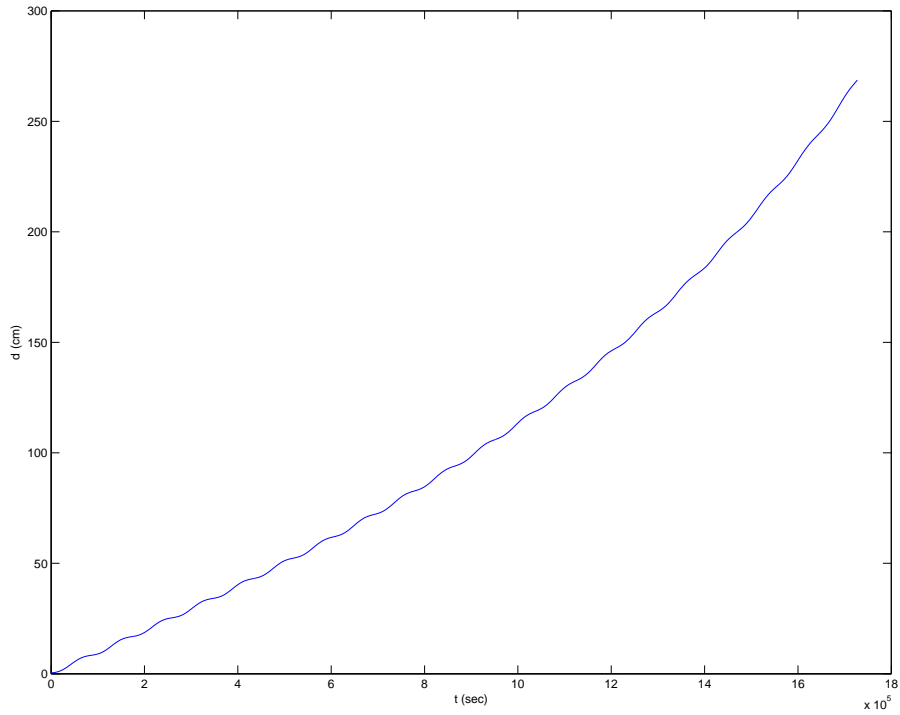
Figure 26: Case 3 for GEO satellites with S2 being closer to the earth than S1, $d = 5$ kilometres, $t = 20$ days, and nonlinear post–Newtonian formulation: Distance between ECI positions of S2 and S1 and the relative position of S2 with respect to S1.
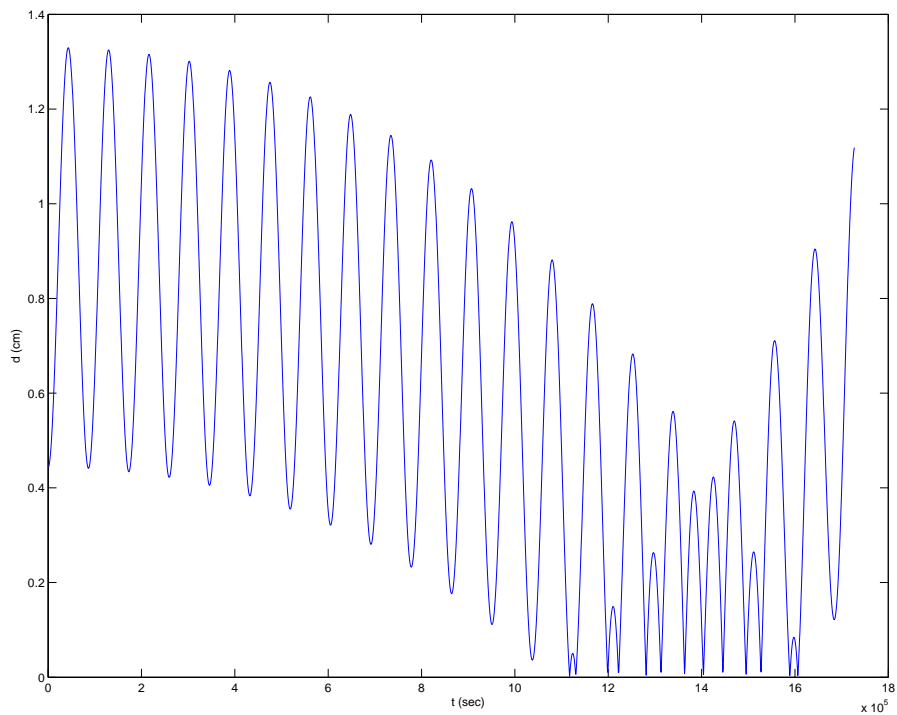

Figure 27: Case 3 for GEO satellites with S2 being closer to the earth than S1, $d = 5$ kilometres, $t = 20$ days, and nonlinear post–Newtonian formulation: This plot, similar to the above one, shows the difference in distances to the ECI center.

24

2.3.2 GEO satellites with S2 being farther away from the Earth than S1

2.3.2.1 Case 1

In this test we showcase the solution for small values in both parameters.
The parameters used for this test are $d = 5$ kilometres and $t = 5$ days.
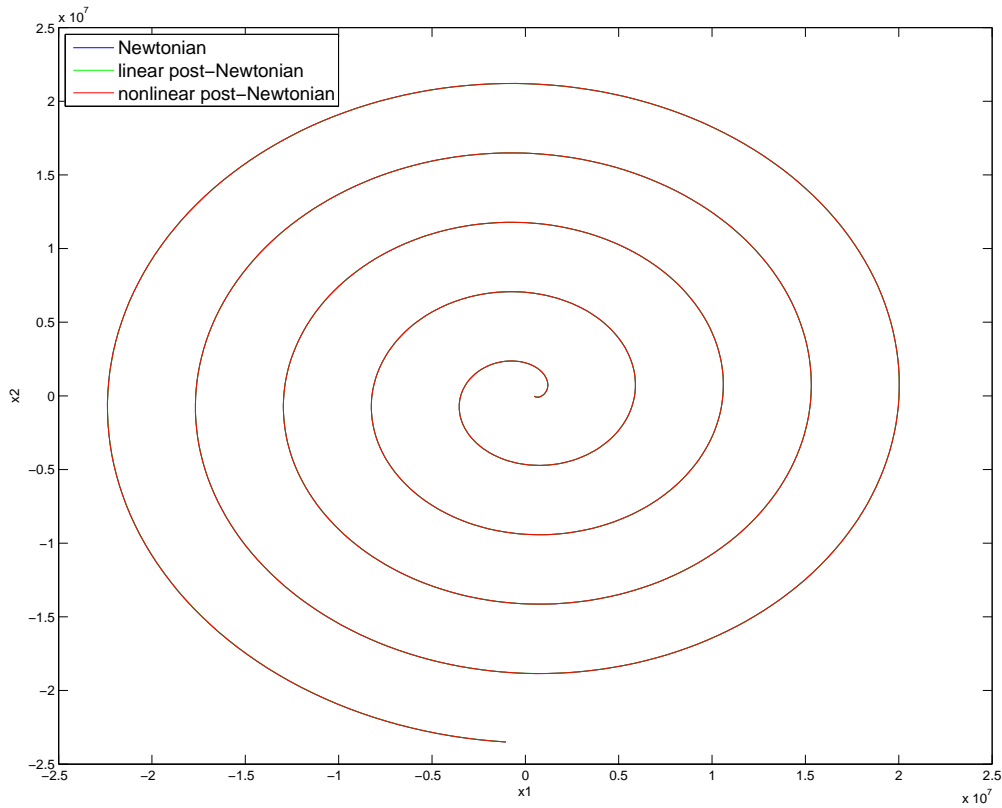
Figure 28: Case 1 for GEO satellites with S2 being farther away from the earth than S1, $d = 5$ kilometres, $t = 5$ days: Relative motion of S2 with respect to S1.
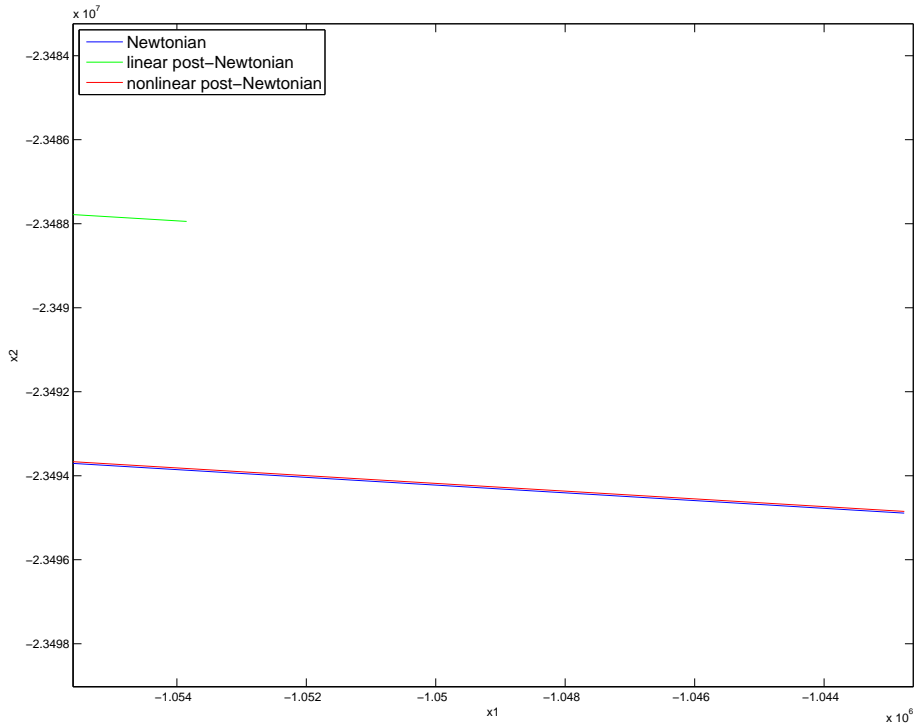
Figure 29: Case 1 for GEO satellites with S2 being farther away from the earth than S1, $d = 5$ kilometres, $t = 5$ days: Zoomed in version of the previous plot. It is now possible to see the difference between solutions from different formulations.
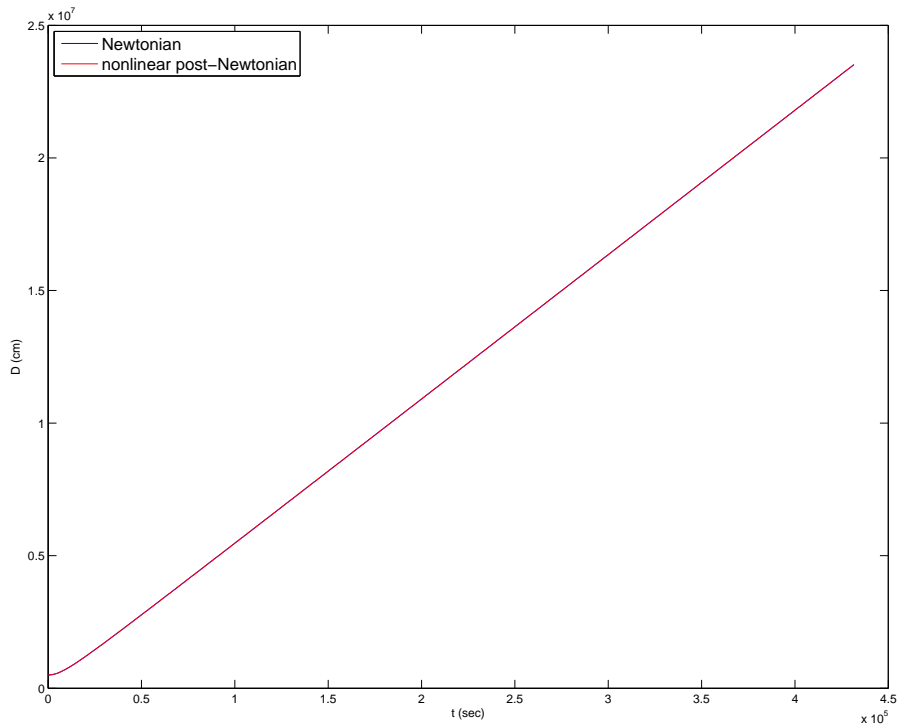

Figure 30: Case 1 for GEO satellites with S2 being farther away from the earth than S1, $d = 5$ kilometres, $t = 5$ days: Absolute distance between S1 and S2.
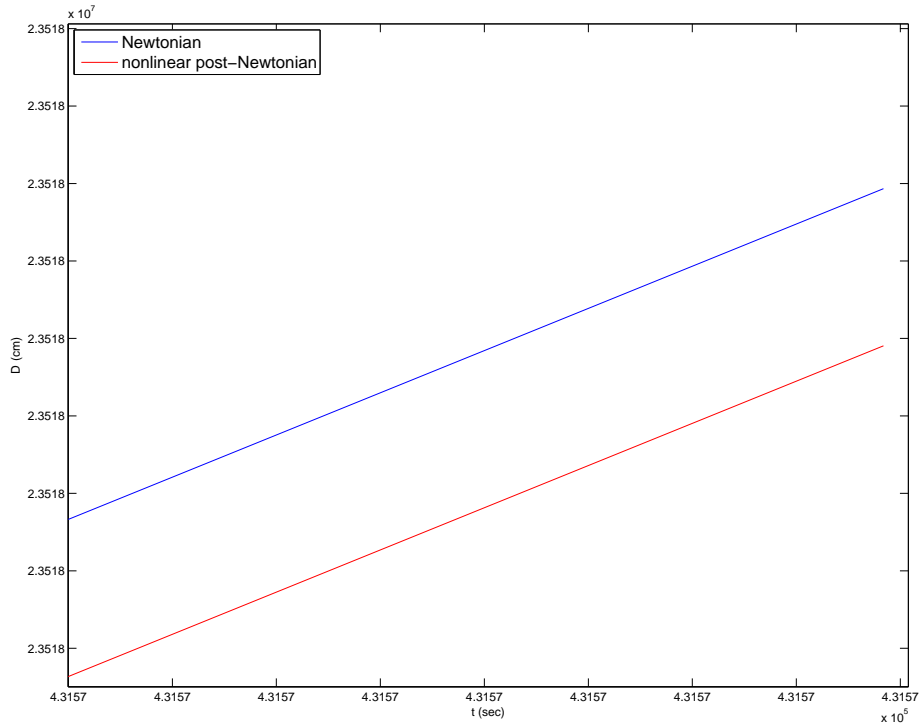
Figure 31: Case 1 for GEO satellites with S2 being farther away from the earth than S1, $d = 5$ kilometres, $t = 5$ days: Zoomed in version of the previous plot. It is now possible to see differences between solutions from different formulations.
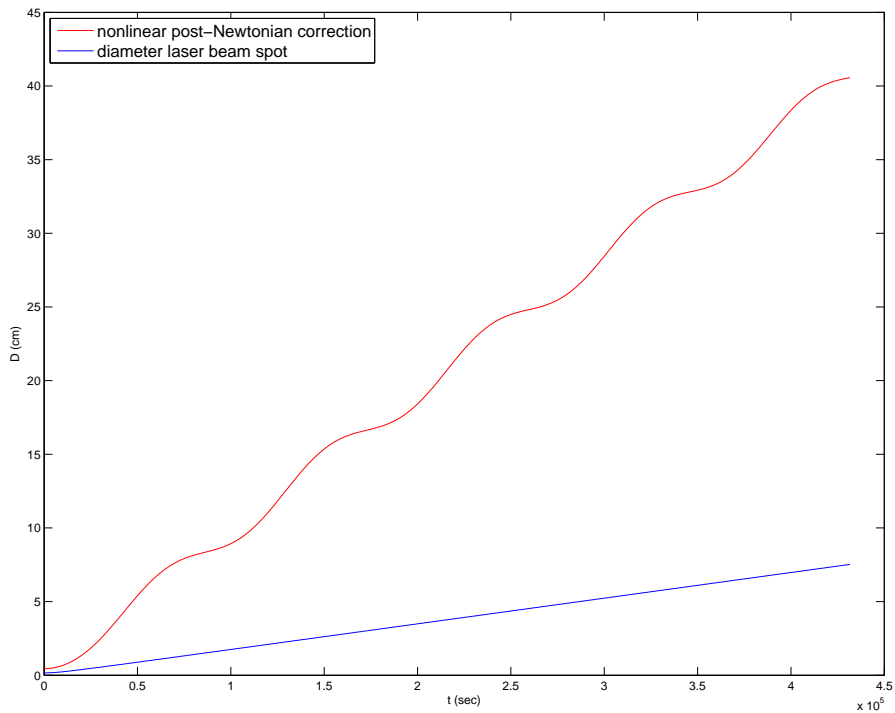

Figure 32: Case 1 for GEO satellites with S2 being farther away from the earth than S1, $d = 5$ kilometres, $t = 5$ days: Correction provided from the nonlinear post–Newtonian equations compared to the laser beam.

27
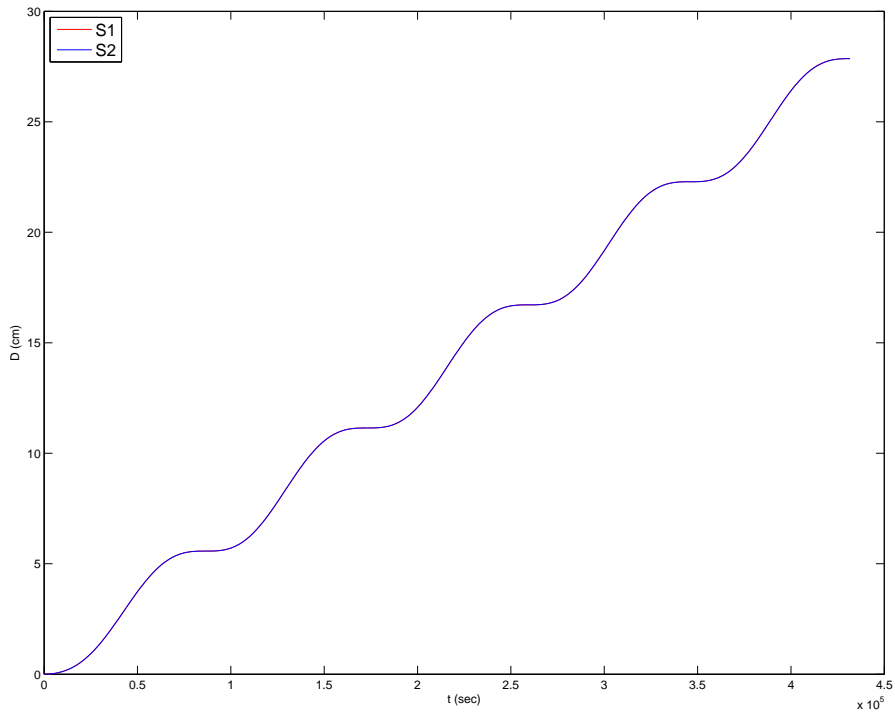
Figure 33: Case 1 for GEO satellites with S2 being farther away from the earth than S1, $d = 5$ kilometres, $t = 5$ days: The distance between the ECI positions of the Newtonian and the nonlinear post–Newtonian solutions, both for S1 and S2, which almost completely overlap.
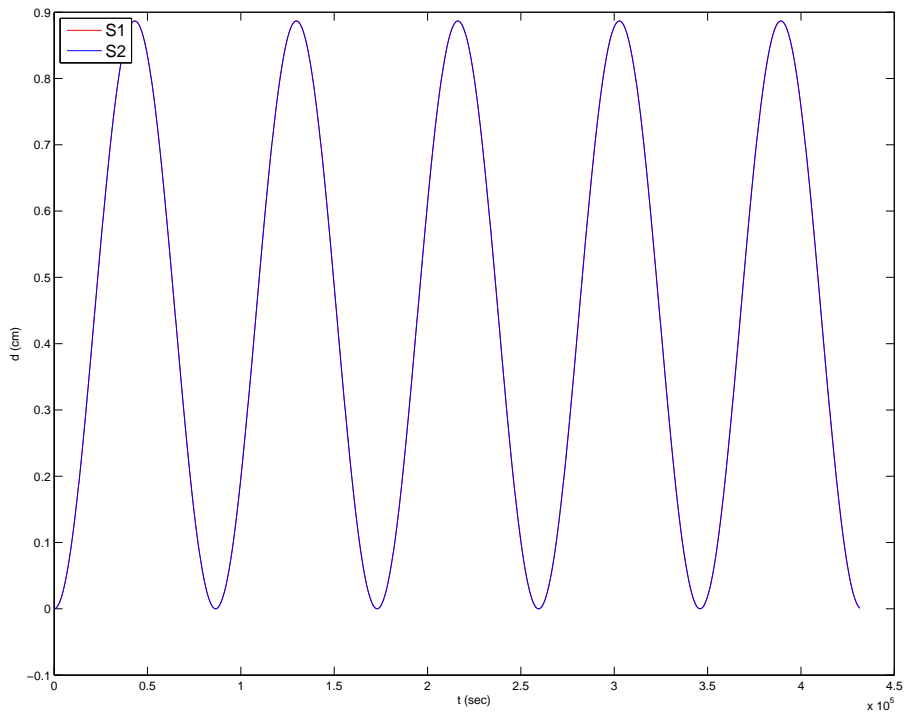

Figure 34: Case 1 for GEO satellites with S2 being farther away from the earth than S1, $d = 5$ kilometres, $t = 5$ days: Difference in distances to the center of the Earth between Newtonian and nonlinear post–Newtonian.
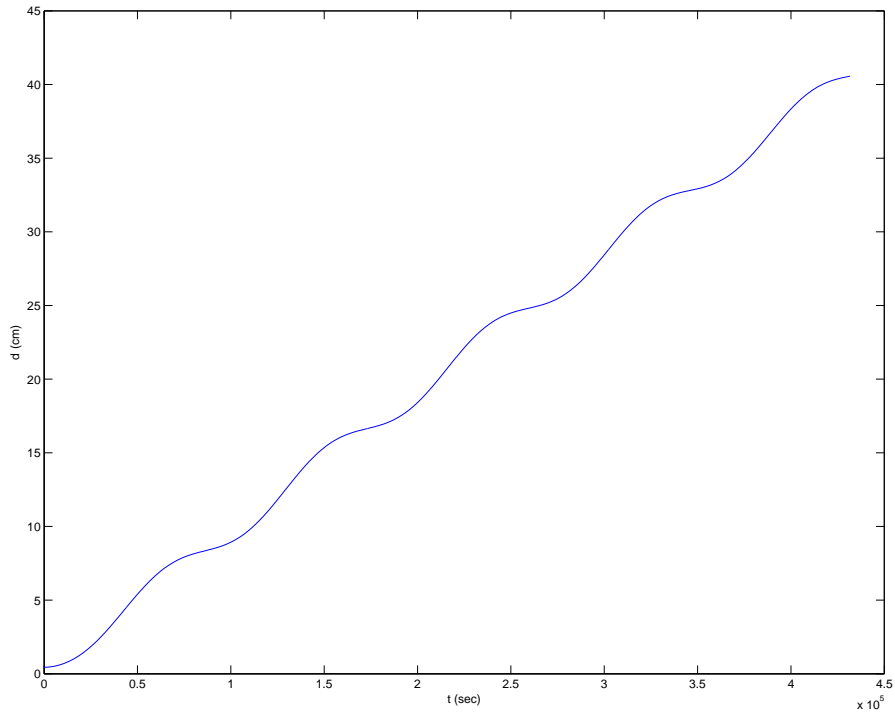
Figure 35: Case 1 for GEO satellites with S2 being farther away from the earth than S1, $d = 5$ kilometres, $t = 5$ days, and nonlinear post–Newtonian formulation: Distance between ECI positions of S2 and S1 and the relative position of S2 with respect to S1.
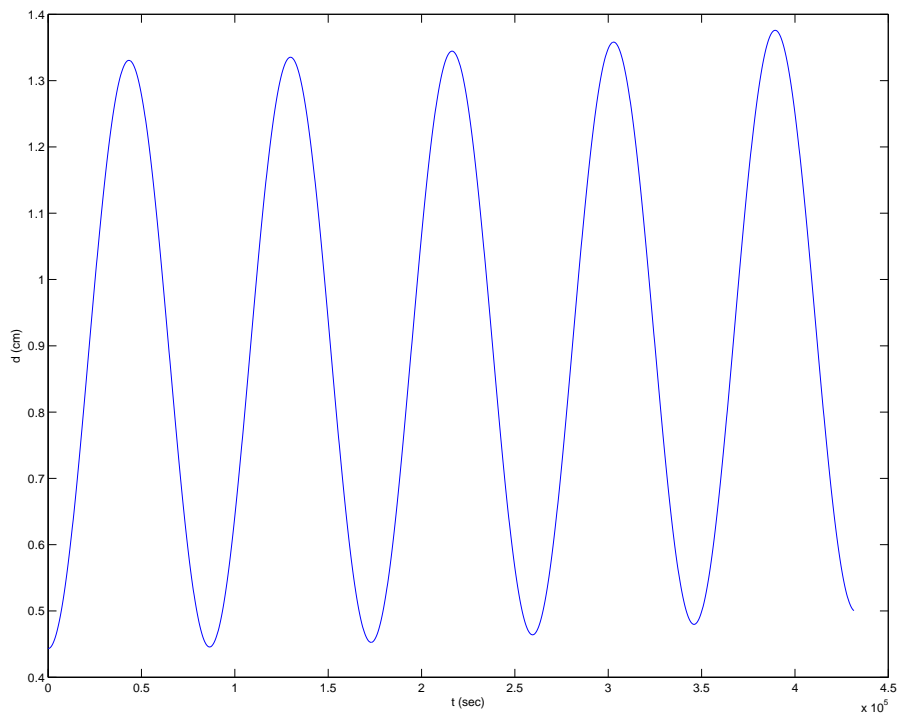

Figure 36: Case 1 for GEO satellites with S2 being farther away from the earth than S1, $d = 5$ kilometres, $t = 5$ days, and nonlinear post–Newtonian formulation: This plot, similar to the above one, shows the difference in distances to the ECI center.

2.3.2.2 Case 2

For this test, the goal was to increase the value of d as much as possible.
The parameters used for this test are $d = 20$ kilometres and $t = 5$ days.
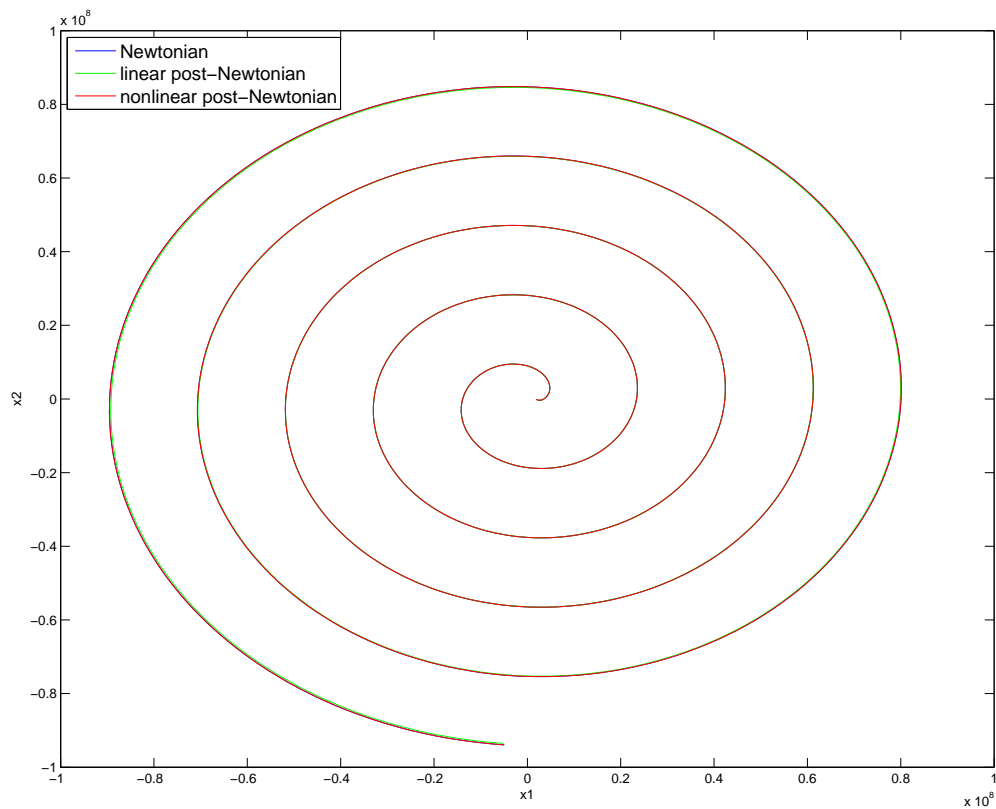

Figure 37: Case 2 for GEO satellites with S2 being farther away from the earth than S1, $d = 20$ kilometres, $t = 5$ days: Relative motion of S2 with respect to S1.
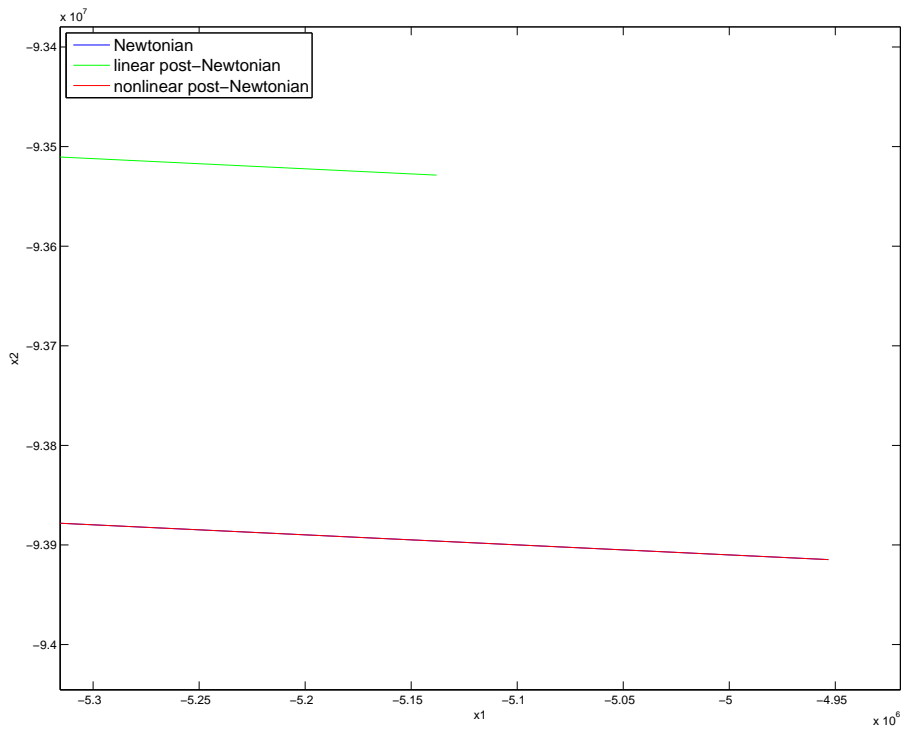
Figure 38: Case 2 for GEO satellites with S2 being farther away from the earth than S1, $d = 20$ kilometres, $t = 5$ days: Zoomed in version of the previous plot. It is now possible to see the difference between solutions from different formulations.
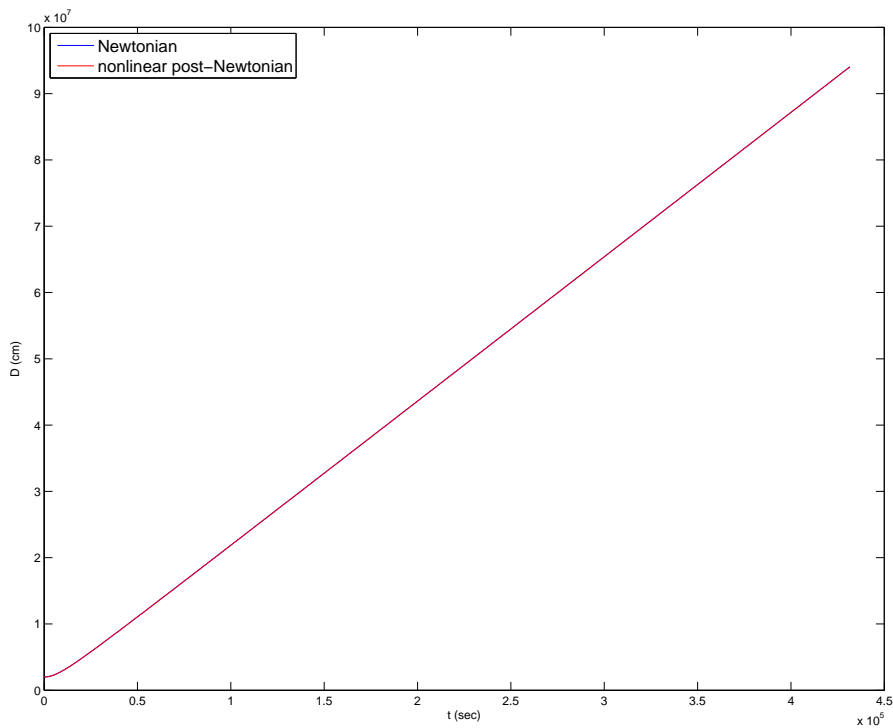

Figure 39: Case 2 for GEO satellites with S2 being farther away from the earth than S1, $d = 20$ kilometres, $t = 5$ days: Absolute distance between S1 and S2.
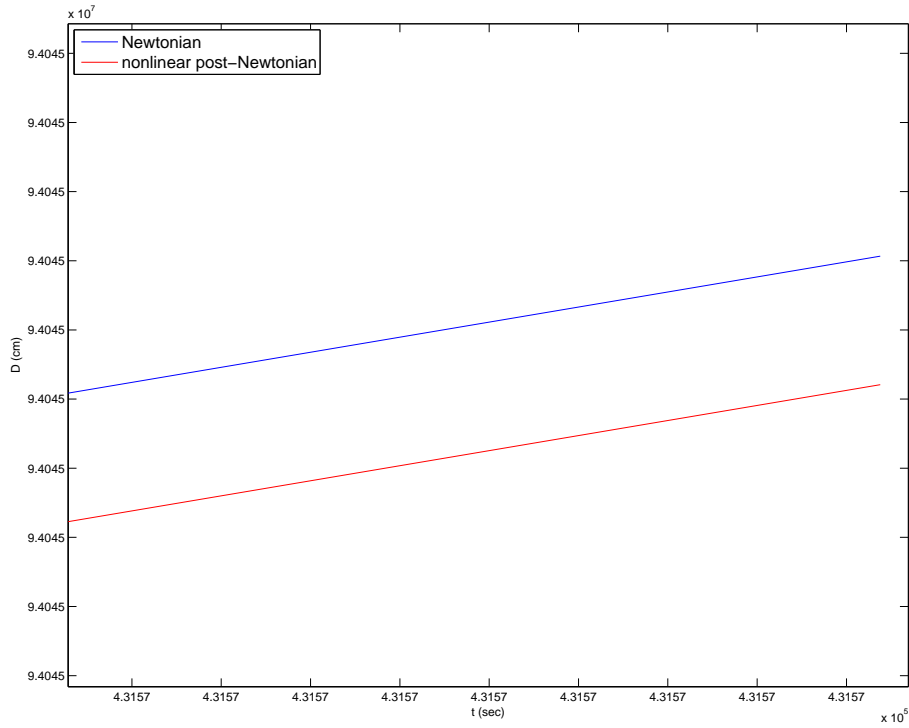
Figure 40: Case 2 for GEO satellites with S2 being farther away from the earth than S1, $d = 20$ kilometres, $t = 5$ days: Zoomed in version of the previous plot. It is now possible to see differences between solutions from different formulations.
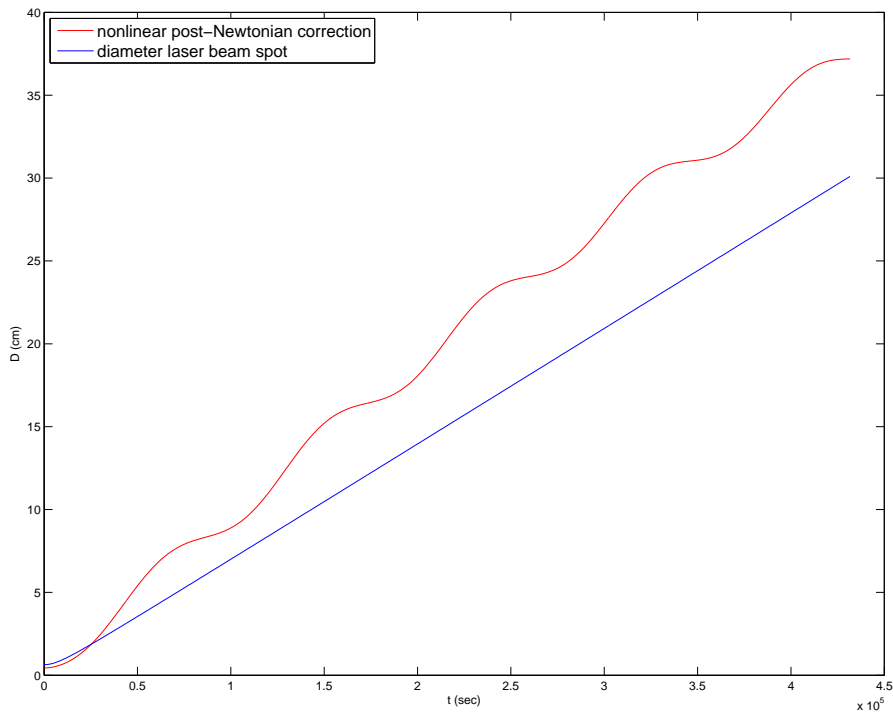

Figure 41: Case 2 for GEO satellites with S2 being farther away from the earth than S1, $d = 20$ kilometres, $t = 5$ days: Correction provided from the nonlinear post–Newtonian equations compared to the laser beam.

32
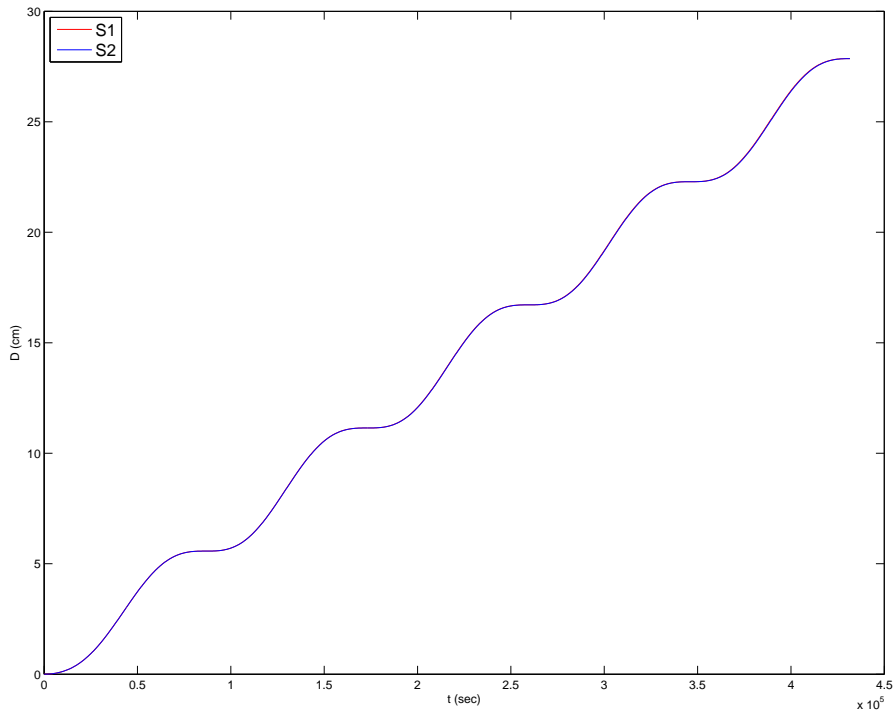
Figure 42: Case 2 for GEO satellites with S2 being farther away from the earth than S1, $d = 20$ kilometres, $t = 5$ days: The distance between the ECI positions of the Newtonian and the nonlinear post–Newtonian solutions, both for S1 and S2, which almost completely overlap.
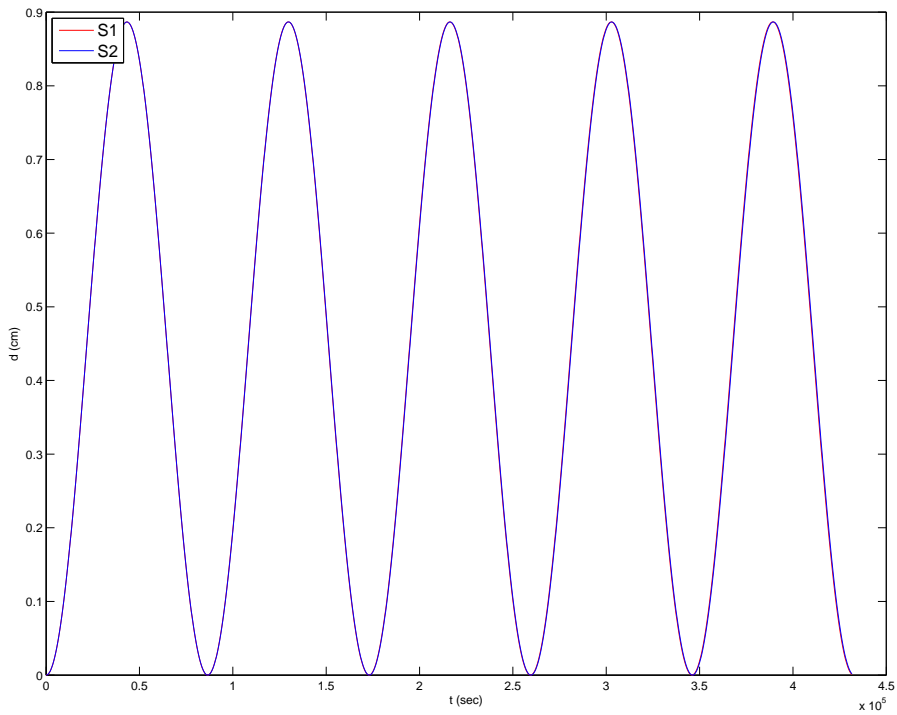

Figure 43: Case 2 for GEO satellites with S2 being farther away from the earth than S1, $d = 20$ kilometres, $t = 5$ days: Difference in distances to the center of the Earth between Newtonian and nonlinear post–Newtonian.
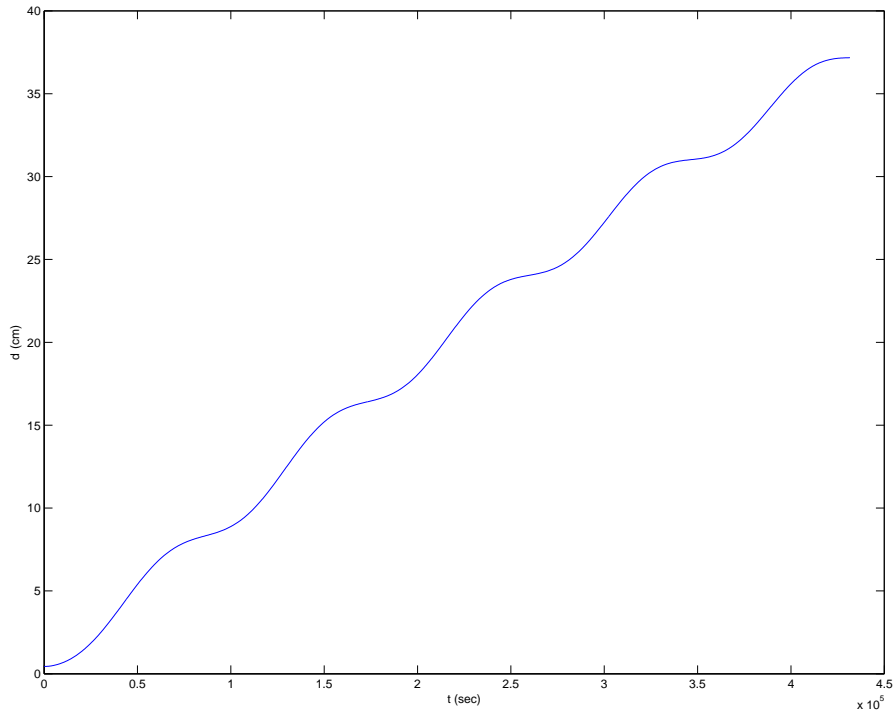
Figure 44: Case 2 for GEO satellites with S2 being farther away from the earth than S1, $d = 20$ kilometres, $t = 5$ days, and nonlinear post–Newtonian formulation: Distance between ECI positions of S2 and S1 and the relative position of S2 with respect to S1.
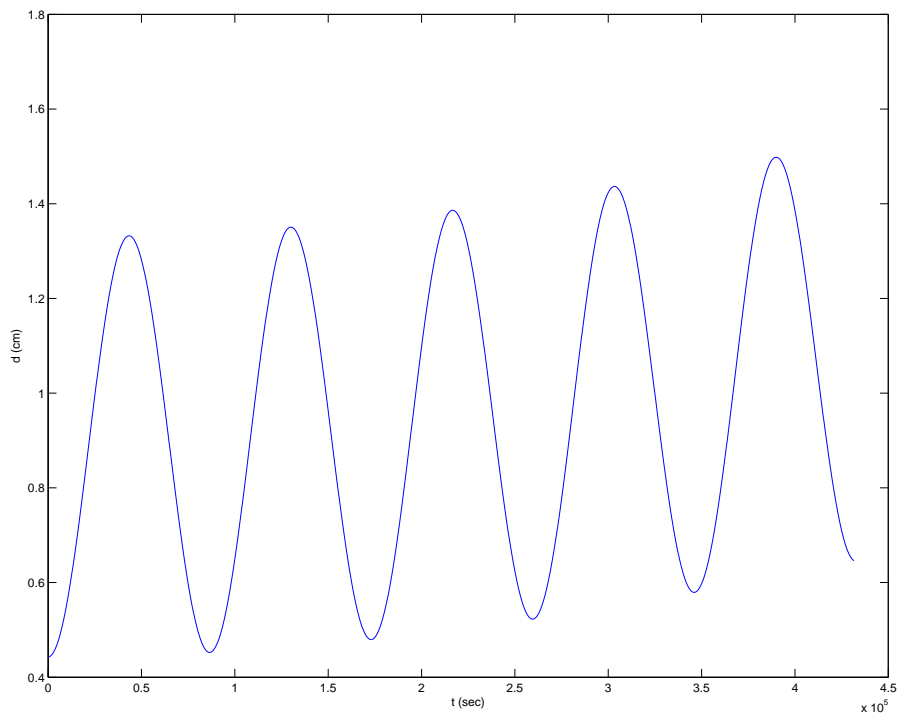

Figure 45: Case 2 for GEO satellites with S2 being farther away from the earth than S1, $d = 20$ kilometres, $t = 5$ days, and nonlinear post–Newtonian formulation: This plot, similar to the above one, shows the difference in distances to the ECI center.

2.3.2.3 Case 3

For this test, the goal was to increase the value of t as much as possible.
The parameters used for this test are $d = 5$ kilometres and $t = 25$ days.
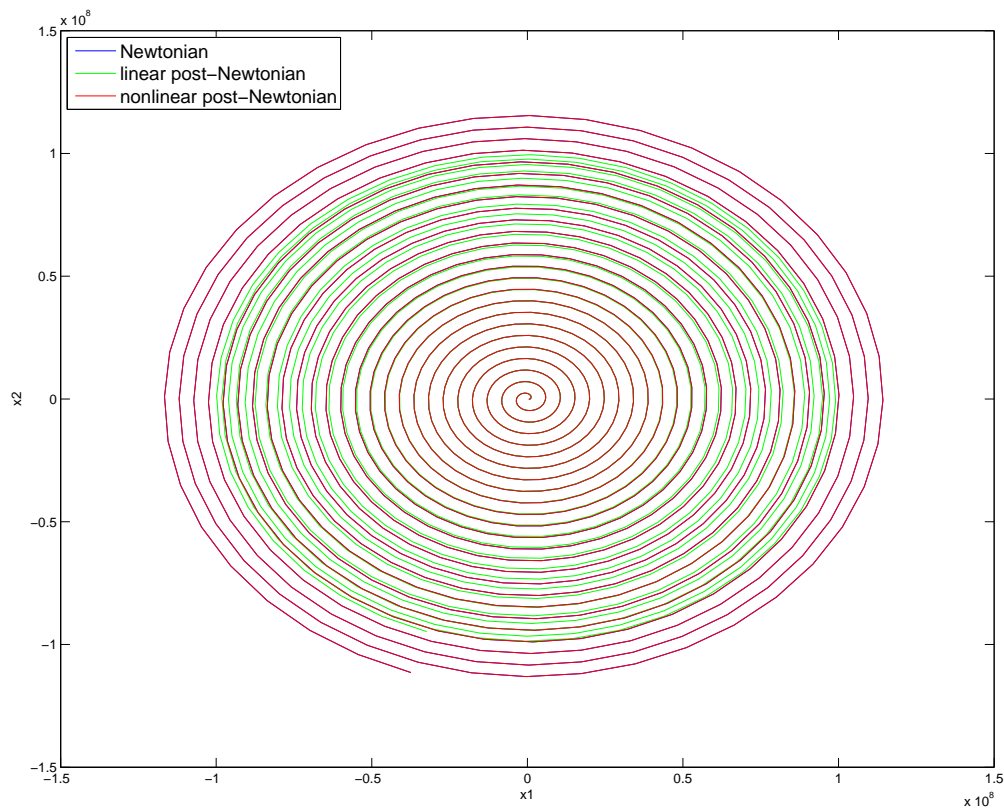

Figure 46: Case 3 for GEO satellites with S2 being farther away from the earth than S1, $d = 5$ kilometres, $t = 25$ days: Relative motion of S2 with respect to S1.
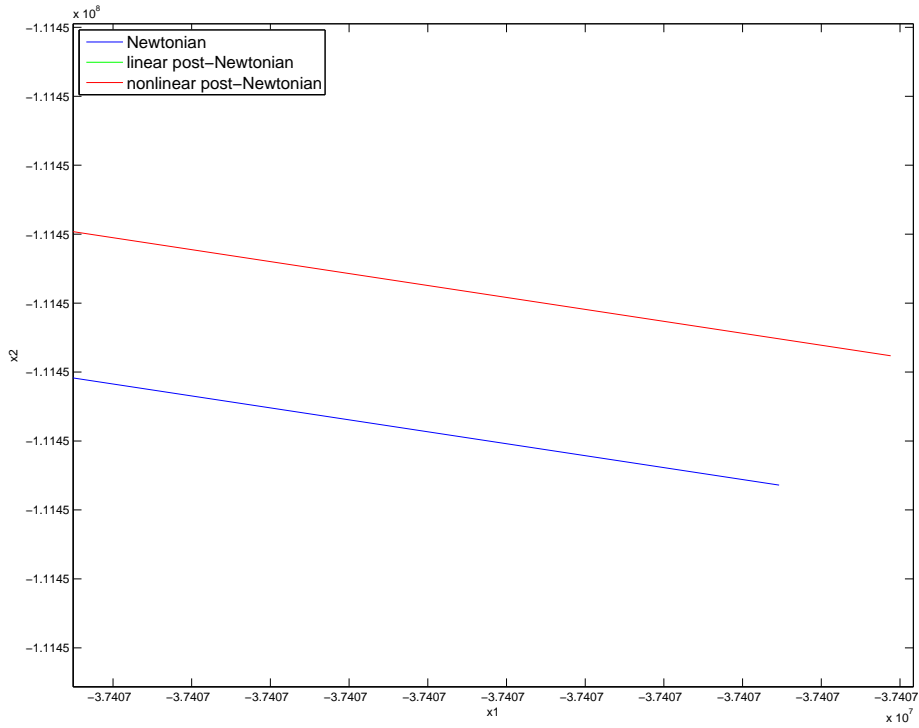
Figure 47: Case 3 for GEO satellites with S2 being farther away from the earth than S1, $d = 5$ kilometres, $t = 25$ days: Zoomed in version of the previous plot. It is now possible to see the difference between solutions from different formulations.
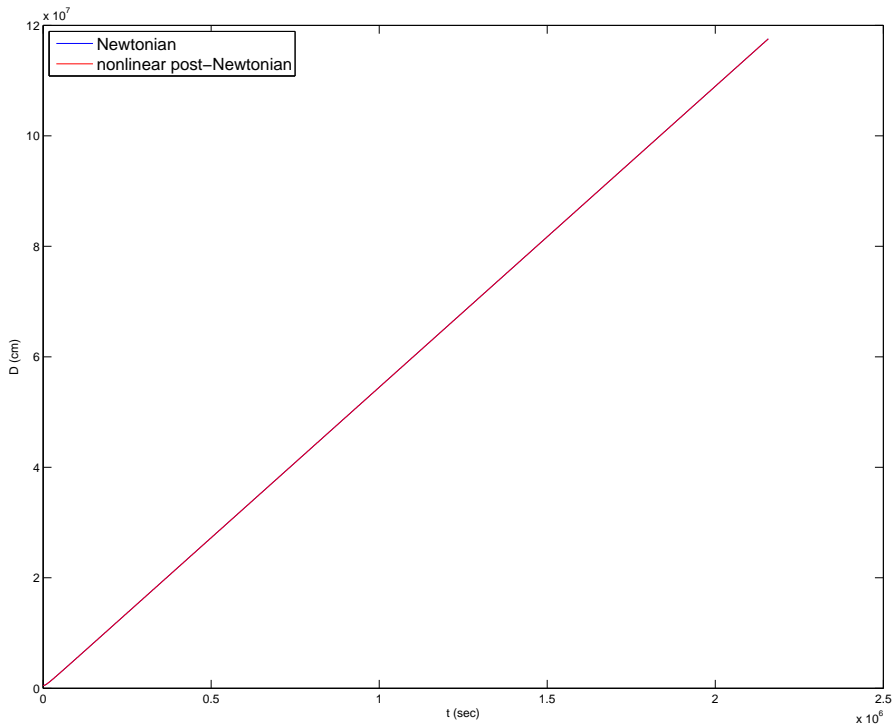
Figure 48: Case 3 for GEO satellites with S2 being farther away from the earth than S1, $d = 5$ kilometres, $t = 25$ days: Absolute distance between S1 and S2.
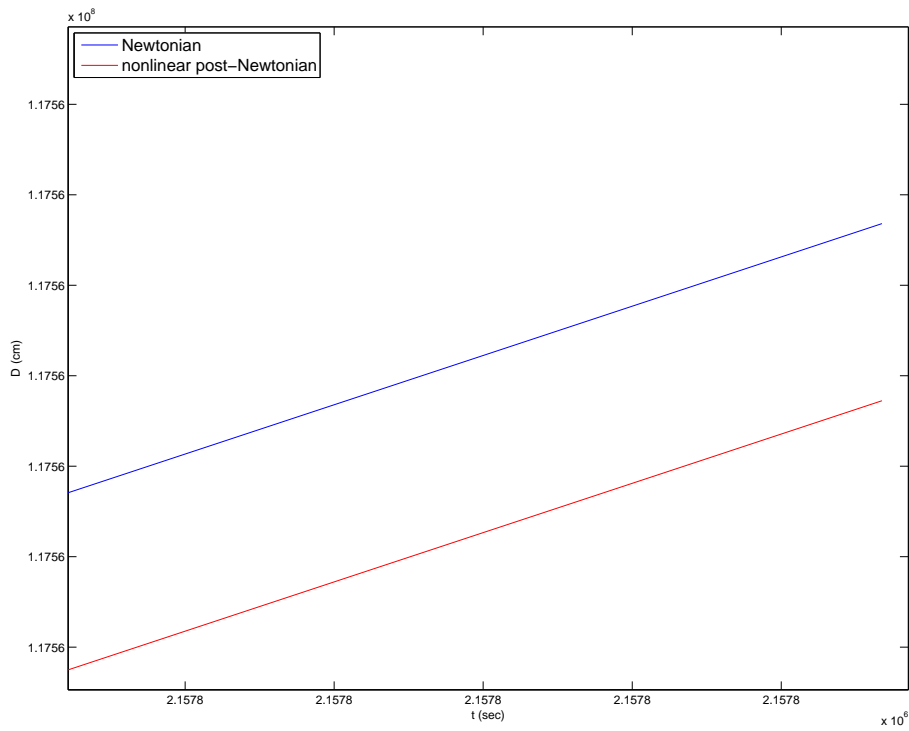
Figure 49: Case 3 for GEO satellites with S2 being farther away from the earth than S1, $d = 5$ kilometres, $t = 25$ days: Zoomed in version of the previous plot. It is now possible to see differences between solutions from different formulations.
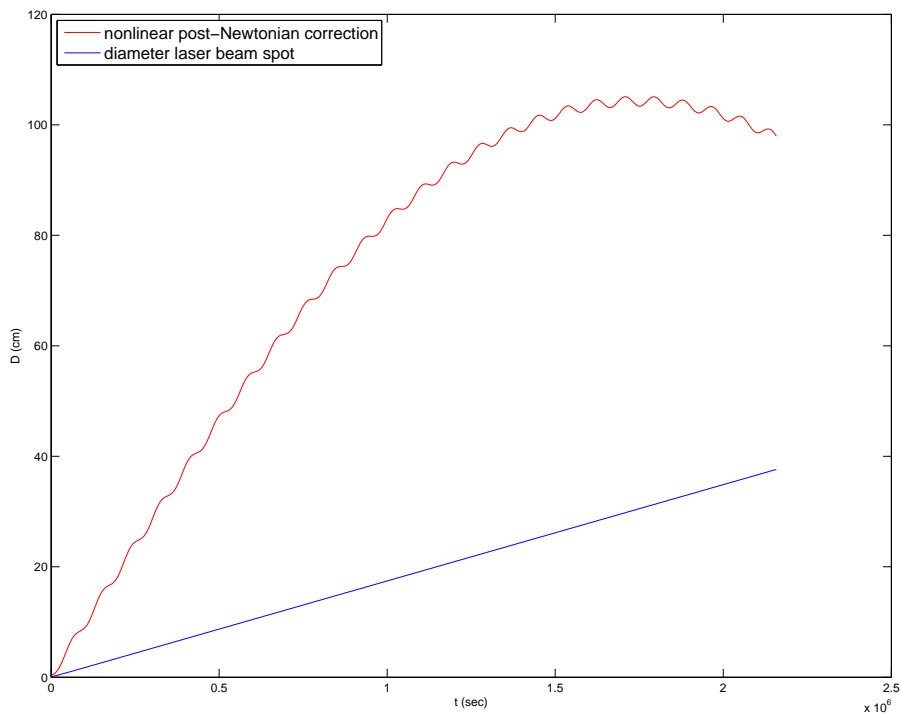

Figure 50: Case 3 for GEO satellites with S2 being farther away from the earth than S1, $d = 5$ kilometres, $t = 25$ days: Correction provided from the nonlinear post–Newtonian equations compared to the laser beam.
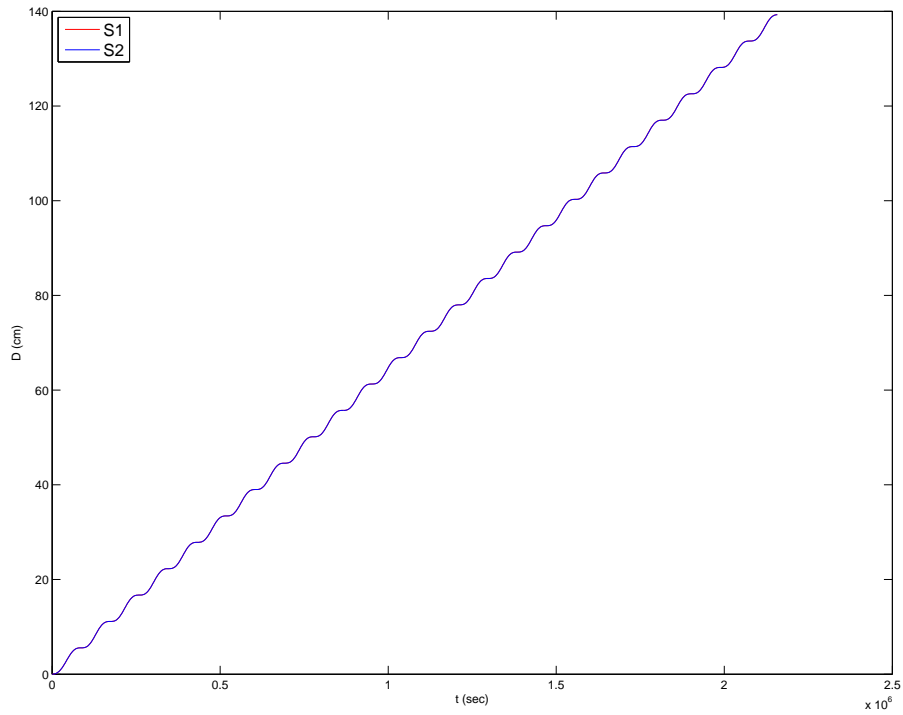
Figure 51: Case 3 for GEO satellites with S2 being farther away from the earth than S1, $d = 5$ kilometres, $t = 25$ days: The distance between the ECI positions of the Newtonian and the nonlinear post–Newtonian solutions, both for S1 and S2, which almost completely overlap.
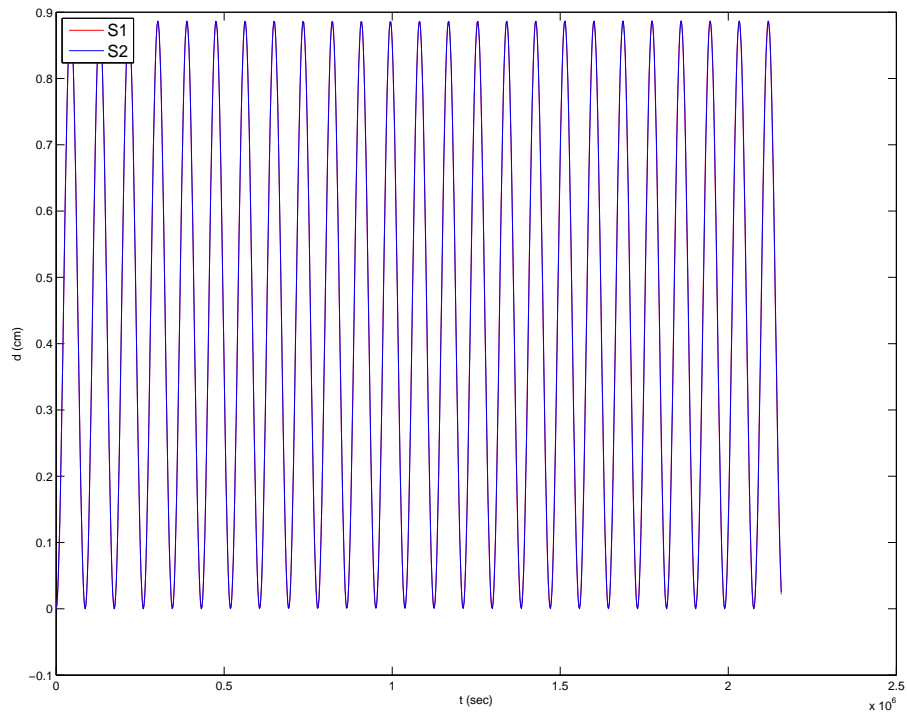

Figure 52: Case 3 for GEO satellites with S2 being farther away from the earth than S1, $d = 5$ kilometres, $t = 25$ days: Difference in distances to the center of the Earth between Newtonian and nonlinear post–Newtonian.

38
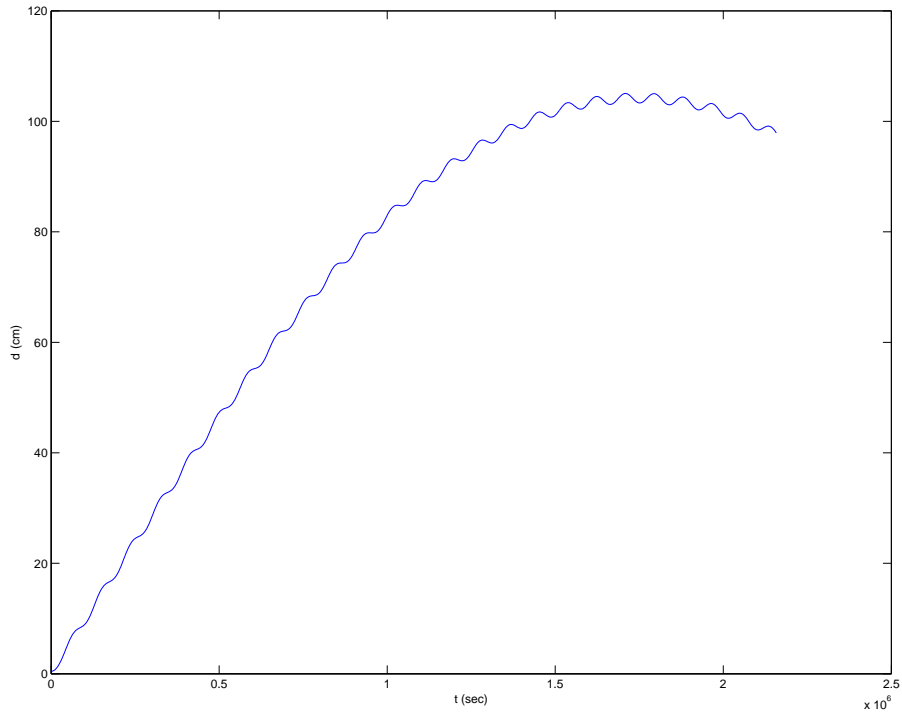
Figure 53: Case 3 for GEO satellites with S2 being farther away from the earth than S1, $d = 5$ kilometres, $t = 25$ days, and nonlinear post–Newtonian formulation: Distance between ECI positions of S2 and S1 and the relative position of S2 with respect to S1.
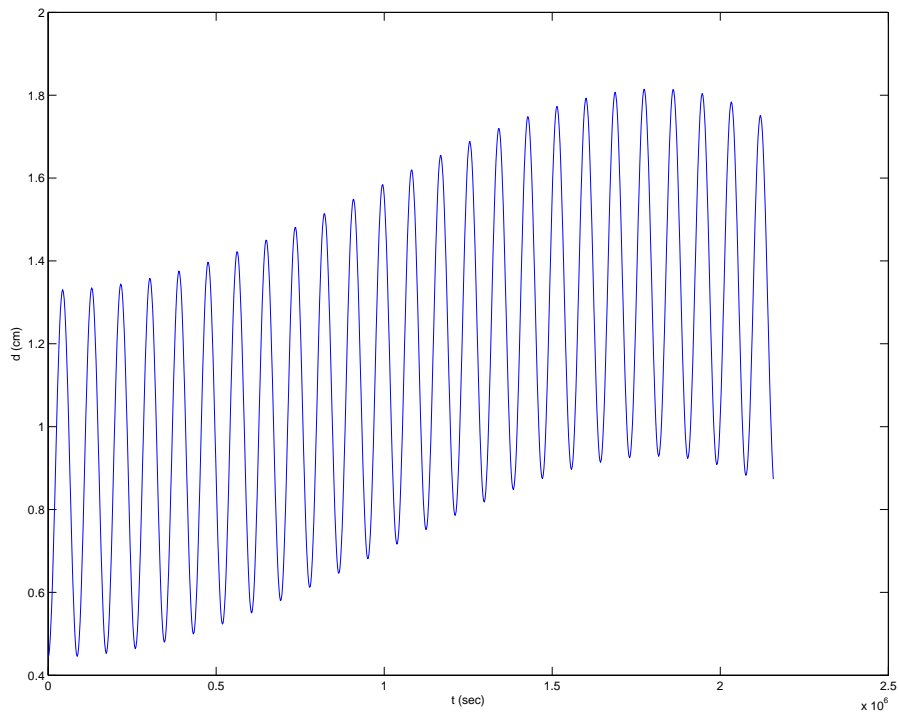
Figure 54: Case 3 for GEO satellites with S2 being farther away from the earth than S1, $d = 5$ kilometres, $t = 25$ days, and nonlinear post–Newtonian formulation: This plot, similar to the above one, shows the difference in distances to the ECI center.

2.3.3 MEO satellites with S2 being closer to the Earth than S1

2.3.3.1 Case 1

In this test we showcase the solution for small values in both parameters. The parameters used for this test are $d = 5$ kilometres and $t = 5$ days.
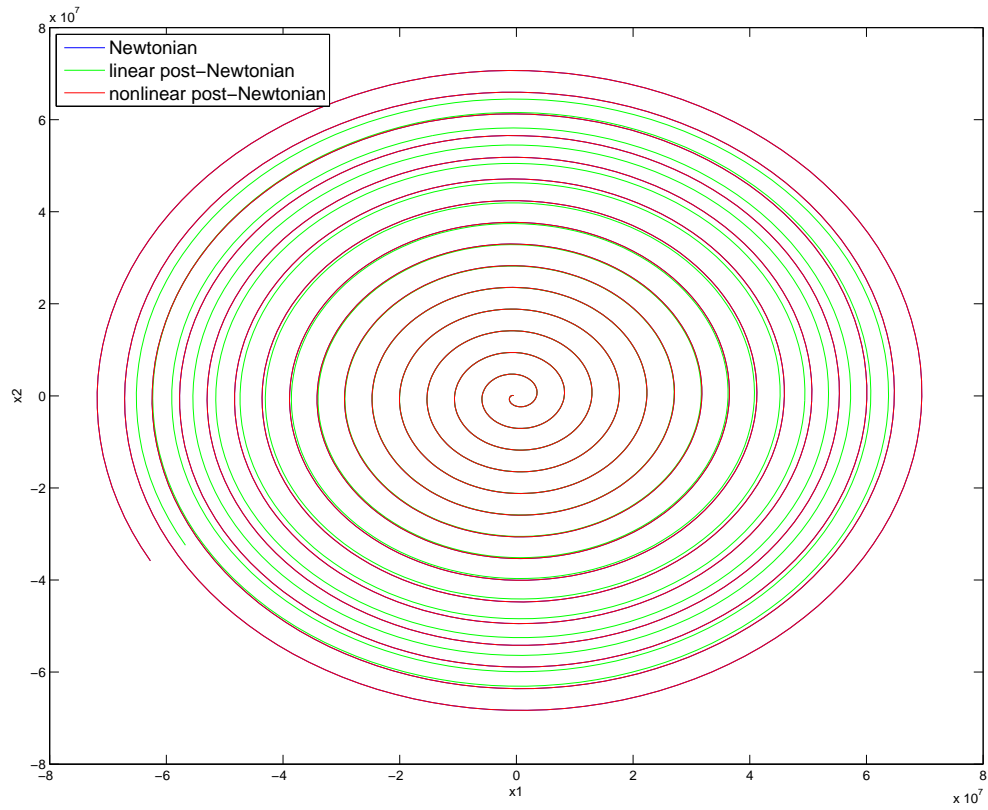

Figure 55: Case 1 for MEO satellites with S2 being closer to the earth than S1, $d = 5$ kilometres, $t = 5$ days: Relative motion of S2 with respect to S1.
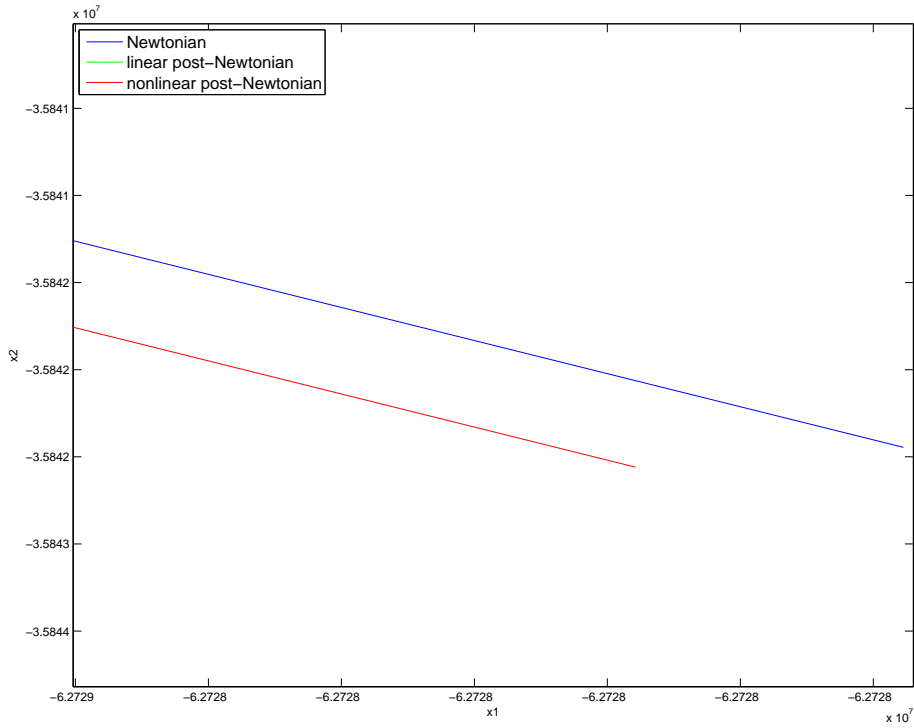
Figure 56: Case 1 for MEO satellites with S2 being closer to the earth than S1, $d = 5$ kilometres, $t = 5$ days: Zoomed in version of the previous plot. It is now possible to see the difference between solutions from different formulations.
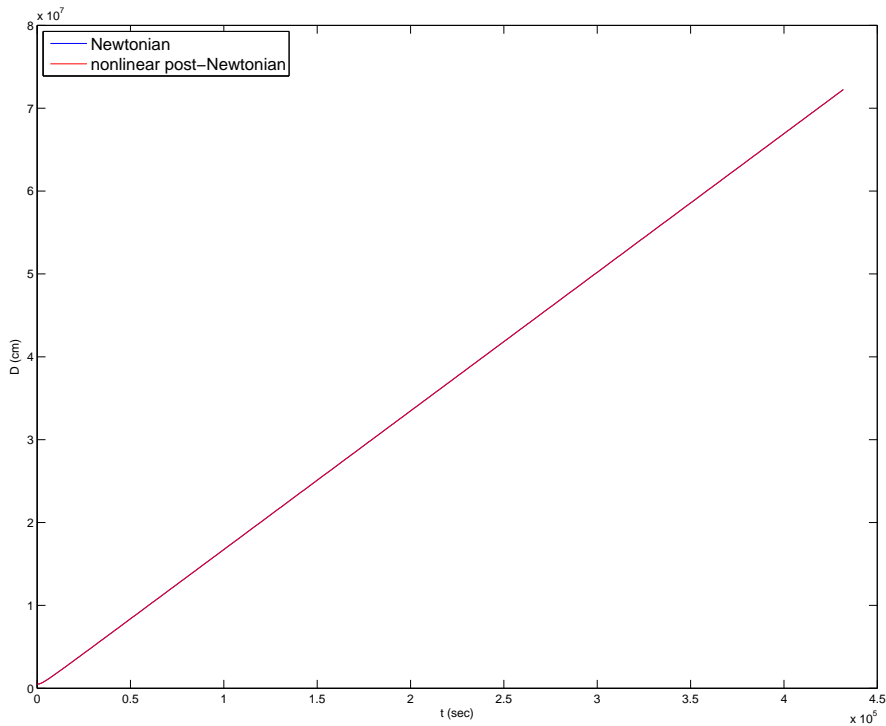
Figure 57: Case 1 for MEO satellites with S2 being closer to the earth than S1, $d = 5$ kilometres, $t = 5$ days: Absolute distance between S1 and S2.
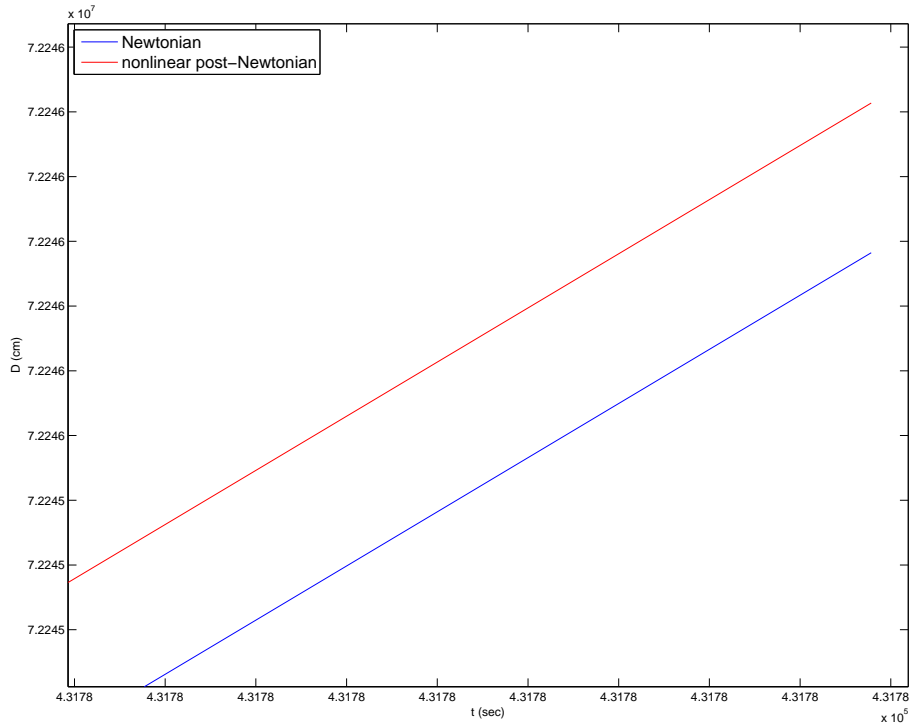
Figure 58: Case 1 for MEO satellites with S2 being closer to the earth than S1, $d = 5$ kilometres, $t = 5$ days: Zoomed in version of the previous plot. It is now possible to see differences between solutions from different formulations.
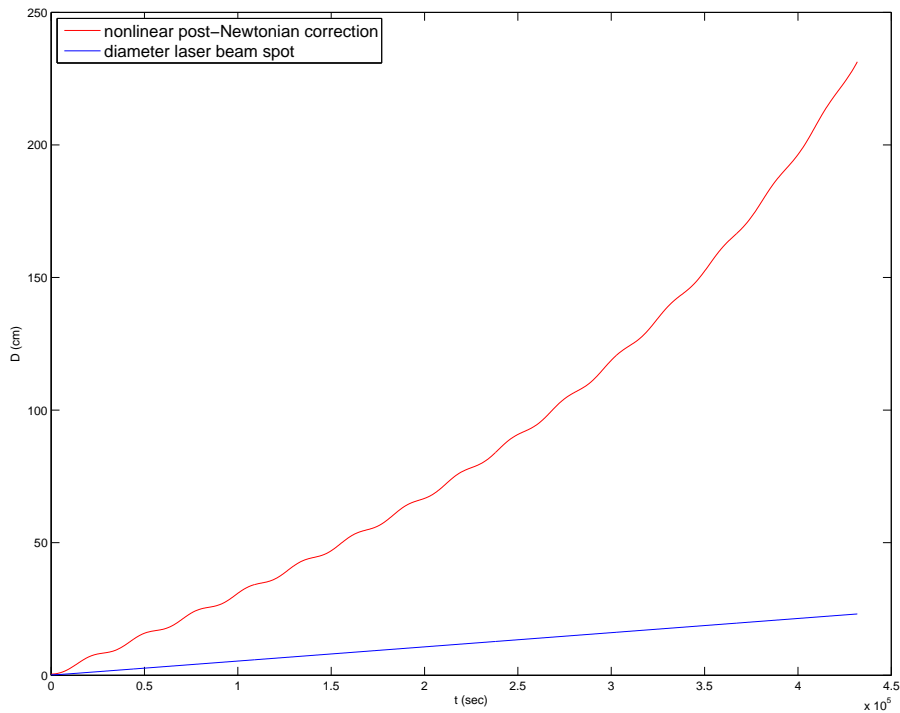

Figure 59: Case 1 for MEO satellites with S2 being closer to the earth than S1, $d = 5$ kilometres, $t = 5$ days: Correction provided from the nonlinear post–Newtonian equations compared to the laser beam.

42
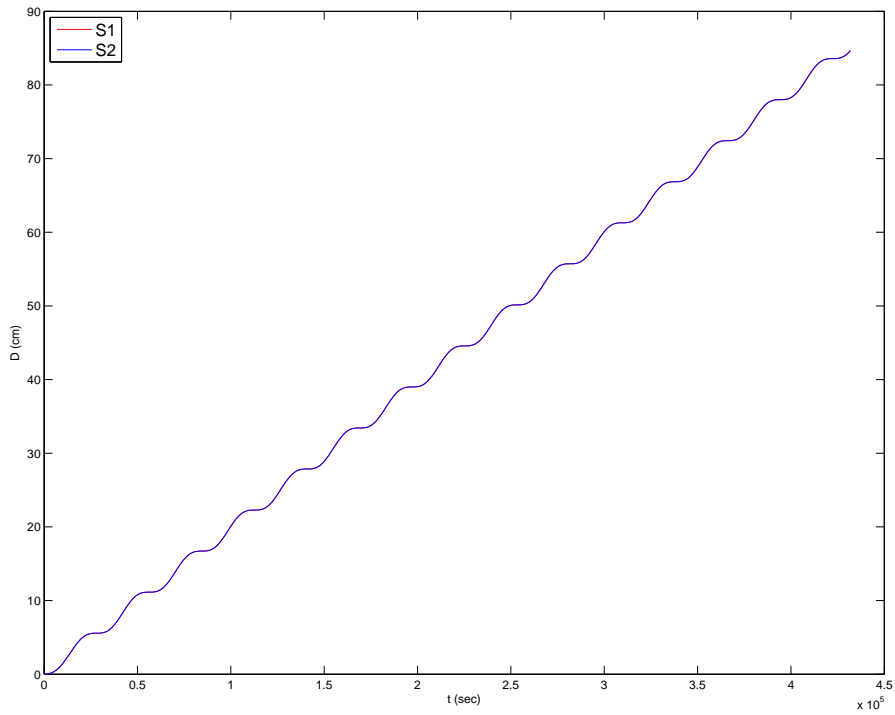
Figure 60: Case 1 for MEO satellites with S2 being closer to the earth than S1, $d = 5$ kilometres, $t = 5$ days: The distance between the ECI positions of the Newtonian and the nonlinear post–Newtonian solutions, both for S1 and S2, which almost completely overlap.
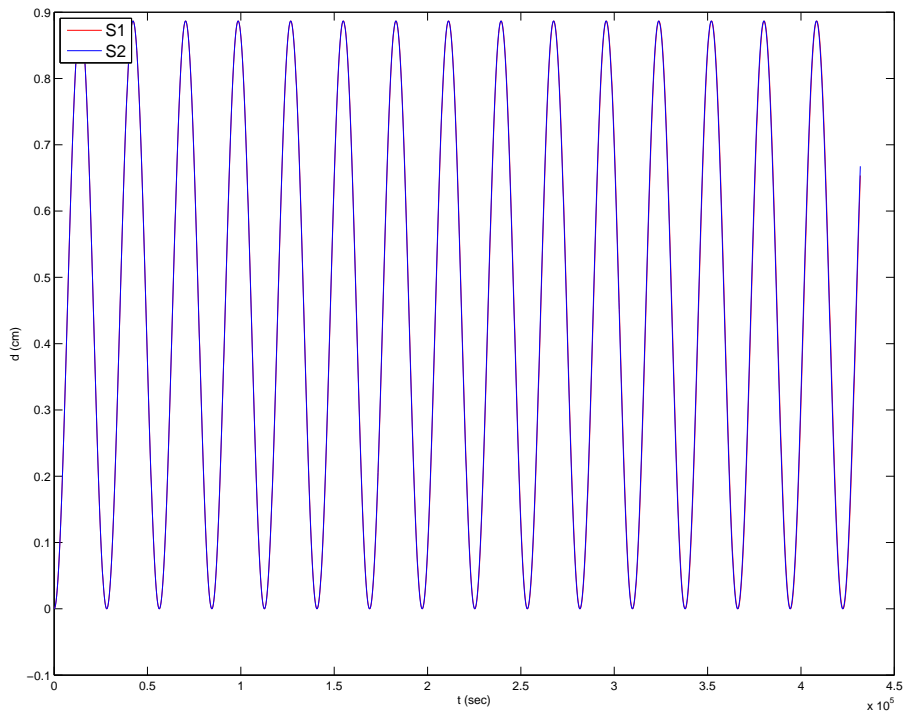

Figure 61: Case 1 for MEO satellites with S2 being closer to the earth than S1, $d = 5$ kilometres, $t = 5$ days: Difference in distances to the center of the Earth between Newtonian and nonlinear post–Newtonian.

43
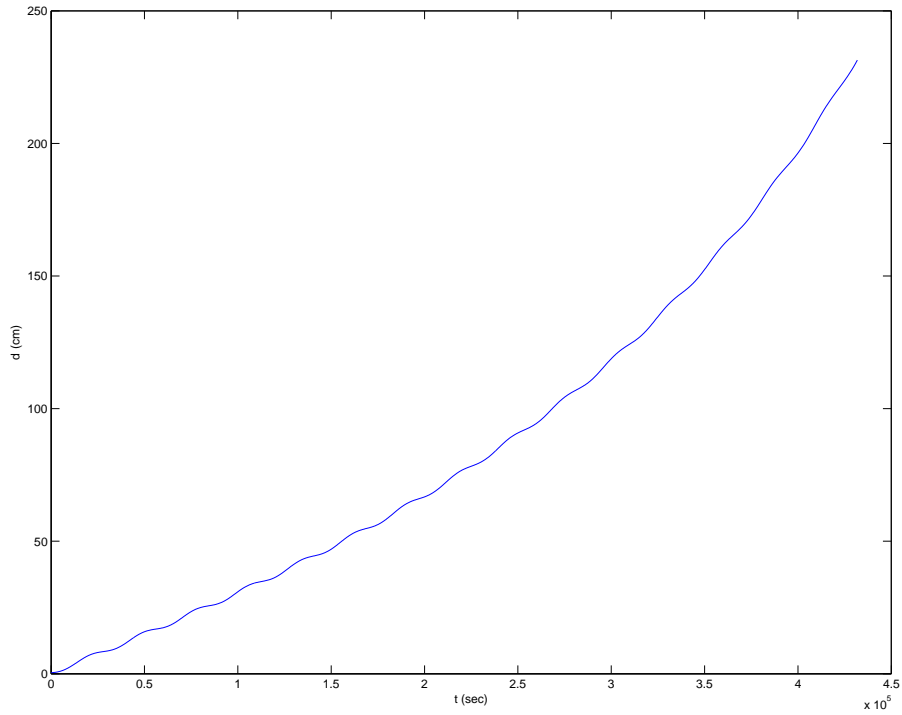
Figure 62: Case 1 for MEO satellites with S2 being closer to the earth than S1, $d = 5$ kilometres, $t = 5$ days, and nonlinear post–Newtonian formulation: Distance between ECI positions of S2 and S1 and the relative position of S2 with respect to S1.
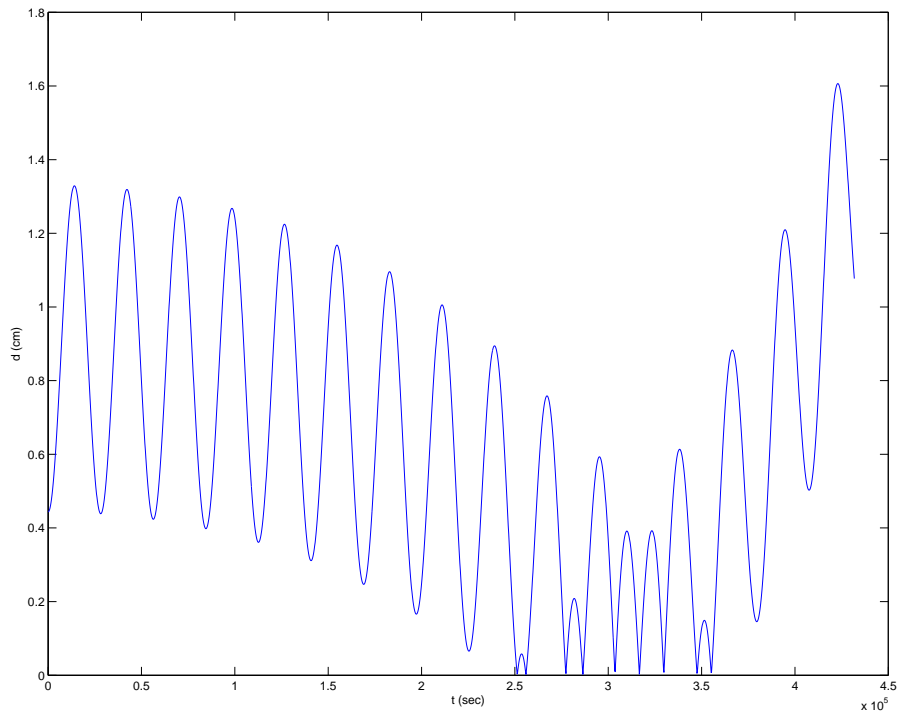


Figure 63: Case 1 for MEO satellites with S2 being closer to the earth than S1, $d = 5$ kilometres, $t = 5$ days, and nonlinear post–Newtonian formulation: This plot, similar to the above one, shows the difference in distances to the ECI center.

2.3.3.2   Case 2

For this test, the goal was to increase the value of d as much as possible.
The parameters used for this test are $d = 40$ kilometres and $t = 2$ days.
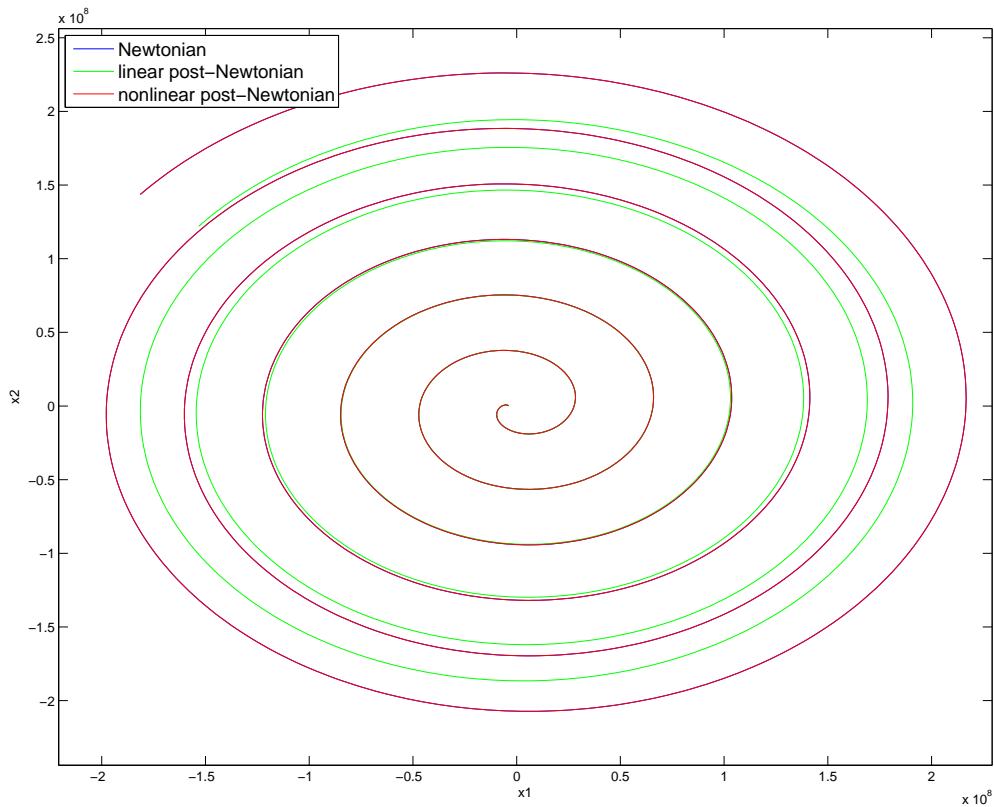

Figure 64: Case 2 for MEO satellites with S2 being closer to the earth than S1, $d = 40$ kilometres, $t = 2$ days: Relative motion of S2 with respect to S1.
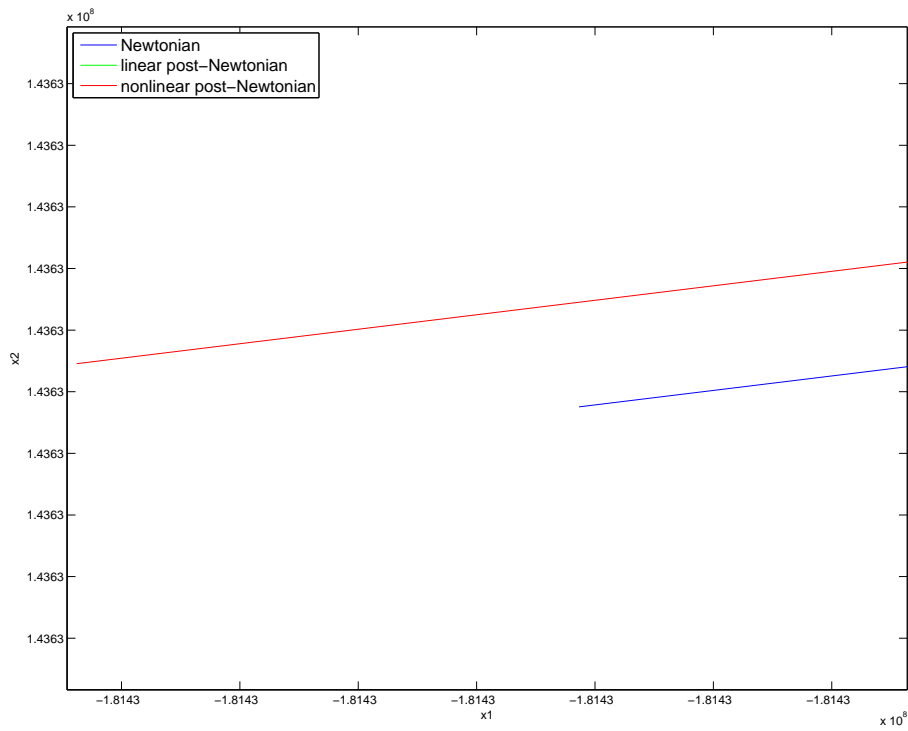
Figure 65: Case 2 for MEO satellites with S2 being closer to the earth than S1, $d = 40$ kilometres, $t = 2$ days: Zoomed in version of the previous plot. It is now possible to see the difference between solutions from different formulations.
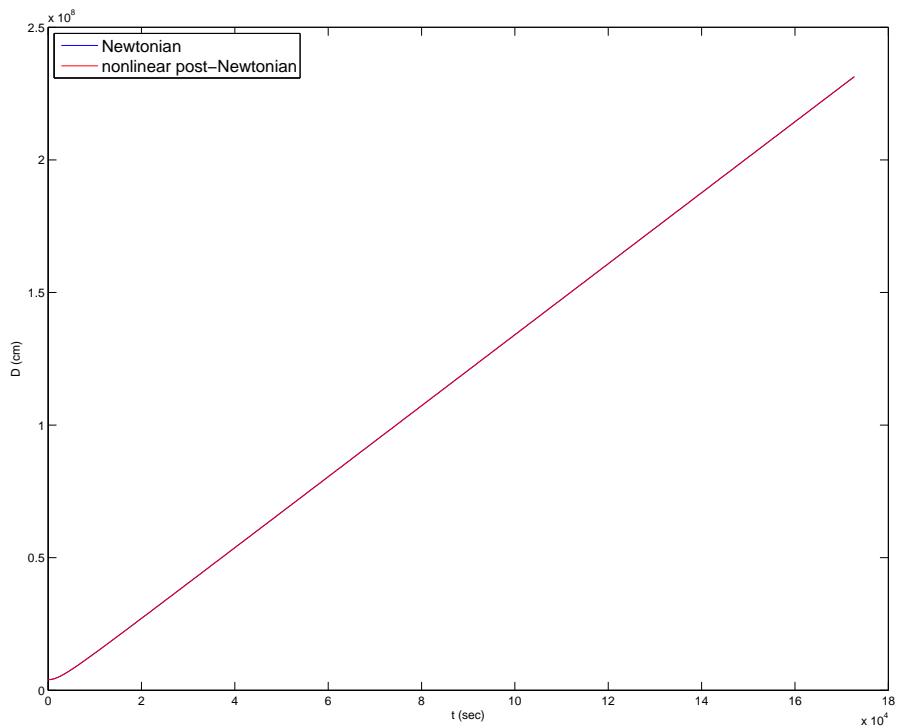
Figure 66: Case 2 for MEO satellites with S2 being closer to the earth than S1, $d = 40$ kilometres, $t = 2$ days: Absolute distance between S1 and S2.
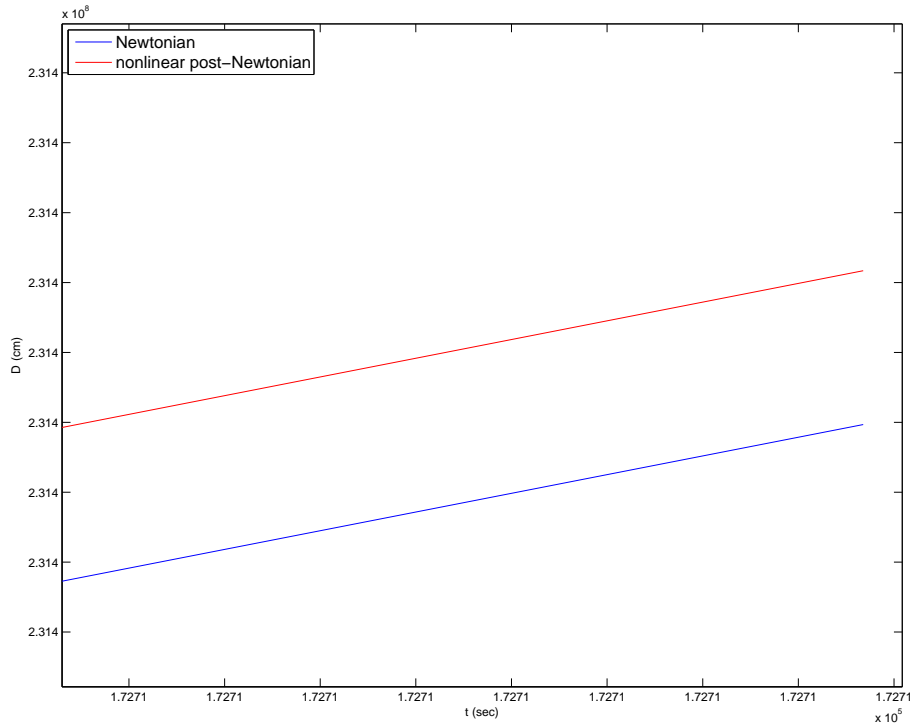
Figure 67: Case 2 for MEO satellites with S2 being closer to the earth than S1, $d = 40$ kilometres, $t = 2$ days: Zoomed in version of the previous plot. It is now possible to see differences between solutions from different formulations.
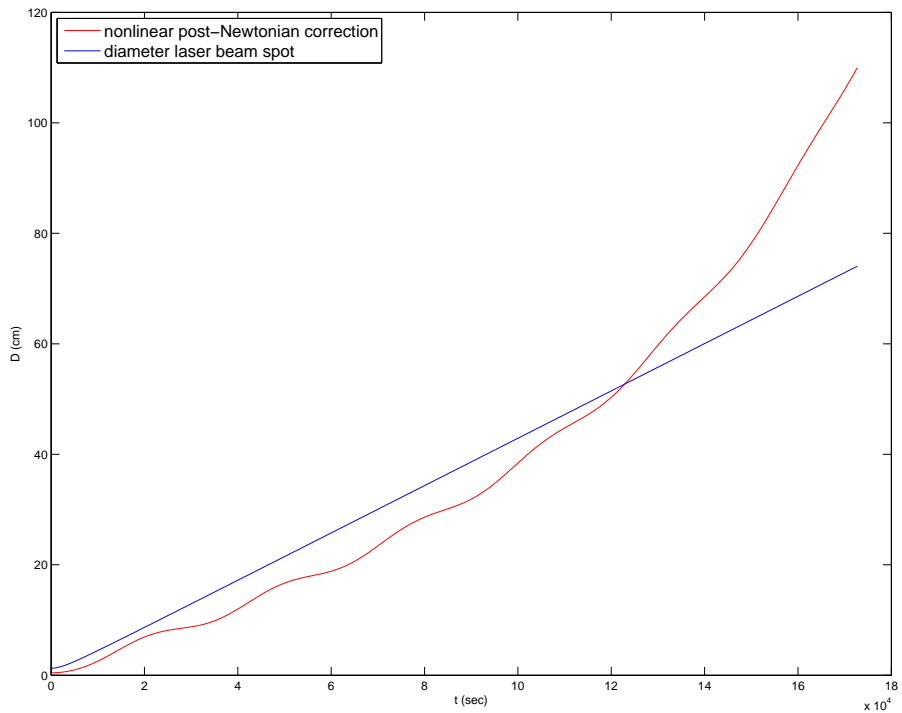

Figure 68: Case 2 for MEO satellites with S2 being closer to the earth than S1, $d = 40$ kilometres, $t = 2$ days: Correction provided from the nonlinear post–Newtonian equations compared to the laser beam.
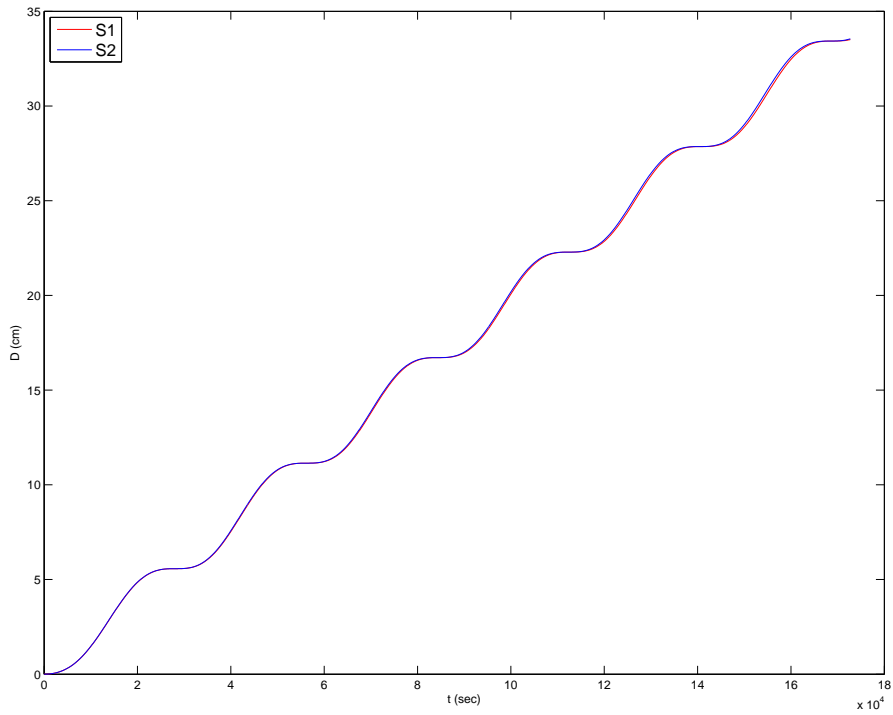
Figure 69: Case 2 for MEO satellites with S2 being closer to the earth than S1, $d = 40$ kilometres, $t = 2$ days: The distance between the ECI positions of the Newtonian and the nonlinear post–Newtonian solutions, both for S1 and S2, which almost completely overlap.
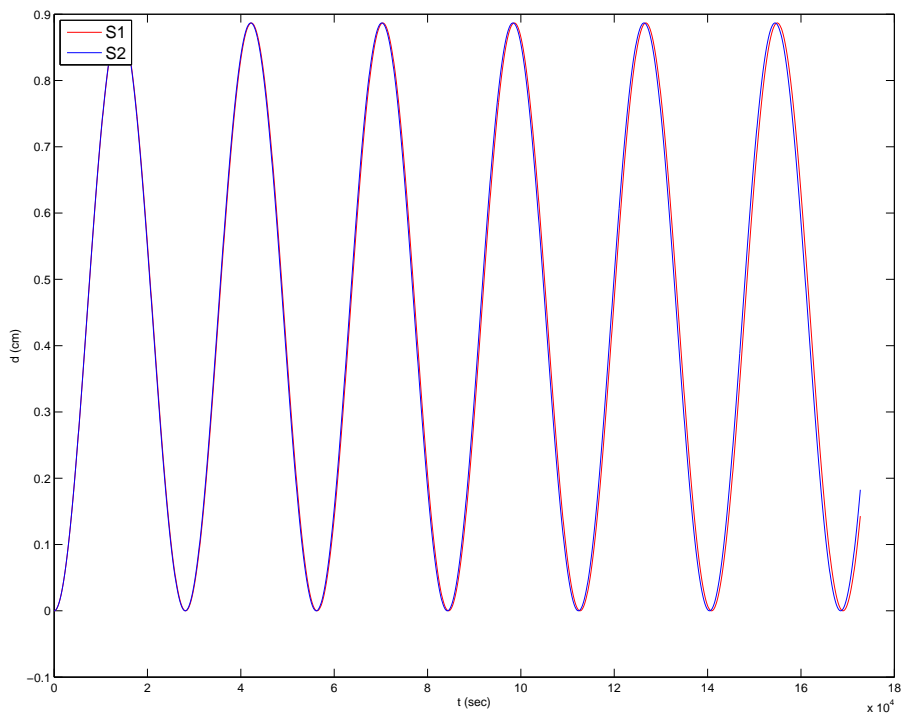

Figure 70: Case 2 for MEO satellites with S2 being closer to the earth than S1, $d = 40$ kilometres, $t = 2$ days: Difference in distances to the center of the Earth between Newtonian and nonlinear post–Newtonian.
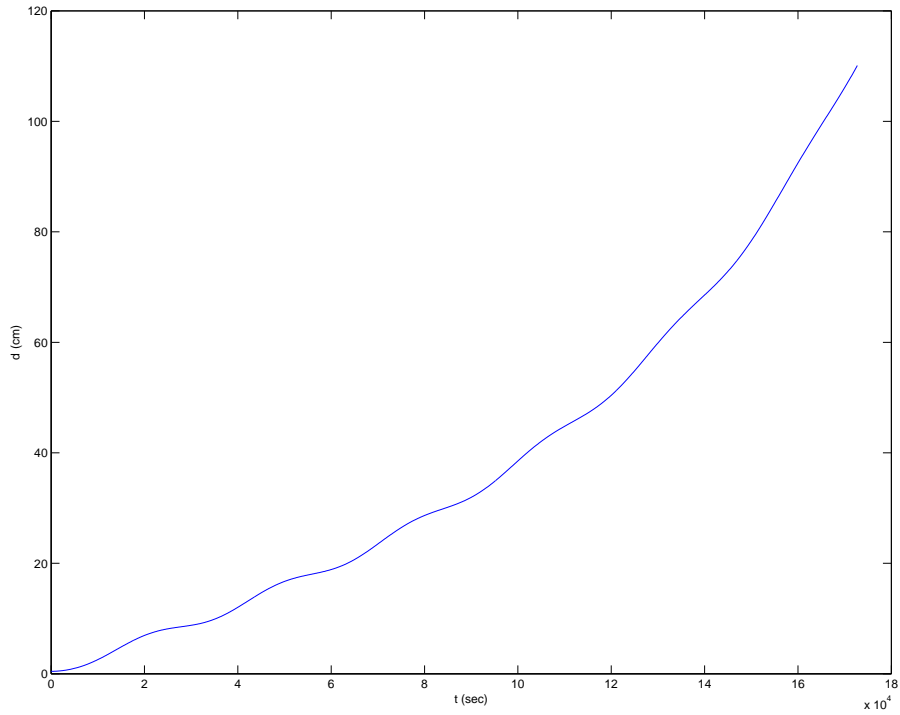
Figure 71: Case 2 for MEO satellites with S2 being closer to the earth than S1, $d = 40$ kilometres, $t = 2$ days, and nonlinear post–Newtonian formulation: Distance between ECI positions of S2 and S1 and the relative position of S2 with respect to S1.
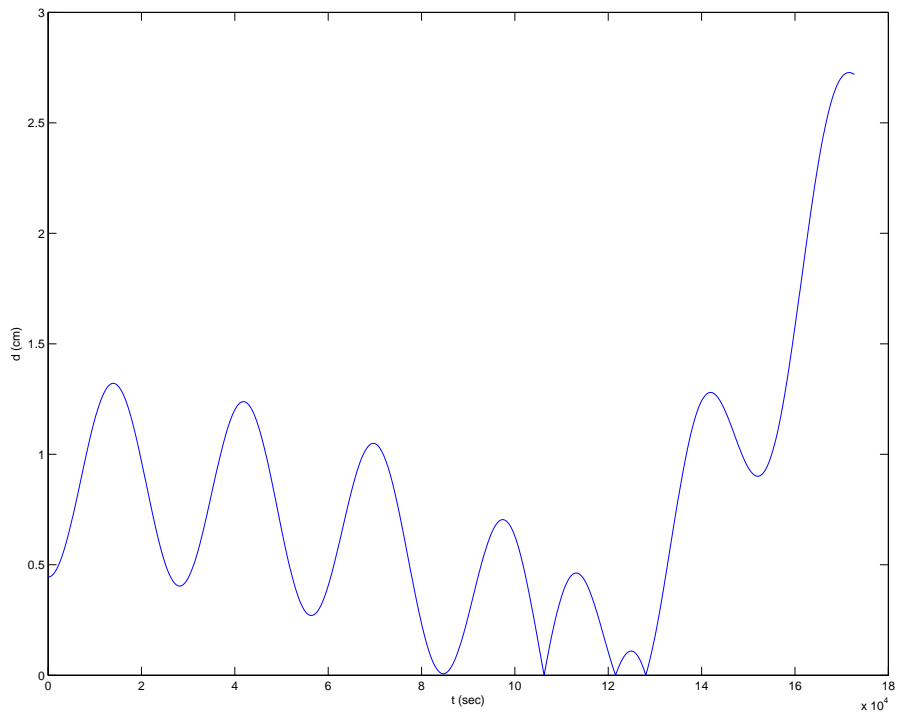

Figure 72: Case 2 for MEO satellites with S2 being closer to the earth than S1, $d = 40$ kilometres, $t = 2$ days, and nonlinear post–Newtonian formulation: This plot, similar to the above one, shows the difference in distances to the ECI center.

2.3.3.3   Case 3

For this test, the goal was to increase the value of t as much as possible.
The parameters used for this test are $d = 2$ kilometres and $t = 15$ days.
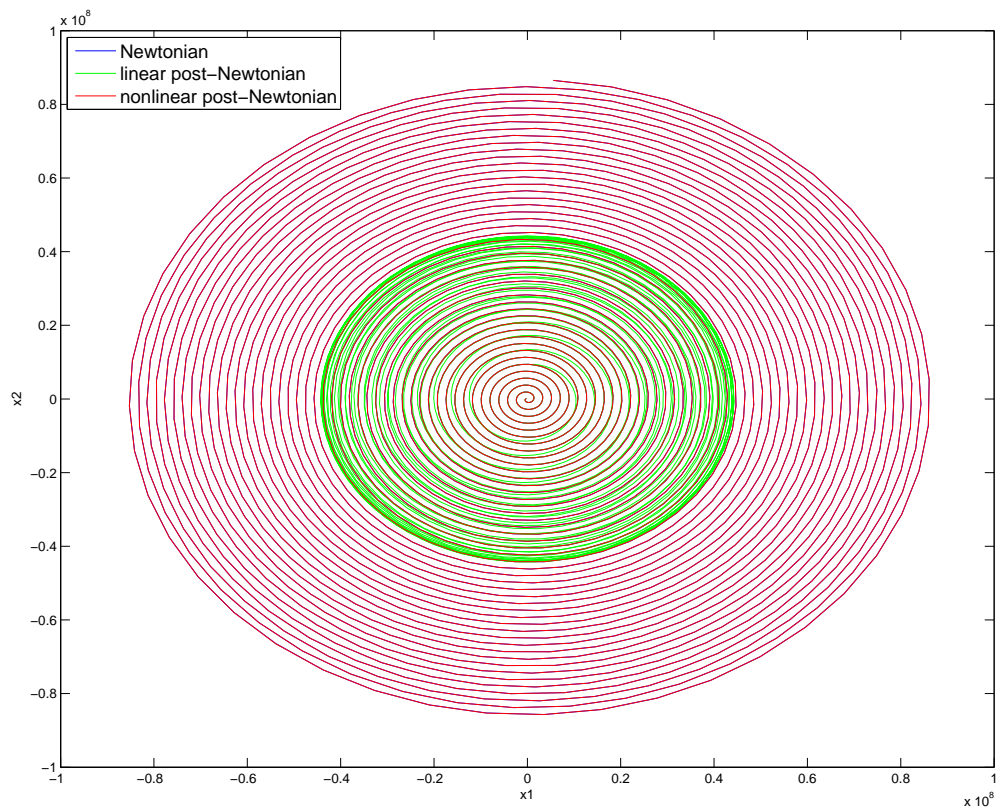
Figure 73: Case 3 for MEO satellites with S2 being closer to the earth than S1, $d = 2$ kilometres, $t = 15$ days: Relative motion of S2 with respect to S1.
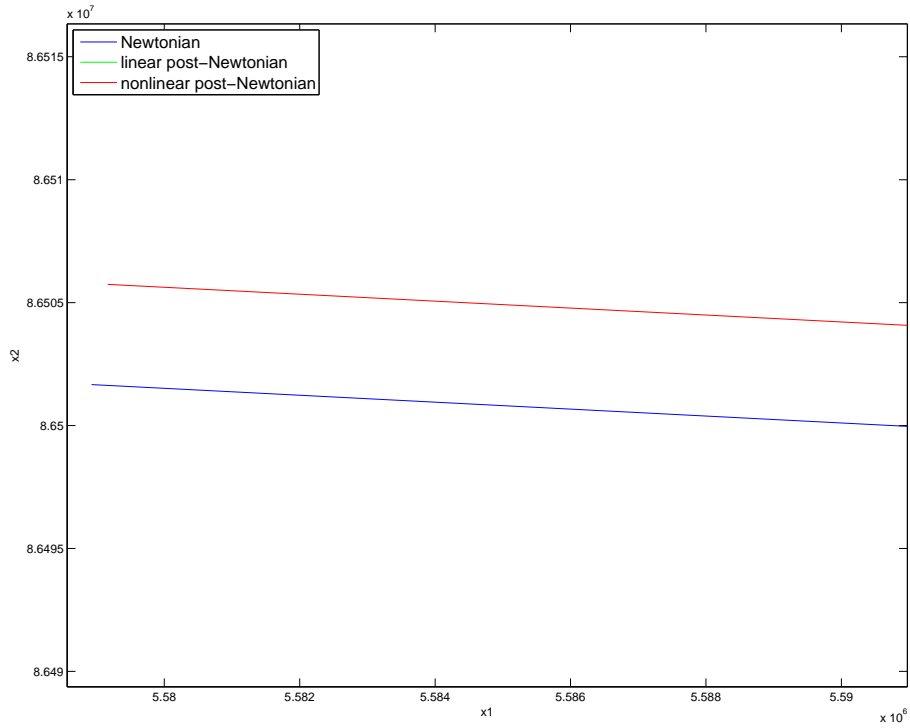
Figure 74: Case 3 for MEO satellites with S2 being closer to the earth than S1, $d = 2$ kilometres, $t = 15$ days: Zoomed in version of the previous plot. It is now possible to see the difference between solutions from different formulations.
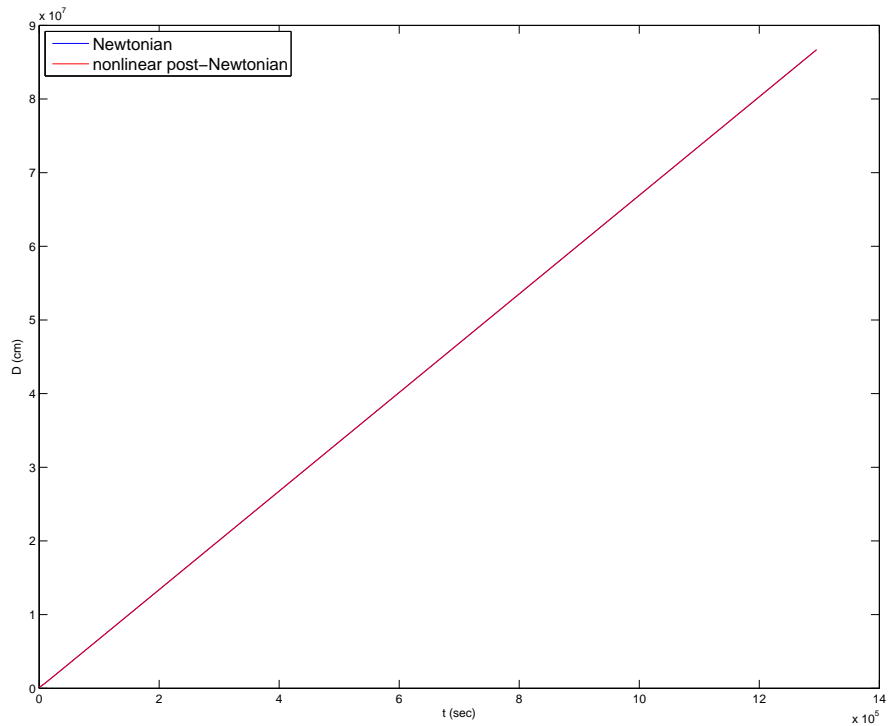
Figure 75: Case 3 for MEO satellites with S2 being closer to the earth than S1, $d = 2$ kilometres, $t = 15$ days: Absolute distance between S1 and S2.

51
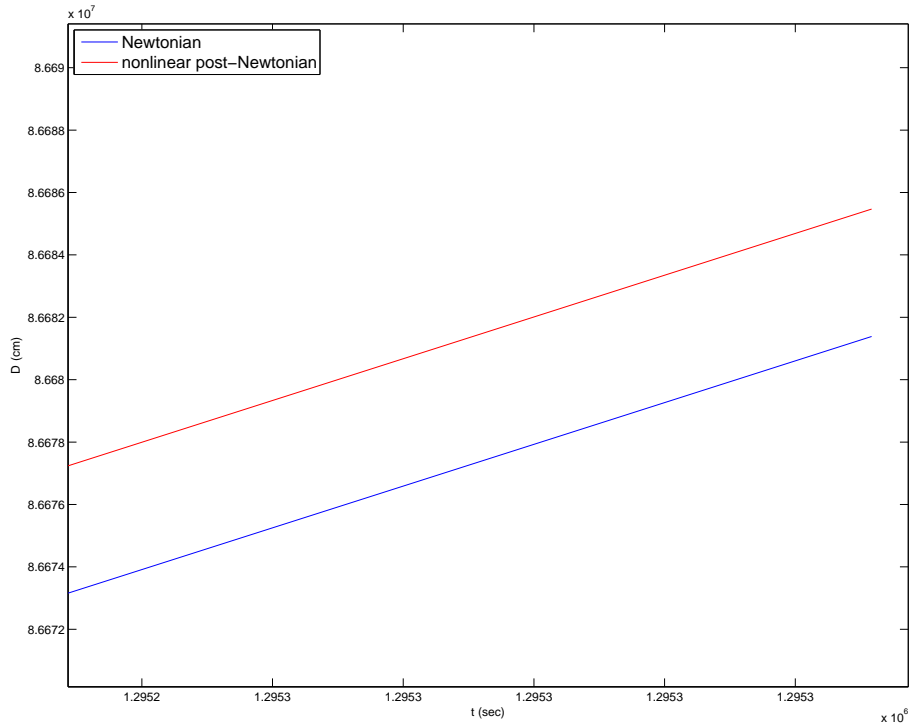
Figure 76: Case 3 for MEO satellites with S2 being closer to the earth than S1, $d = 2$ kilometres, $t = 15$ days: Zoomed in version of the previous plot. It is now possible to see differences between solutions from different formulations.
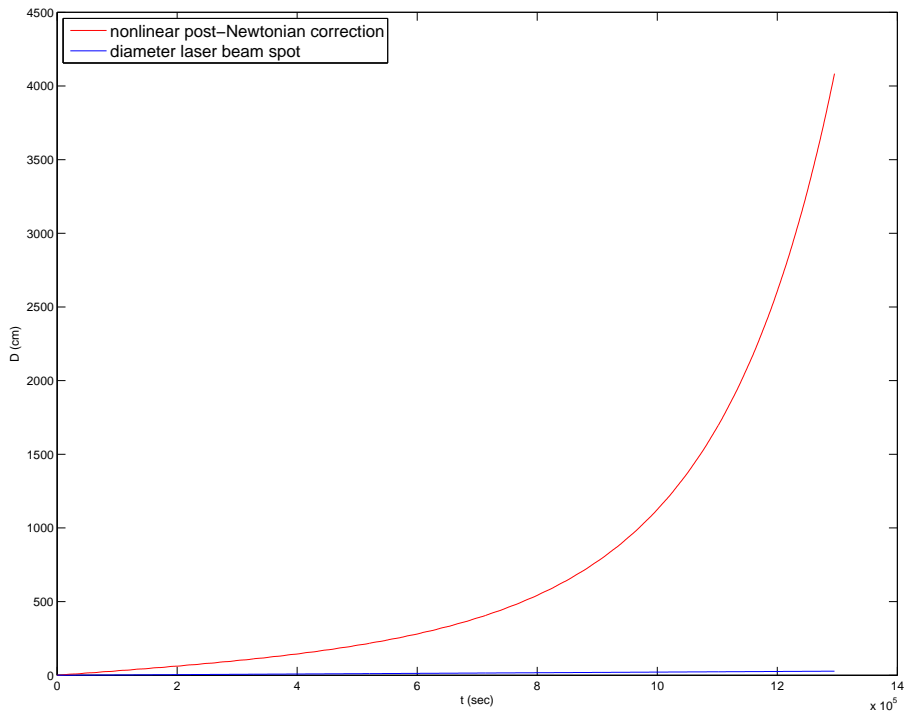

Figure 77: Case 3 for MEO satellites with S2 being closer to the earth than S1, $d = 2$ kilometres, $t = 15$ days: Correction provided from the nonlinear post–Newtonian equations compared to the laser beam.
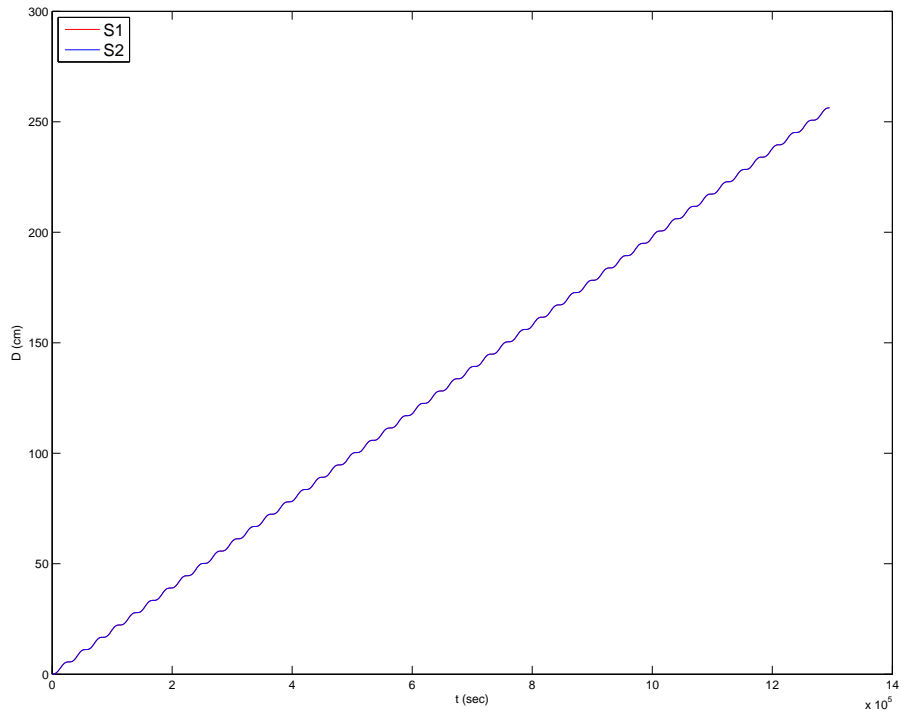
Figure 78: Case 3 for MEO satellites with S2 being closer to the earth than S1, $d = 2$ kilometres, $t = 15$ days: The distance between the ECI positions of the Newtonian and the nonlinear post–Newtonian solutions, both for S1 and S2, which almost completely overlap.
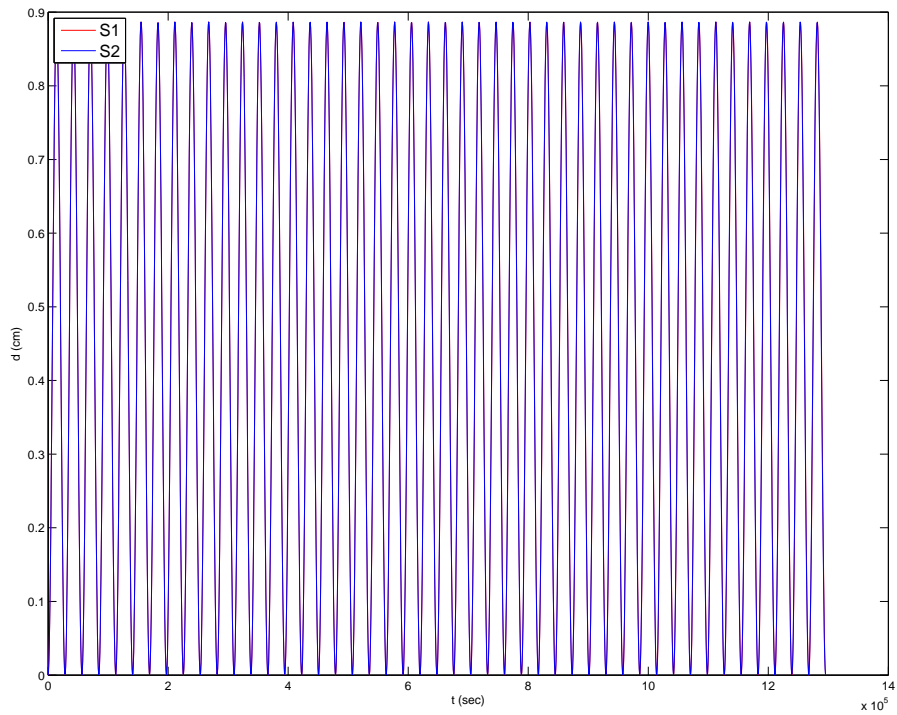
Figure 79: Case 3 for MEO satellites with S2 being closer to the earth than S1, $d = 2$ kilometres, $t = 15$ days: Difference in distances to the center of the Earth between Newtonian and nonlinear post–Newtonian.

53
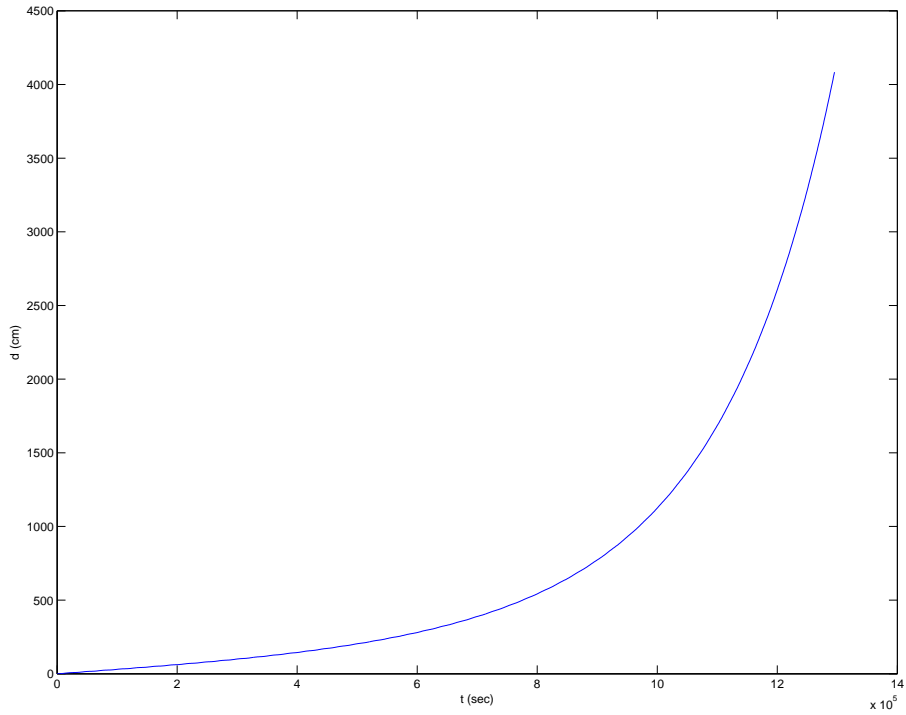
Figure 80: Case 3 for MEO satellites with S2 being closer to the earth than S1, $d = 2$ kilometres, $t = 15$ days, and nonlinear post–Newtonian formulation: Distance between ECI positions of S2 and S1 and the relative position of S2 with respect to S1.
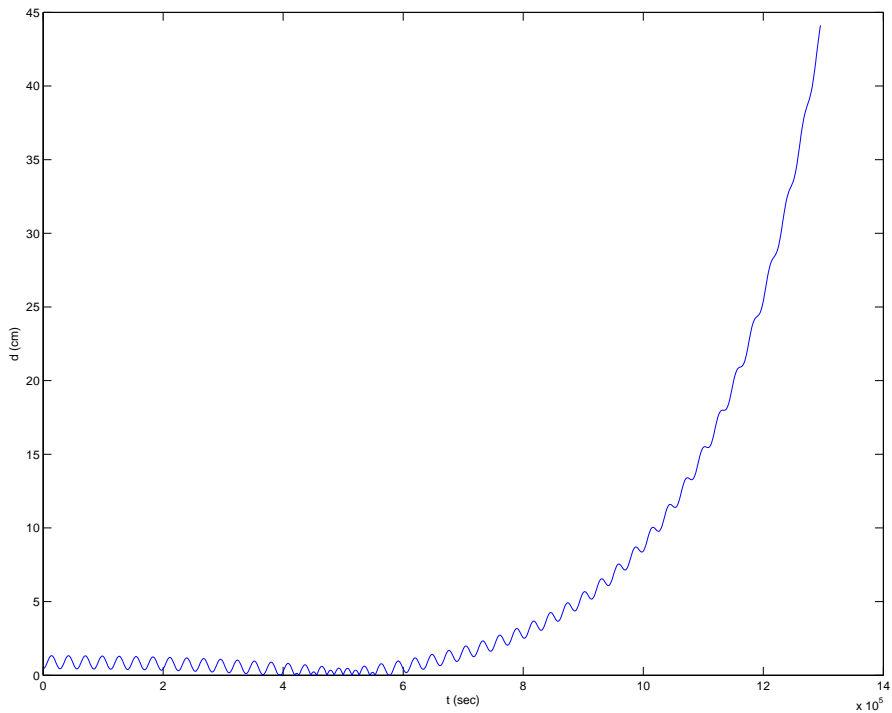
Figure 81: Case 3 for MEO satellites with S2 being closer to the earth than S1, $d = 2$ kilometres, $t = 15$ days, and nonlinear post–Newtonian formulation: This plot, similar to the above one, shows the difference in distances to the ECI center.

2.3.4 MEO satellites with S2 being farther away from the Earth than S1

2.3.4.1 Case 1

In this test we showcase the solution for small values in both parameters.
The parameters used for this test are $d = 5$ kilometres and $t = 5$ days.
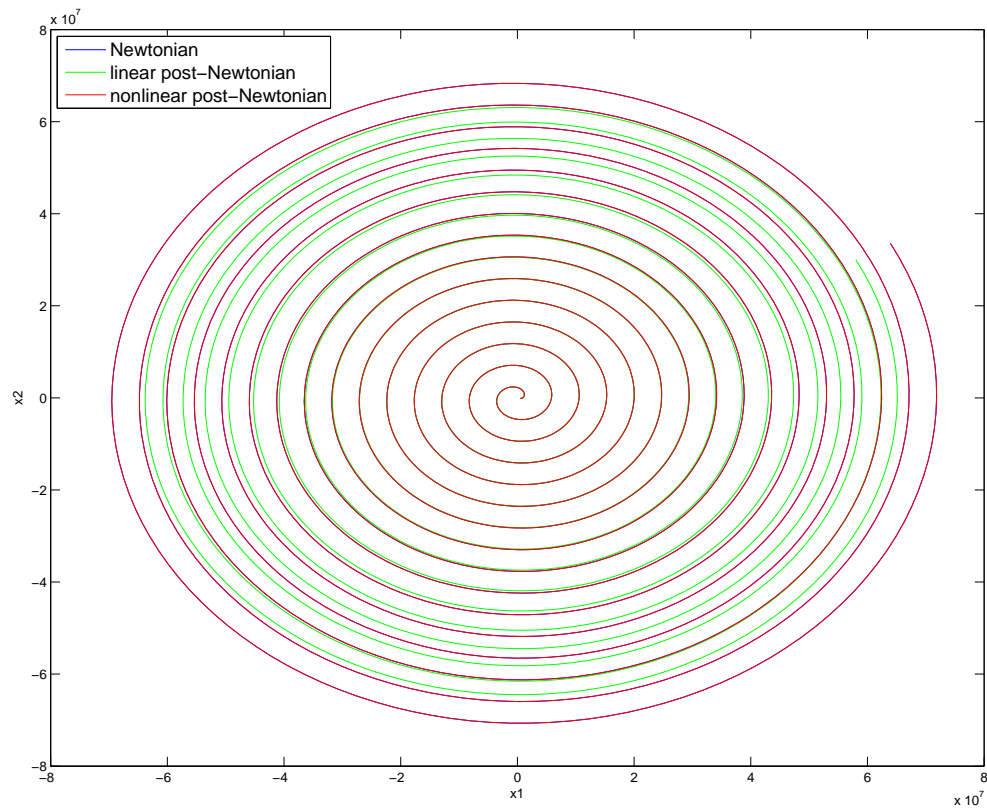
Figure 82: Case 1 for MEO satellites with S2 being farther away from the earth than S1, $d = 5$ kilometres, $t = 5$ days: Relative motion of S2 with respect to S1.
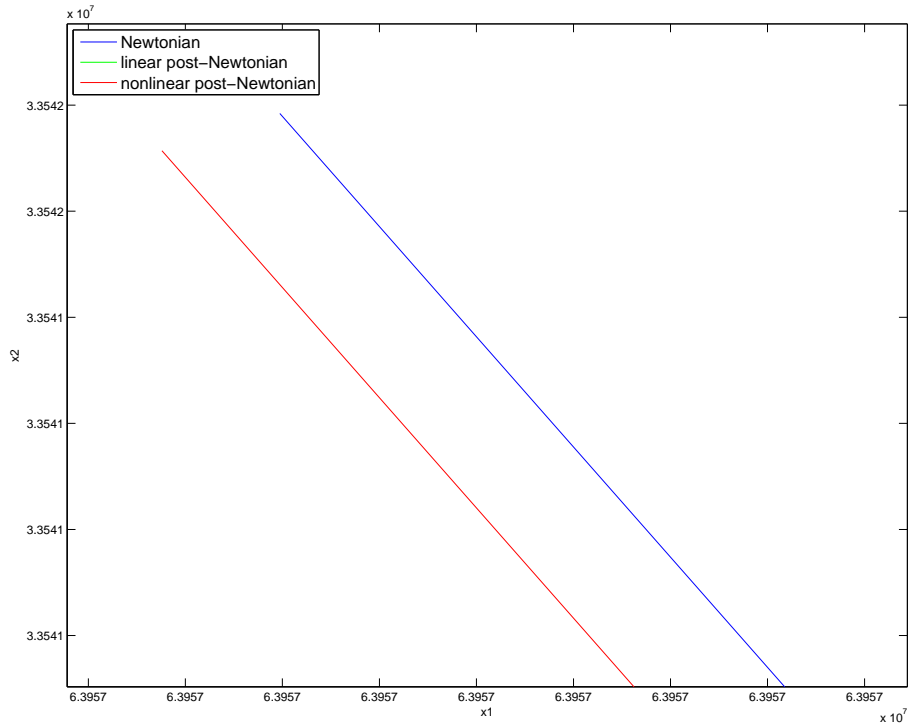
Figure 83: Case 1 for MEO satellites with S2 being farther away from the earth than S1, $d = 5$ kilometres, $t = 5$ days: Zoomed in version of the previous plot. It is now possible to see the difference between solutions from different formulations.
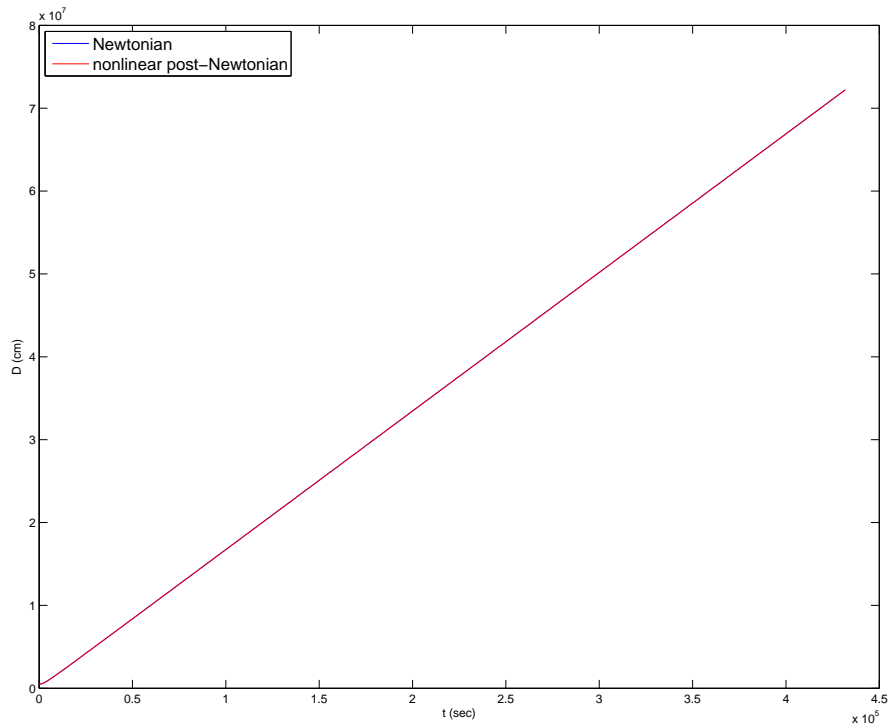
Figure 84: Case 1 for MEO satellites with S2 being farther away from the earth than S1, $d = 5$ kilometres, $t = 5$ days: Absolute distance between S1 and S2.
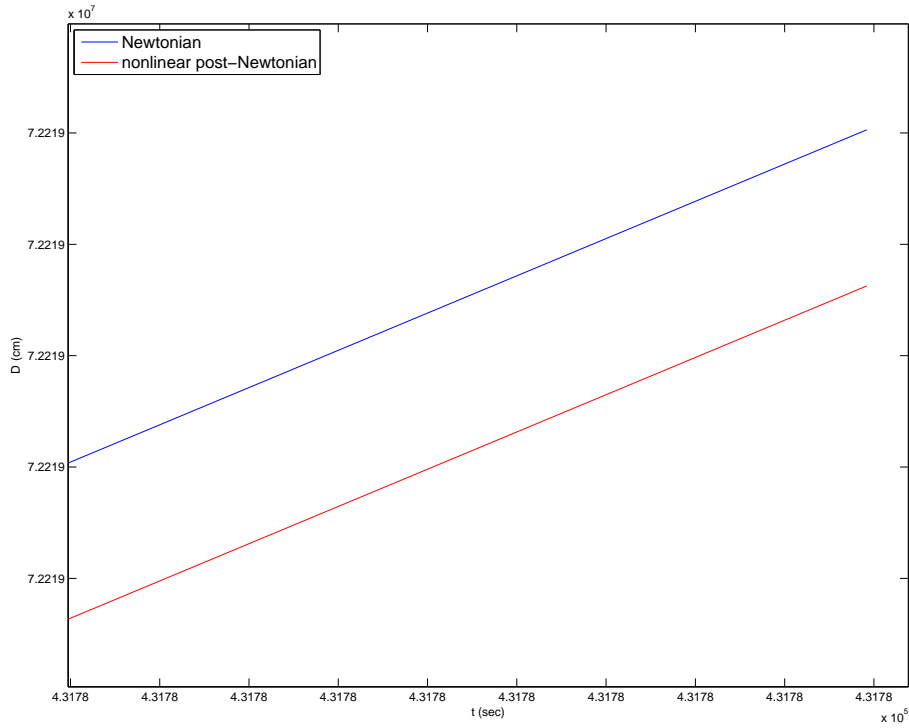
Figure 85: Case 1 for MEO satellites with S2 being farther away from the earth than S1, $d = 5$ kilometres, $t = 5$ days: Zoomed in version of the previous plot. It is now possible to see differences between solutions from different formulations.
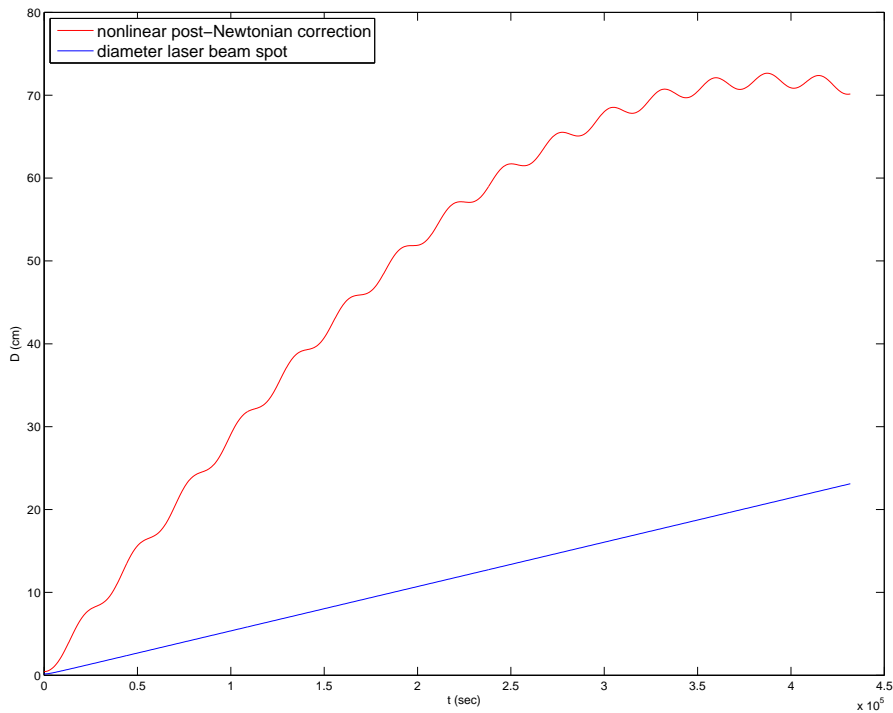
Figure 86: Case 1 for MEO satellites with S2 being farther away from the earth than S1, $d = 5$ kilometres, $t = 5$ days: Correction provided from the nonlinear post–Newtonian equations compared to the laser beam.
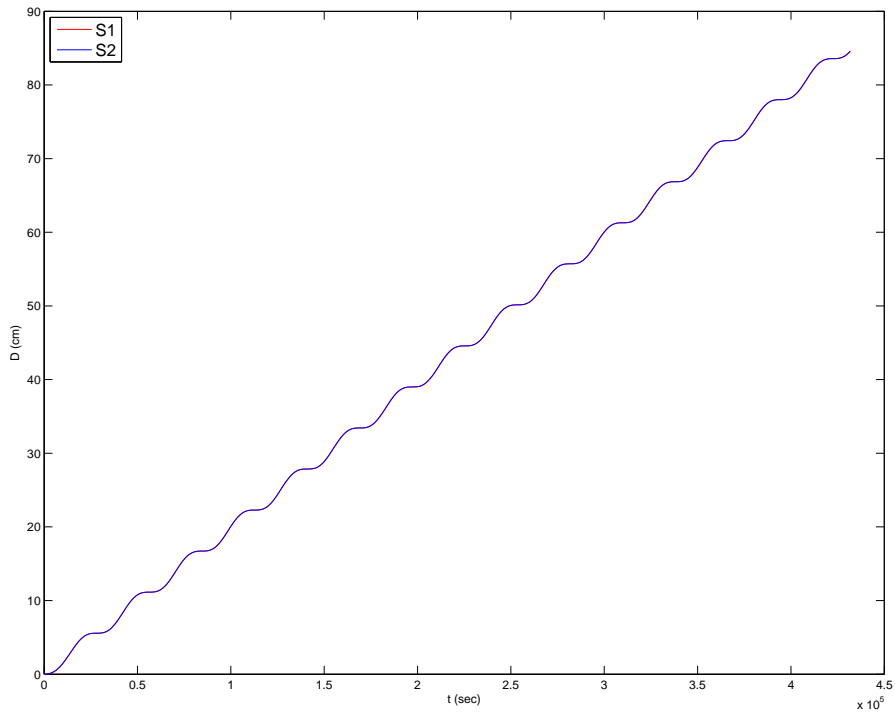
Figure 87: Case 1 for MEO satellites with S2 being farther away from the earth than S1, $d = 5$ kilometres, $t = 5$ days: The distance between the ECI positions of the Newtonian and the nonlinear post–Newtonian solutions, both for S1 and S2, which almost completely overlap.
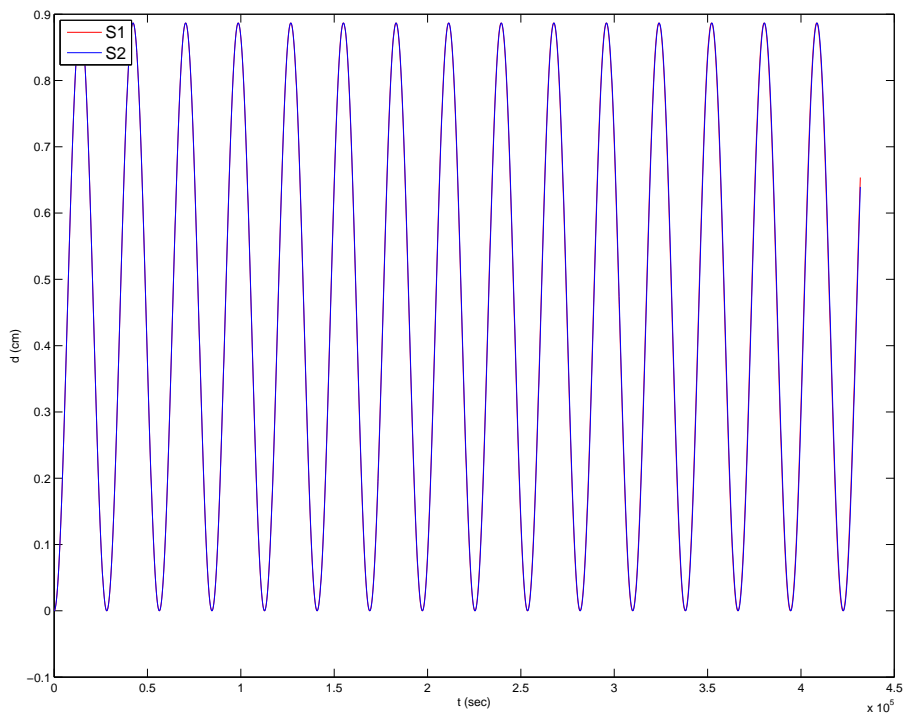

Figure 88: Case 1 for MEO satellites with S2 being farther away from the earth than S1, $d = 5$ kilometres, $t = 5$ days: Difference in distances to the center of the Earth between Newtonian and nonlinear post–Newtonian.
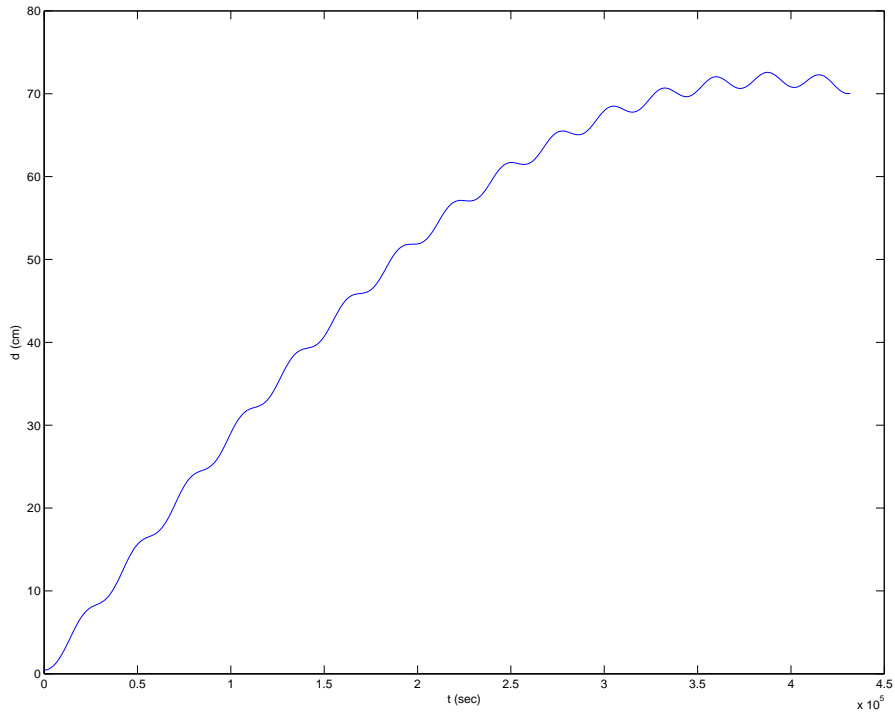
Figure 89: Case 1 for MEO satellites with S2 being farther away from the earth than S1, $d = 5$ kilometres, $t = 5$ days, and nonlinear post–Newtonian formulation: Distance between ECI positions of S2 and S1 and the relative position of S2 with respect to S1.
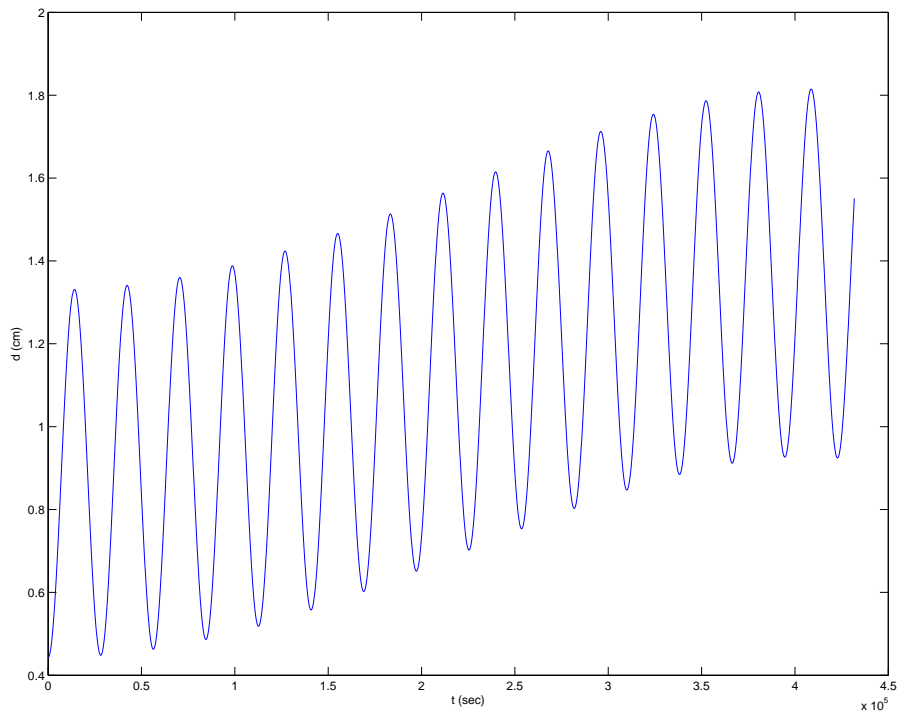
Figure 90: Case 1 for MEO satellites with S2 being farther away from the earth than S1, $d = 5$ kilometres, $t = 5$ days, and nonlinear post–Newtonian formulation: This plot, similar to the above one, shows the difference in distances to the ECI center.

59

2.3.4.2 Case 2

For this test, the goal was to increase the value of d as much as possible. The parameters used for this test are $d = 18$ kilometres and $t = 2$ days.
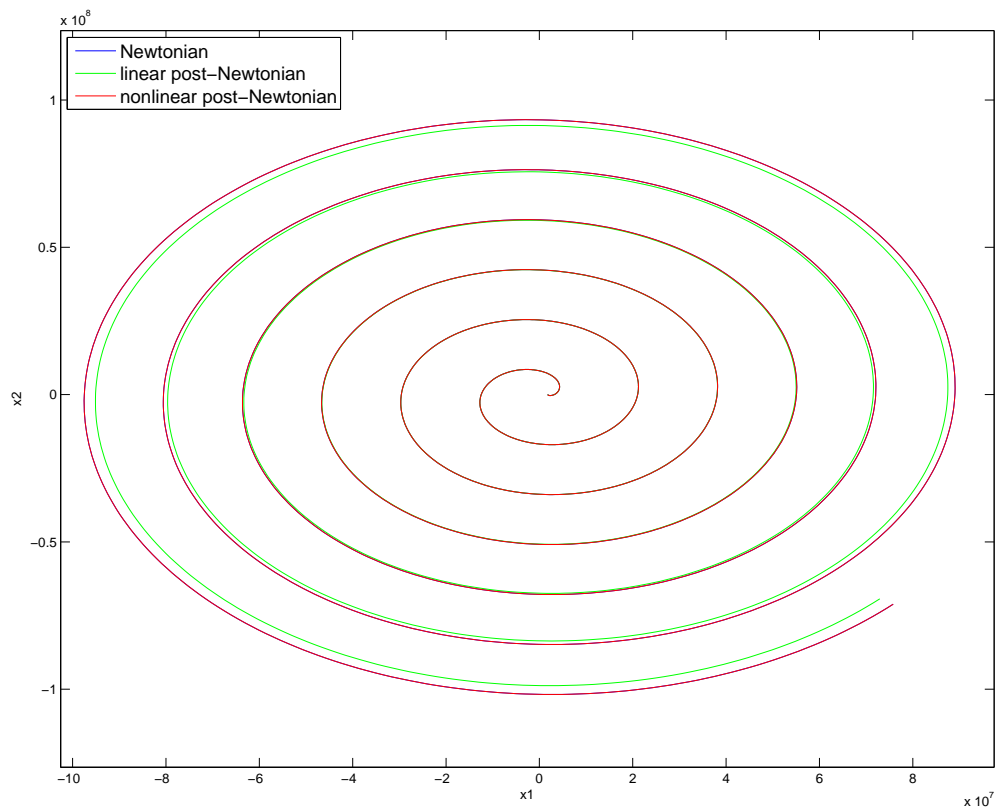
Figure 91: Case 2 for MEO satellites with S2 being farther away from the earth than S1, $d = 18$ kilometres, $t = 2$ days: Relative motion of S2 with respect to S1.
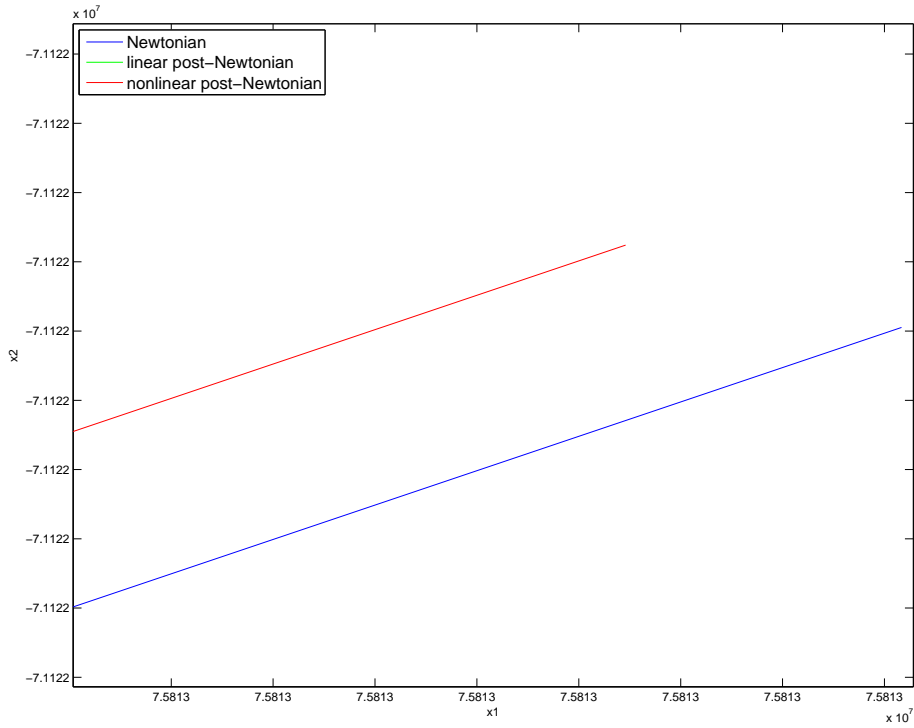
Figure 92: Case 2 for MEO satellites with S2 being farther away from the earth than S1, $d = 18$ kilometres, $t = 2$ days: Zoomed in version of the previous plot. It is now possible to see the difference between solutions from different formulations.
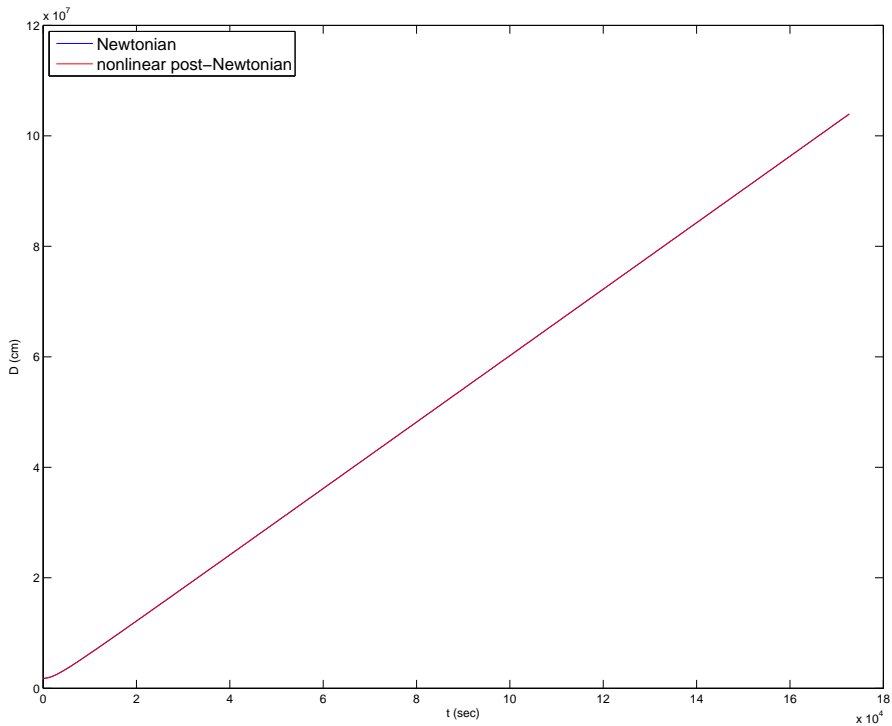

Figure 93: Case 2 for MEO satellites with S2 being farther away from the earth than S1, $d = 18$ kilometres, $t = 2$ days: Absolute distance between S1 and S2.
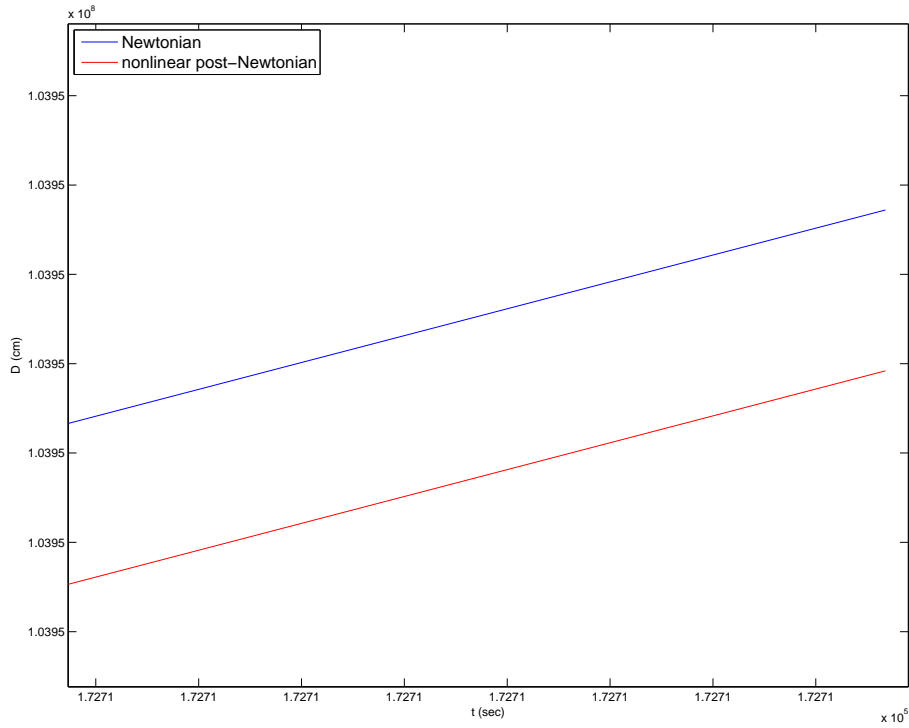
Figure 94: Case 2 for MEO satellites with S2 being farther away from the earth than S1, $d = 18$ kilometres, $t = 2$ days: Zoomed in version of the previous plot. It is now possible to see differences between solutions from different formulations.
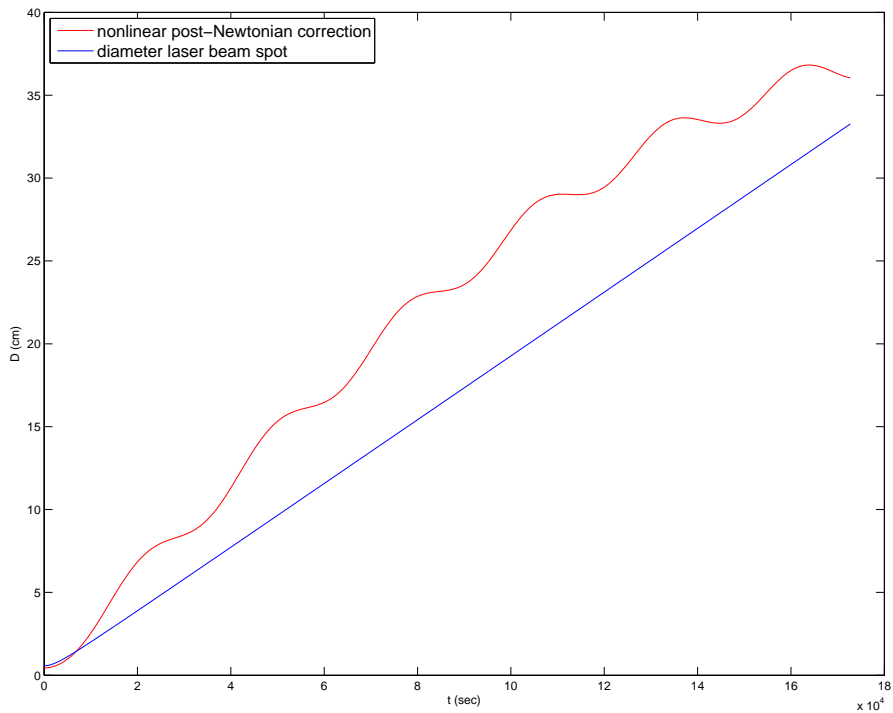

Figure 95: Case 2 for MEO satellites with S2 being farther away from the earth than S1, $d = 18$ kilometres, $t = 2$ days: Correction provided from the nonlinear post–Newtonian equations compared to the laser beam.
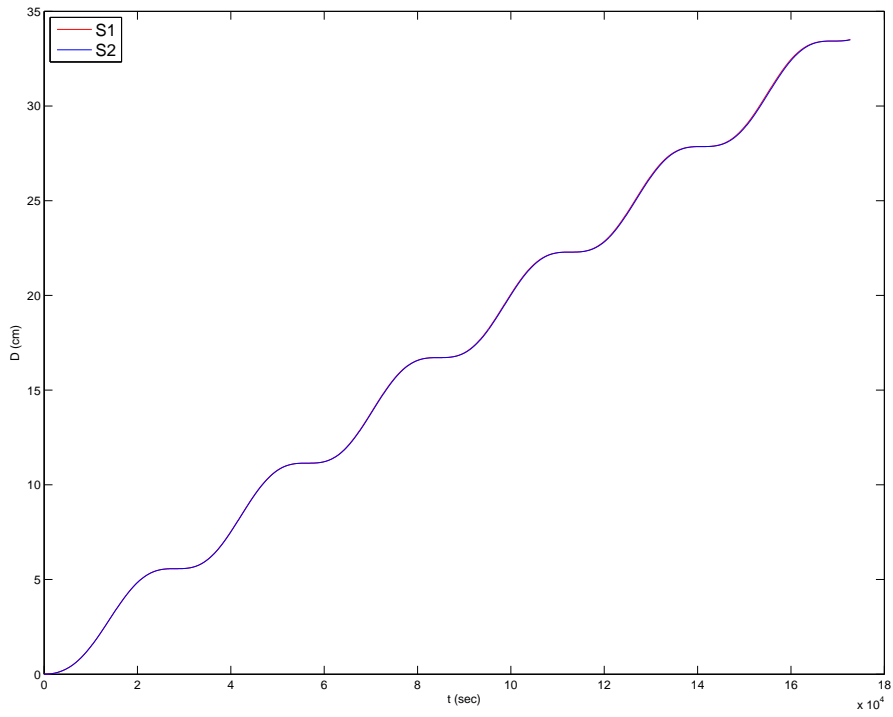
Figure 96: Case 2 for MEO satellites with S2 being farther away from the earth than S1, $d = 18$ kilometres, $t = 2$ days: The distance between the ECI positions of the Newtonian and the nonlinear post–Newtonian solutions, both for S1 and S2, which almost completely overlap.
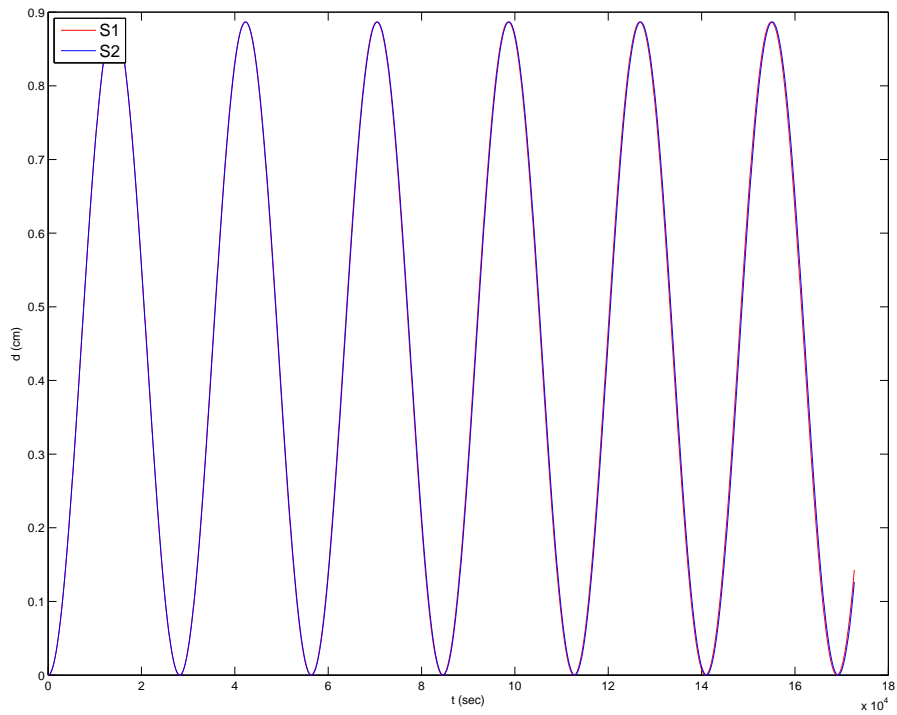

Figure 97: Case 2 for MEO satellites with S2 being farther away from the earth than S1, $d = 18$ kilometres, $t = 2$ days: Difference in distances to the center of the Earth between Newtonian and nonlinear post–Newtonian.
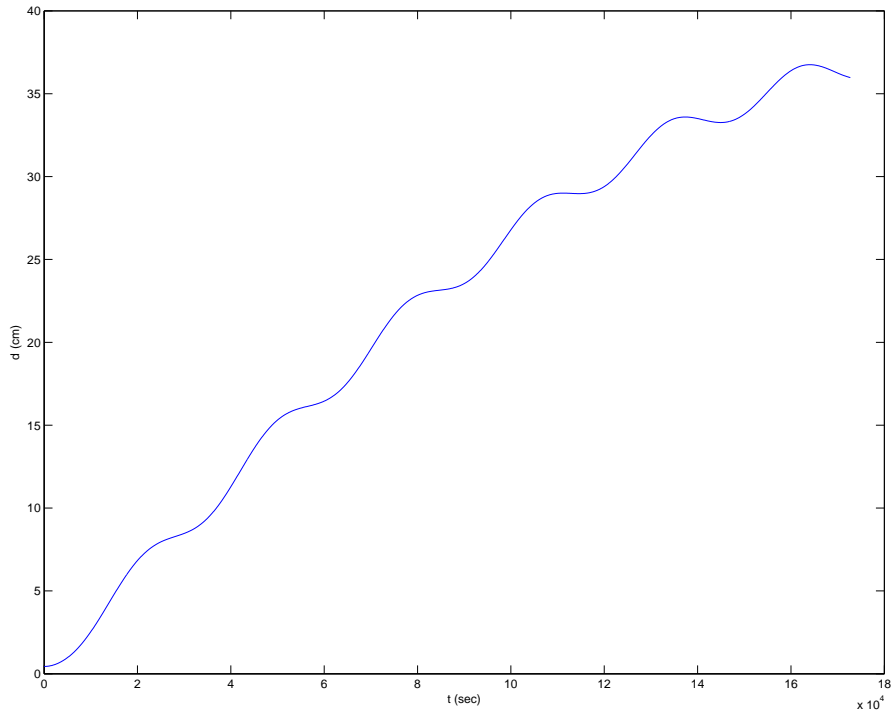
Figure 98: Case 2 for MEO satellites with S2 being farther away from the earth than S1, $d = 18$ kilometres, $t = 2$ days, and nonlinear post–Newtonian formulation: Distance between ECI positions of S2 and S1 and the relative position of S2 with respect to S1.
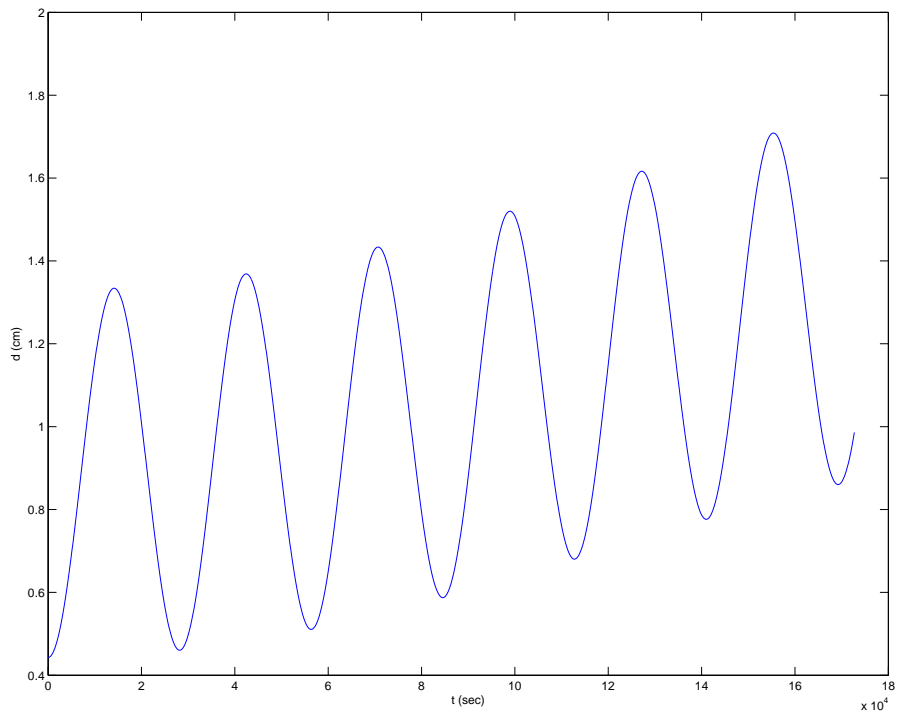
Figure 99: Case 2 for MEO satellites with S2 being farther away from the earth than S1, $d = 18$ kilometres, $t = 2$ days, and nonlinear post–Newtonian formulation: This plot, similar to the above one, shows the difference in distances to the ECI center.

2.3.4.3 Case 3

For this test, the goal was to increase the value of t as much as possible.
The parameters used for this test are $d = 2$ kilometres and $t = 20$ days.
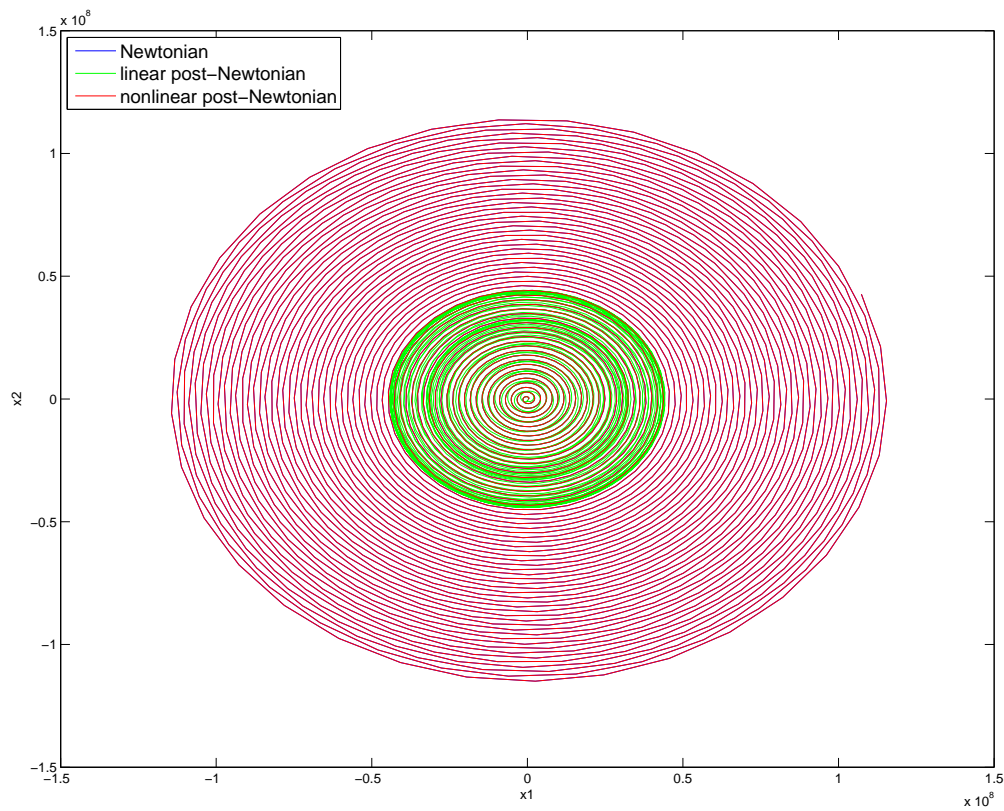
Figure 100: Case 3 for MEO satellites with S2 being farther away from the earth than
S1, $d = 2$ kilometres, $t = 20$ days: Relative motion of S2 with respect to S1.
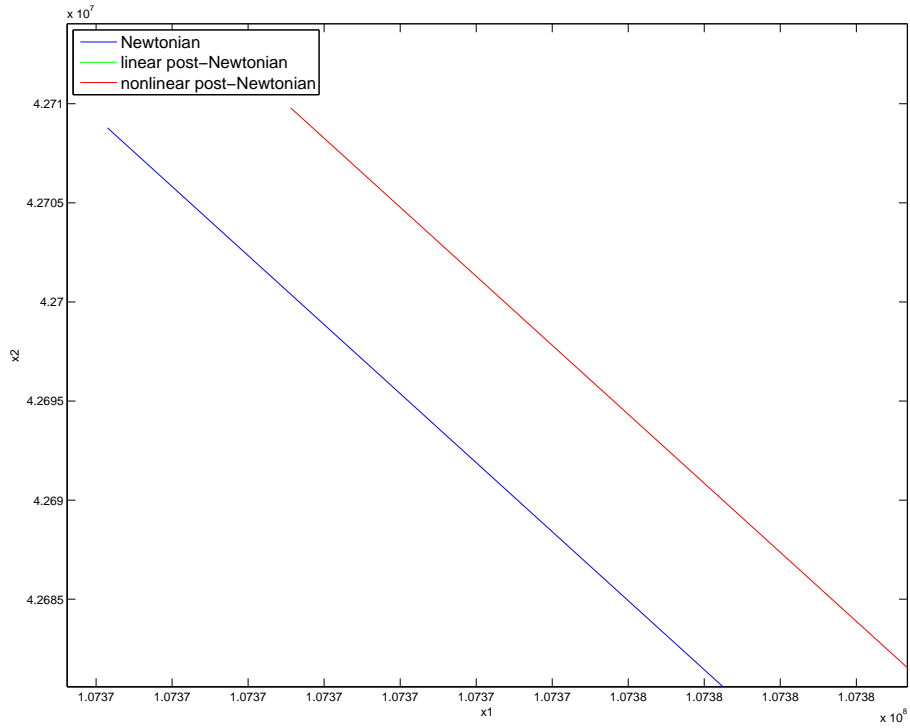
Figure 101: Case 3 for MEO satellites with S2 being farther away from the earth than S1, $d = 2$ kilometres, $t = 20$ days: Zoomed in version of the previous plot. It is now possible to see the difference between solutions from different formulations.
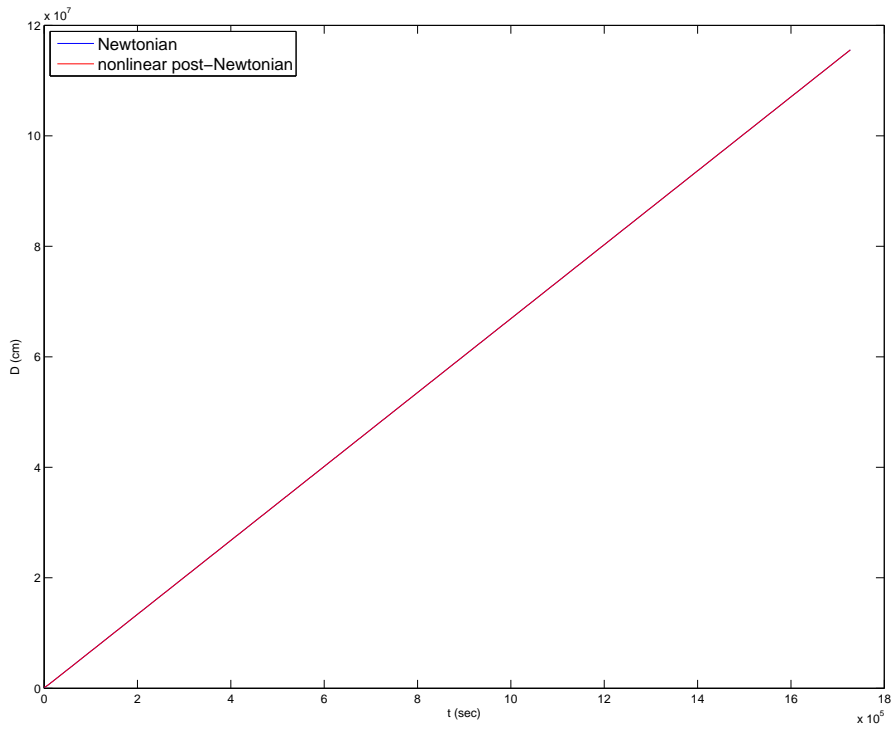

Figure 102: Case 3 for MEO satellites with S2 being farther away from the earth than S1, $d = 2$ kilometres, $t = 20$ days: Absolute distance between S1 and S2.
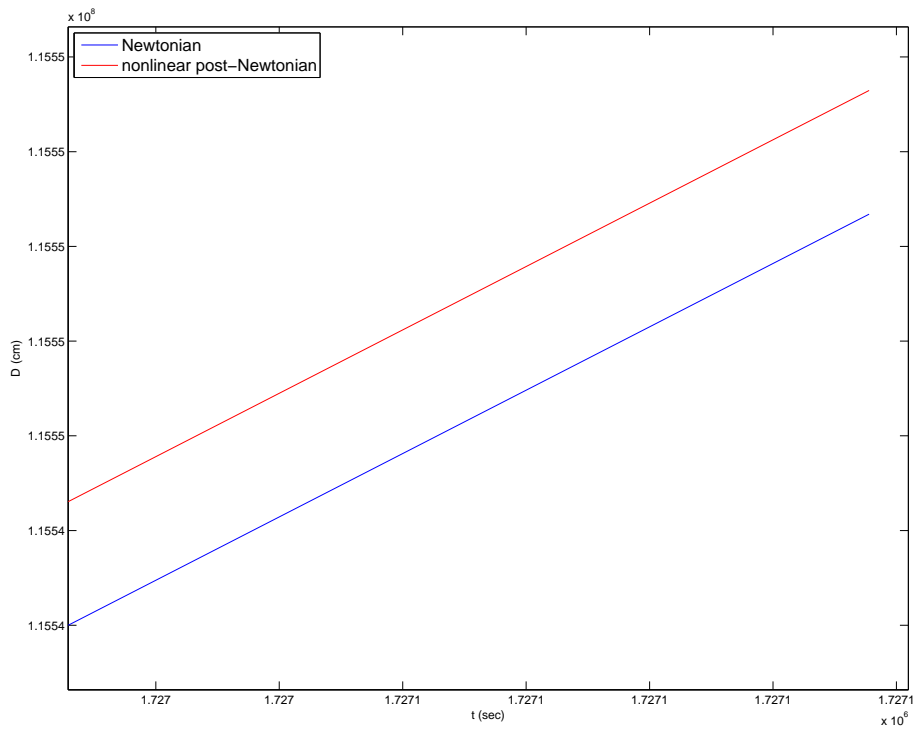
Figure 103: Case 3 for MEO satellites with S2 being farther away from the earth than S1, $d = 2$ kilometres, $t = 20$ days: Zoomed in version of the previous plot. It is now possible to see differences between solutions from different formulations.
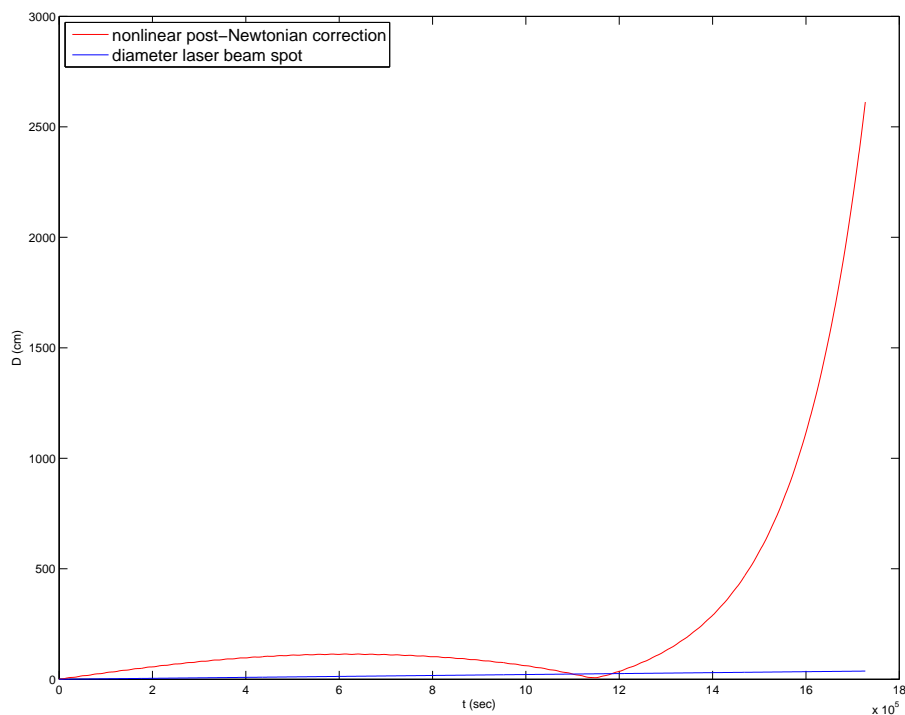

Figure 104: Case 3 for MEO satellites with S2 being farther away from the earth than S1, $d = 2$ kilometres, $t = 20$ days: Correction provided from the nonlinear post–Newtonian equations compared to the laser beam.
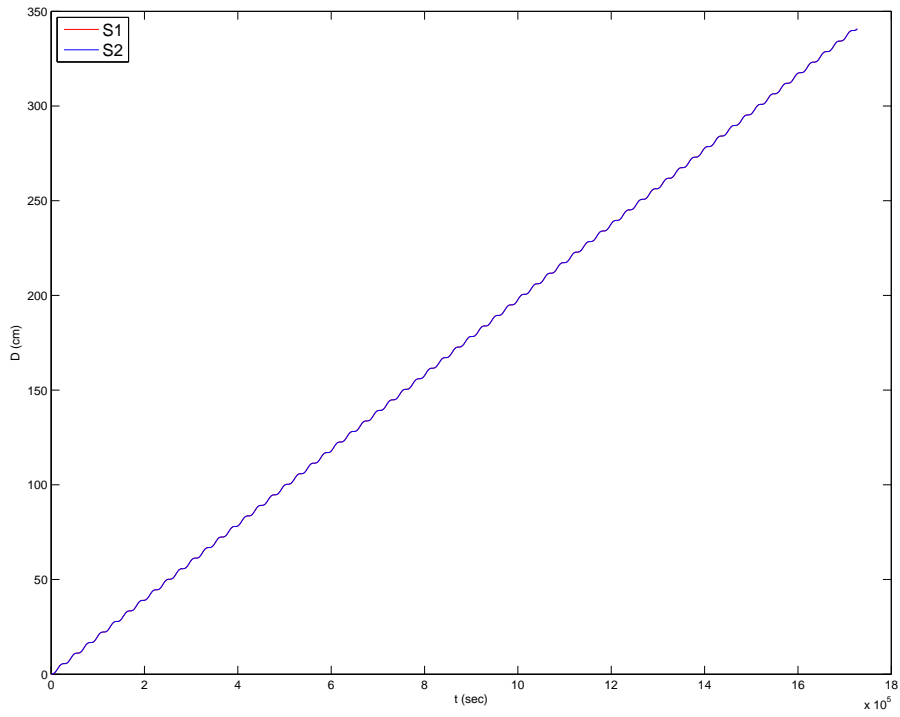
Figure 105: Case 3 for MEO satellites with S2 being farther away from the earth than S1, $d = 2$ kilometres, $t = 20$ days: The distance between the ECI positions of the Newtonian and the nonlinear post–Newtonian solutions, both for S1 and S2, which almost completely overlap.
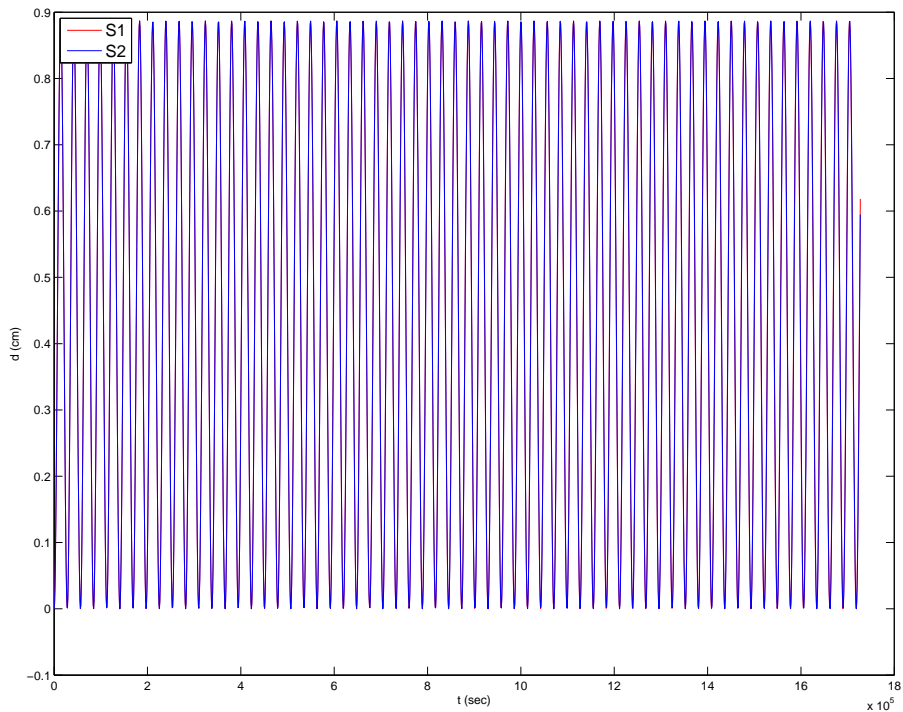
Figure 106: Case 3 for MEO satellites with S2 being farther away from the earth than S1, $d = 2$ kilometres, $t = 20$ days: Difference in distances to the center of the Earth between Newtonian and nonlinear post–Newtonian.

68
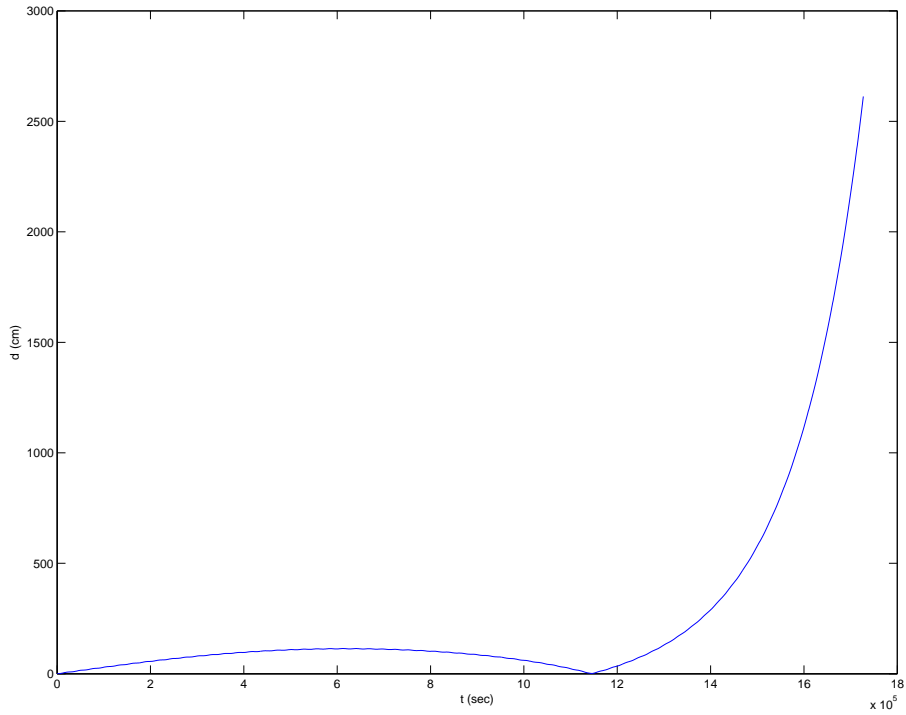
Figure 107: Case 3 for MEO satellites with S2 being farther away from the earth than S1, $d = 2$ kilometres, $t = 20$ days, and nonlinear post–Newtonian formulation: Distance between ECI positions of S2 and S1 and the relative position of S2 with respect to S1.
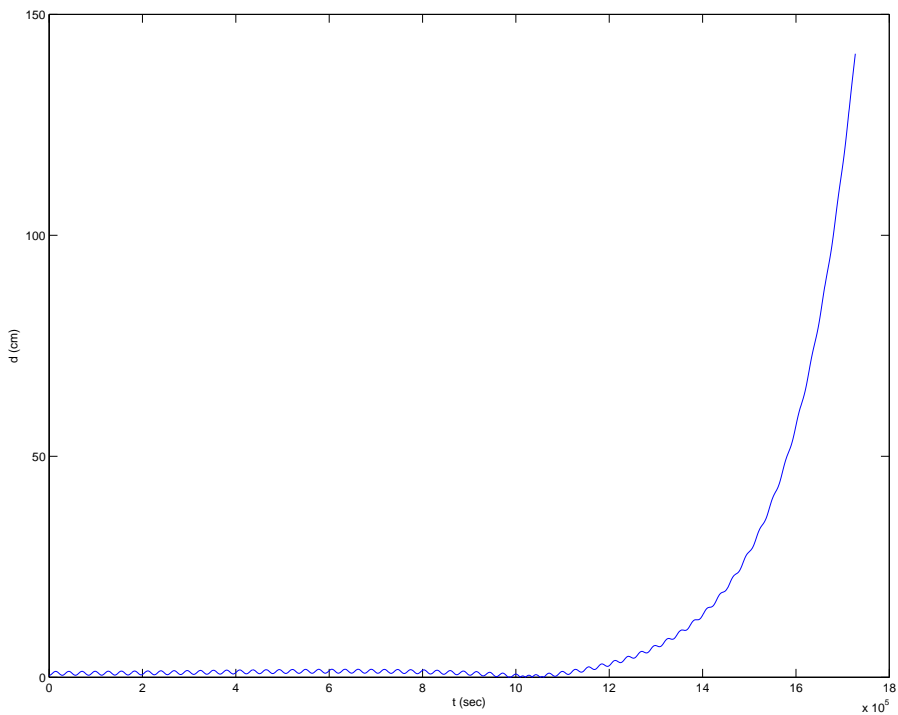
Figure 108: Case 3 for MEO satellites with S2 being farther away from the earth than S1, $d = 2$ kilometres, $t = 20$ days, and nonlinear post–Newtonian formulation: This plot, similar to the above one, shows the difference in distances to the ECI center.

69

2.3.5 LEO satellites with S2 being closer to the Earth than S1

2.3.5.1 Case 1

In this test we showcase the solution for small values in both parameters.
The parameters used for this test are $d = 5$ kilometres and $t = 5$ hours.
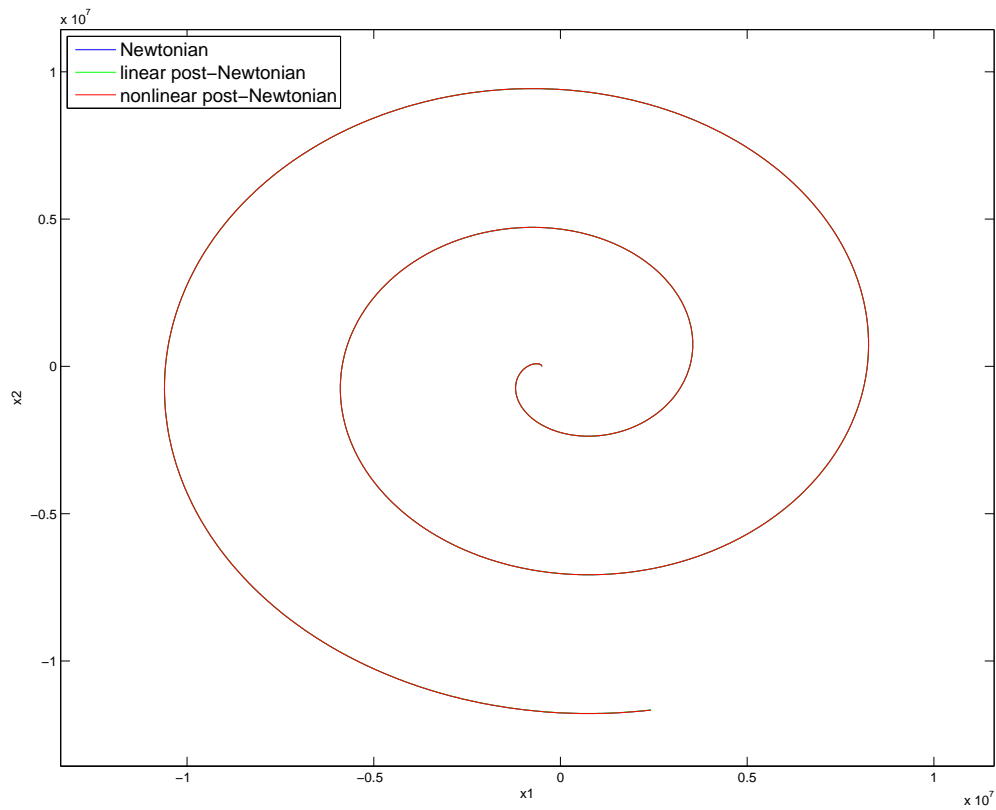
Figure 109: Case 1 for LEO satellites with S2 being closer to the earth than S1, $d = 5$ kilometres, $t = 5$ hours: Relative motion of S2 with respect to S1.
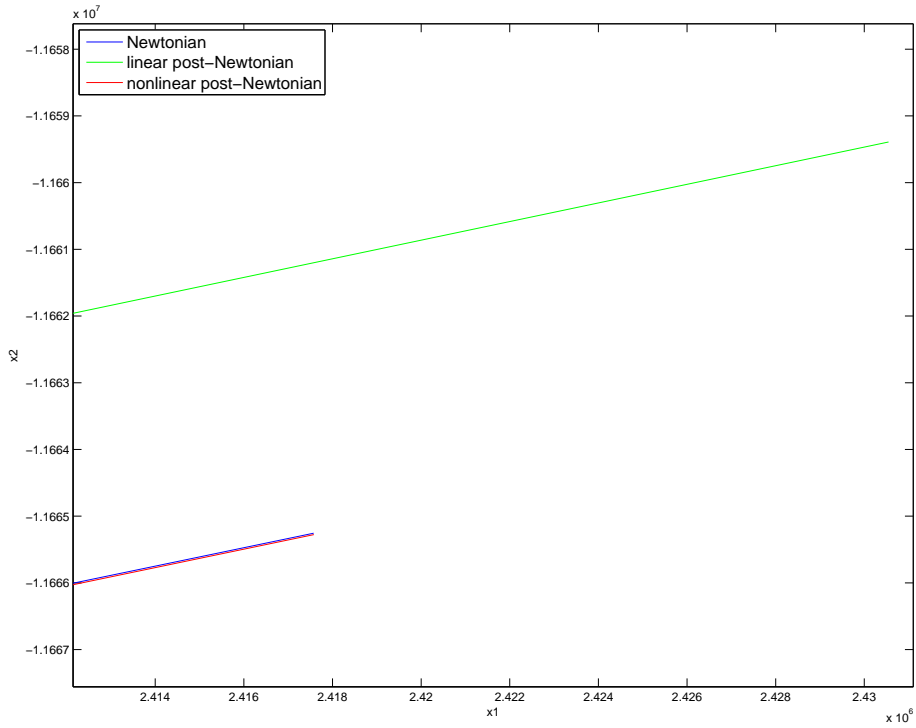
Figure 110: Case 1 for LEO satellites with S2 being closer to the earth than S1, $d = 5$ kilometres, $t = 5$ hours: Zoomed in version of the previous plot. It is now possible to see the difference between solutions from different formulations.
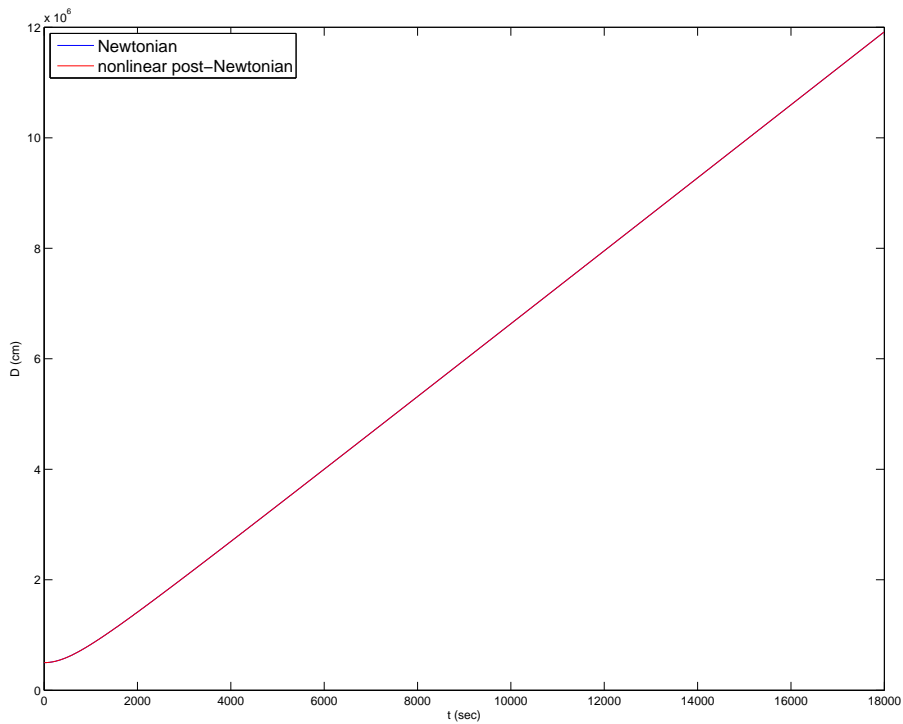

Figure 111: Case 1 for LEO satellites with S2 being closer to the earth than S1, $d = 5$ kilometres, $t = 5$ hours: Absolute distance between S1 and S2.

71
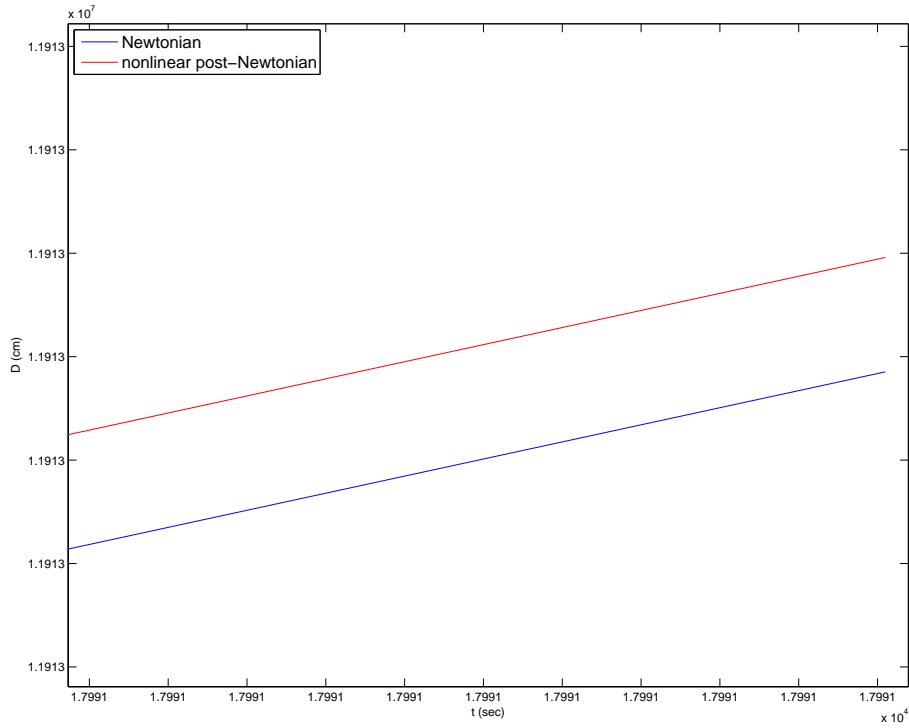
Figure 112: Case 1 for LEO satellites with S2 being closer to the earth than S1, $d = 5$ kilometres, $t = 5$ hours: Zoomed in version of the previous plot. It is now possible to see differences between solutions from different formulations.
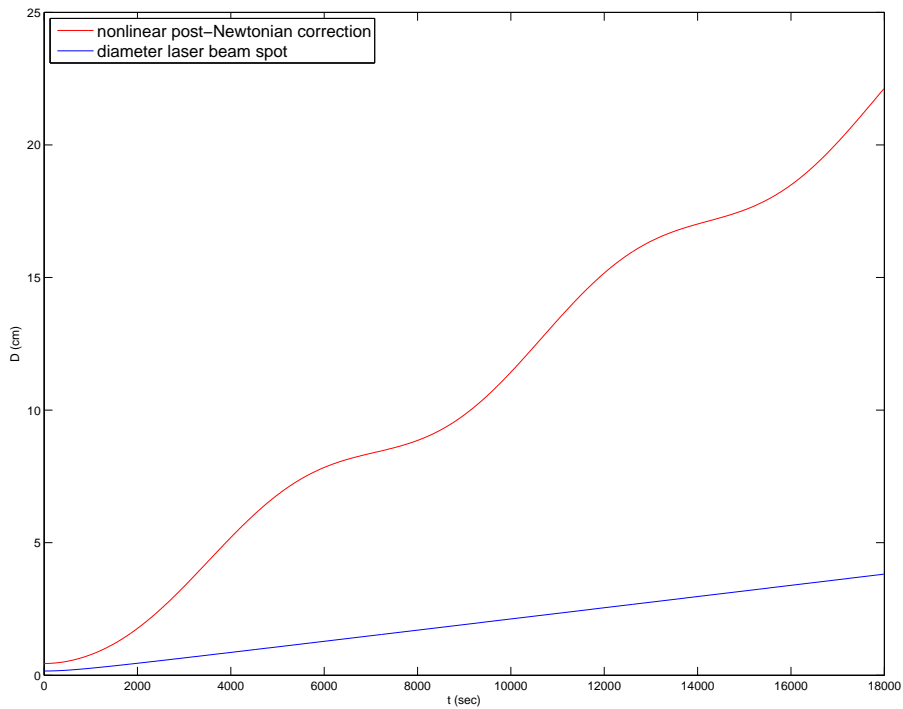
Figure 113: Case 1 for LEO satellites with S2 being closer to the earth than S1, $d = 5$ kilometres, $t = 5$ hours: Correction provided from the nonlinear post–Newtonian equations compared to the laser beam.
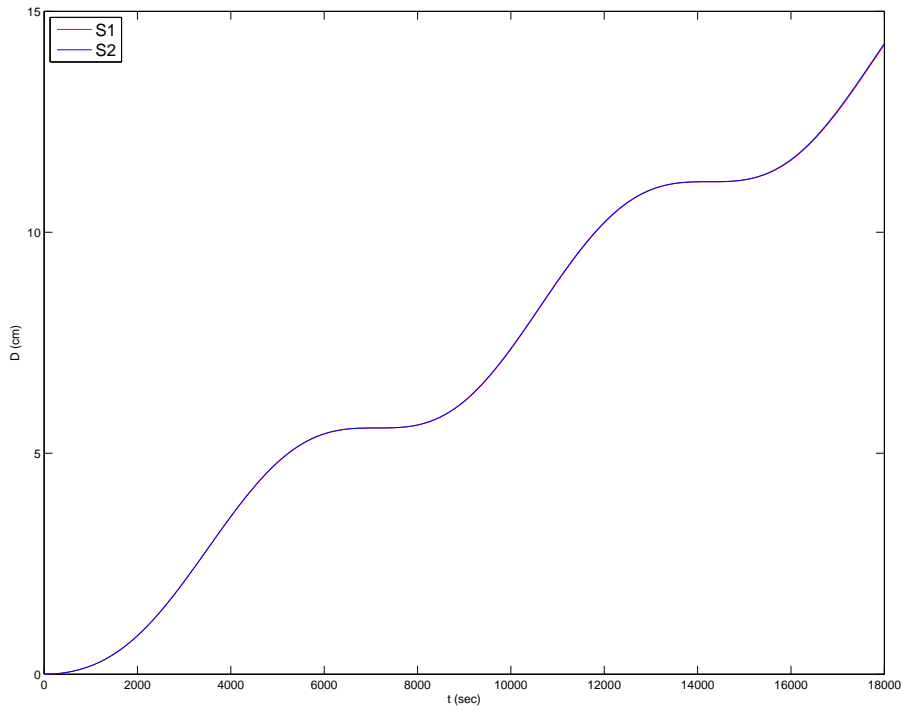
Figure 114: Case 1 for LEO satellites with S2 being closer to the earth than S1, $d = 5$ kilometres, $t = 5$ hours: The distance between the ECI positions of the Newtonian and the nonlinear post–Newtonian solutions, both for S1 and S2, which almost completely overlap.
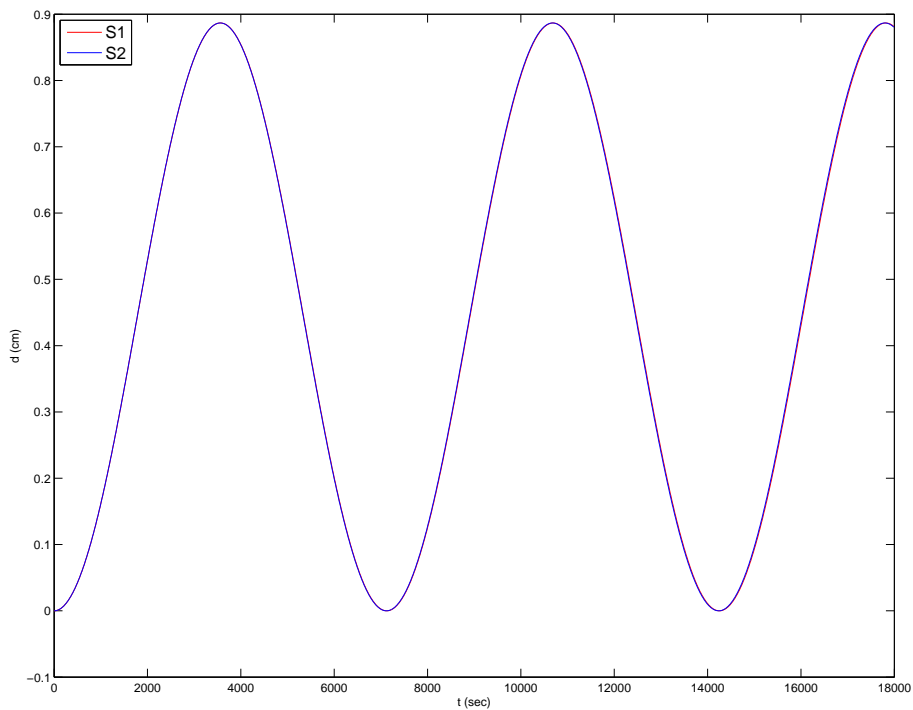
Figure 115: Case 1 for LEO satellites with S2 being closer to the earth than S1, $d = 5$ kilometres, $t = 5$ hours: Difference in distances to the center of the Earth between Newtonian and nonlinear post–Newtonian.
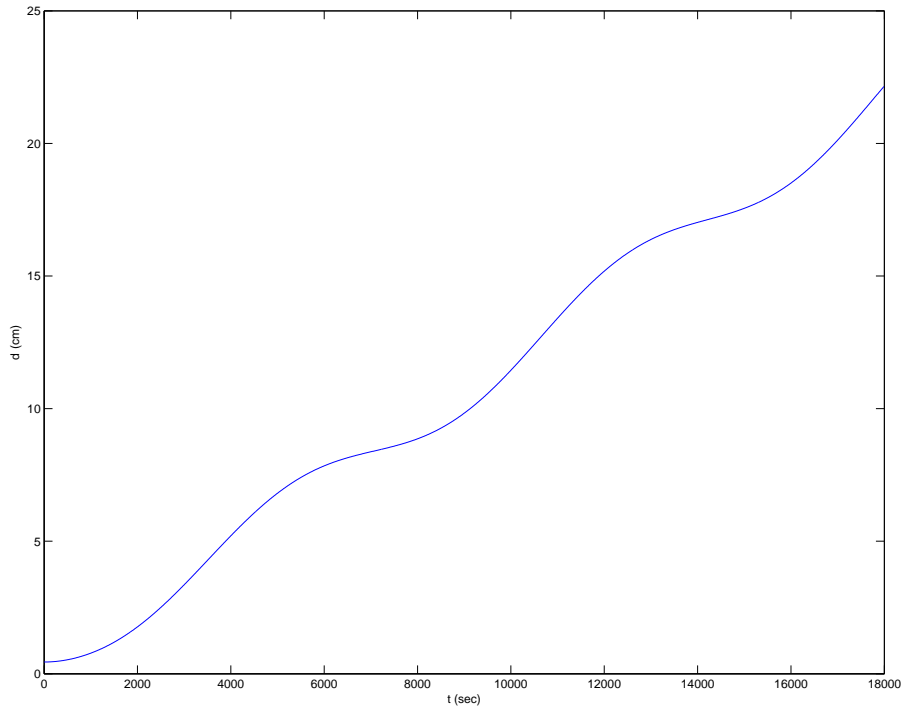
Figure 116: Case 1 for LEO satellites with S2 being closer to the earth than S1, $d = 5$ kilometres, $t = 5$ hours, and nonlinear post–Newtonian formulation: Distance between ECI positions of S2 and S1 and the relative position of S2 with respect to S1.
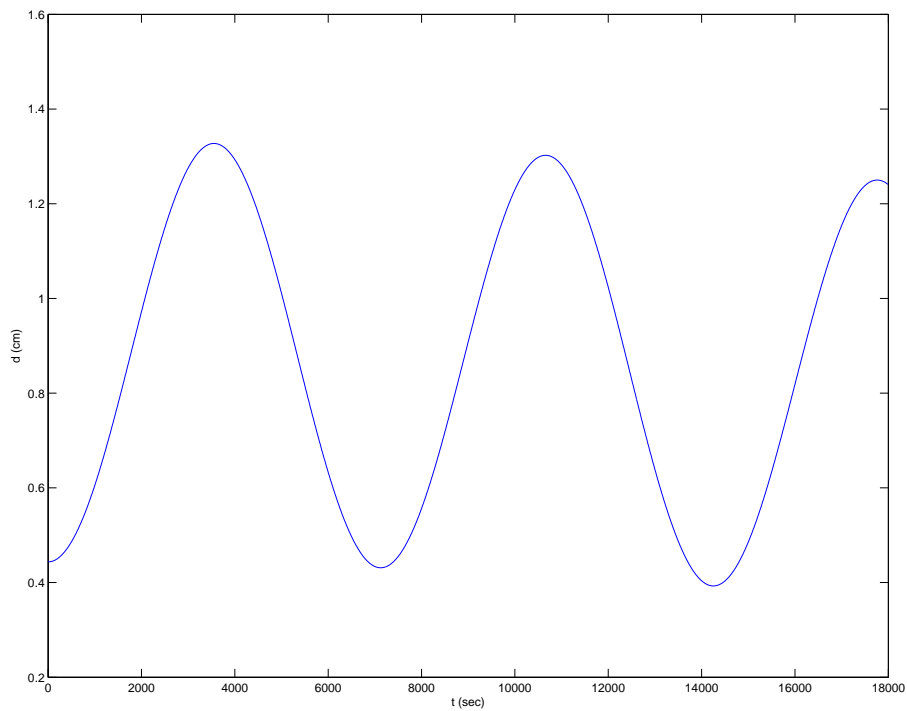
Figure 117: Case 1 for LEO satellites with S2 being closer to the earth than S1, $d = 5$ kilometres, $t = 5$ hours, and nonlinear post–Newtonian formulation: This plot, similar to the above one, shows the difference in distances to the ECI center.

2.3.5.2   Case 2

For this test, the goal was to increase the value of d as much as possible.
The parameters used for this test are $d = 25$ kilometres and $t = 3$ hours.
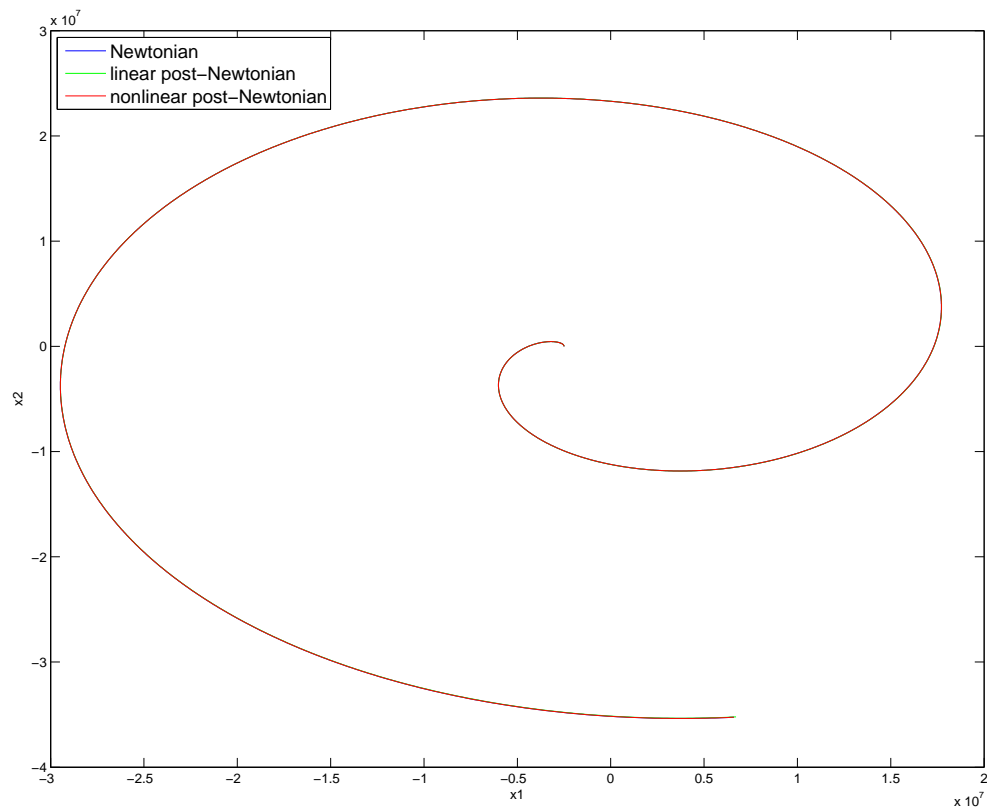
Figure 118: Case 2 for LEO satellites with S2 being closer to the earth than S1, $d = 25$ kilometres, $t = 3$ hours: Relative motion of S2 with respect to S1.
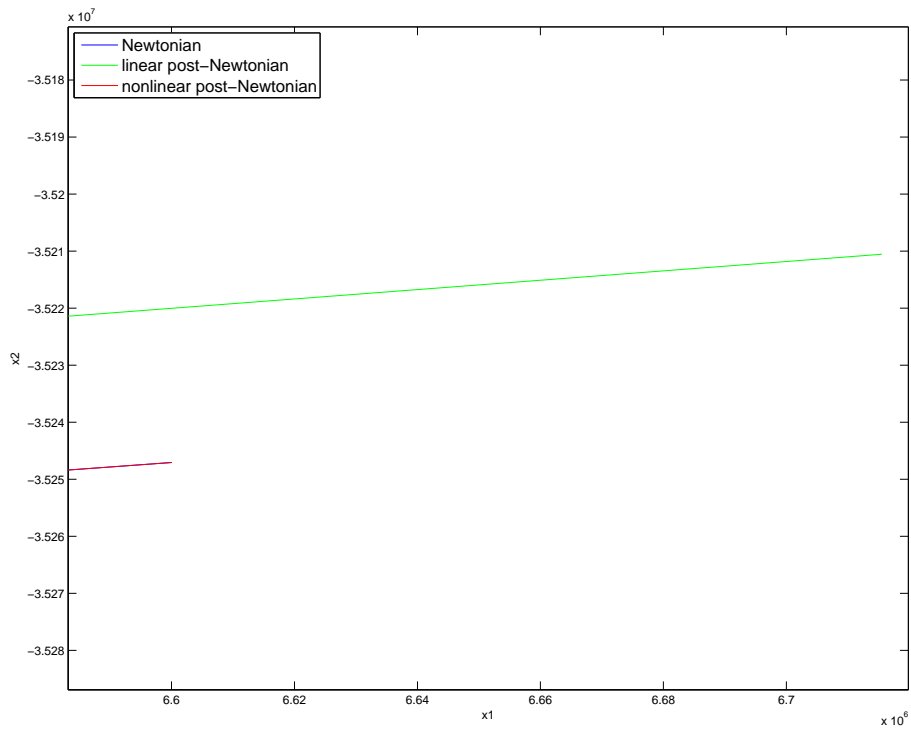
Figure 119: Case 2 for LEO satellites with S2 being closer to the earth than S1, $d = 25$ kilometres, $t = 3$ hours: Zoomed in version of the previous plot. It is now possible to see the difference between solutions from different formulations.
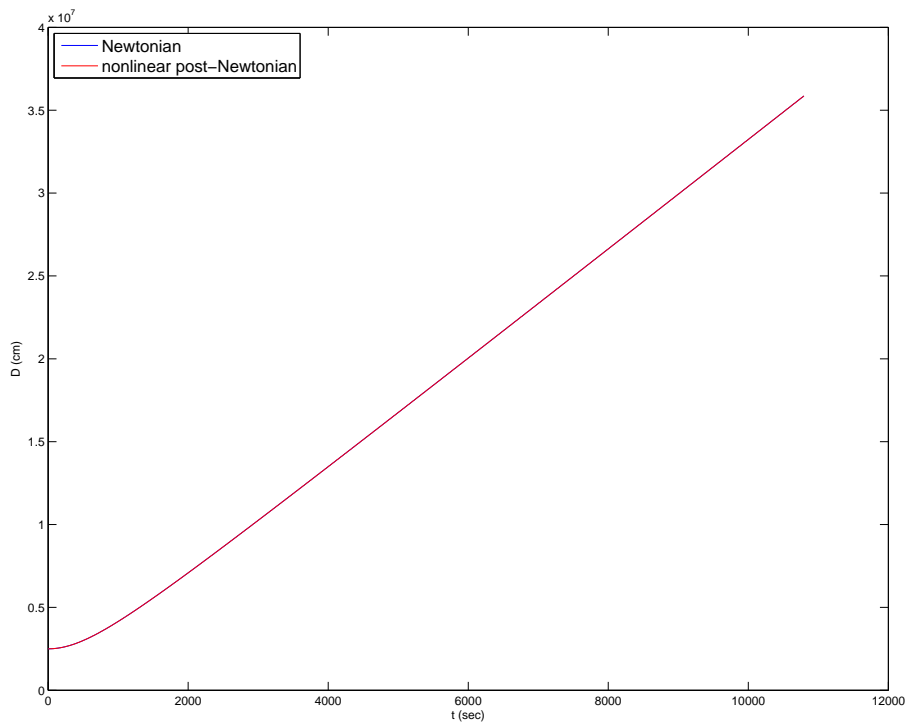
Figure 120: Case 2 for LEO satellites with S2 being closer to the earth than S1, $d = 25$ kilometres, $t = 3$ hours: Absolute distance between S1 and S2.

76
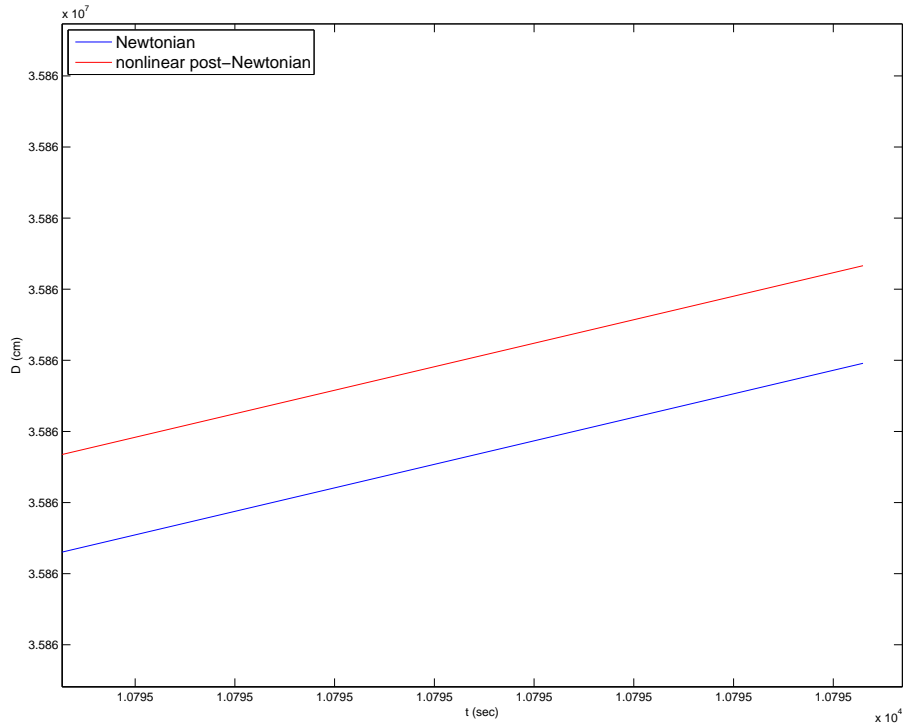
Figure 121: Case 2 for LEO satellites with S2 being closer to the earth than S1, $d = 25$ kilometres, $t = 3$ hours: Zoomed in version of the previous plot. It is now possible to see differences between solutions from different formulations.
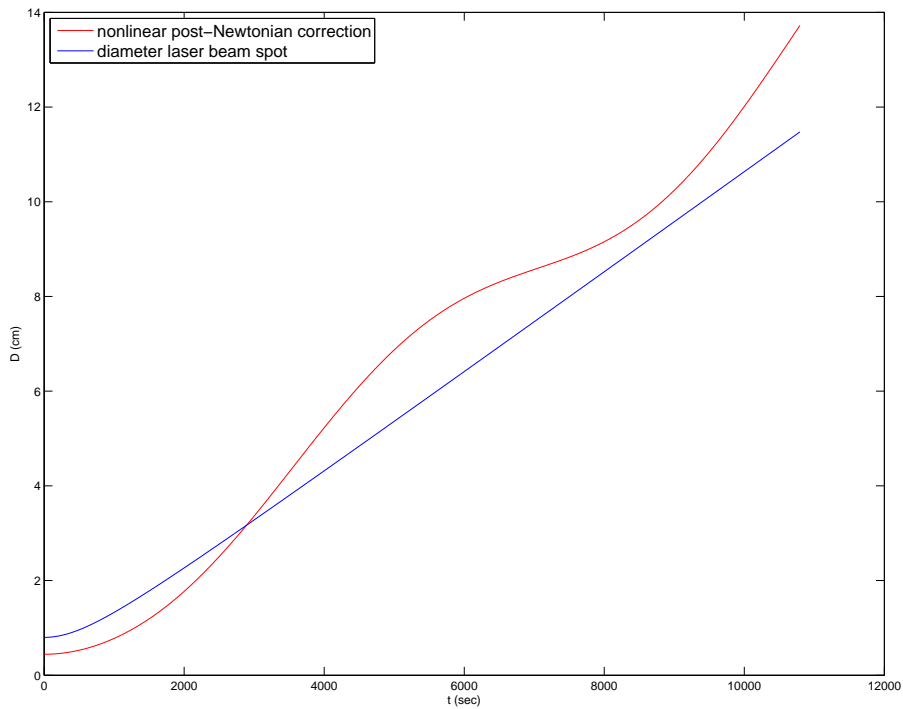
Figure 122: Case 2 for LEO satellites with S2 being closer to the earth than S1, $d = 25$ kilometres, $t = 3$ hours: Correction provided from the nonlinear post–Newtonian equations compared to the laser beam.

77
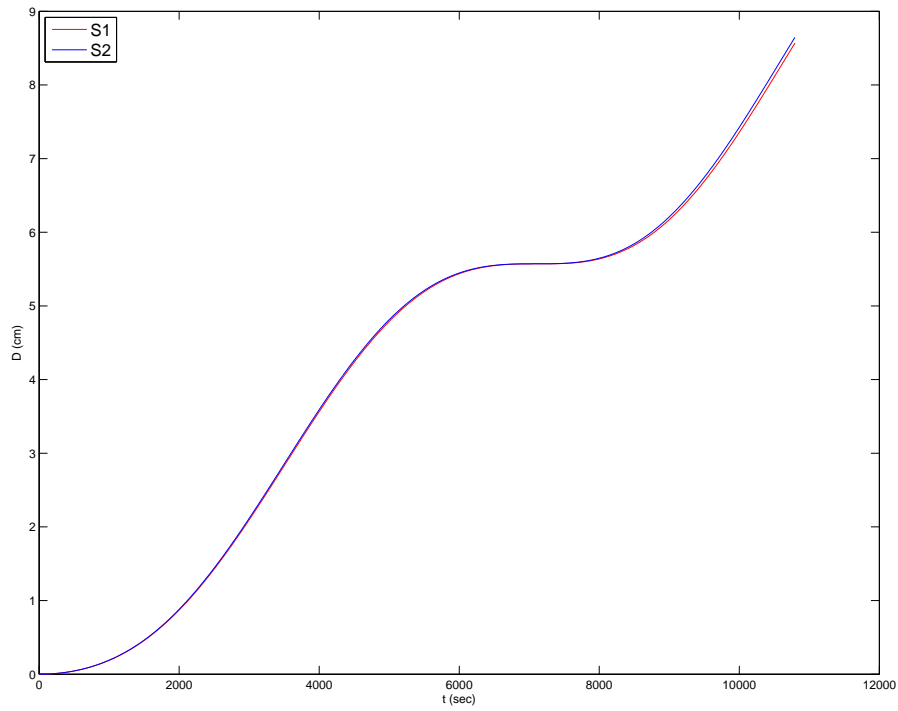
Figure 123: Case 2 for LEO satellites with S2 being closer to the earth than S1, $d = 25$ kilometres, $t = 3$ hours: The distance between the ECI positions of the Newtonian and the nonlinear post–Newtonian solutions, both for S1 and S2, which almost completely overlap.
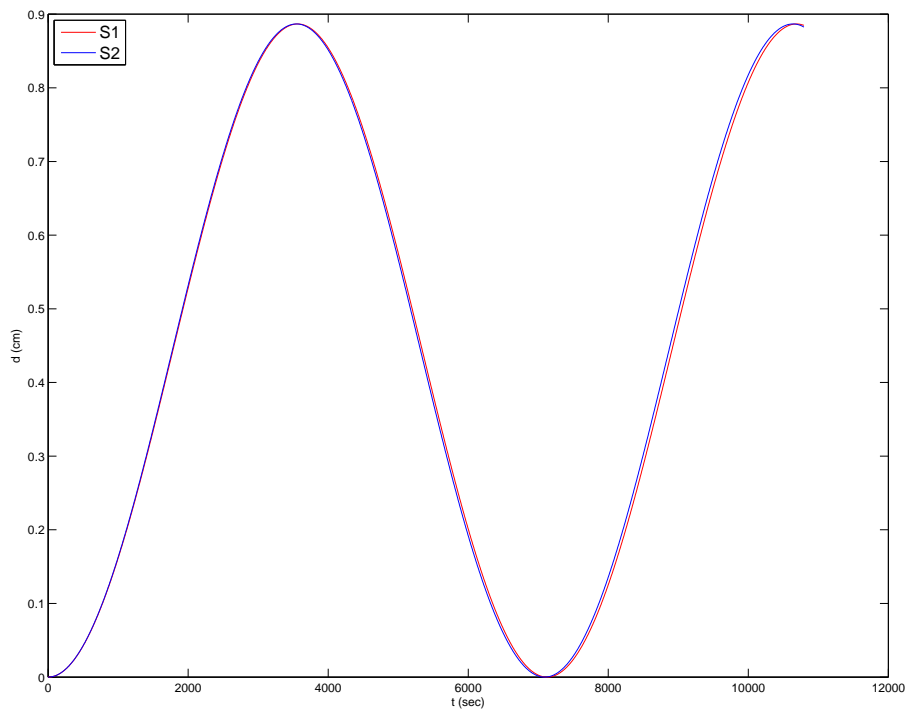

Figure 124: Case 2 for LEO satellites with S2 being closer to the earth than S1, $d = 25$ kilometres, $t = 3$ hours: Difference in distances to the center of the Earth between Newtonian and nonlinear post–Newtonian.
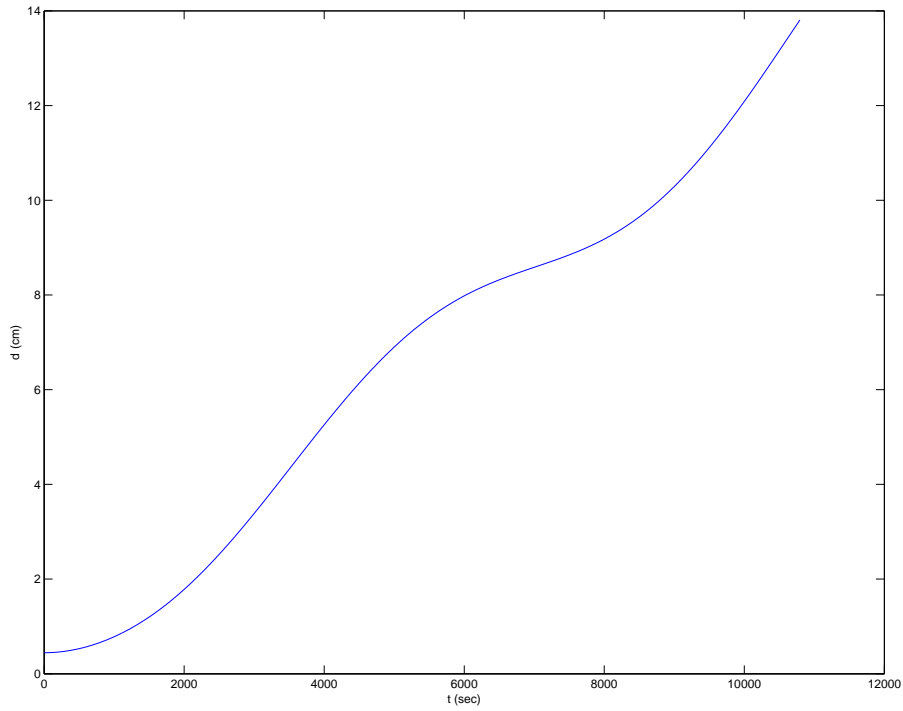
Figure 125: Case 2 for LEO satellites with S2 being closer to the earth than S1, $d = 25$ kilometres, $t = 3$ hours, and nonlinear post–Newtonian formulation: Distance between ECI positions of S2 and S1 and the relative position of S2 with respect to S1.
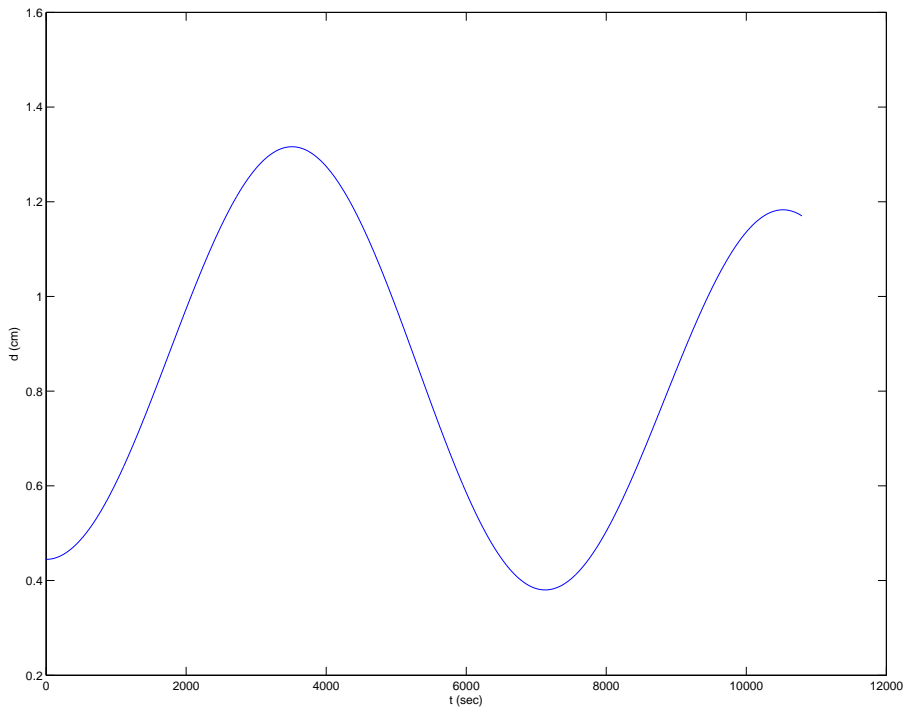

Figure 126: Case 2 for LEO satellites with S2 being closer to the earth than S1, $d = 25$ kilometres, $t = 3$ hours, and nonlinear post–Newtonian formulation: This plot, similar to the above one, shows the difference in distances to the ECI center.

2.3.5.3 Case 3

For this test, the goal was to increase the value of t as much as possible. The parameters used for this test are $d = 3$ kilometres and $t = 72$ hours.
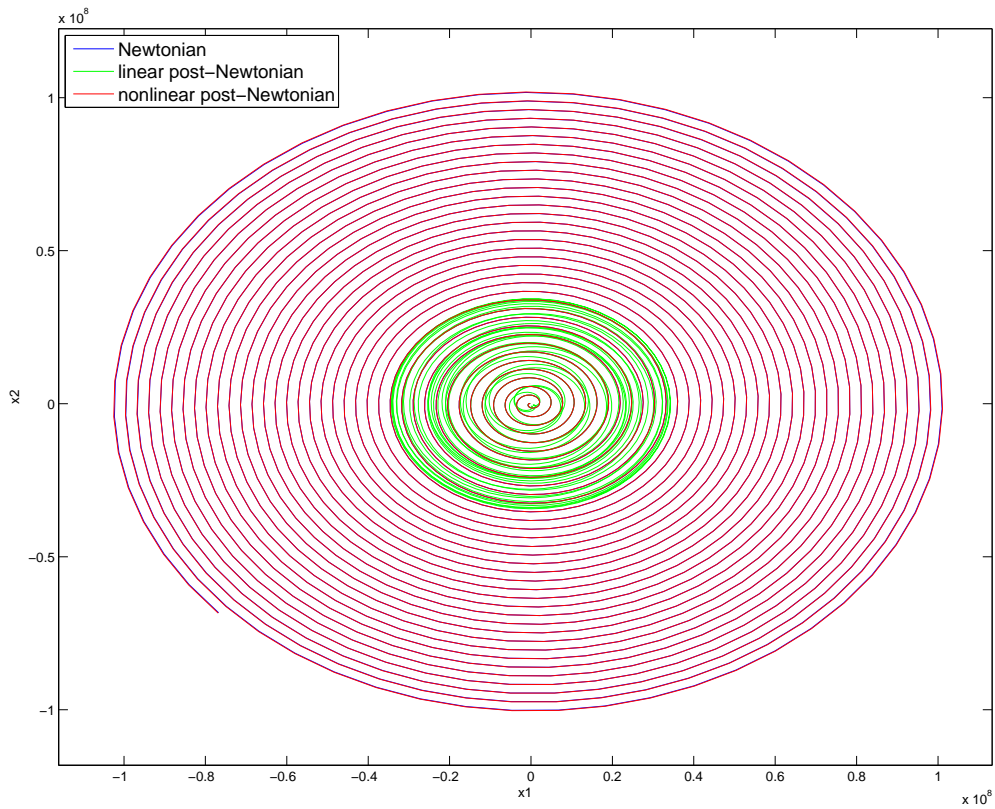

Figure 127: Case 3 for LEO satellites with S2 being closer to the earth than S1, $d = 3$ kilometres, $t = 72$ hours: Relative motion of S2 with respect to S1.
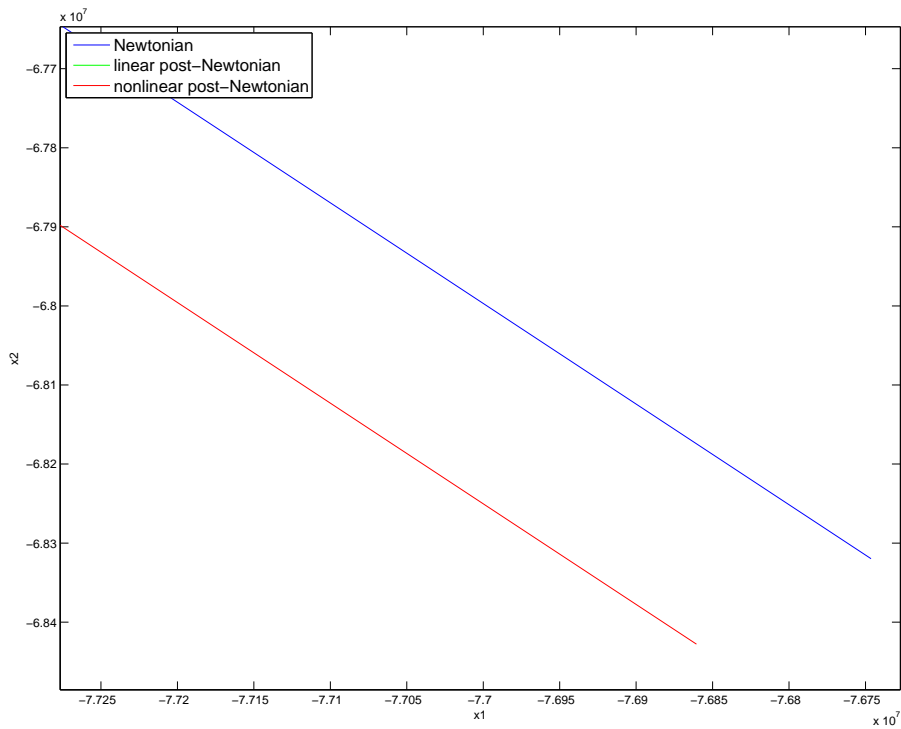
Figure 128: Case 3 for LEO satellites with S2 being closer to the earth than S1, $d = 3$ kilometres, $t = 72$ hours: Zoomed in version of the previous plot. It is now possible to see the difference between solutions from different formulations.
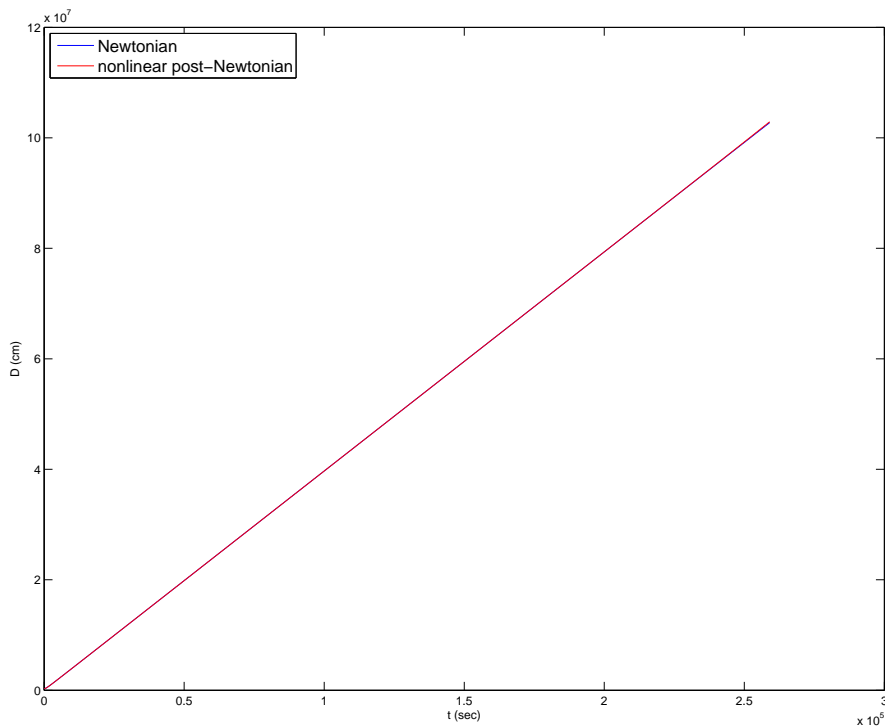

Figure 129: Case 3 for LEO satellites with S2 being closer to the earth than S1, $d = 3$ kilometres, $t = 72$ hours: Absolute distance between S1 and S2.
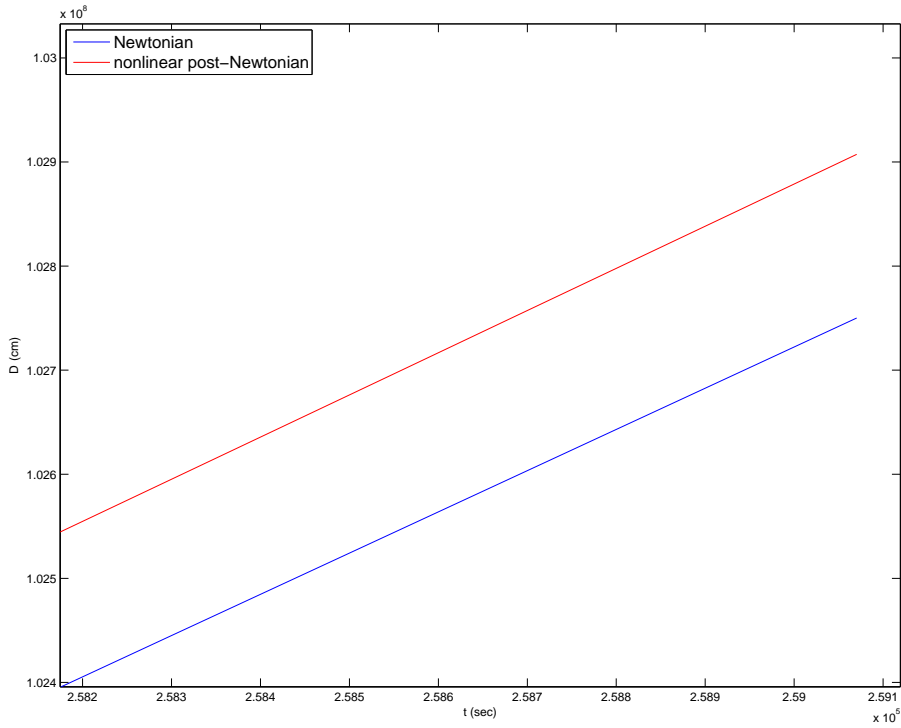
Figure 130: Case 3 for LEO satellites with S2 being closer to the earth than S1, $d = 3$ kilometres, $t = 72$ hours: Zoomed in version of the previous plot. It is now possible to see differences between solutions from different formulations.
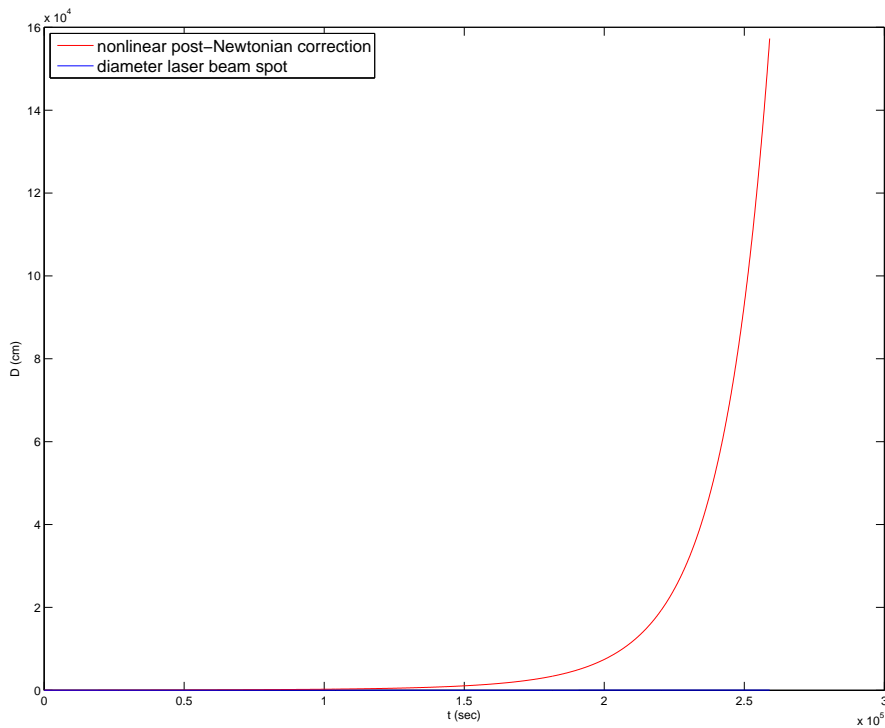

Figure 131: Case 3 for LEO satellites with S2 being closer to the earth than S1, $d = 3$ kilometres, $t = 72$ hours: Correction provided from the nonlinear post–Newtonian equations compared to the laser beam.
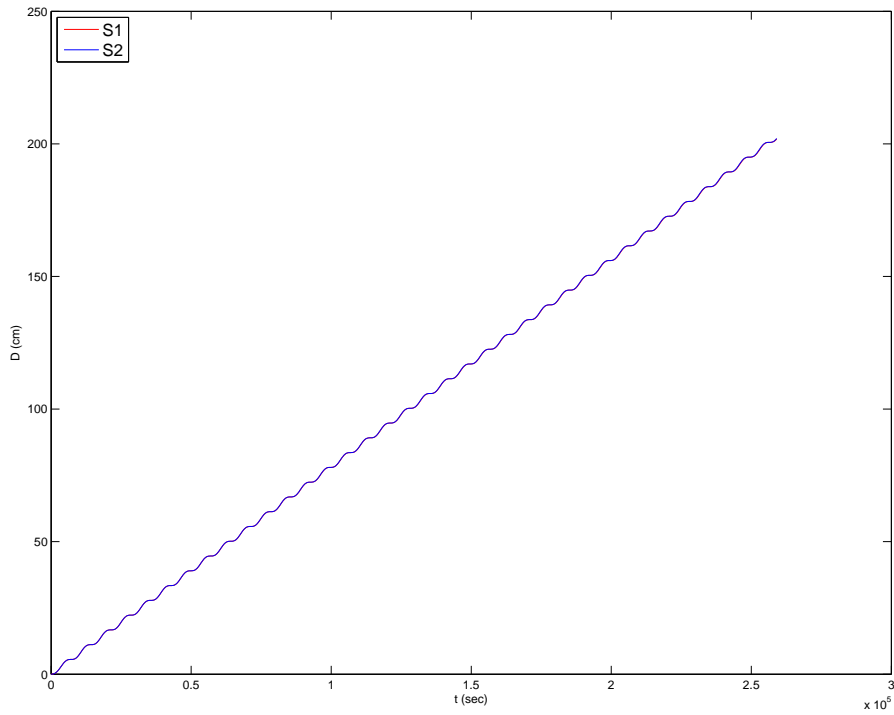
Figure 132: Case 3 for LEO satellites with S2 being closer to the earth than S1, $d = 3$ kilometres, $t = 72$ hours: The distance between the ECI positions of the Newtonian and the nonlinear post–Newtonian solutions, both for S1 and S2, which almost completely overlap.
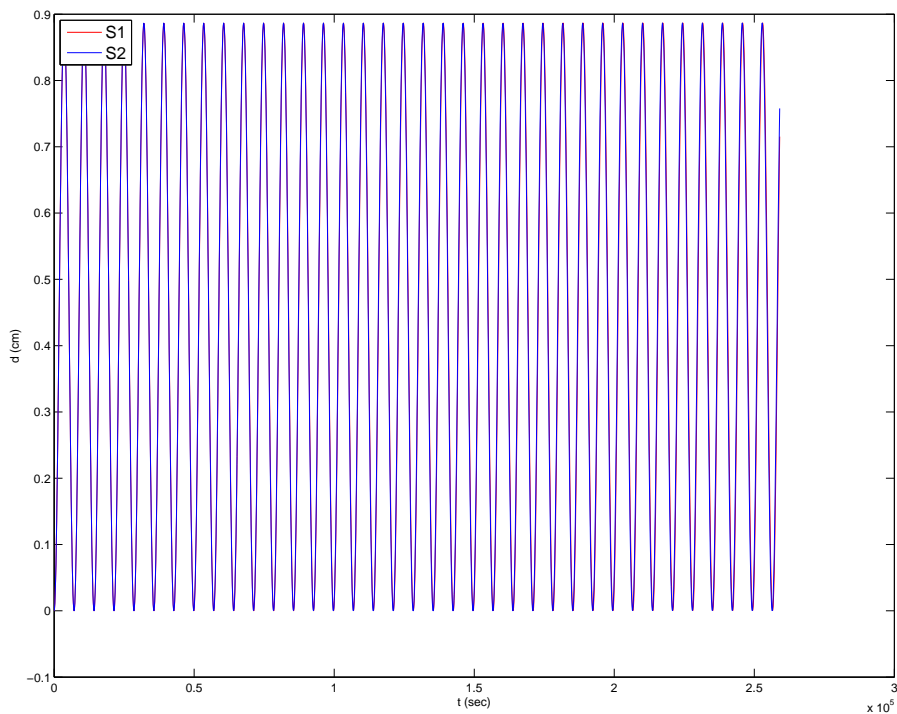

Figure 133: Case 3 for LEO satellites with S2 being closer to the earth than S1, $d = 3$ kilometres, $t = 72$ hours: Difference in distances to the center of the Earth between Newtonian and nonlinear post–Newtonian.
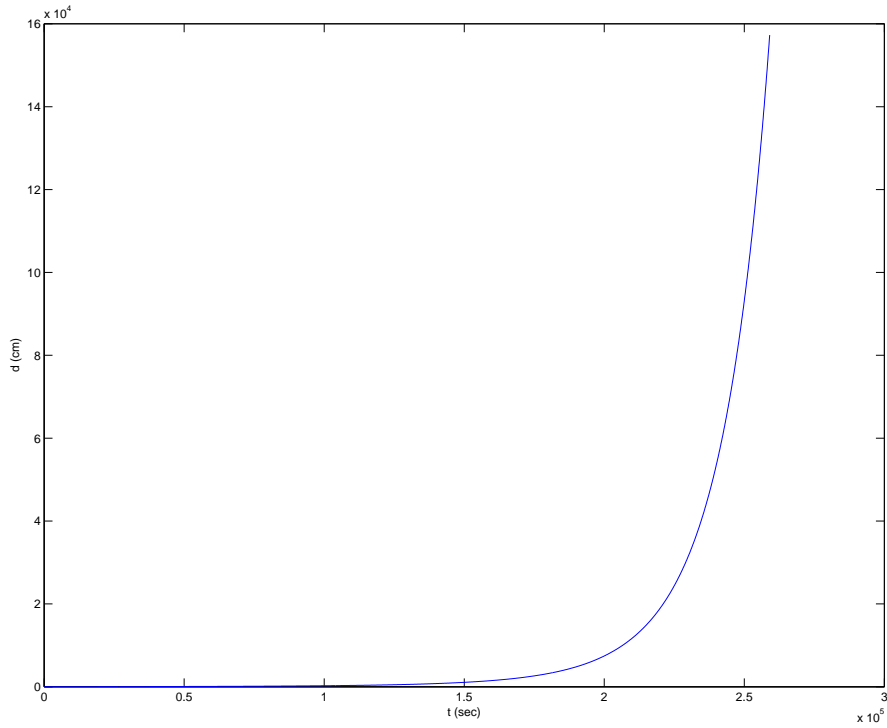
Figure 134: Case 3 for LEO satellites with S2 being closer to the earth than S1, $d = 3$ kilometres, $t = 72$ hours, and nonlinear post–Newtonian formulation: Distance between ECI positions of S2 and S1 and the relative position of S2 with respect to S1.
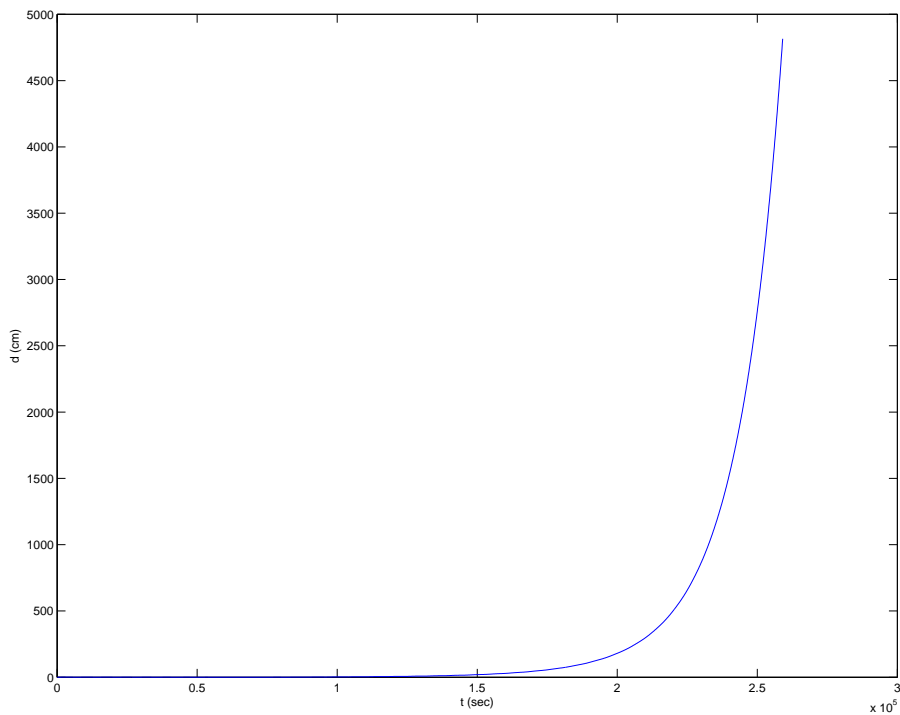

Figure 135: Case 3 for LEO satellites with S2 being closer to the earth than S1, $d = 3$ kilometres, $t = 72$ hours, and nonlinear post–Newtonian formulation: This plot, similar to the above one, shows the difference in distances to the ECI center.

2.3.6 LEO satellites with S2 being farther away from the Earth than S1

2.3.6.1 Case 1

In this test we showcase the solution for small values in both parameters.
The parameters used for this test are $d = 5$ kilometres and $t = 5$ hours.
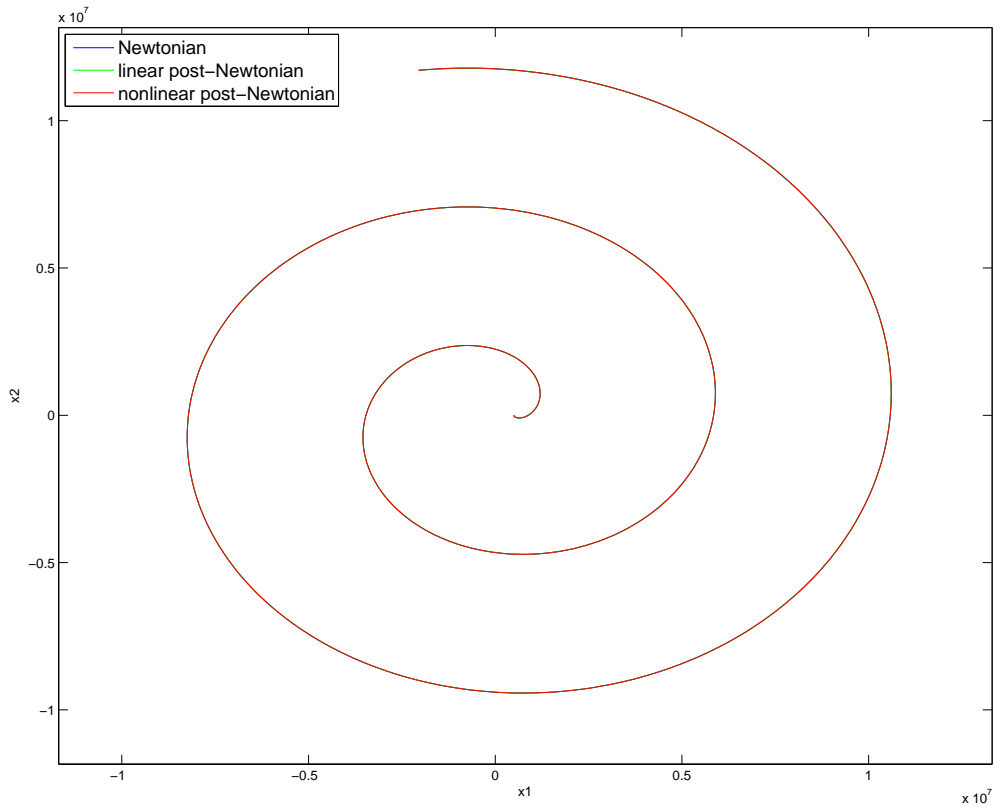
Figure 136: Case 1 for LEO satellites with S2 being farther away from the earth than S1, $d = 5$ kilometres, $t = 5$ hours: Relative motion of S2 with respect to S1.
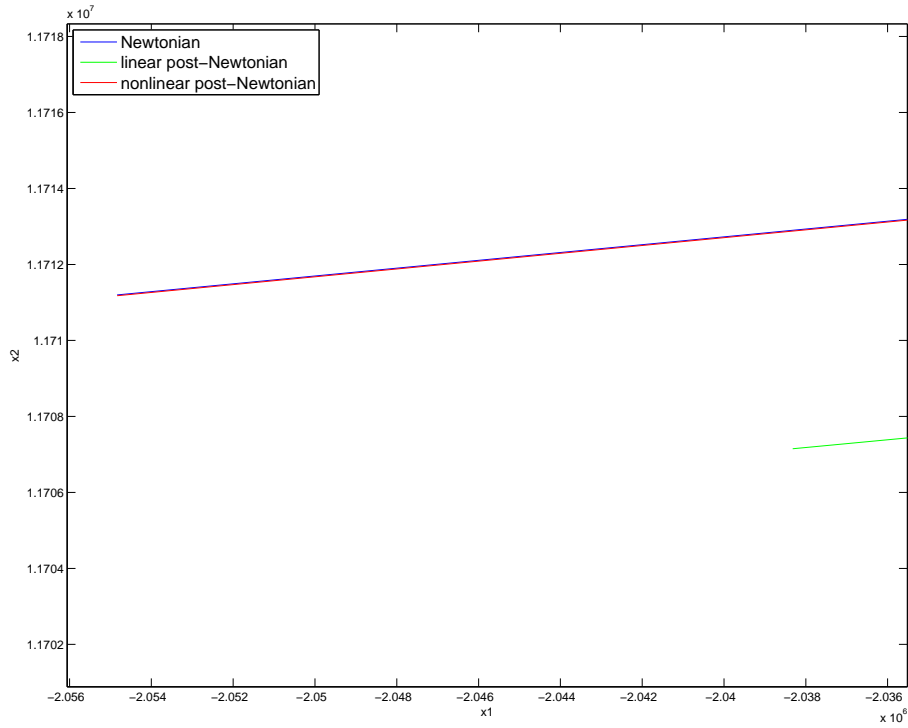
Figure 137: Case 1 for LEO satellites with S2 being farther away from the earth than S1, $d = 5$ kilometres, $t = 5$ hours: Zoomed in version of the previous plot. It is now possible to see the difference between solutions from different formulations.
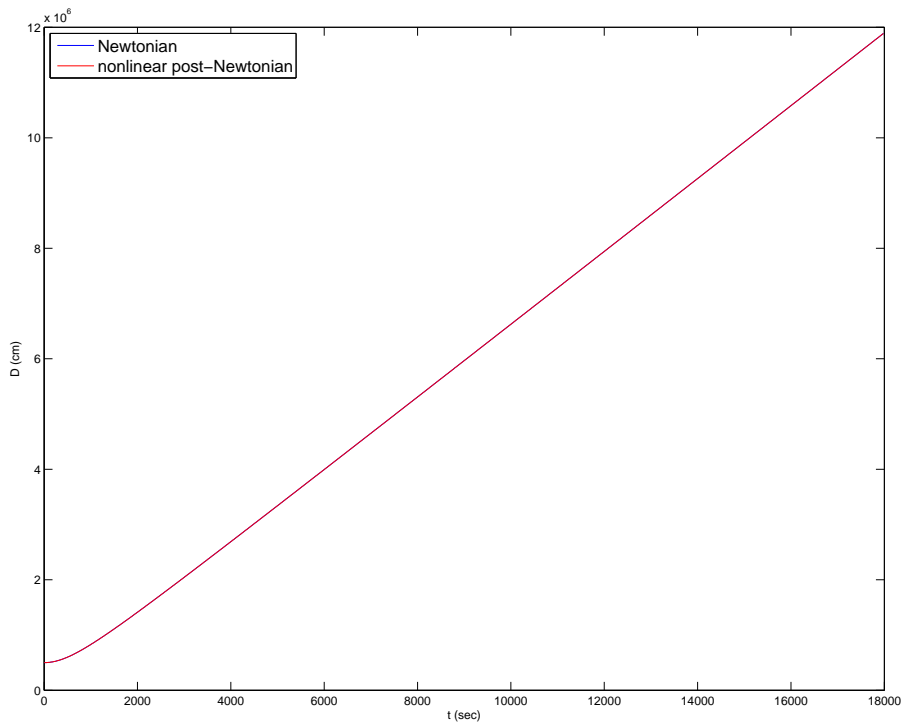

Figure 138: Case 1 for LEO satellites with S2 being farther away from the earth than S1, $d = 5$ kilometres, $t = 5$ hours: Absolute distance between S1 and S2.
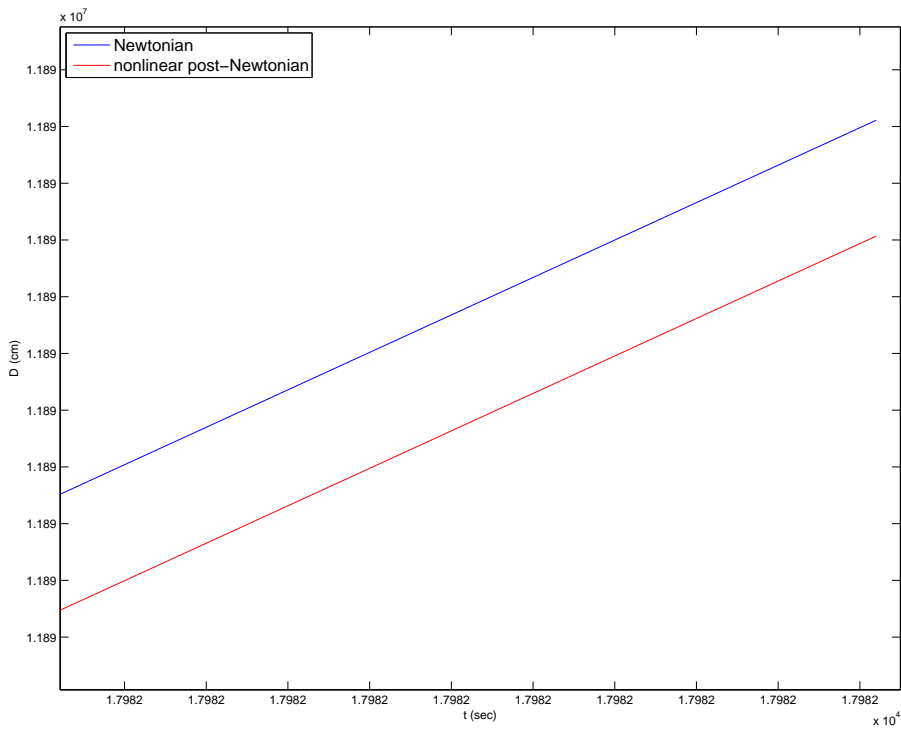
Figure 139: Case 1 for LEO satellites with S2 being farther away from the earth than S1, $d = 5$ kilometres, $t = 5$ hours: Zoomed in version of the previous plot. It is now possible to see differences between solutions from different formulations.
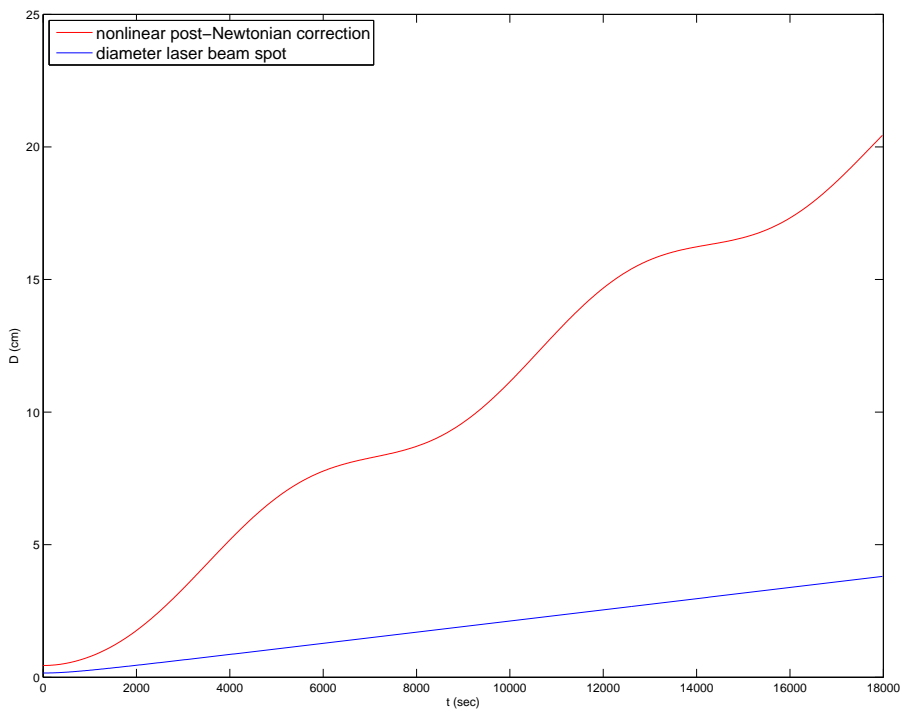

Figure 140: Case 1 for LEO satellites with S2 being farther away from the earth than S1, $d = 5$ kilometres, $t = 5$ hours: Correction provided from the nonlinear post–Newtonian equations compared to the laser beam.
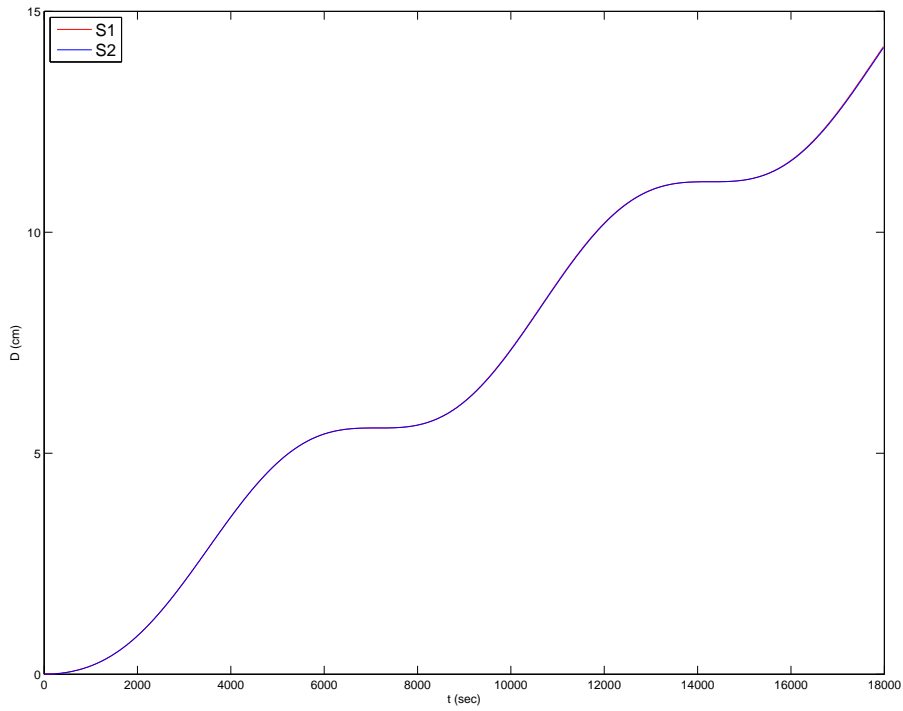
Figure 141: Case 1 for LEO satellites with S2 being farther away from the earth than S1, $d = 5$ kilometres, $t = 5$ hours: The distance between the ECI positions of the Newtonian and the nonlinear post–Newtonian solutions, both for S1 and S2, which almost completely overlap.
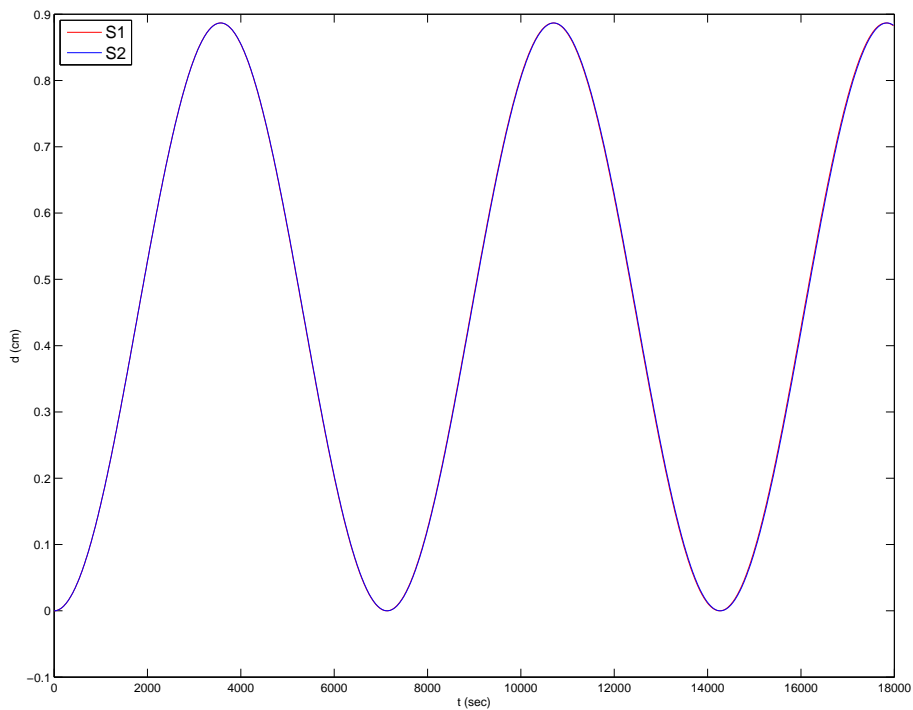

Figure 142: Case 1 for LEO satellites with S2 being farther away from the earth than S1, $d = 5$ kilometres, $t = 5$ hours: Difference in distances to the center of the Earth between Newtonian and nonlinear post–Newtonian.
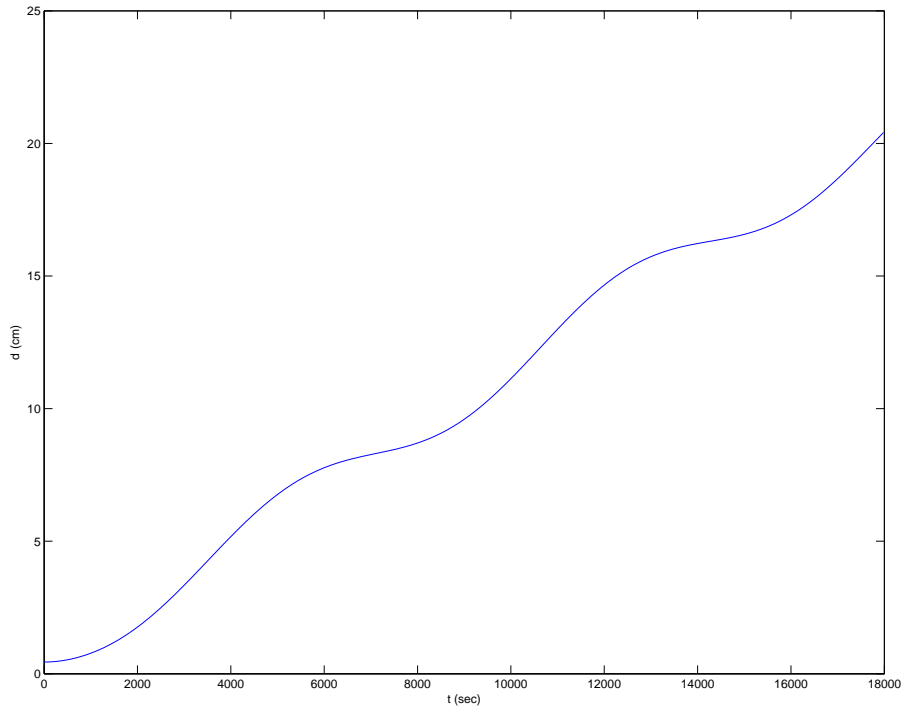
Figure 143: Case 1 for LEO satellites with S2 being farther away from the earth than S1, $d = 5$ kilometres, $t = 5$ hours, and nonlinear post–Newtonian formulation: Distance between ECI positions of S2 and S1 and the relative position of S2 with respect to S1.
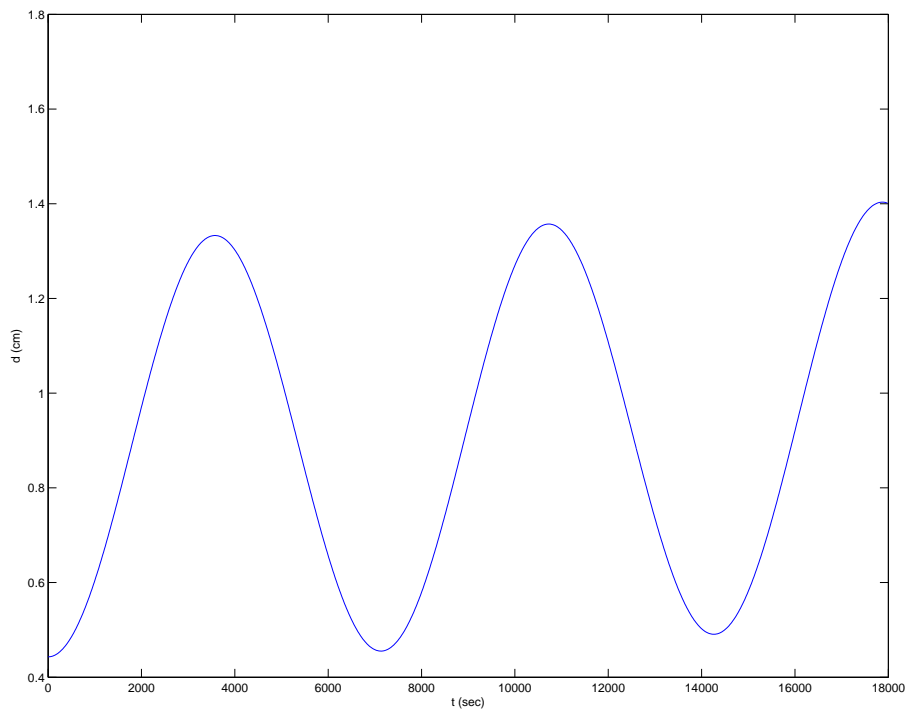

Figure 144: Case 1 for LEO satellites with S2 being farther away from the earth than S1, $d = 5$ kilometres, $t = 5$ hours, and nonlinear post–Newtonian formulation: This plot, similar to the above one, shows the difference in distances to the ECI center.

2.3.6.2 Case 2

For this test, the goal was to increase the value of d as much as possible. The parameters used for this test are $d = 22$ kilometres and $t = 3$ hours.
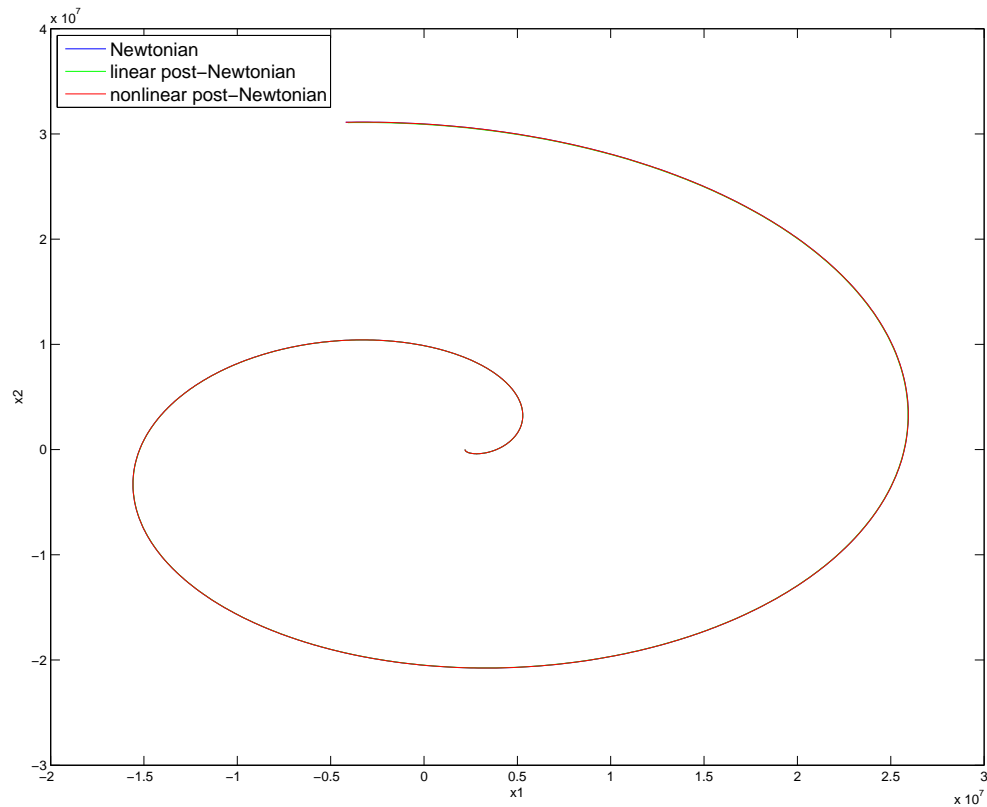

Figure 145: Case 2 for LEO satellites with S2 being farther away from the earth than S1, $d = 22$ kilometres, $t = 3$ hours: Relative motion of S2 with respect to S1.
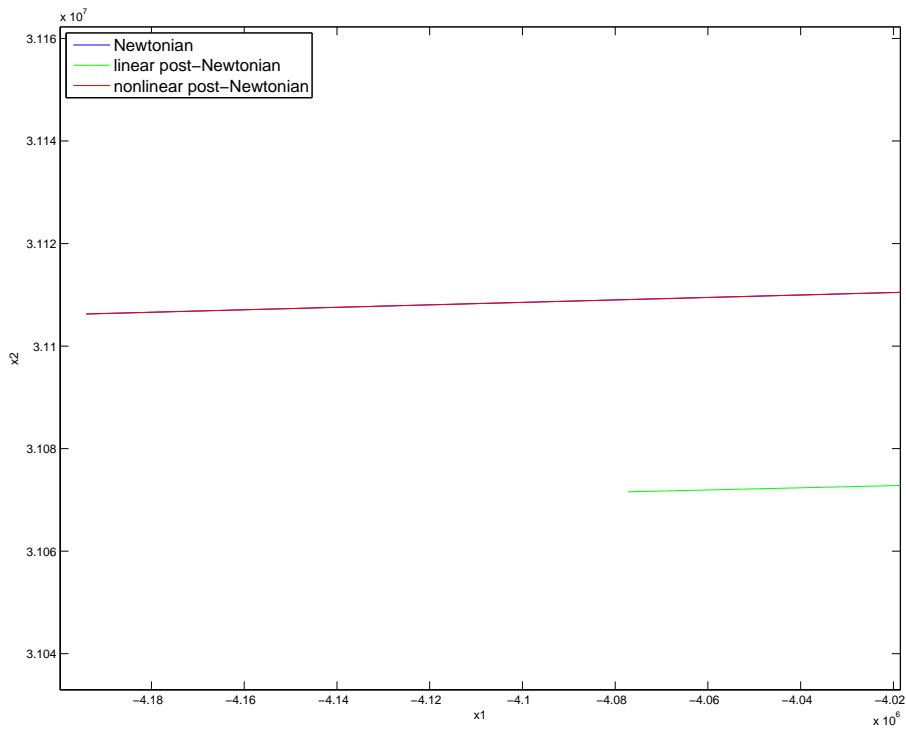
Figure 146: Case 2 for LEO satellites with S2 being farther away from the earth than S1, $d = 22$ kilometres, $t = 3$ hours: Zoomed in version of the previous plot. It is now possible to see the difference between solutions from different formulations.
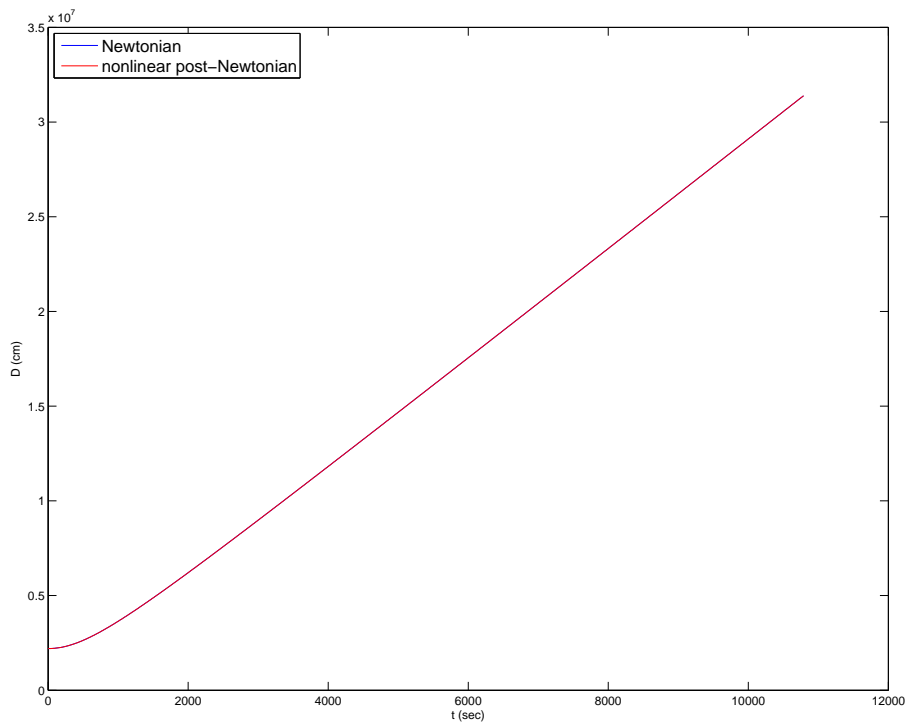

Figure 147: Case 2 for LEO satellites with S2 being farther away from the earth than S1, $d = 22$ kilometres, $t = 3$ hours: Absolute distance between S1 and S2.

91
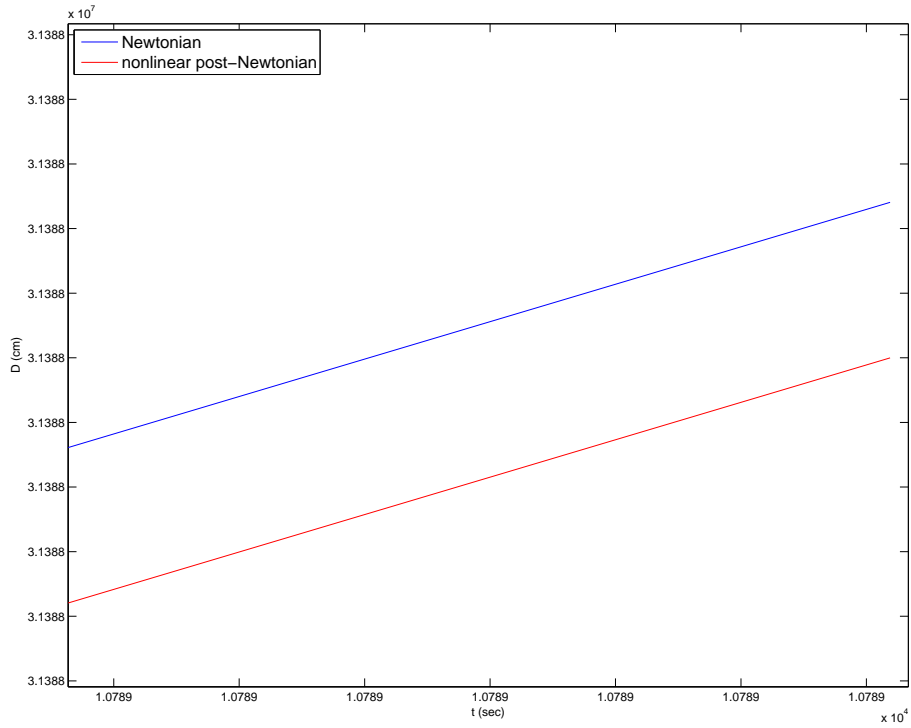
Figure 148: Case 2 for LEO satellites with S2 being farther away from the earth than S1, $d = 22$ kilometres, $t = 3$ hours: Zoomed in version of the previous plot. It is now possible to see differences between solutions from different formulations.
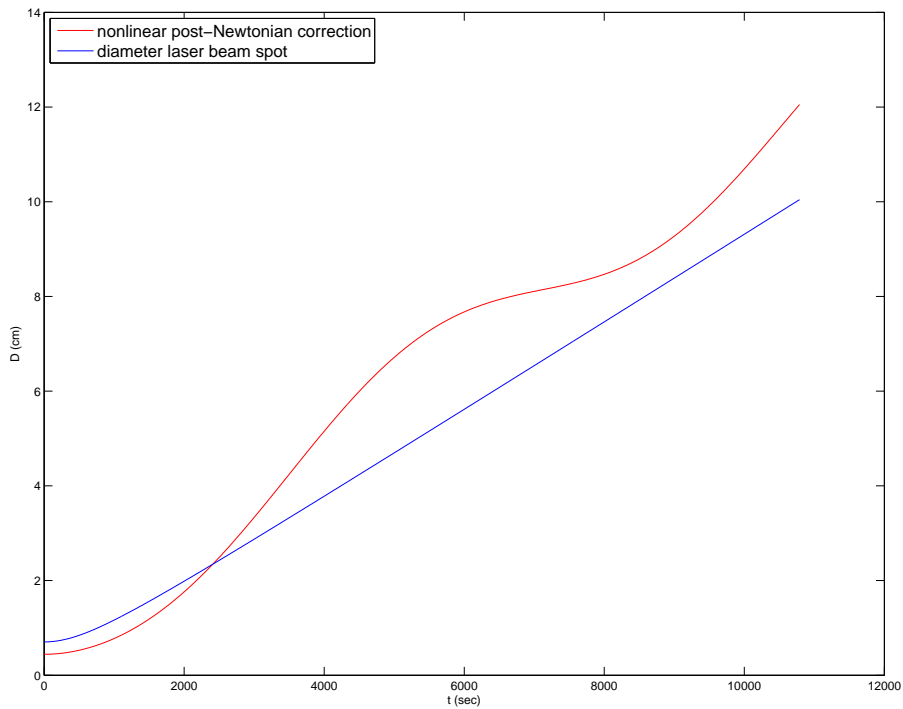

Figure 149: Case 2 for LEO satellites with S2 being farther away from the earth than S1, $d = 22$ kilometres, $t = 3$ hours: Correction provided from the nonlinear post–Newtonian equations compared to the laser beam.
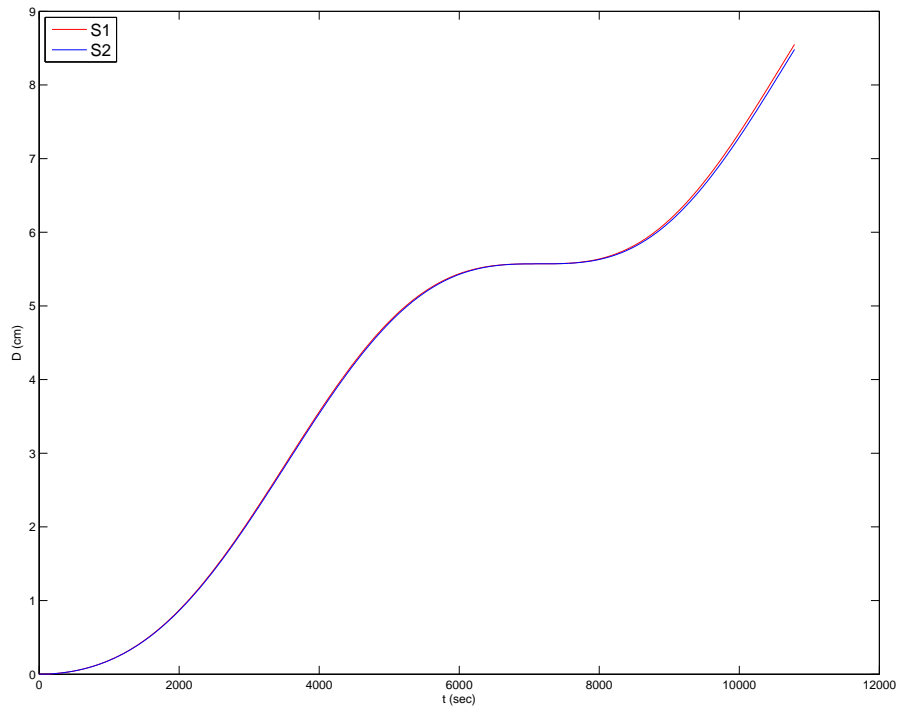
Figure 150: Case 2 for LEO satellites with S2 being farther away from the earth than S1, $d = 22$ kilometres, $t = 3$ hours: The distance between the ECI positions of the Newtonian and the nonlinear post–Newtonian solutions, both for S1 and S2, which almost completely overlap.
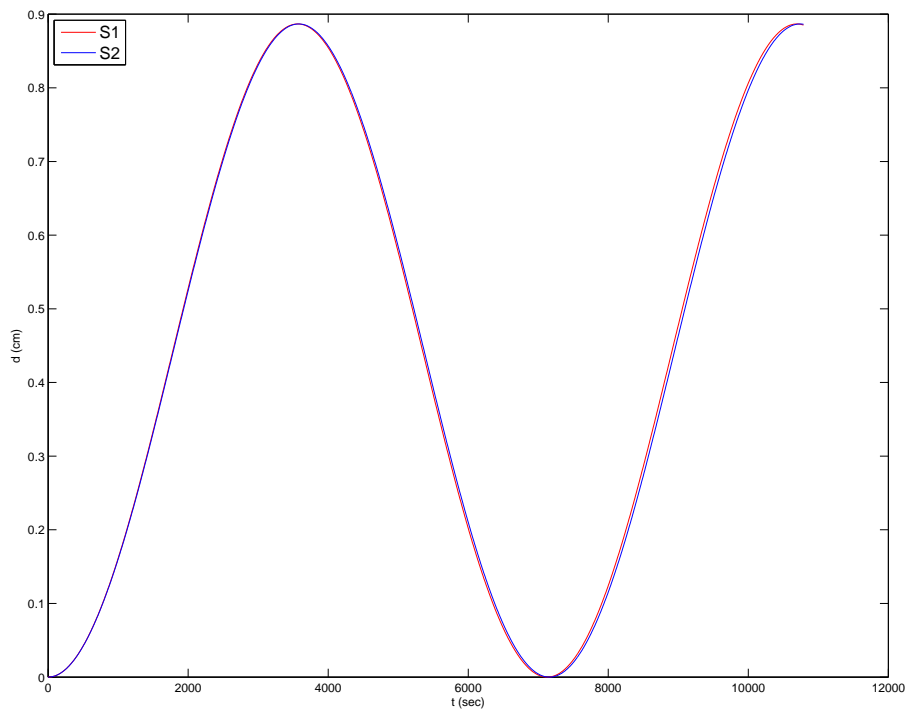

Figure 151: Case 2 for LEO satellites with S2 being farther away from the earth than S1, $d = 22$ kilometres, $t = 3$ hours: Difference in distances to the center of the Earth between Newtonian and nonlinear post–Newtonian.
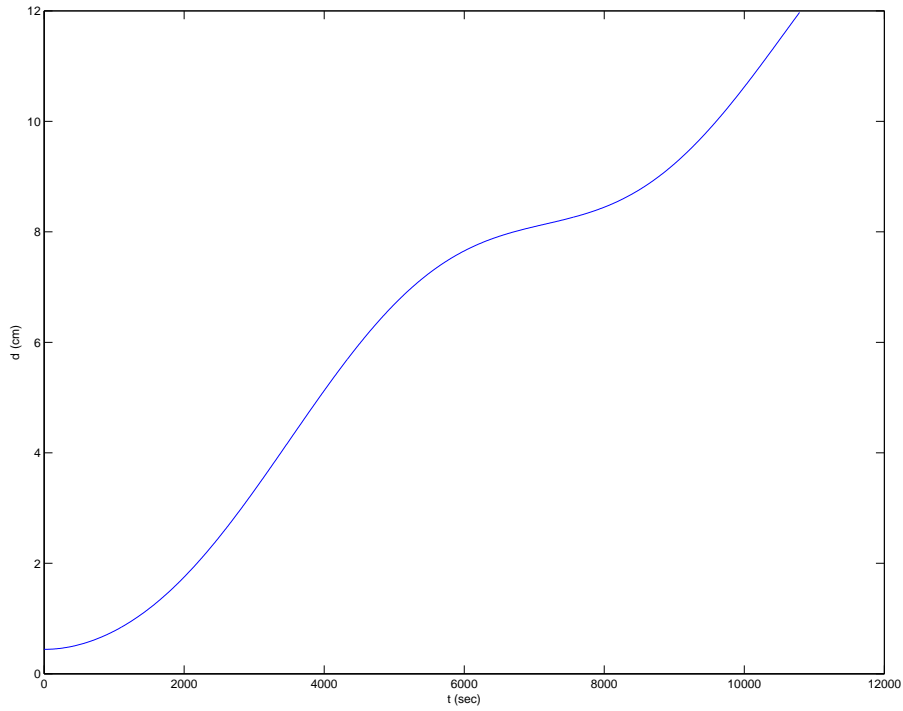
Figure 152: Case 2 for LEO satellites with S2 being farther away from the earth than S1, $d = 22$ kilometres, $t = 3$ hours, and nonlinear post–Newtonian formulation: Distance between ECI positions of S2 and S1 and the relative position of S2 with respect to S1.
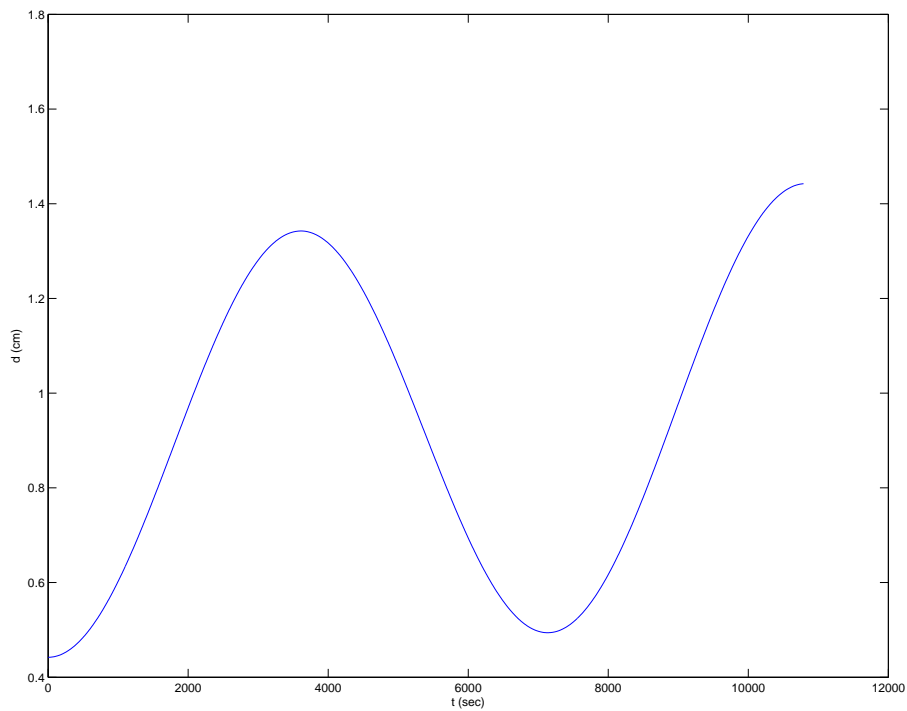

Figure 153: Case 2 for LEO satellites with S2 being farther away from the earth than S1, $d = 22$ kilometres, $t = 3$ hours, and nonlinear post–Newtonian formulation: This plot, similar to the above one, shows the difference in distances to the ECI center.

2.3.6.3   Case 3

For this test, the goal was to increase the value of t as much as possible. The parameters used for this test are $d = 3$ kilometres and $t = 36$ hours.
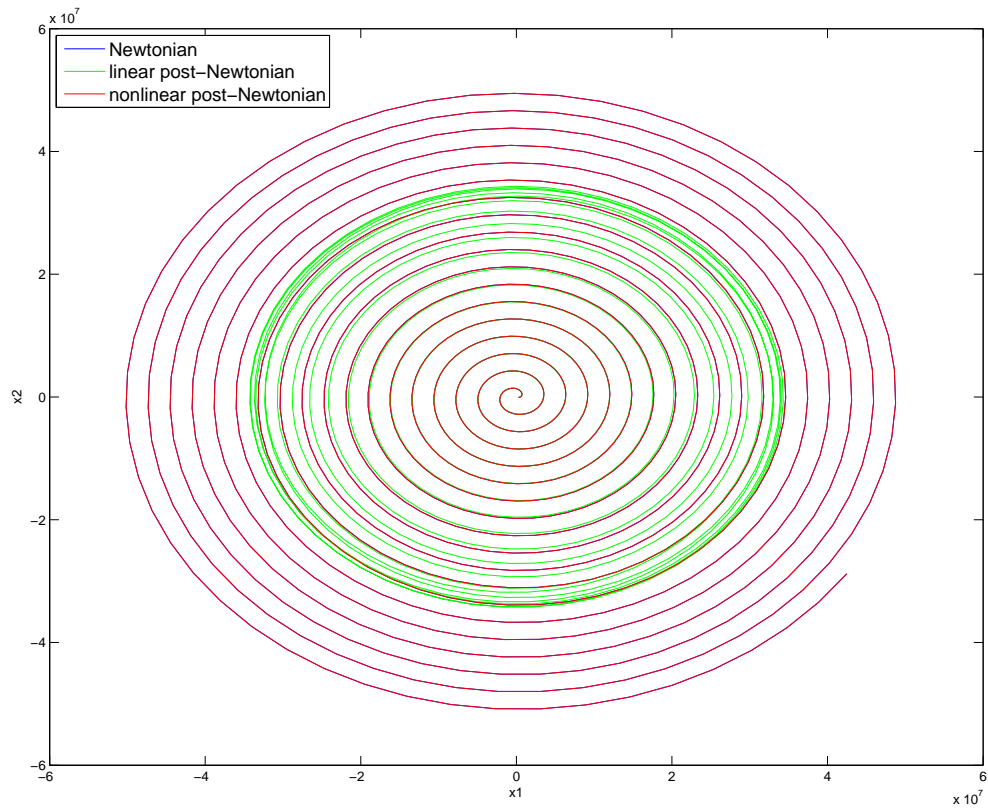

Figure 154: Case 3 for LEO satellites with S2 being farther away from the earth than S1, $d = 3$ kilometres, $t = 36$ hours: Relative motion of S2 with respect to S1.
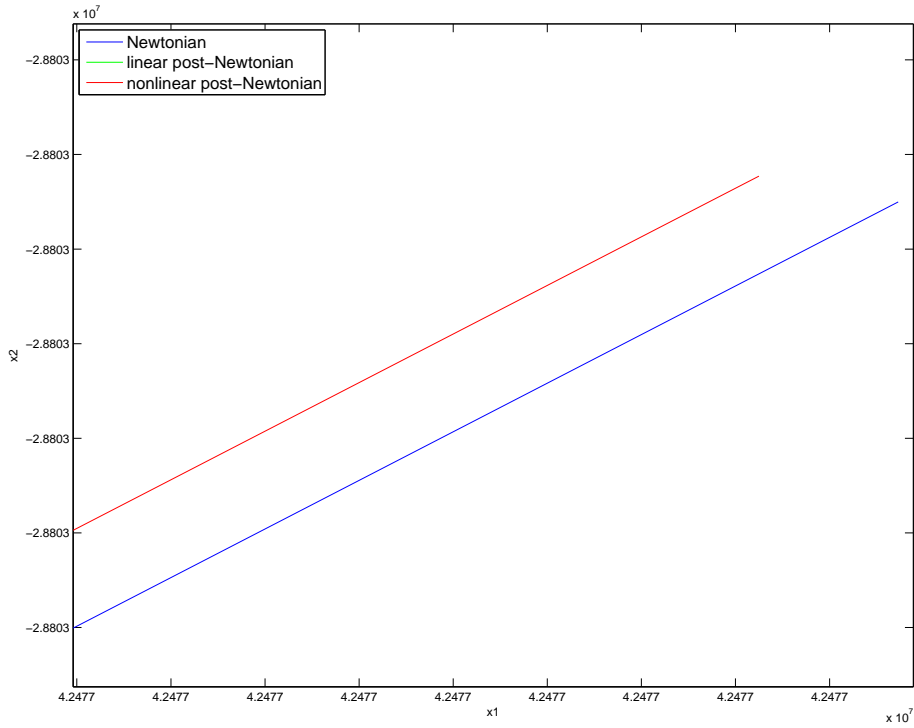
Figure 155: Case 3 for LEO satellites with S2 being farther away from the earth than S1, $d = 3$ kilometres, $t = 36$ hours: Zoomed in version of the previous plot. It is now possible to see the difference between solutions from different formulations.
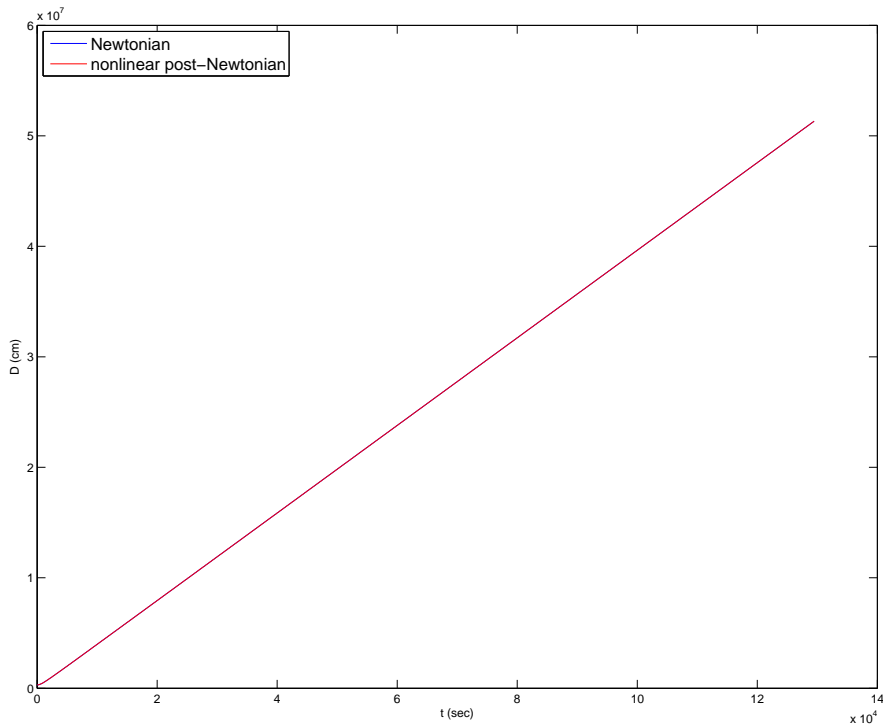
Figure 156: Case 3 for LEO satellites with S2 being farther away from the earth than S1, $d = 3$ kilometres, $t = 36$ hours: Absolute distance between S1 and S2.
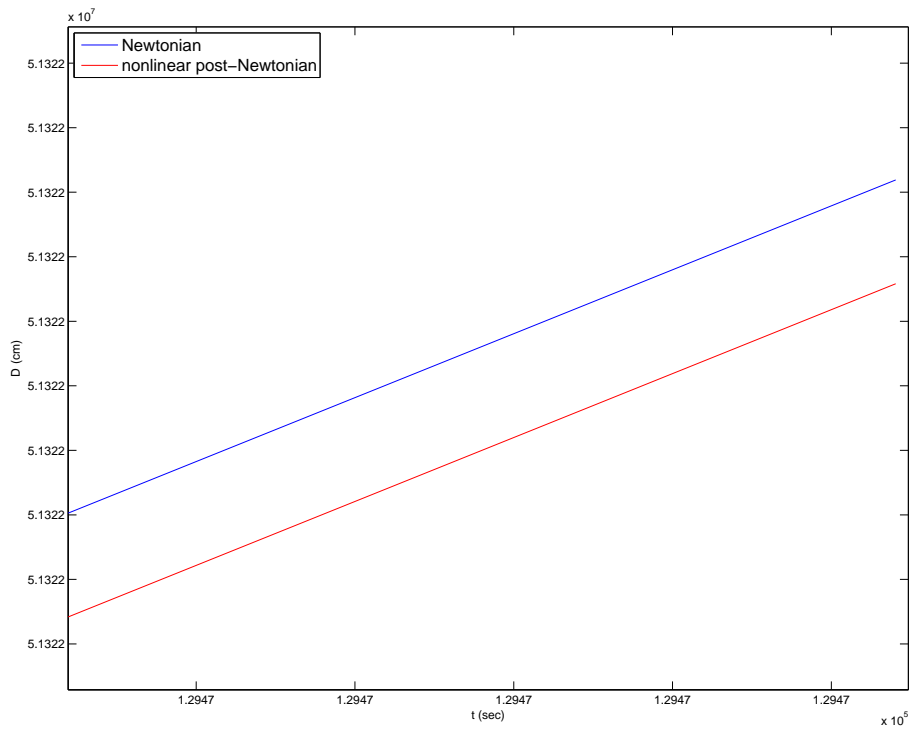
Figure 157: Case 3 for LEO satellites with S2 being farther away from the earth than S1, $d = 3$ kilometres, $t = 36$ hours: Zoomed in version of the previous plot. It is now possible to see differences between solutions from different formulations.
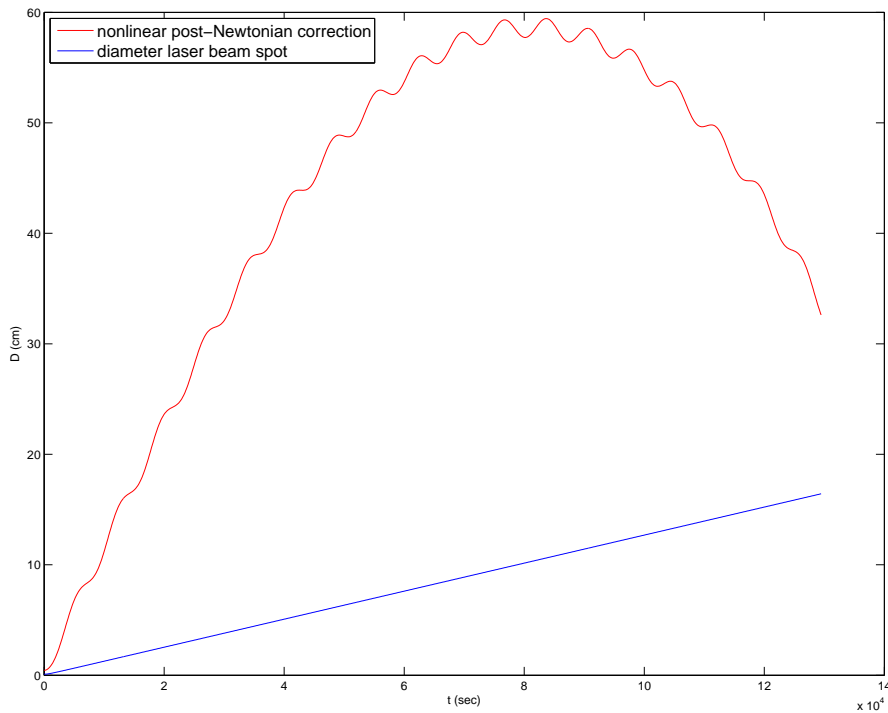

Figure 158: Case 3 for LEO satellites with S2 being farther away from the earth than S1, $d = 3$ kilometres, $t = 36$ hours: Correction provided from the nonlinear post–Newtonian equations compared to the laser beam.

97
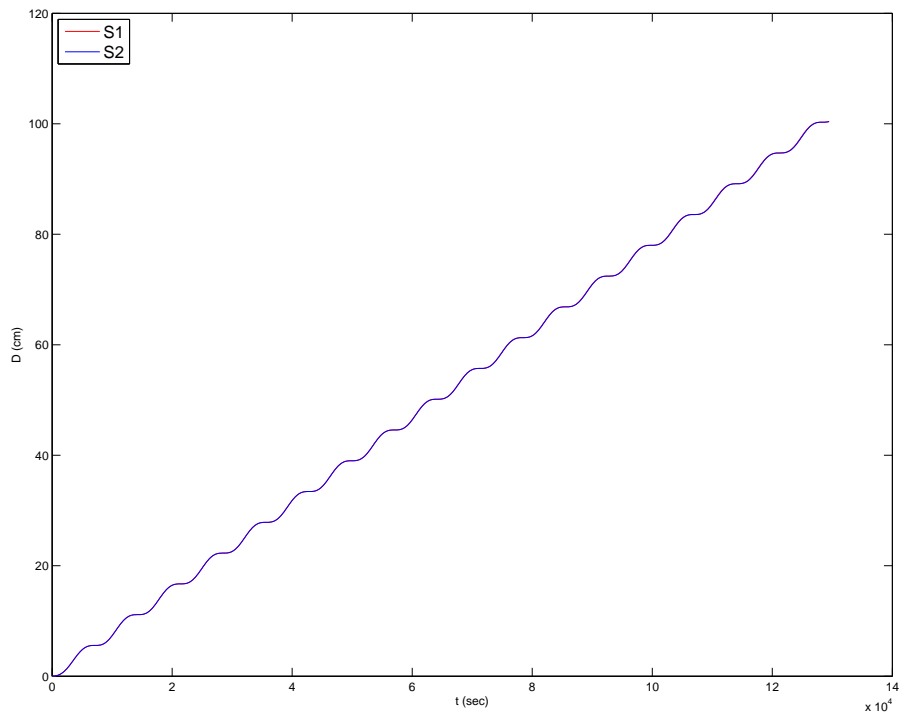
Figure 159: Case 3 for LEO satellites with S2 being farther away from the earth than S1, $d = 3$ kilometres, $t = 36$ hours: The distance between the ECI positions of the Newtonian and the nonlinear post–Newtonian solutions, both for S1 and S2, which almost completely overlap.
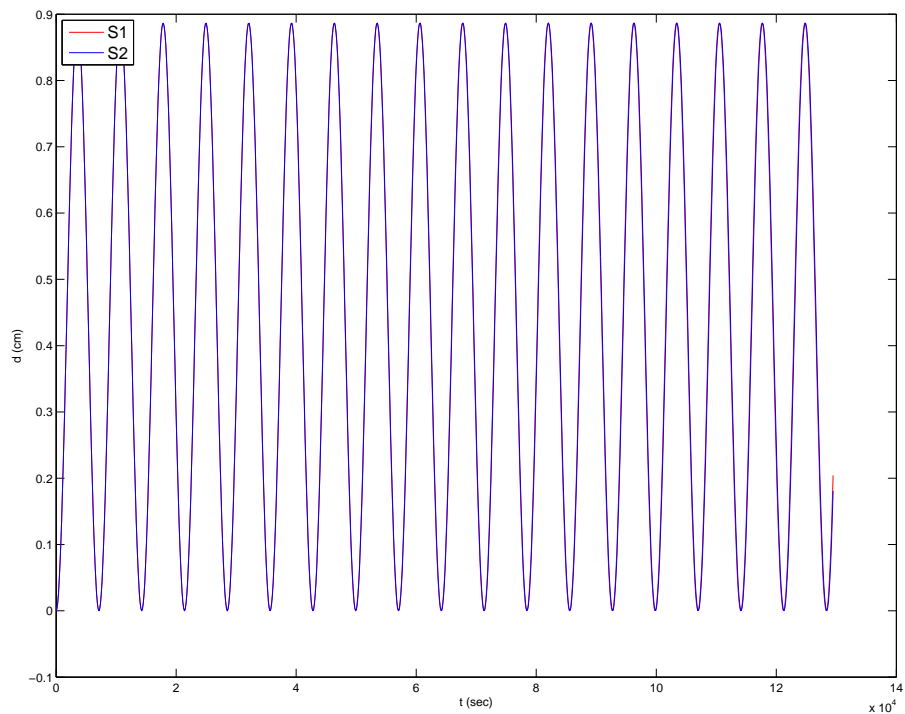

Figure 160: Case 3 for LEO satellites with S2 being farther away from the earth than S1, $d = 3$ kilometres, $t = 36$ hours: Difference in distances to the center of the Earth between Newtonian and nonlinear post–Newtonian.
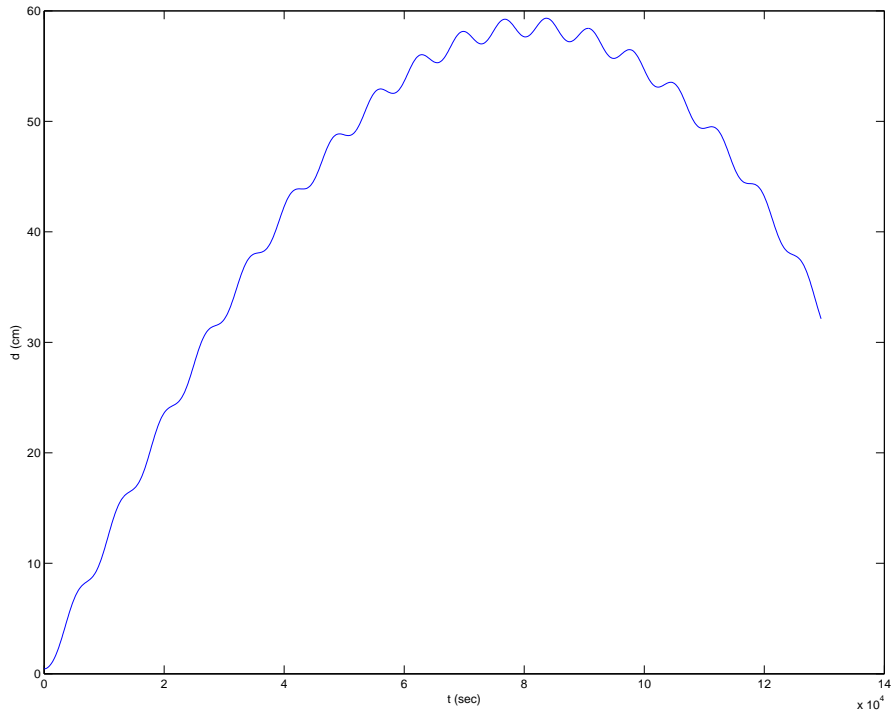
Figure 161: Case 3 for LEO satellites with S2 being farther away from the earth than S1, $d = 3$ kilometres, $t = 36$ hours, and nonlinear post–Newtonian formulation: Distance between ECI positions of S2 and S1 and the relative position of S2 with respect to S1.
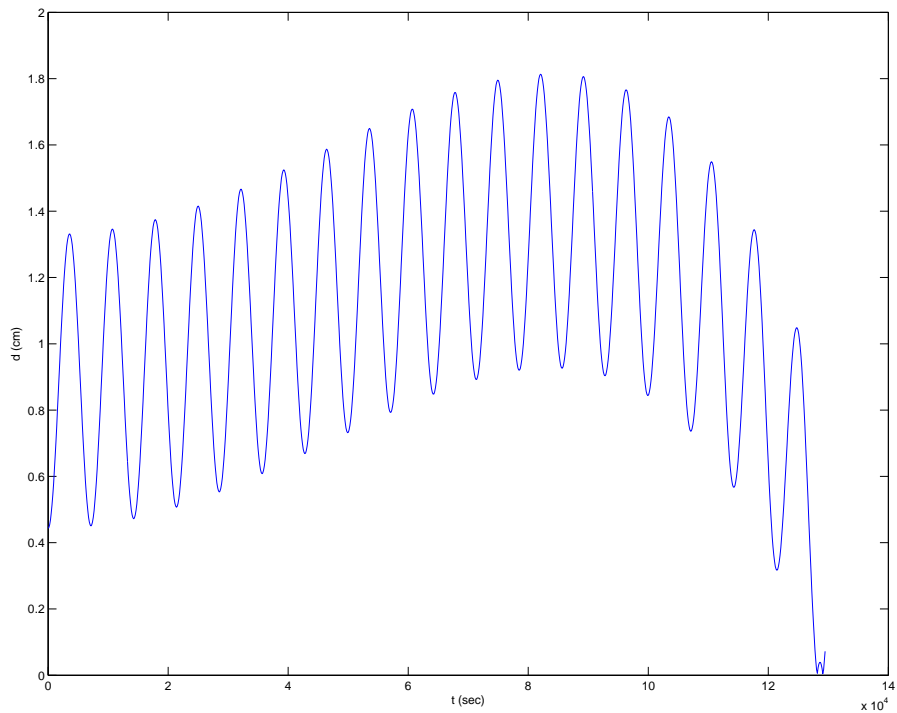

Figure 162: Case 3 for LEO satellites with S2 being farther away from the earth than S1, $d = 3$ kilometres, $t = 36$ hours, and nonlinear post–Newtonian formulation: This plot, similar to the above one, shows the difference in distances to the ECI center.

2.4 Conclusions

The simulations carried out in the present work, suggest to conclude that in all considered scenarios, where GEO, MEO and LEO satellites are involved, the post–Newtonian linear equations for the relative motion are not appropriate to model the two–way laser links from the APT systems to the destination objects at practically any instant. The reason is that the absence of the nonlinear terms modifies the behaviour of the solutions significantly, even at the early stages of the integrations, cf. Figures 1–2, 10–11, 19–20, 28–29, 37–38, 46–47, 55–56, 64–65, 73–74, 82–83, 91–92, 100–101, 109–110, 118–119, 127–128, 136–137, 145–146, and 154–155.

In fact, the solutions of the nonlinear equations appear to be more reliable than those of the linear equations when computing the post–Newtonian corrections to the Newtonian solutions, because their size fits rather well with the size of the gravitational corrections included in the post–Newtonian approximation of the Schwarzschild field for the neighborhood of the Earth (1). On the other hand, the contributions of the nonlinear terms amount to quantities that increase, along with the distance from the APT systems to the targets, as the integration time increases. In fact, these quantities are measurable at practically any instant prefixed to perform the link procedure, so that they are susceptible of being taken into account, at least within the intervals considered for d in each case. The reason is that the diameter of the spot of the laser beam supposedly used by the systems stays smaller than the size of the corrections from instants very close to the initial integration instant, see Figures 5, 14, 23, 32, 41, 50, 59, 68, 77, 86, 95, 104, 113, 122, 131, 140, 149, and 158.

Finally, it is clear that the curved structure of space around the Earth described by the post–Newtonian model in (1) manifests itself in the post–Newtonian nonlinear equations for the relative motion. In fact, unlike for the Newtonian equations, there are significant differences in all the scenarios considered here between the predictions obtained with these equations and those predicted by taking the differences between the post–Newtonian ECI orbital equations for the destination objects and the APT systems, see Figures 8–9, 17–18, 26–27, 35–36, 44–45, 53–54, 62–63, 71–72, 80–81, 89–90, 98–99, 107–108, 116–117, 125–126, 134–135, 143–144, 152–153, and 161–162.

3   Stationary Wigner Equation

3.1   Introduction

This part of the thesis is dedicated to the numerical simulation of the stationary Wigner equation, in a kinetic formulation from quantum mechanics.

The problem in its standard form is an Index-2 differential algebraic equation (DAE). Here, standard form means that $v = 0$ is one of the discrete velocities and the aim is to find the associated solution. If $v \neq 0$, the problem becomes an easily solvable ordinary differential equation (ODE).

For the numerical tests, we therefore, introduce the parameter $v := \varepsilon$, which will deviate the problem away from the standard form. By letting $\varepsilon \to 0$, we shall observe how the solution of the ODE converges to the limit solution of a DAE.

After the first series of tests, we will introduce an additional parameter, μ, and simulate the problem again. The purpose of the second simulation is to understand the preliminary results and validate the conclusions drawn from the first series of tests. Although, we could gain some inside in the problem structure, further investigations are still required.

3.2   Analytical problem and its discretization

The continuous equation has the following form [24]:

$$vw_x(x,v) - \Theta[V]w(x,v) = 0, \quad 0 < x < L, \quad v \in \mathbb{R},$$

where

$$\Theta[V]w(x,v) = \frac{1}{\sqrt{2\pi}} \int_{\mathbb{R}} \delta V(x,\eta)\hat{w}(x,\eta)\exp(iv\eta)d\eta,$$

$$\delta V(x,\eta) = i\left[V\left(x + \frac{\eta}{2}\right) - V\left(x - \frac{\eta}{2}\right)\right],$$

$$\hat{w}(x,\eta) = \frac{1}{\sqrt{2\pi}} \int_{\mathbb{R}} w(x,v)\exp(-iv\eta)dv.$$

In the first step, we discretize the operator Θ and obtain

$$(A(x)w)_j = \sum_{k \in \mathbb{Z}} w_k a_{j-k}(x), \quad j \in \mathbb{Z},$$

where

$$a_j(x) = \frac{1}{2\eta_0} \int_{-\eta_0}^{\eta_0} \delta V(x,\eta)\exp\left(\frac{i\pi j\eta}{\eta_0}\right)d\eta.$$

The parameter η_0 specifies the finite support of the potential V, which we focus on next. In Figure 163, one can see the potential $V(x) = v_0\chi_{[-l,l]}$ which was chosen for the numerical simulation. Since η_0 is the bandwidth of the potential, it follows that $\eta_0 = 2l$.
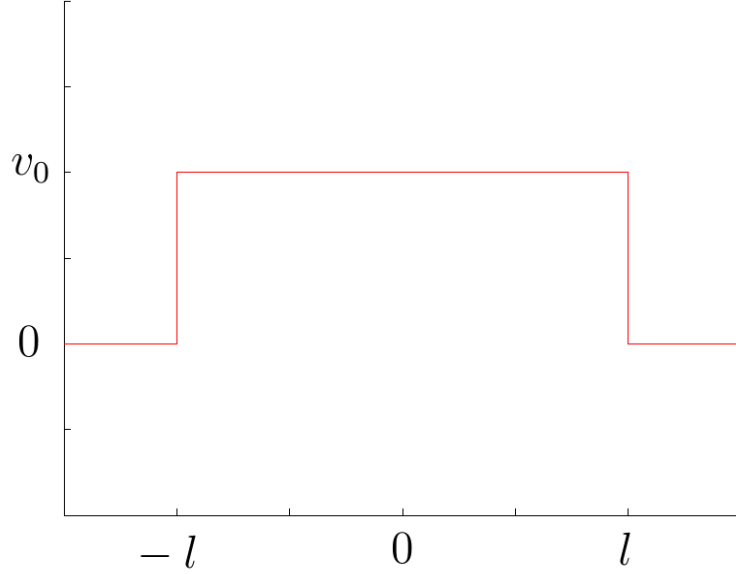
Figure 163: Image of the potential V used for the numerical tests.

This potential results in δV of the form

$$\delta V = iv_0 \left[\chi_{[-l,l]} \left(x + \frac{\eta}{2} \right) - \chi_{[-l,l]} \left(x - \frac{\eta}{2} \right) \right].$$

From the above definitions, after few simplifying steps, we obtain the following representation for a_j,

$$a_j(x) = \frac{v_0}{j} \begin{cases} \cos \left[j\pi \left(1 + \frac{2x}{\eta_0} \right) \right] - (-1)^j, & 0 < x < \eta_0, \\ -\cos \left[j\pi \left(1 + \frac{2x}{\eta_0} \right) \right] + (-1)^j, & -\eta_0 < x \le 0. \end{cases} \tag{3}$$

This result allows us to reformulate the original problem, with $L = \eta_0 = 2l$. The new equation is

$$T w_x(x,v) - A(x)w(x,v) = 0, \quad -L < x < L, \tag{4}$$

with $w(x)$ being now a vector valued function. The length of this vector is defined by the set J, which in our simulations is either $J = \{-1,0,1,2\}$ or $J = \{-2,-1,0,1,2,3\}$. In Figure 164, the discretization of w is shown, The arrows indicate where the boundary conditions are formulated.
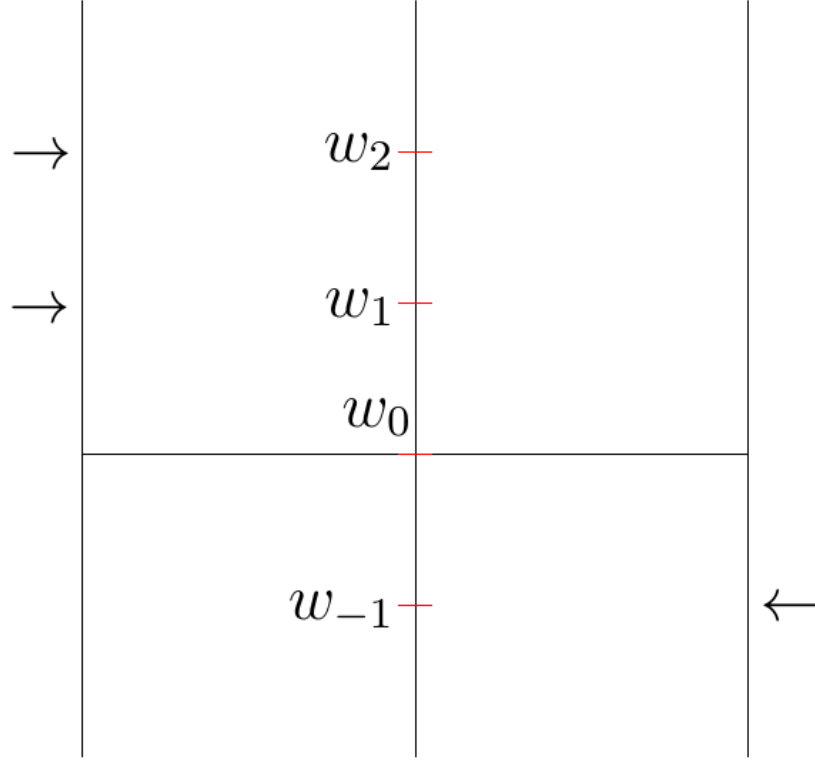
Figure 164: Discretization of w for $J = \{-1, 0, 1, 2\}$.

Clearly, after fixing J, we obtain either

$$w(x) = \begin{cases} w_{-1}(x), \\ w_0(x), \\ w_1(x), \\ w_2(x), \end{cases} \quad \text{or} \quad w(x) = \begin{cases} w_{-2}(x), \\ w_{-1}(x), \\ w_0(x), \\ w_1(x), \\ w_2(x), \\ w_3(x), \end{cases}$$

where the matrix T is defined as

$$T = \operatorname{diag}(v_j)_{j \in J} \in \mathbb{R}^{|J| \times |J|}, \quad v_j = \frac{(j - \varepsilon)\pi}{L}.$$

Here, one can see how the parameter ε, mentioned in the introduction, enters the system. As already said, for $\varepsilon = 0$ the problem is a system of DAEs, while for $\varepsilon > 0$ it is a system of ODEs, linear in each case.

The matrix A, a discretization of Θ, is a skew-symmetric, Toeplitz matrix, which means $a_{jk}(x) = a_{j-k}(x)$. The values for $a_j(x)$ are given in (3).

To summarize all this, we will show how the complete system looks for the two cases of J.

First, $J = \{-1, 0, 1, 2\}$

$$\begin{pmatrix} \frac{(-1-\varepsilon)\pi}{\eta_0} & 0 & 0 & 0 \\ 0 & \frac{-\varepsilon\pi}{\eta_0} & 0 & 0 \\ 0 & 0 & \frac{(1-\varepsilon)\pi}{\eta_0} & 0 \\ 0 & 0 & 0 & \frac{(2-\varepsilon)\pi}{\eta_0} \end{pmatrix} \begin{pmatrix} \frac{dw_{-1}}{dx} \\ \frac{dw_0}{dx} \\ \frac{dw_1}{dx} \\ \frac{dw_2}{dx} \end{pmatrix} -$$

$$\begin{pmatrix} a_0(x) & a_{-1}(x) & a_{-2}(x) & a_{-3}(x) \\ a_1(x) & a_0(x) & a_{-1}(x) & a_{-2}(x) \\ a_2(x) & a_1(x) & a_0(x) & a_{-1}(x) \\ a_3(x) & a_2(x) & a_1(x) & a_0(x) \end{pmatrix} \begin{pmatrix} w_{-1} \\ w_0 \\ w_1 \\ w_2 \end{pmatrix} = 0,$$

and for $J = \{-2, -1, 0, 1, 2, 3\}$

$$\begin{pmatrix} \frac{(-2-\varepsilon)\pi}{\eta_0} & 0 & 0 & 0 & 0 & 0 \\ 0 & \frac{(-1-\varepsilon)\pi}{\eta_0} & 0 & 0 & 0 & 0 \\ 0 & 0 & \frac{-\varepsilon\pi}{\eta_0} & 0 & 0 & 0 \\ 0 & 0 & 0 & \frac{(1-\varepsilon)\pi}{\eta_0} & 0 & 0 \\ 0 & 0 & 0 & 0 & \frac{(2-\varepsilon)\pi}{\eta_0} & 0 \\ 0 & 0 & 0 & 0 & 0 & \frac{(3-\varepsilon)\pi}{\eta_0} \end{pmatrix} \begin{pmatrix} \frac{dw_{-2}}{dx} \\ \frac{dw_{-1}}{dx} \\ \frac{dw_0}{dx} \\ \frac{dw_1}{dx} \\ \frac{dw_2}{dx} \\ \frac{dw_3}{dx} \end{pmatrix} -$$

$$\begin{pmatrix} a_0(x) & a_{-1}(x) & a_{-2}(x) & a_{-3}(x) & a_{-4}(x) & a_{-5}(x) \\ a_1(x) & a_0(x) & a_{-1}(x) & a_{-2}(x) & a_{-3}(x) & a_{-4}(x) \\ a_2(x) & a_1(x) & a_0(x) & a_{-1}(x) & a_{-2}(x) & a_{-3}(x) \\ a_3(x) & a_2(x) & a_1(x) & a_0(x) & a_{-1}(x) & a_{-2}(x) \\ a_4(x) & a_3(x) & a_2(x) & a_1(x) & a_0(x) & a_{-1}(x) \\ a_5(x) & a_4(x) & a_3(x) & a_2(x) & a_1(x) & a_0(x) \end{pmatrix} \begin{pmatrix} w_{-2} \\ w_{-1} \\ w_0 \\ w_1 \\ w_2 \\ w_3 \end{pmatrix} = 0.$$

Finally, we specify the boundary conditions,

$$w_j(-L) = 0, \quad j \geq 0, \quad w_j(L) = 1, \quad j < 0.$$

3.3 Numerical algorithm

In this section, we specify the solution algorithm, which is a standard polynomial collocation methods known from the ODE context, and its modification suitable to deal with higher index DAEs.

3.3.1 Collocation method for systems of ODEs

In order to specify the collocation method [25], we first introduce a mesh

$$\pi := \{a = t_0 < t_1 < \ldots < t_i < t_{i+1} < \ldots < t_N = b\},$$

with the step sizes $h_i := t_{i+1} - t_i$, $i = 0, \ldots, N-1$. In each subinterval $[t_i, t_{i+1}]$, we insert m collocation points $\tau_{ik} := t_i + h_i \rho_k$, $k = 1, \ldots, m$, using m values $0 \le \rho_1 < \ldots < \rho_m \le 1$, see Figure 165.
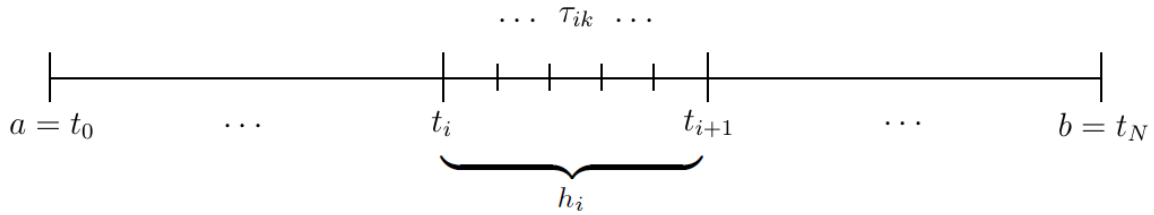
Figure 165: Computational grid, including all mesh and collocation points.

As a solution ansatz, we choose a globally continuous piecewise polynomial function which reduces to a polynomial of the degree $\le m$ in each subinterval of the mesh. In order to calculate the coefficients in the ansatz, we require that the ODE system is exactly (up to the round-off errors) satisfied in each collocation point and satisfies the initial/boundary conditions.

3.3.2 Least Square Collocation method for DAEs

Since, we intend to solve an Index-2 DAE system which is ill-posed, the above standard collocation is not a method of choice, since it shows a divergent behaviour in general. Therefore, we designed a variant of the collocation [26], which shows a convergent behaviour for higher index DAEs. The idea of this modification is as follows: In addition to the collocation points specified by the set $\{\rho_i\}_{i=1}^s$, we introduce new collocation points defined by $\{\sigma_i\}_{i=1}^q \in [0, 1]$ and we require the DAE system to be satisfied exactly at those additional points as well. Clearly, the resulting discrete system is overdetermined and will be solved in the least squares sense.
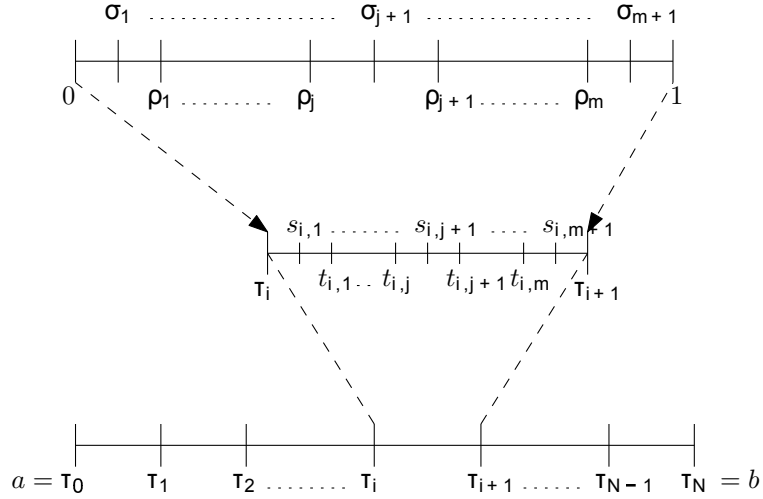
Figure 166: Standard collocation points and additional points for the least squares variant of the collocation.

The choice of the parameters $\{\sigma_i\}_{i=1}^q \in [0,1]$ is somewhat free and so, we decided for the the following: $q = m+1$,

$$\sigma_i := \begin{cases} \frac{\rho_1}{2}, & i = 1, \\ \frac{\rho_i + \rho_{i+1}}{2}, & 1 < i \leq m, \\ \frac{\rho_m + 1}{2}, & i = m+1. \end{cases}$$

3.4 First results

The results documented in this chapter were calculated with $N = 200$ equidistant grid points and $m = 5$ Gaussian collocation points. Our aim here is to observe how the solution changes when $\varepsilon \to 0$.

3.4.1 $\mathbf{J = \{-2, -1, 0, 1, 2, 3\}}$

3.4.1.1 Solution component w_{-2}
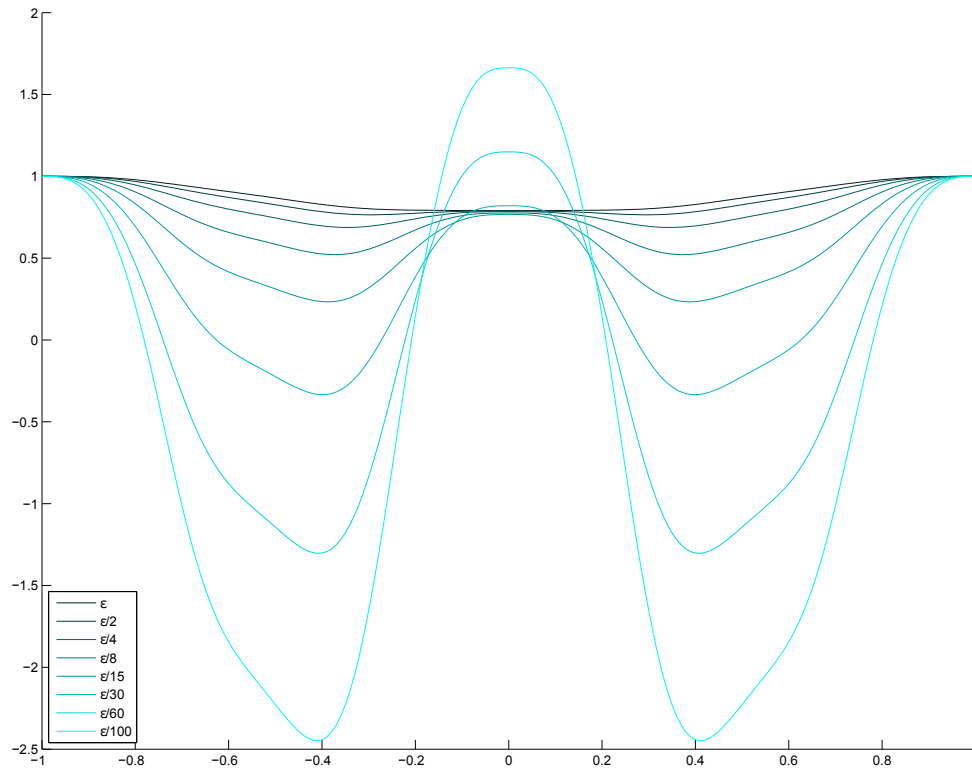
Figure 167: Solution component w_{-2} for ε varying between $1e - 1$ and $1e - 3$.
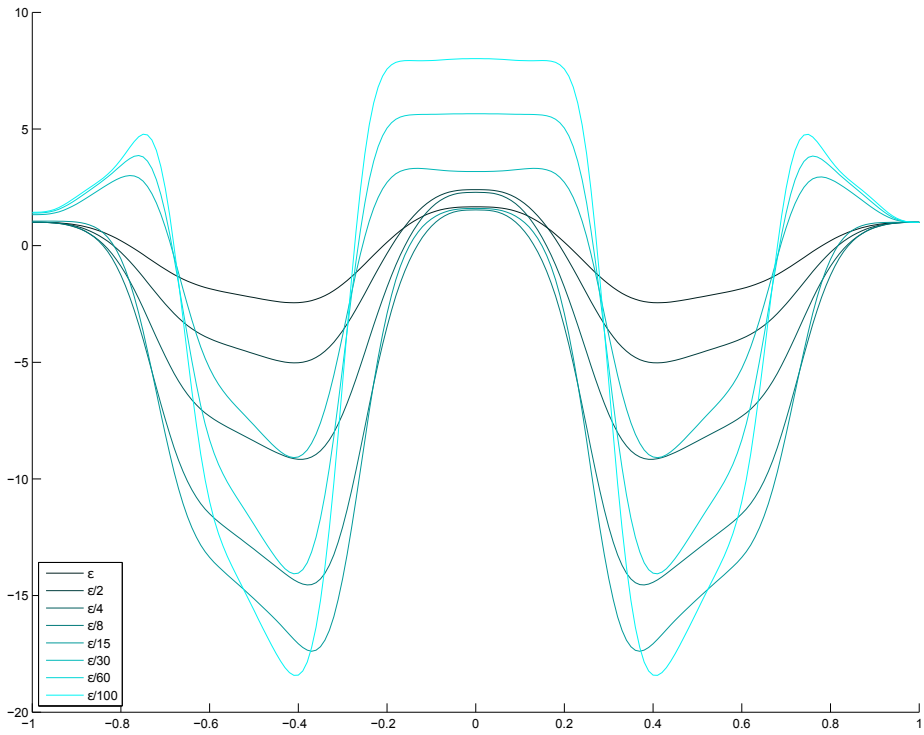
Figure 168: Solution component w_{-2} for ε varying between $1e-3$ and $1e-5$.
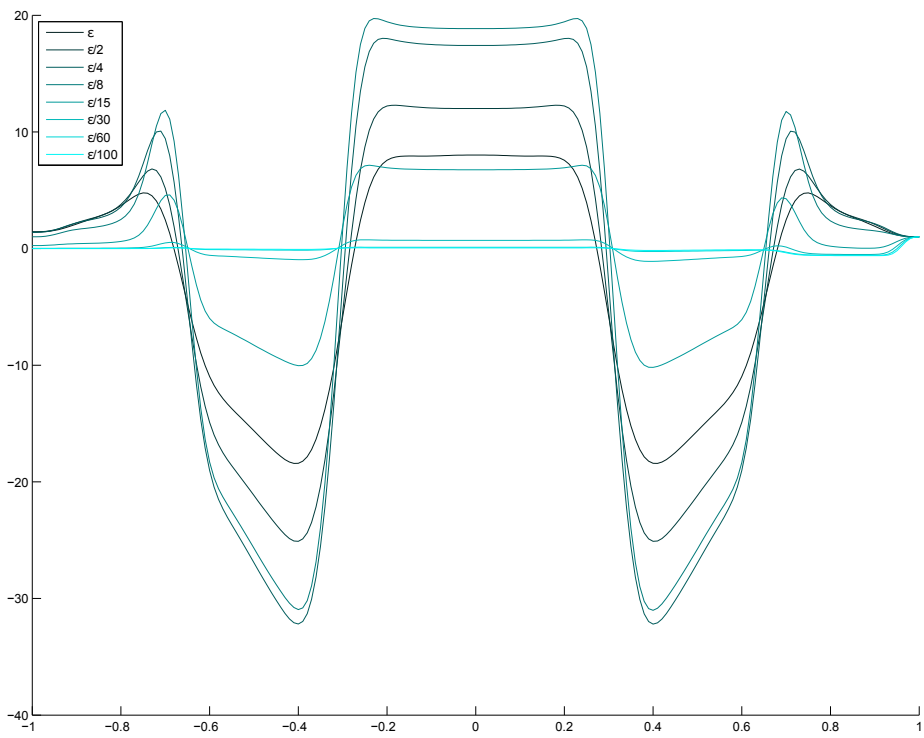
Figure 169: Solution component w_{-2} for ε varying between $1e-5$ and $1e-7$.

108
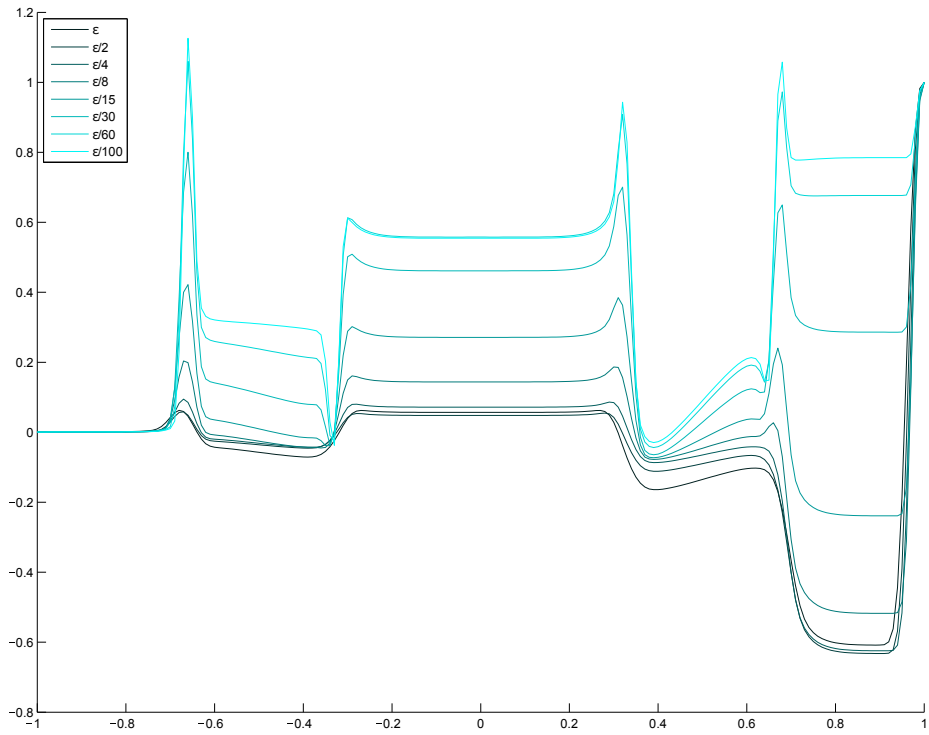
Figure 170: Solution component w_{-2} for ε varying between $1e - 7$ and $1e - 9$.
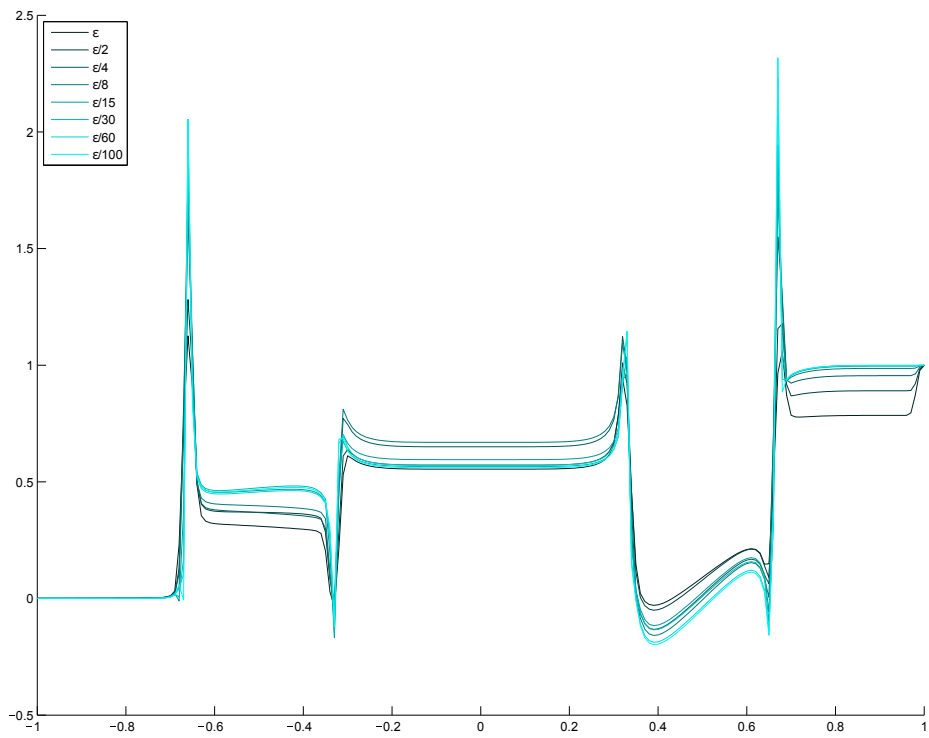
Figure 171: Solution component w_{-2} for ε varying between $1e - 9$ and $1e - 11$.
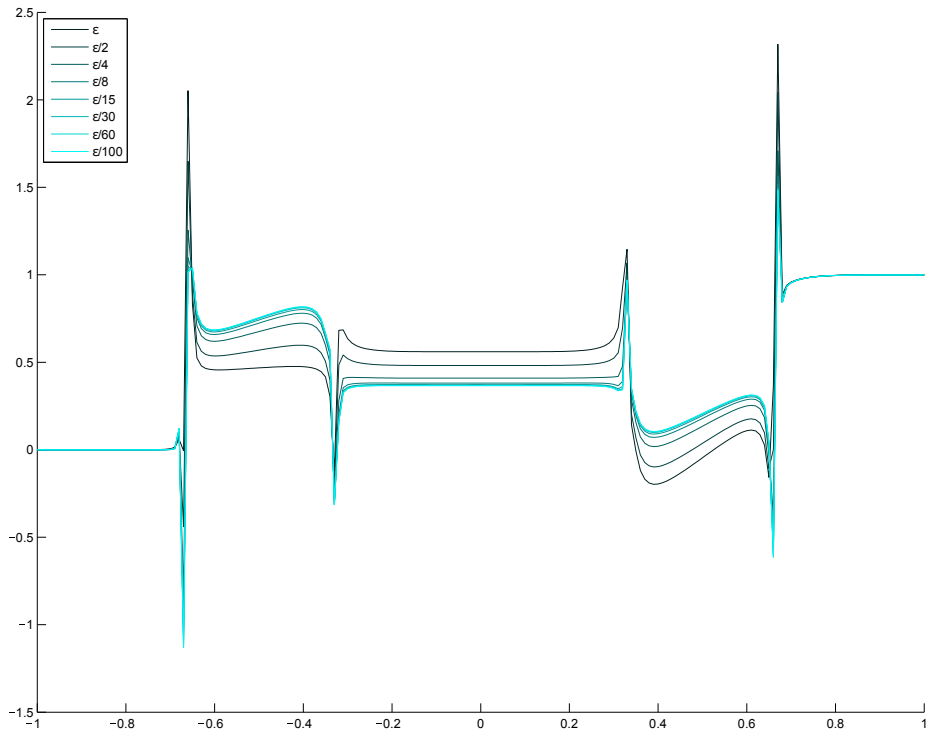
Figure 172: Solution component w_{-2} for ε varying between $1e-11$ and $1e-13$.
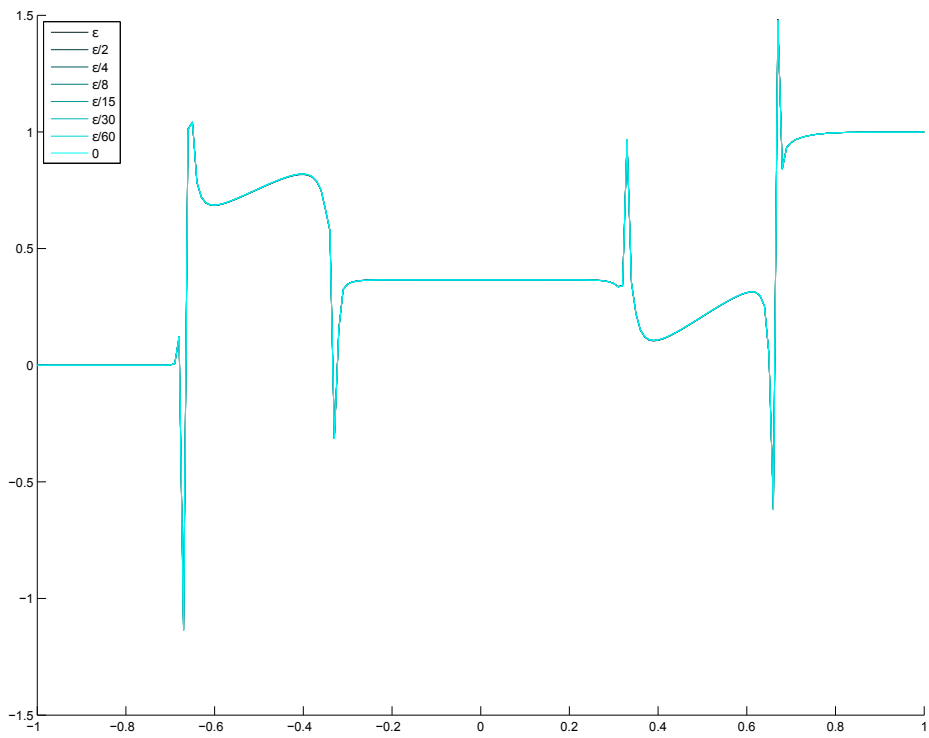
Figure 173: Solution component w_{-2} for ε varying between $1e-13$ and 0.

3.4.1.2   Solution component w_{-1}
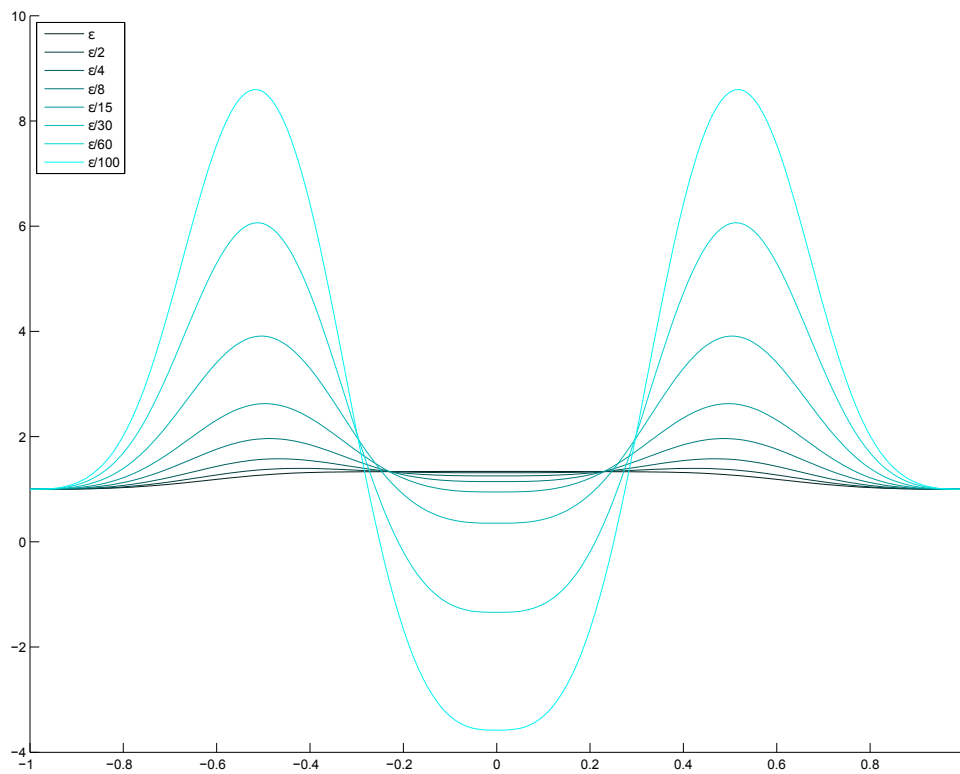
Figure 174: Solution component w_{-1} for ε varying between $1e-1$ and $1e-3$.
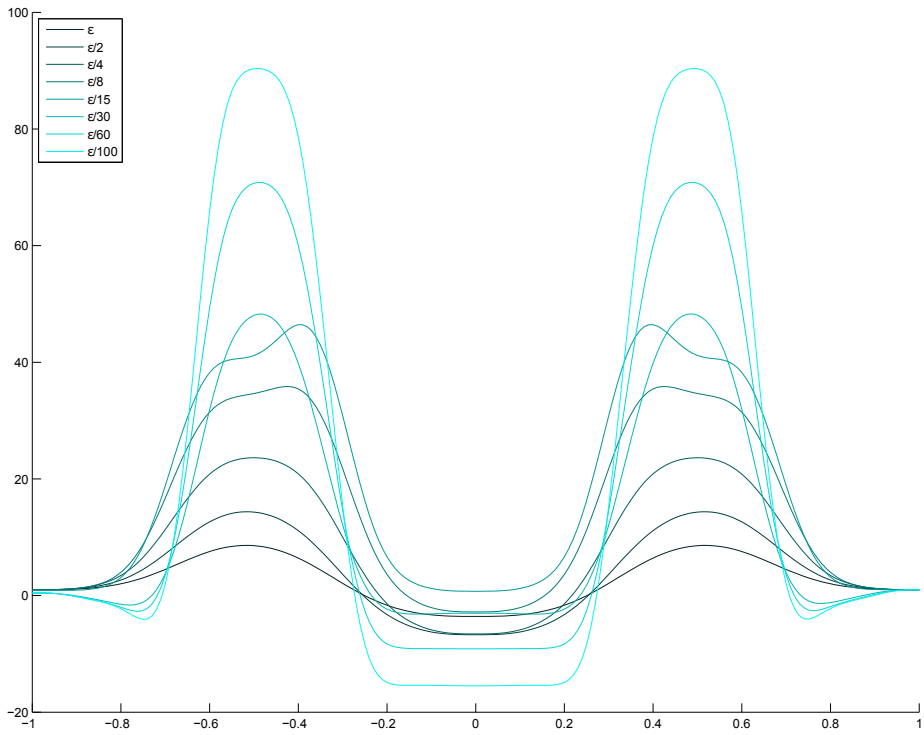
Figure 175: Solution component w_{-1} for ε varying between $1e-3$ and $1e-5$.
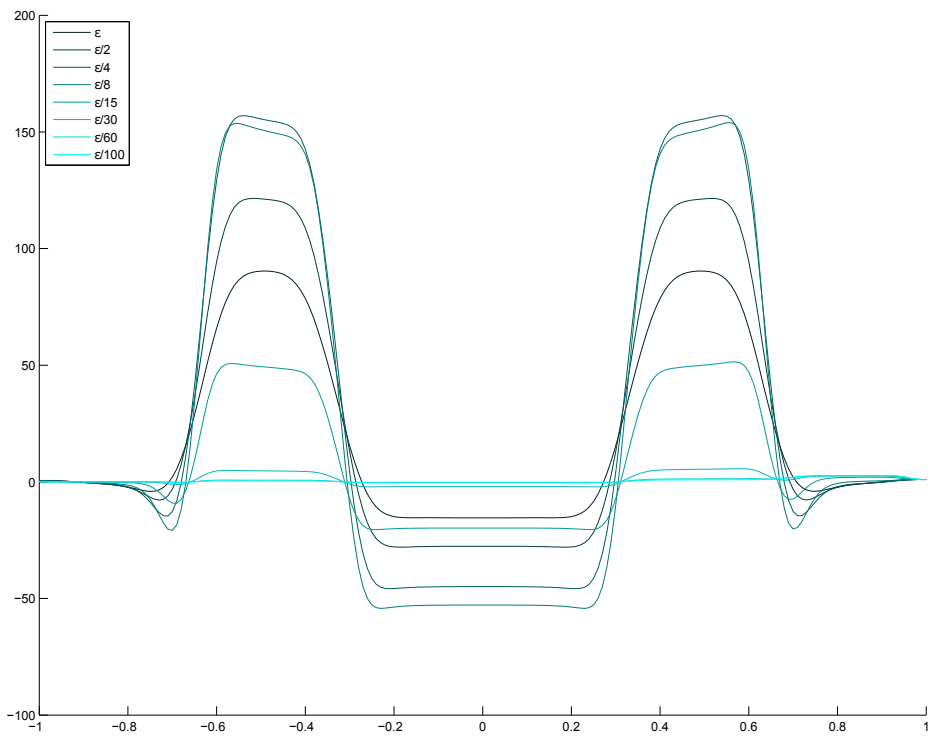
Figure 176: Solution component w_{-1} for ε varying between $1e-5$ and $1e-7$.
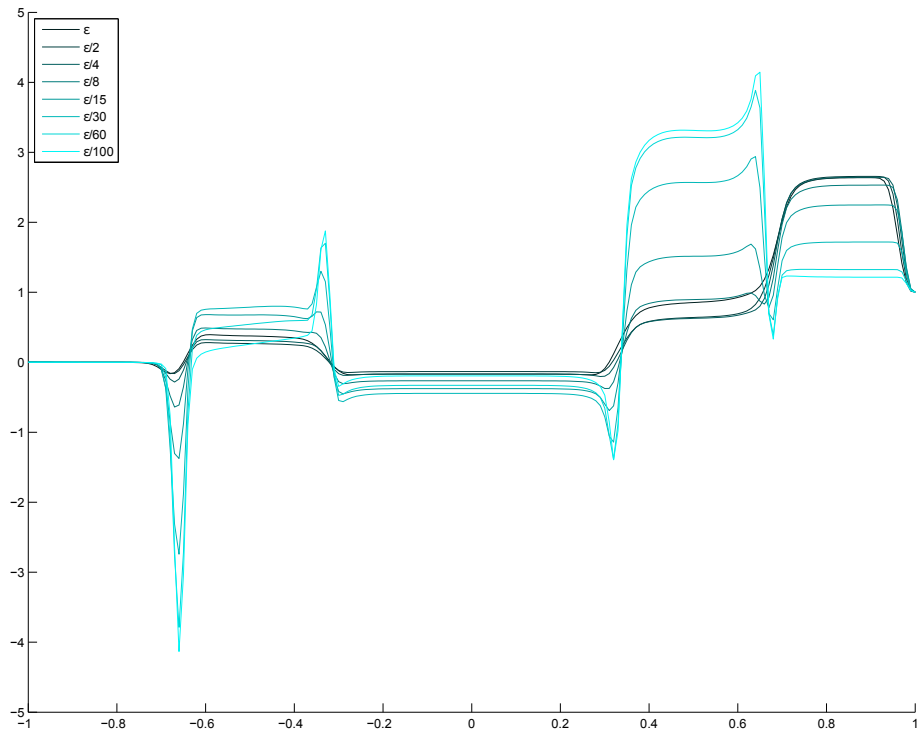
Figure 177: Solution component w_{-1} for ε varying between $1e-7$ and $1e-9$.
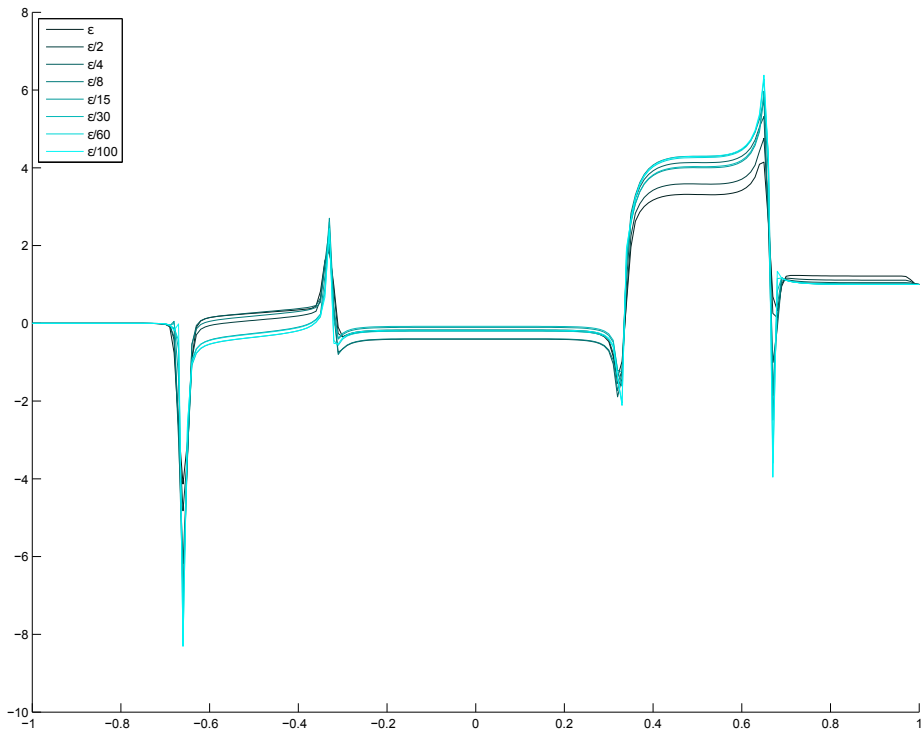
Figure 178: Solution component w_{-1} for ε varying between $1e-9$ and $1e-11$.
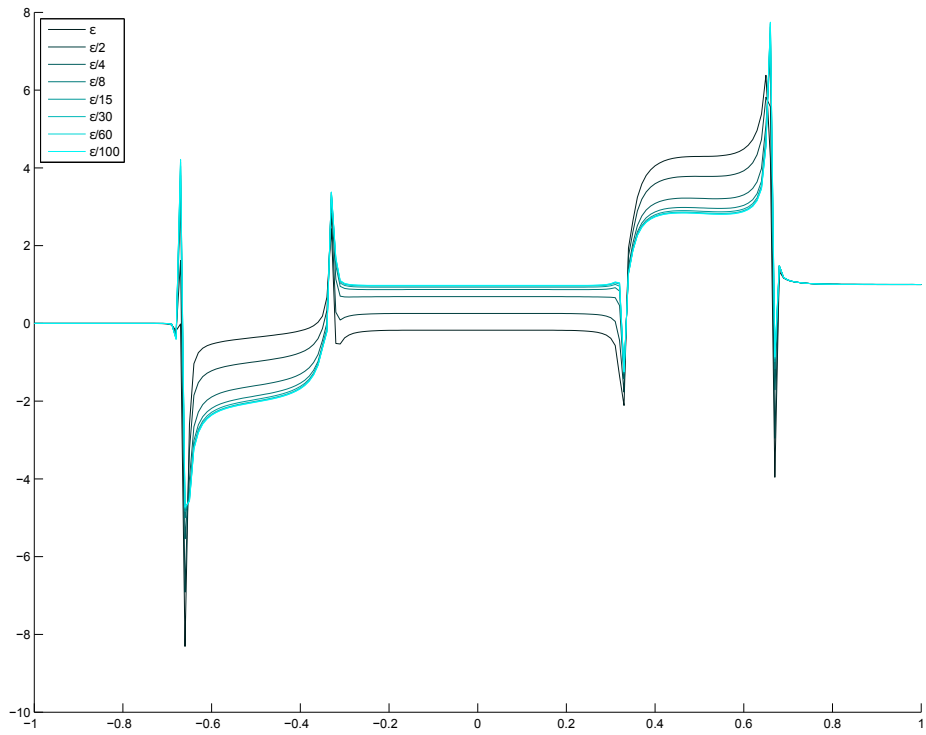
Figure 179: Solution component w_{-1} for ε varying between $1e-11$ and $1e-13$.
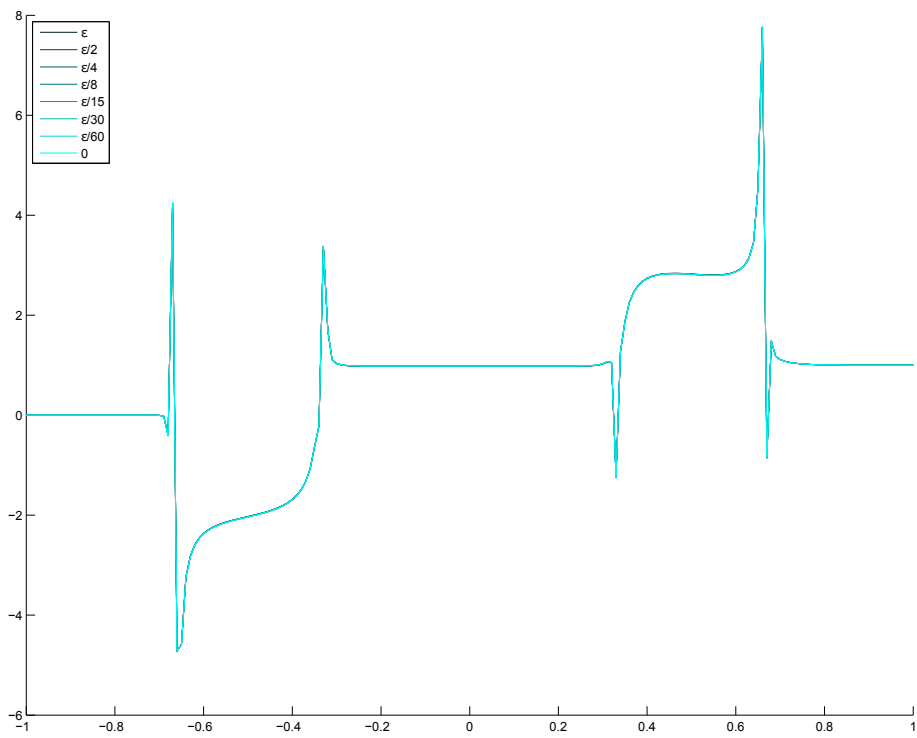
Figure 180: Solution component w_{-1} for ε varying between $1e-13$ and 0.

114

3.4.1.3   Solution component w_0
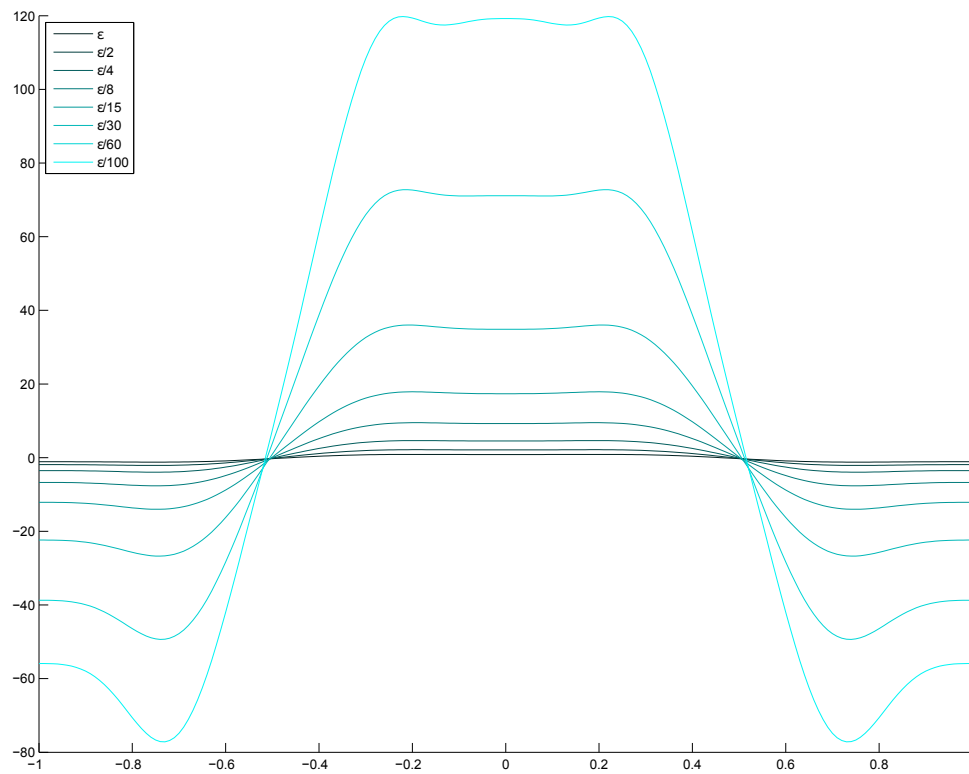
Figure 181: Solution component w_0 for ε varying between $1e - 1$ and $1e - 3$.
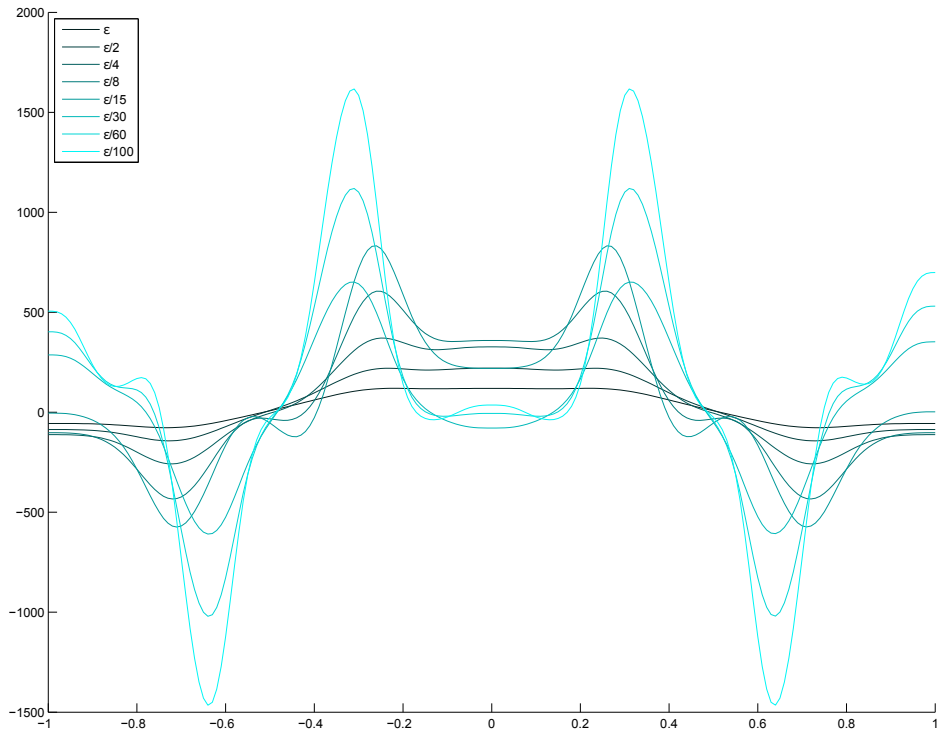
Figure 182: Solution component w_0 for ε varying between $1e-3$ and $1e-5$.
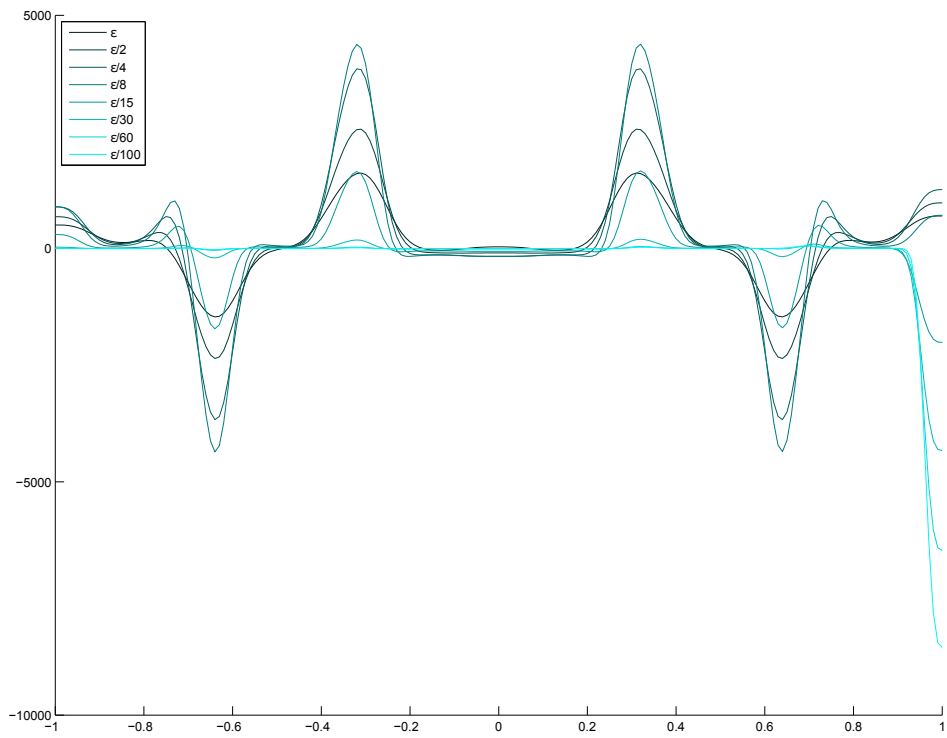
Figure 183: Solution component w_0 for ε varying between $1e-5$ and $1e-7$.
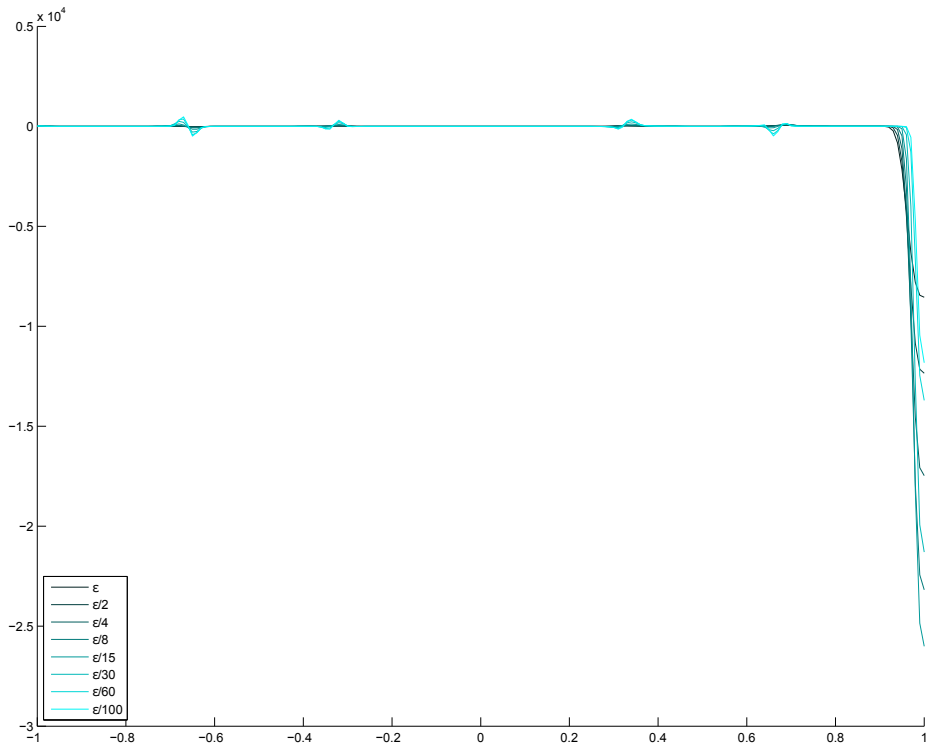
Figure 184: Solution component w_0 for ε varying between $1e-7$ and $1e-9$.
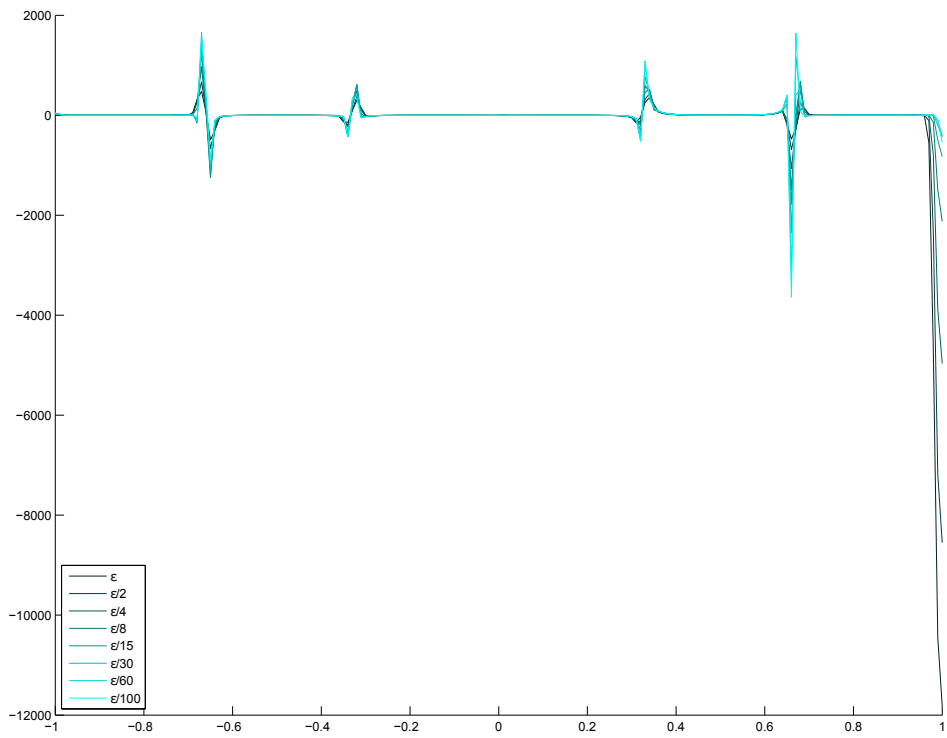
Figure 185: Solution component w_0 for ε varying between $1e-9$ and $1e-11$.
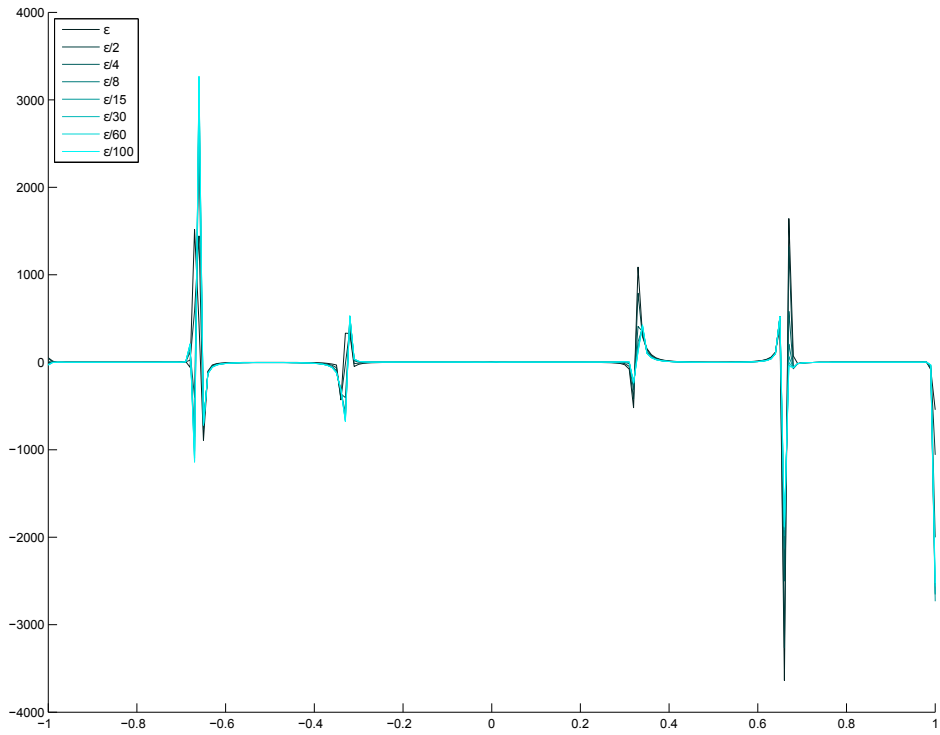
Figure 186: Solution component w_0 for ε varying between $1e-11$ and $1e-13$.
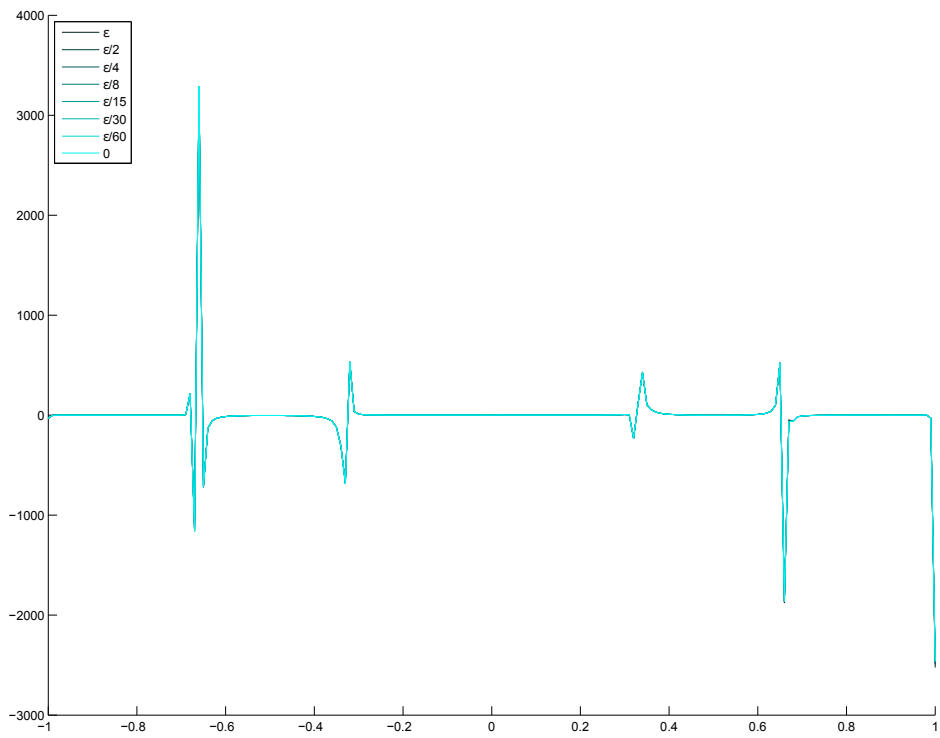
Figure 187: Solution component w_0 for ε varying between $1e-13$ and 0.

3.4.1.4   Solution component w_1
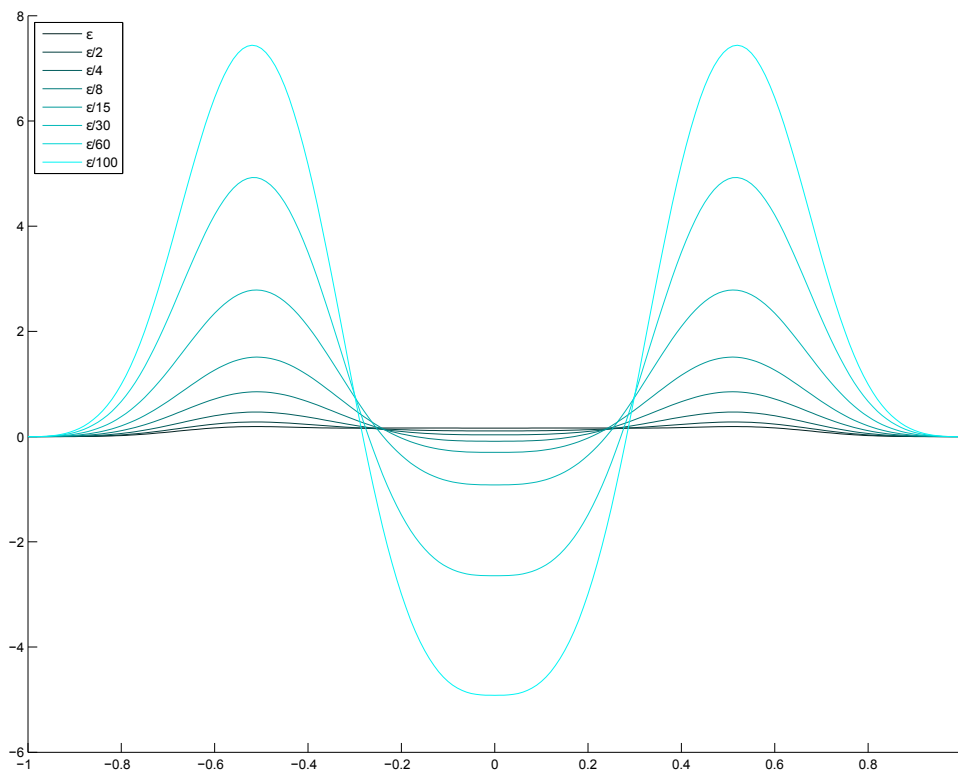
Figure 188: Solution component w_1 for ε varying between $1e-1$ and $1e-3$.
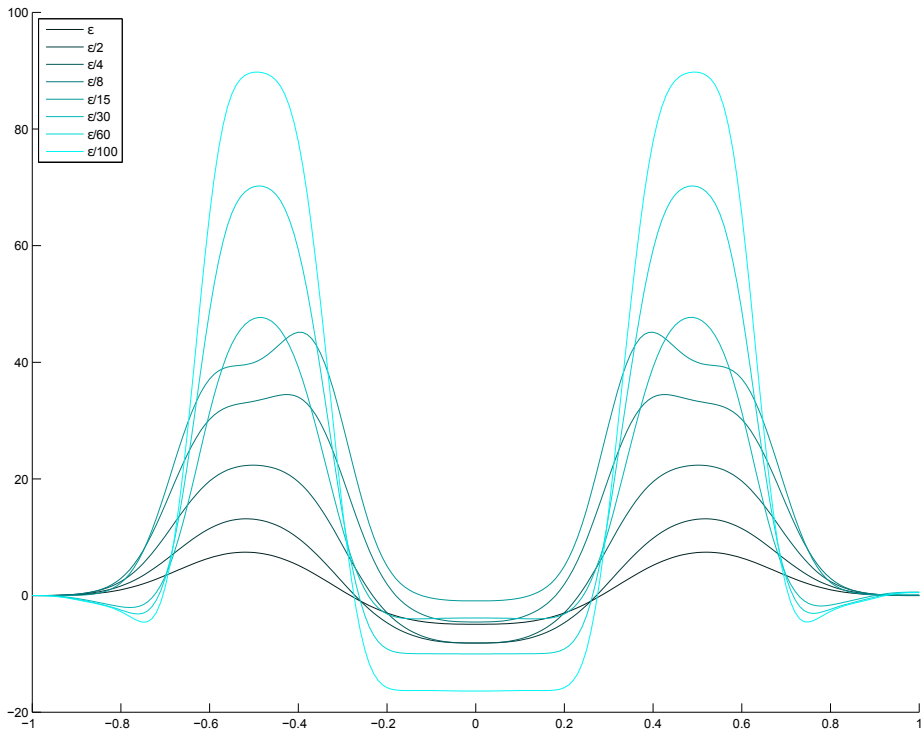
Figure 189: Solution component w_1 for ε varying between $1e - 3$ and $1e - 5$.
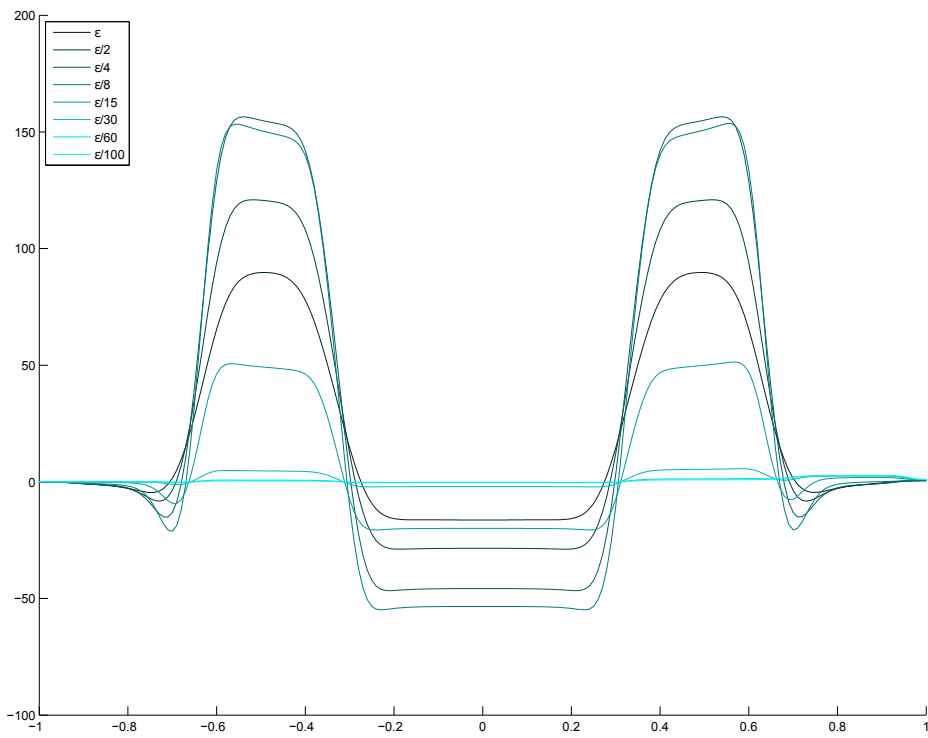
Figure 190: Solution component w_1 for ε varying between $1e - 5$ and $1e - 7$.
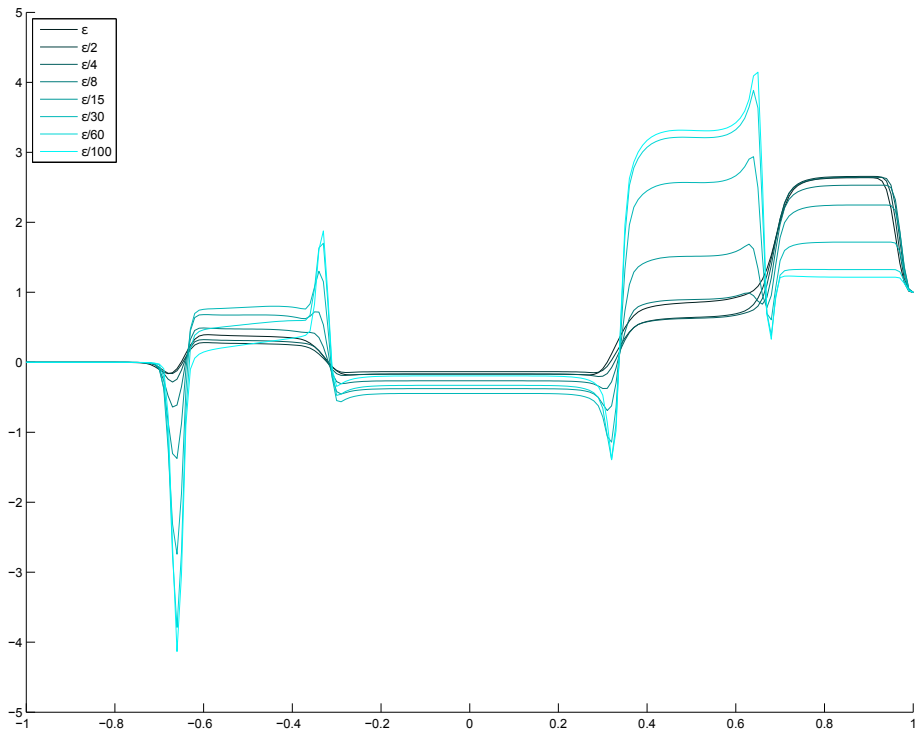
Figure 191: Solution component w_1 for ε varying between $1e - 7$ and $1e - 9$.
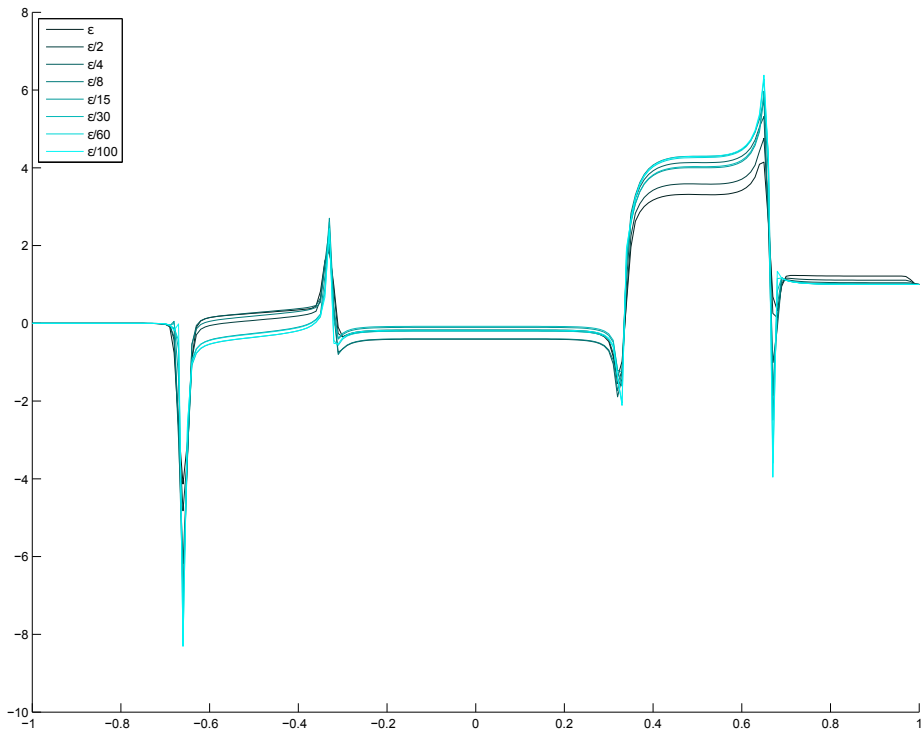
Figure 192: Solution component w_1 for ε varying between $1e - 9$ and $1e - 11$.
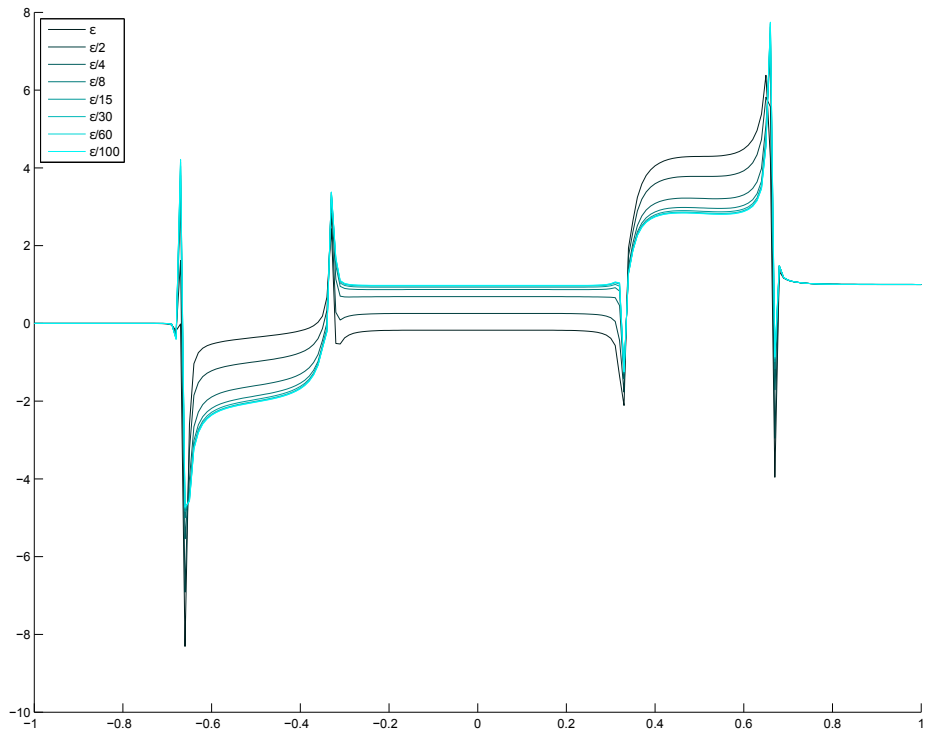
Figure 193: Solution component w_1 for ε varying between $1e-11$ and $1e-13$.
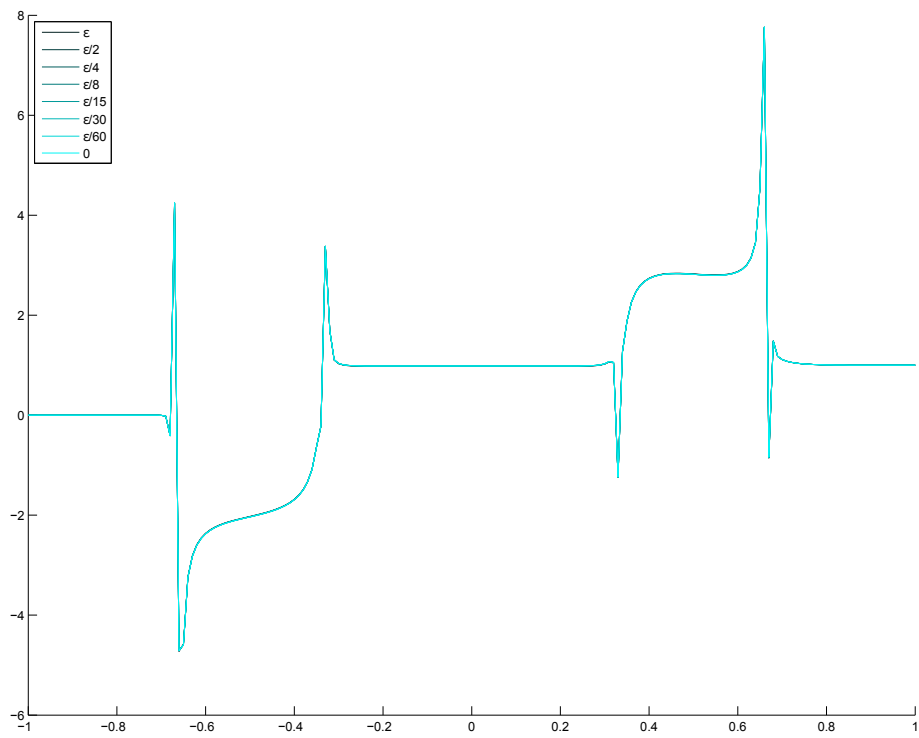
Figure 194: Solution component w_1 for ε varying between $1e-13$ and 0.

3.4.1.5   Solution component w_2
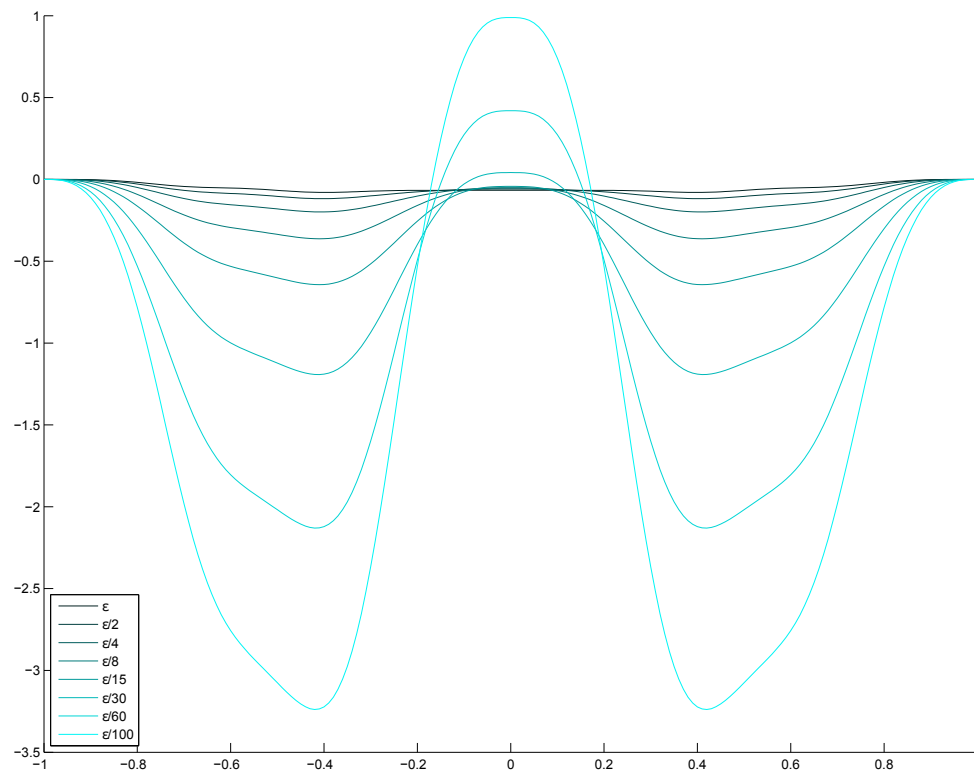
Figure 195: Solution component w_2 for ε varying between $1e-1$ and $1e-3$.
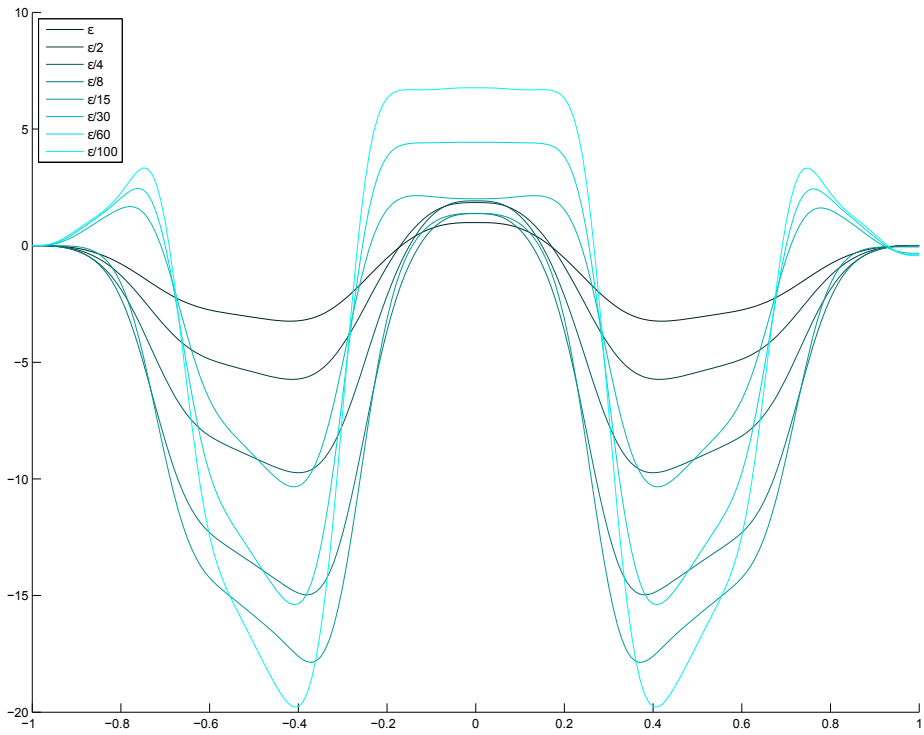
Figure 196: Solution component w_2 for ε varying between $1e-3$ and $1e-5$.
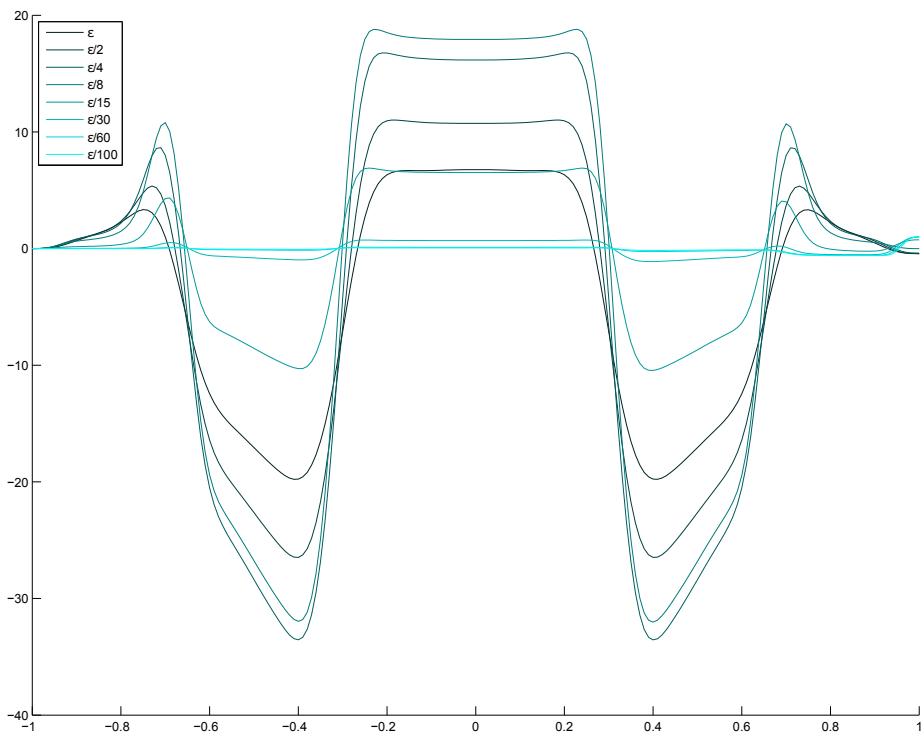
Figure 197: Solution component w_2 for ε varying between $1e-5$ and $1e-7$.

124
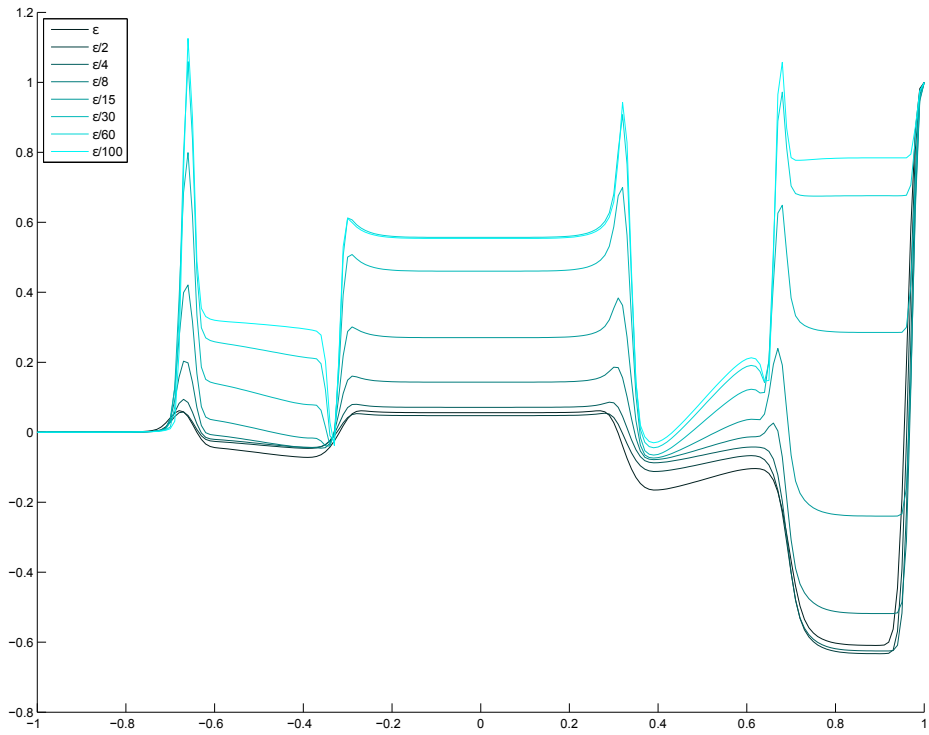
Figure 198: Solution component w_2 for ε varying between $1e-7$ and $1e-9$.
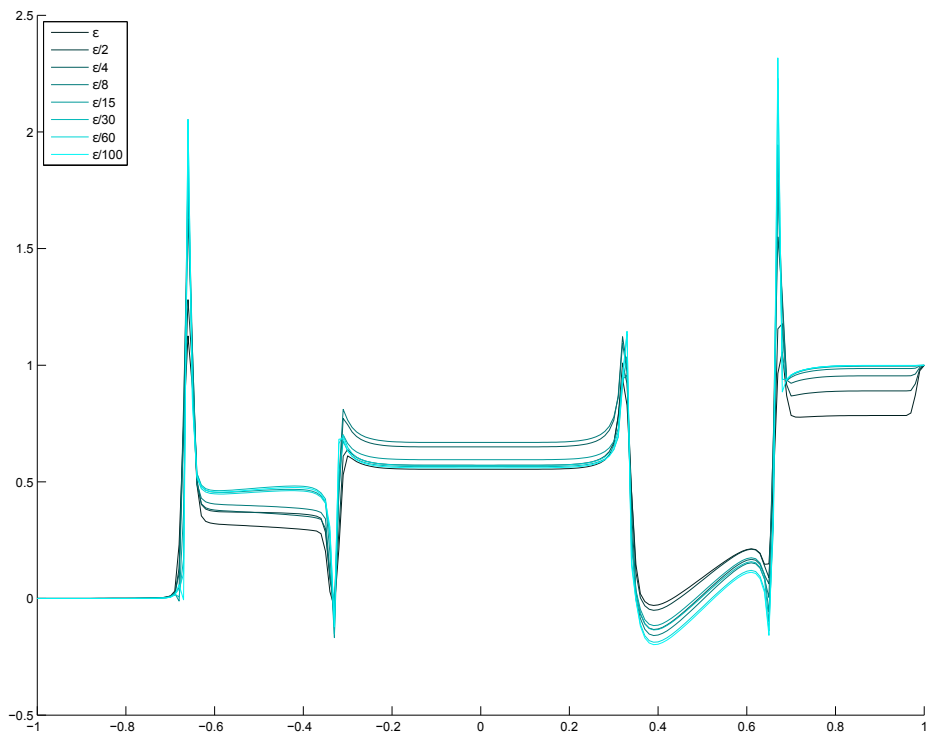
Figure 199: Solution component w_2 for ε varying between $1e-9$ and $1e-11$.
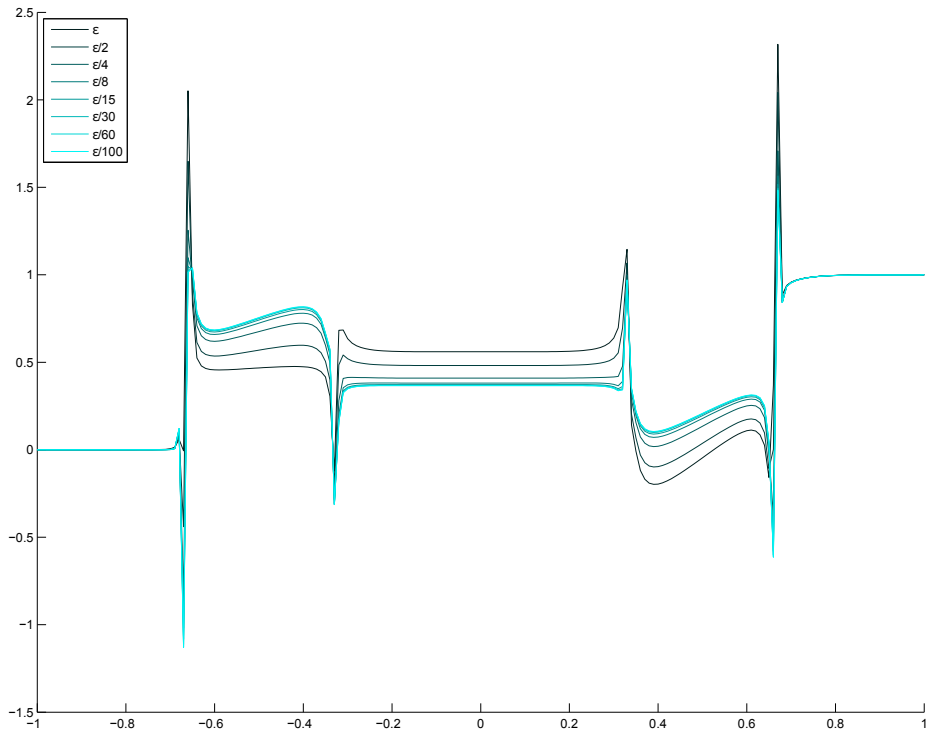
Figure 200: Solution component w_2 for ε varying between $1e - 11$ and $1e - 13$.
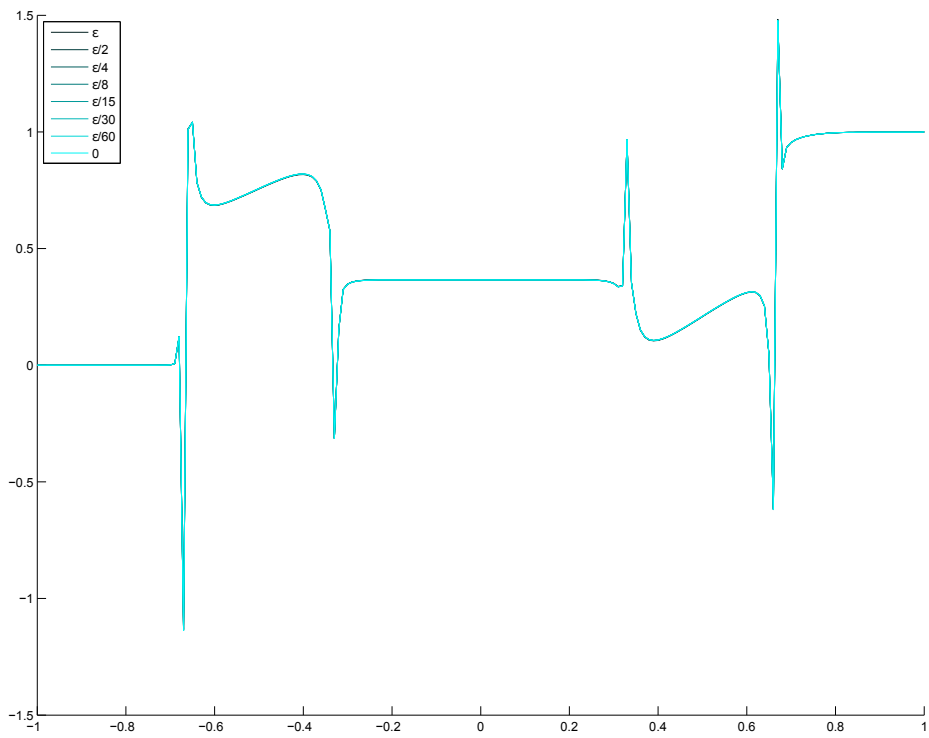
Figure 201: Solution component w_2 for ε varying between $1e - 13$ and 0.

3.4.1.6 Solution component w_3
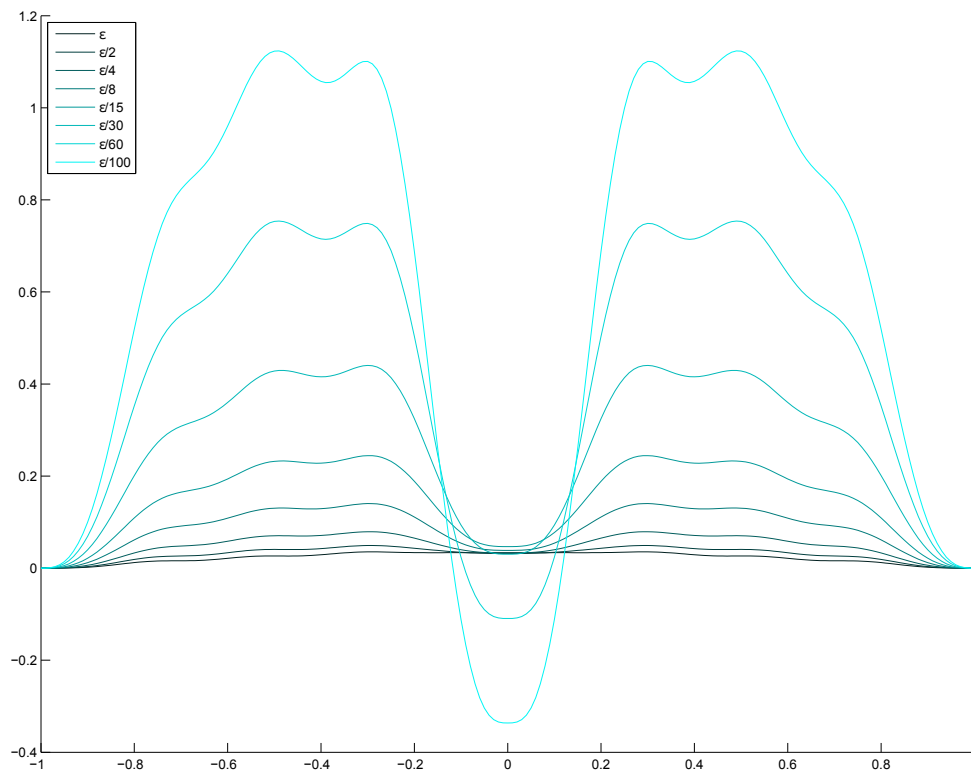
Figure 202: Solution component w_3 for ε varying between $1e-1$ and $1e-3$.
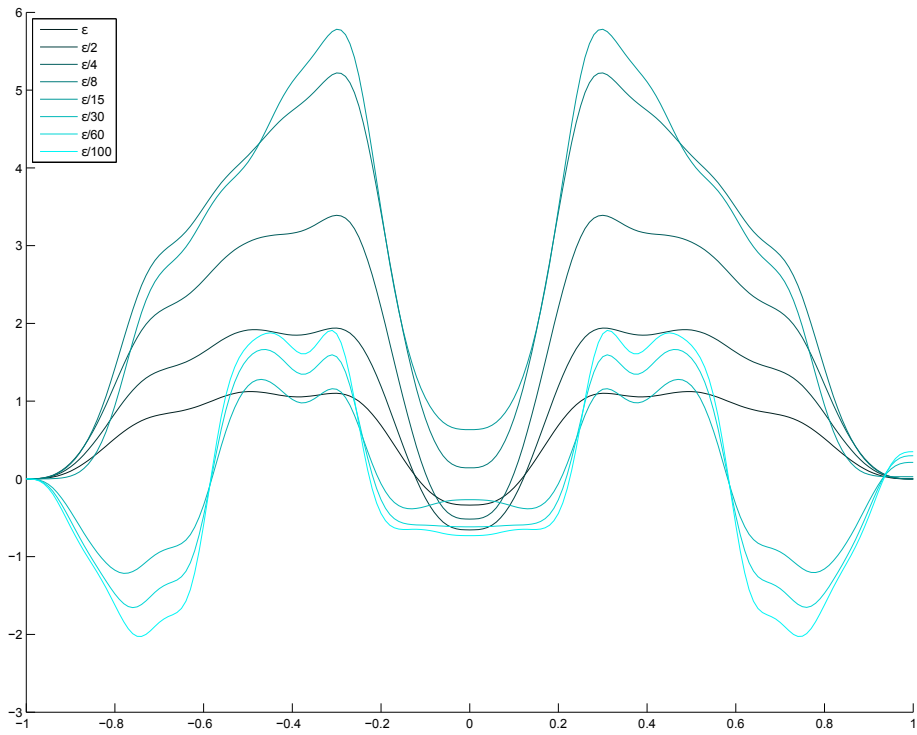
Figure 203: Solution component w_3 for ε varying between $1e-3$ and $1e-5$.
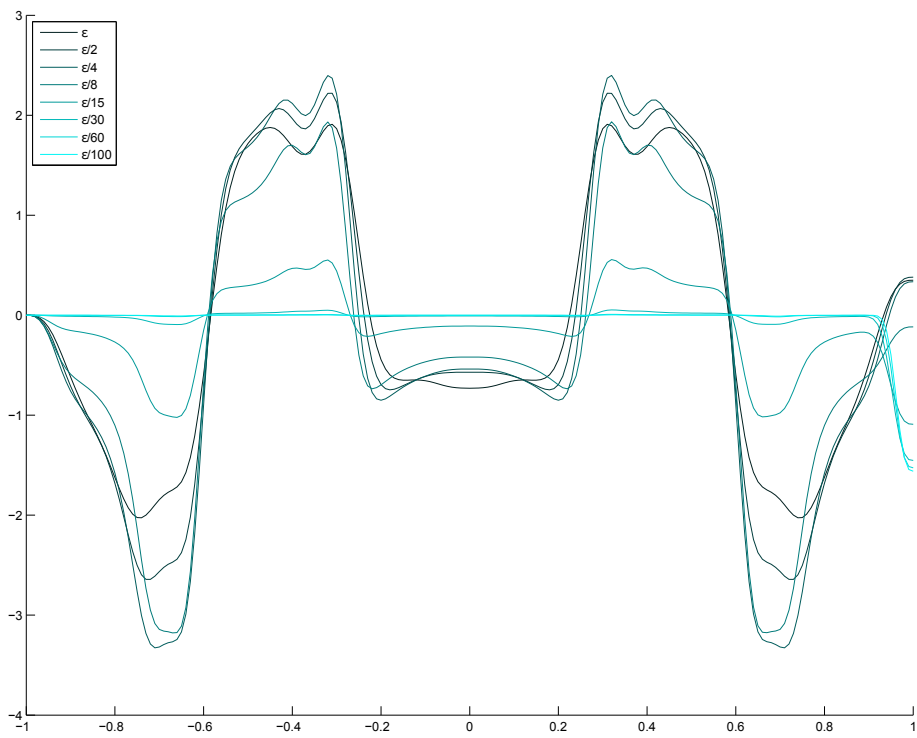
Figure 204: Solution component w_3 for ε varying between $1e-5$ and $1e-7$.
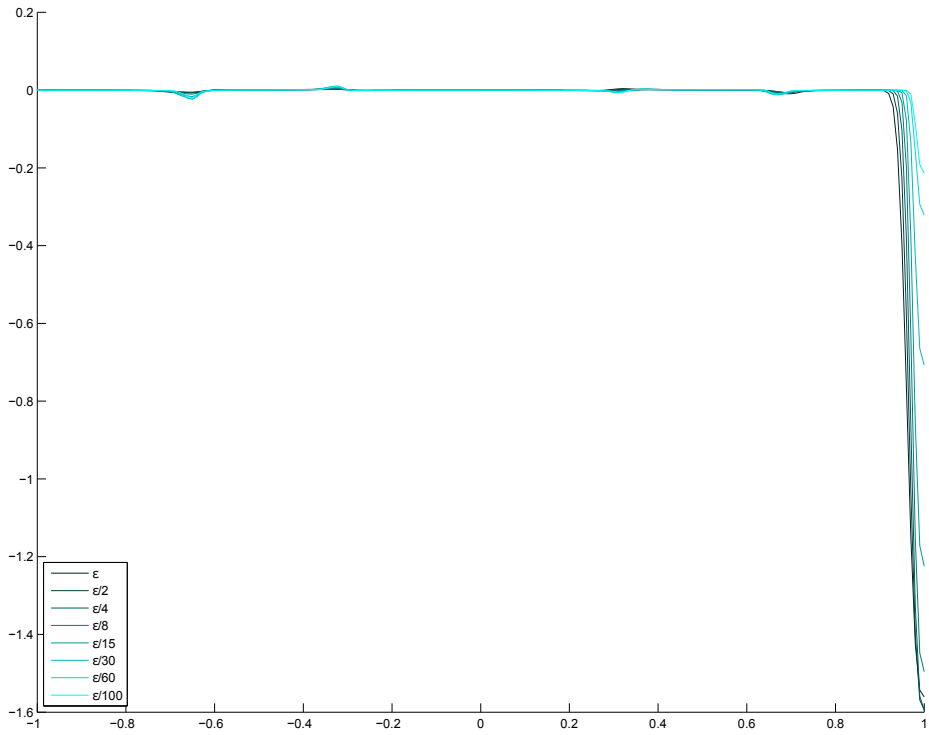
Figure 205: Solution component w_3 for ε varying between $1e - 7$ and $1e - 9$.
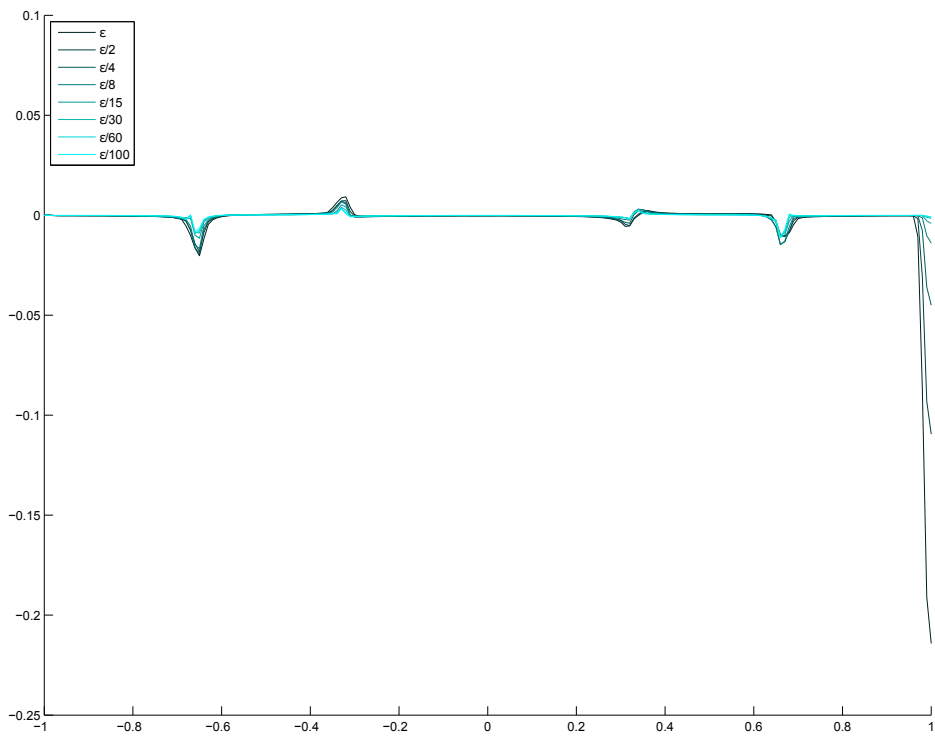
Figure 206: Solution component w_3 for ε varying between $1e - 9$ and $1e - 11$.
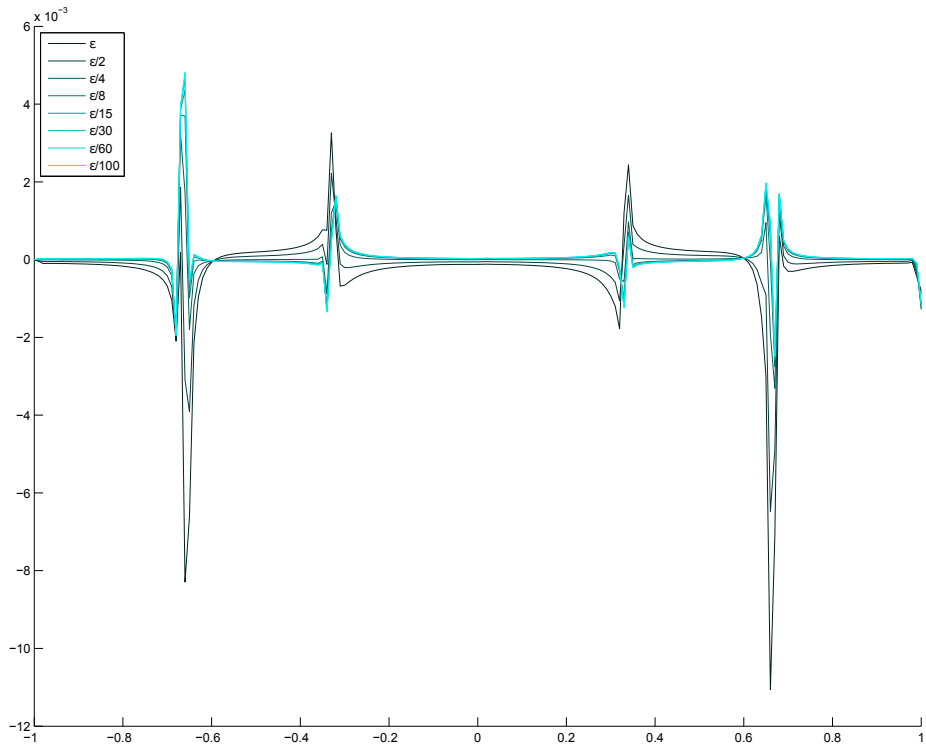
Figure 207: Solution component w_3 for ε varying between $1e-11$ and $1e-13$.
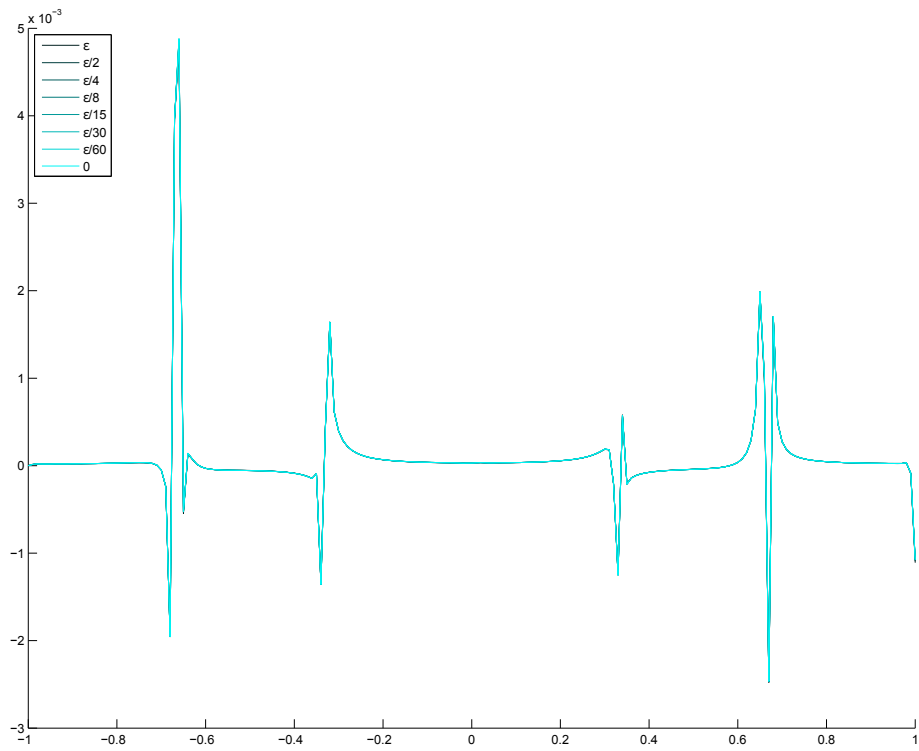
Figure 208: Solution component w_3 for ε varying between $1e-13$ and 0.

3.4.2   J = {−1, 0, 1, 2}

3.4.2.1   Solution component w_{-1}
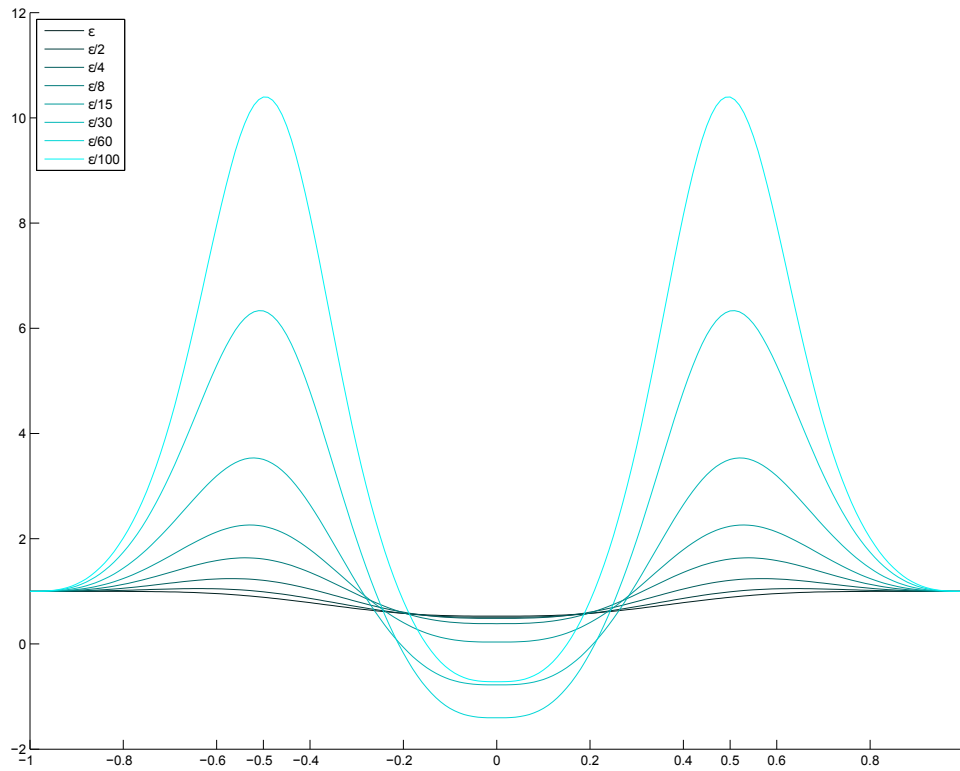
Figure 209: Solution component w_{-1} for ε varying between $1e-1$ and $1e-3$.
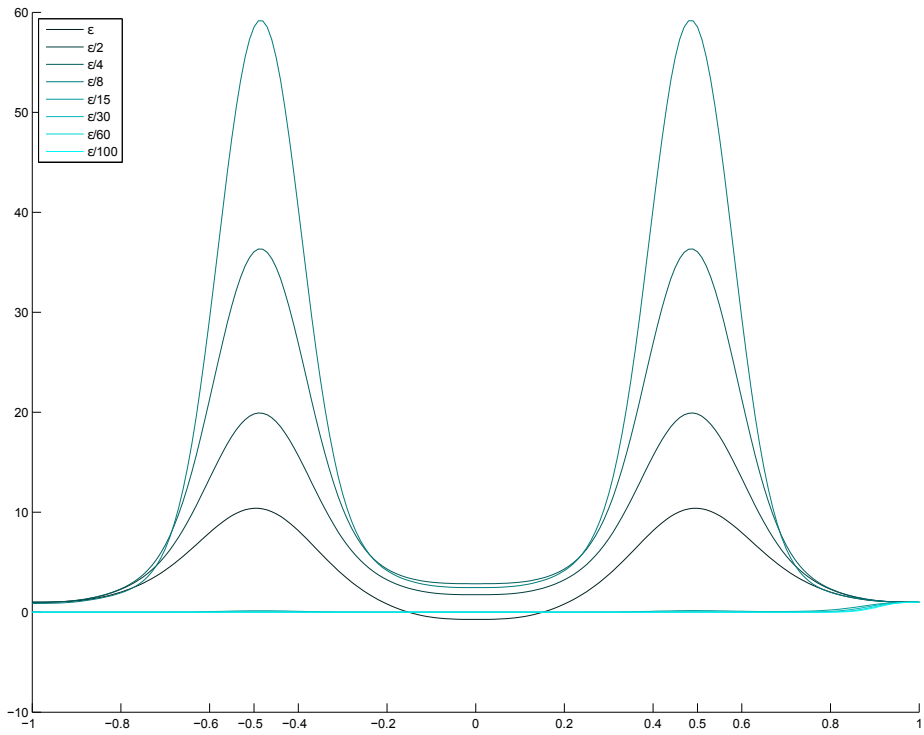
Figure 210: Solution component w_{-1} for ε varying between $1e-3$ and $1e-5$.
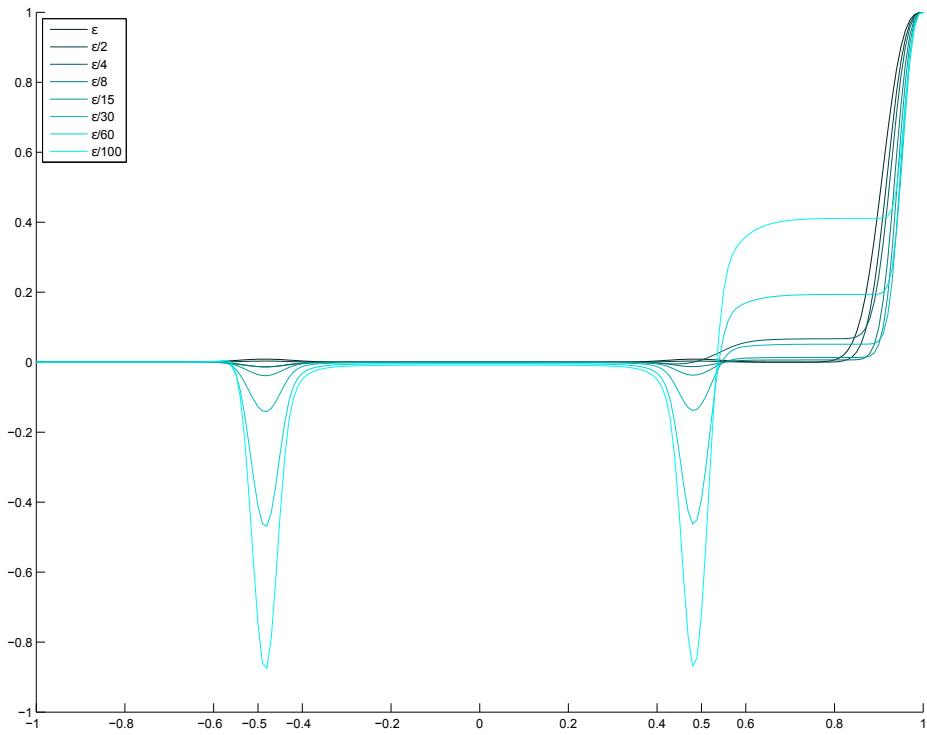
Figure 211: Solution component w_{-1} for ε varying between $1e-5$ and $1e-7$.
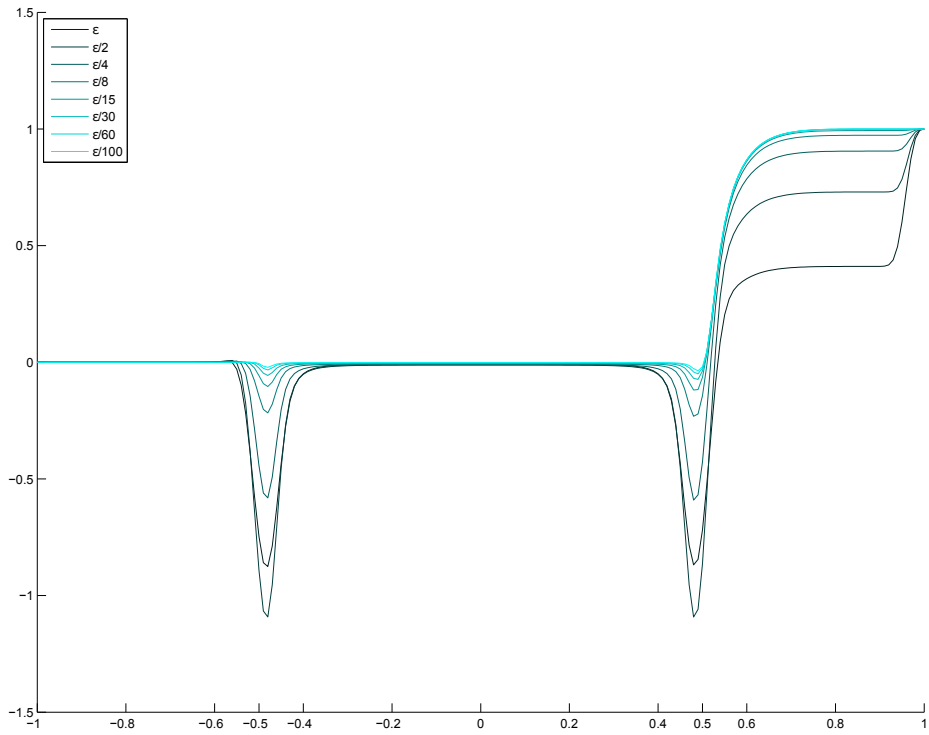
Figure 212: Solution component w_{-1} for ε varying between $1e-7$ and $1e-9$.
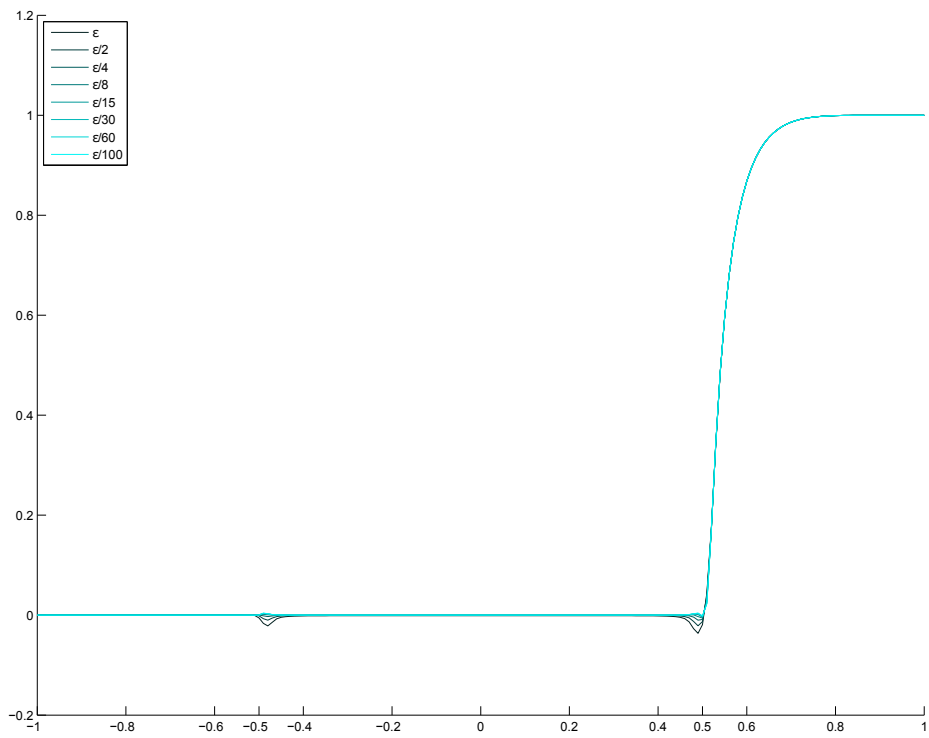
Figure 213: Solution component w_{-1} for ε varying between $1e-9$ and $1e-11$.

133
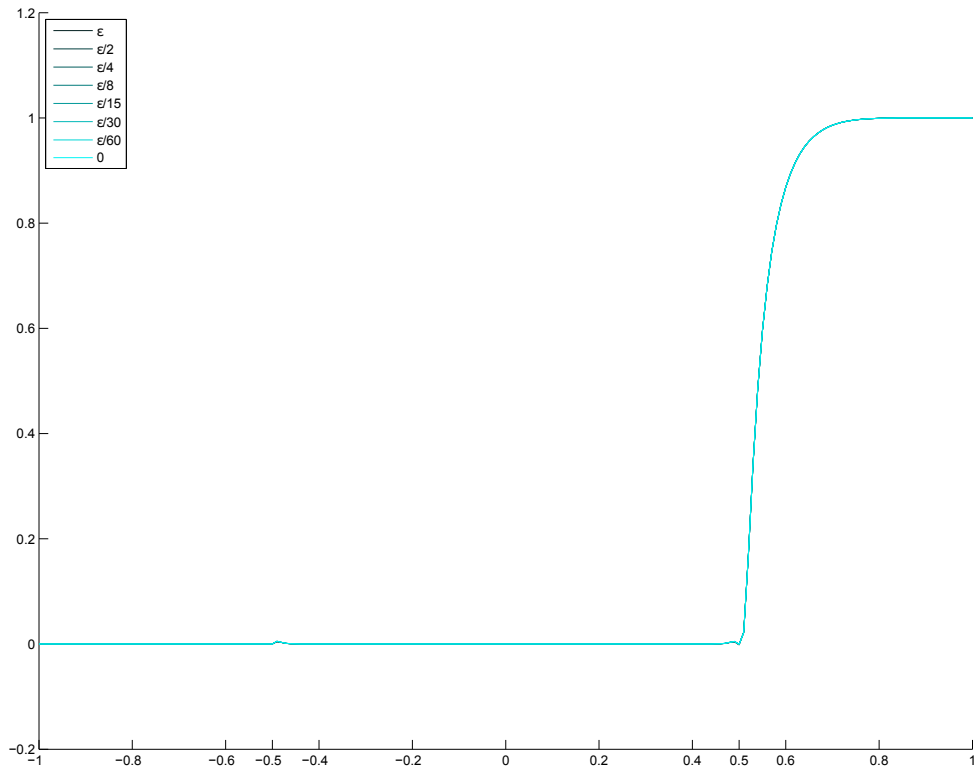
Figure 214: Solution component w_{-1} for ε varying between $1e - 11$ and 0.

3.4.2.2   Solution component w_0
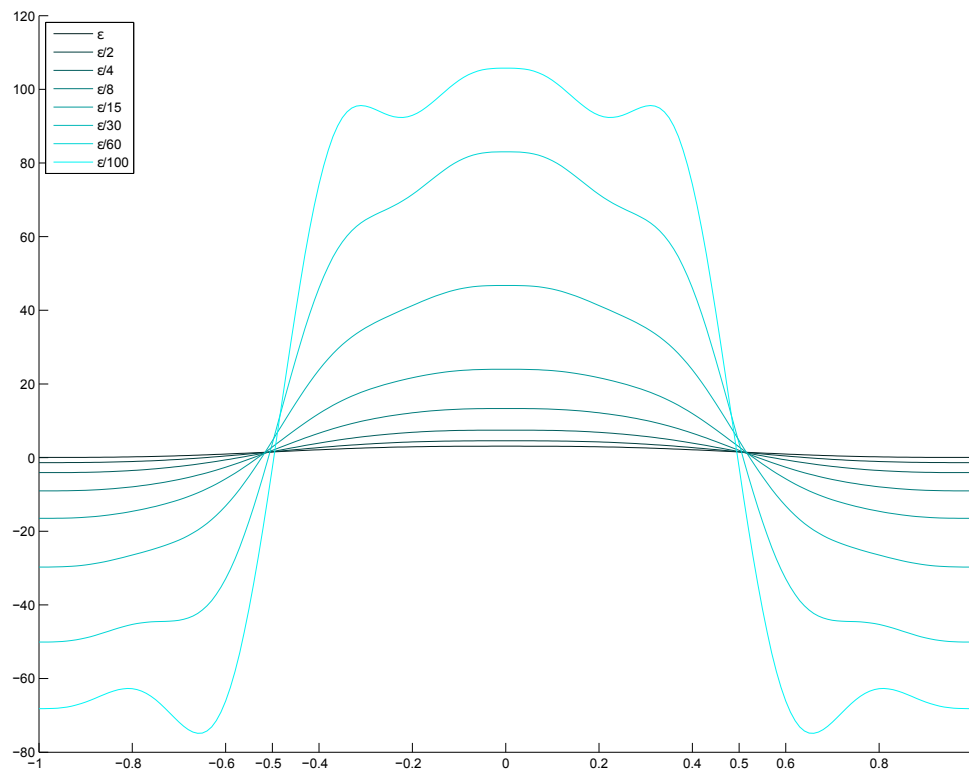
Figure 215: Solution component w_0 for ε varying between $1e - 1$ and $1e - 3$.
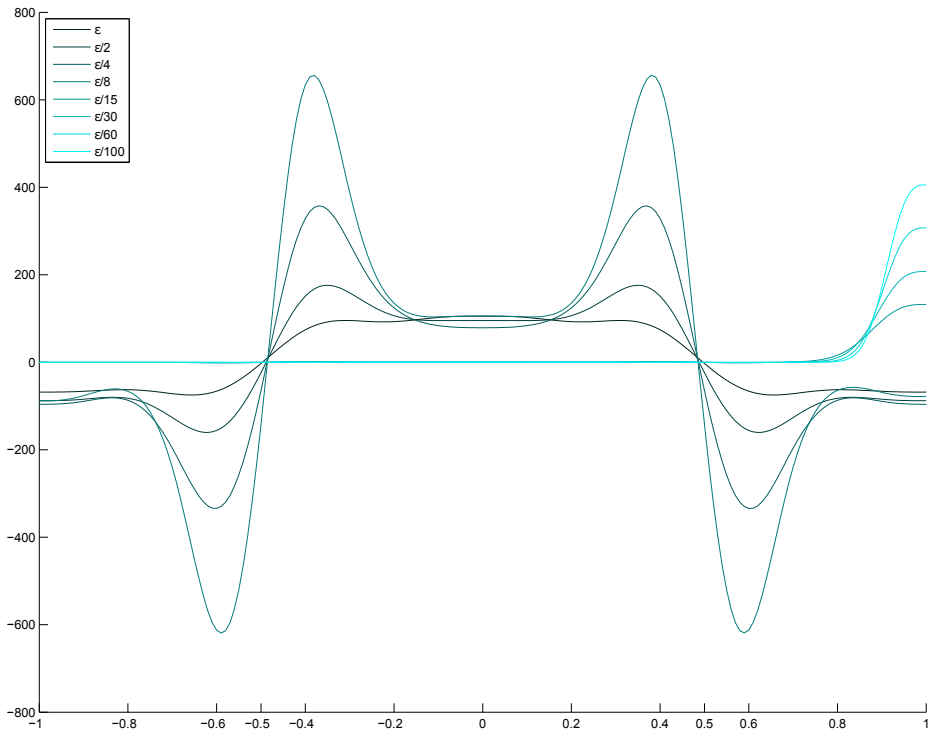
Figure 216: Solution component w_0 for ε varying between $1e-3$ and $1e-5$.
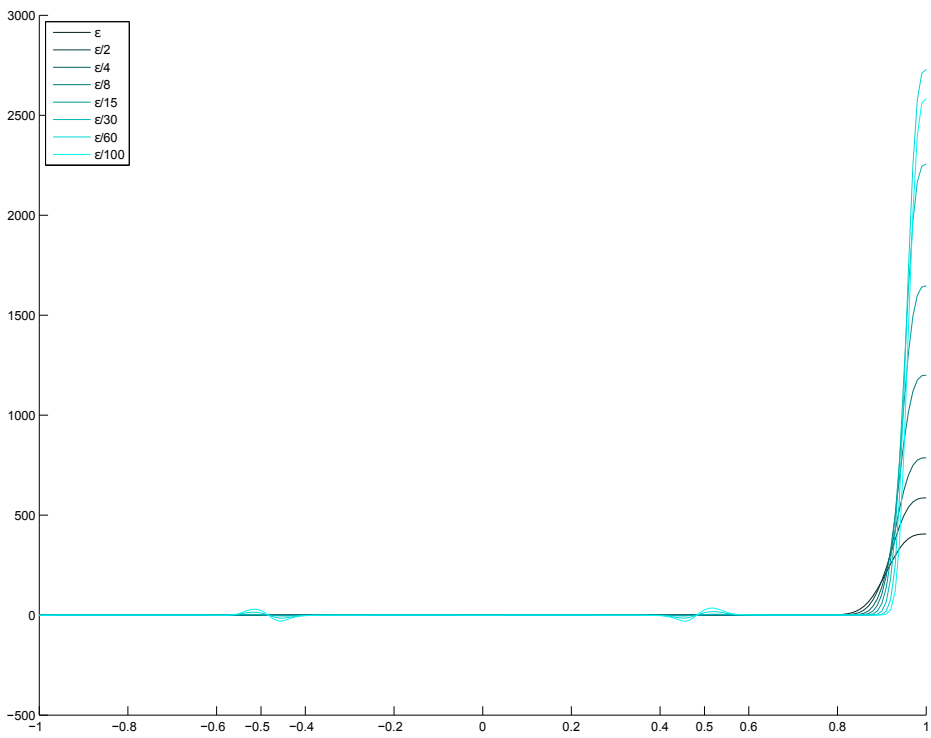
Figure 217: Solution component w_0 for ε varying between $1e-5$ and $1e-7$.
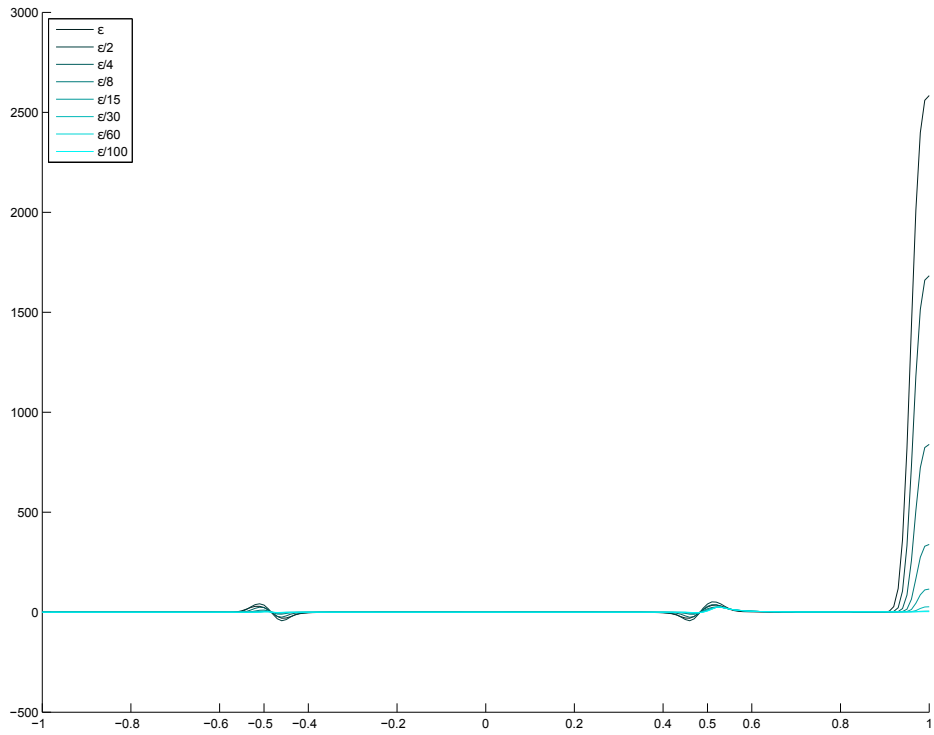
Figure 218: Solution component w_0 for ε varying between $1e-7$ and $1e-9$.
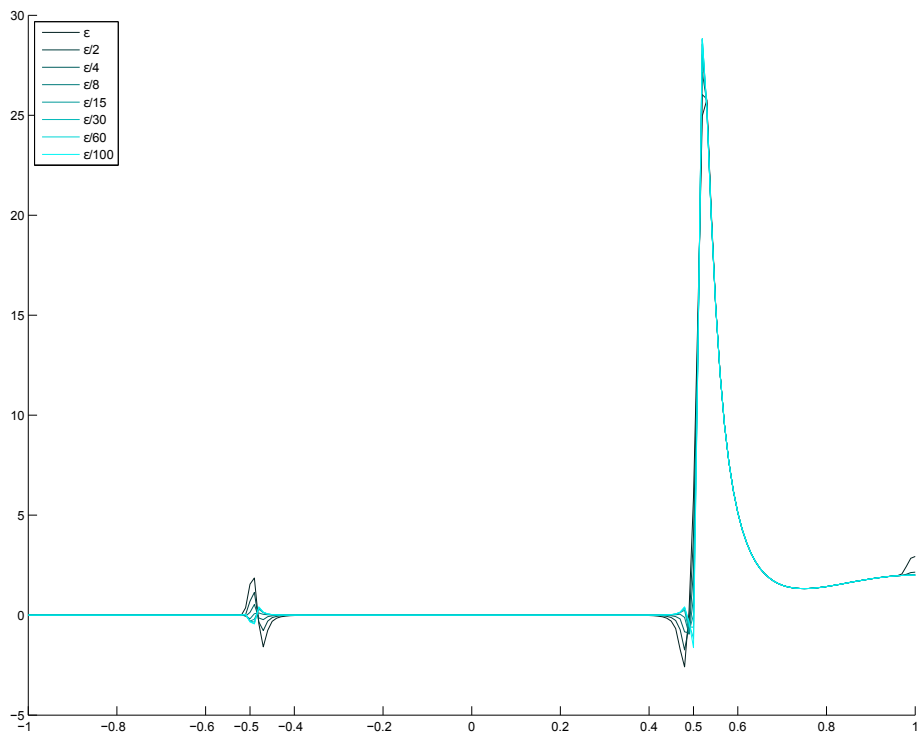
Figure 219: Solution component w_0 for ε varying between $1e-9$ and $1e-11$.
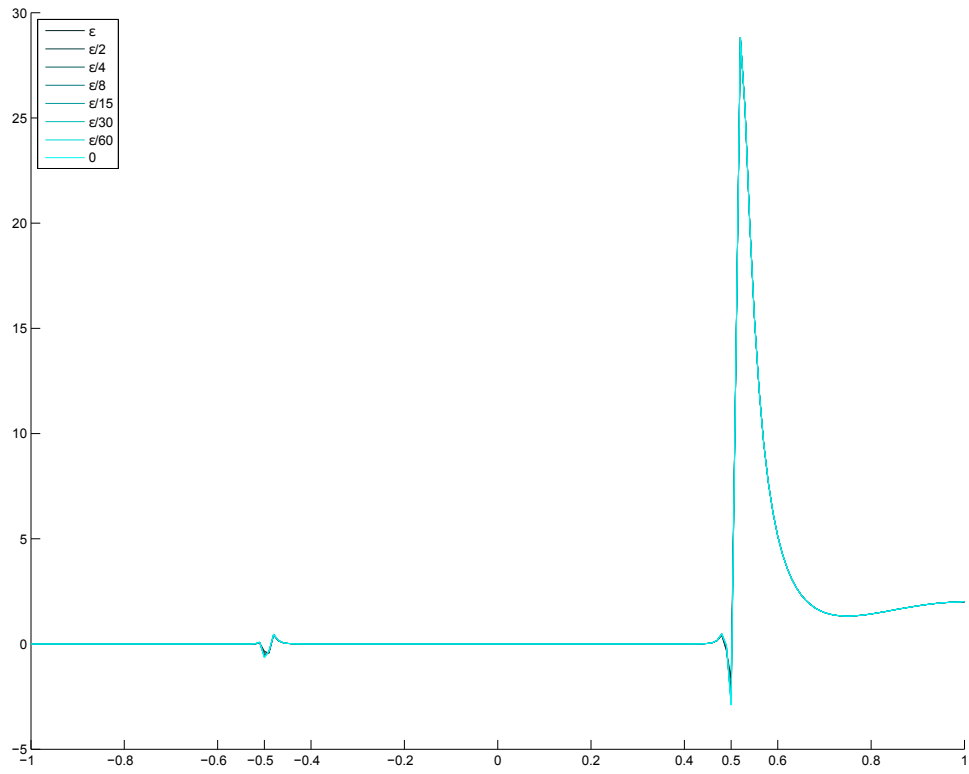
Figure 220: Solution component w_0 for ε varying between $1e-11$ and 0.

3.4.2.3 Solution component w_1
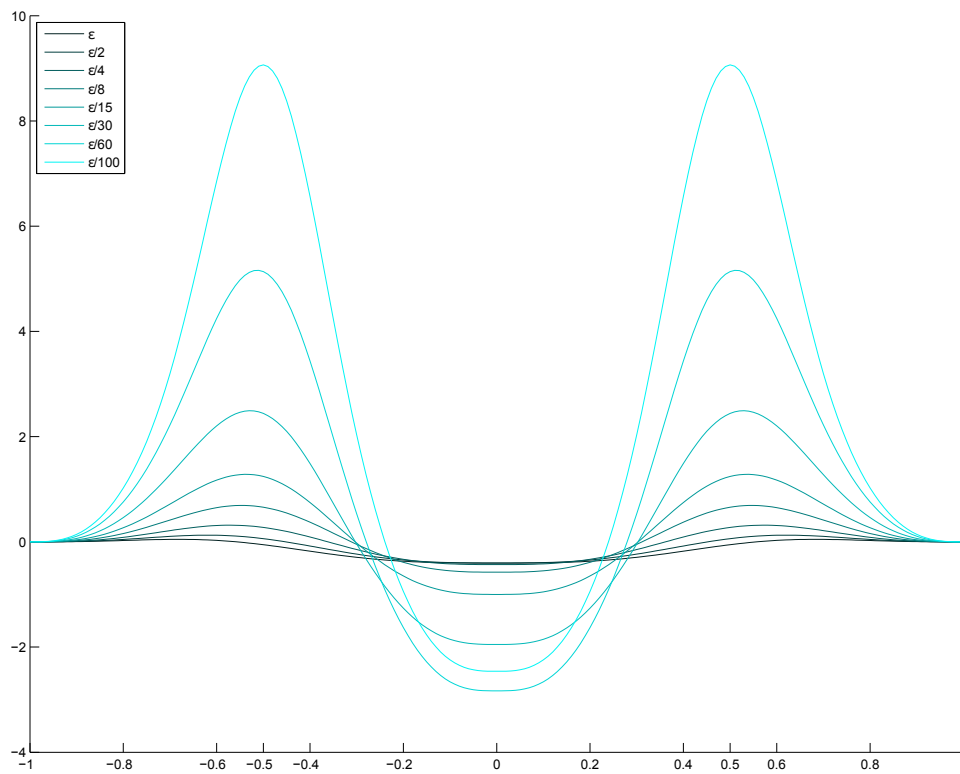
Figure 221: Solution component w_1 for ε varying between $1e - 1$ and $1e - 3$.
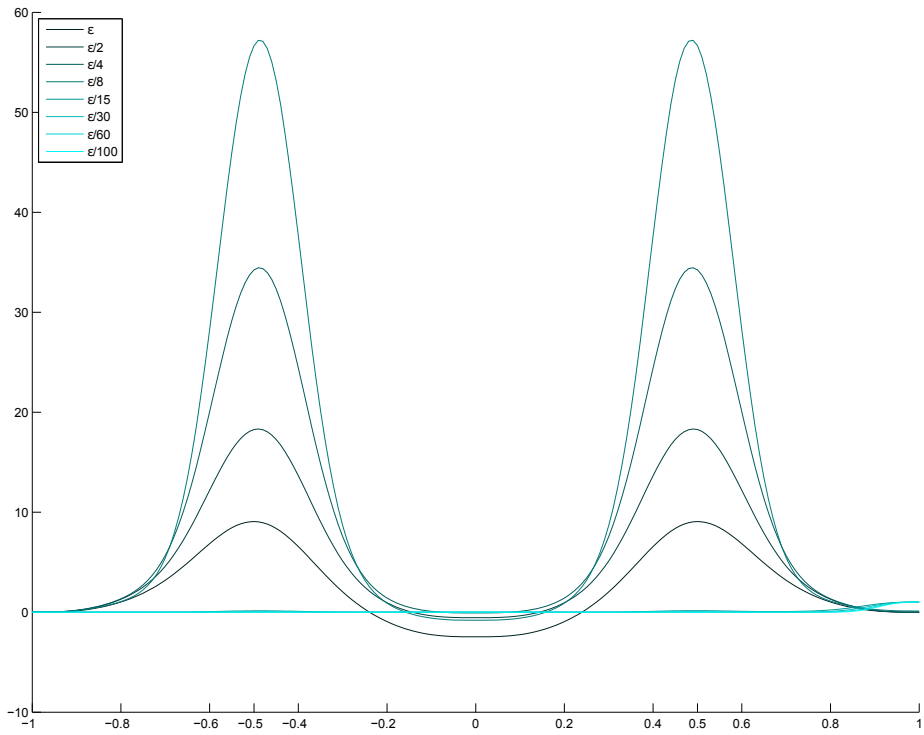
Figure 222: Solution component w_1 for ε varying between $1e-3$ and $1e-5$.
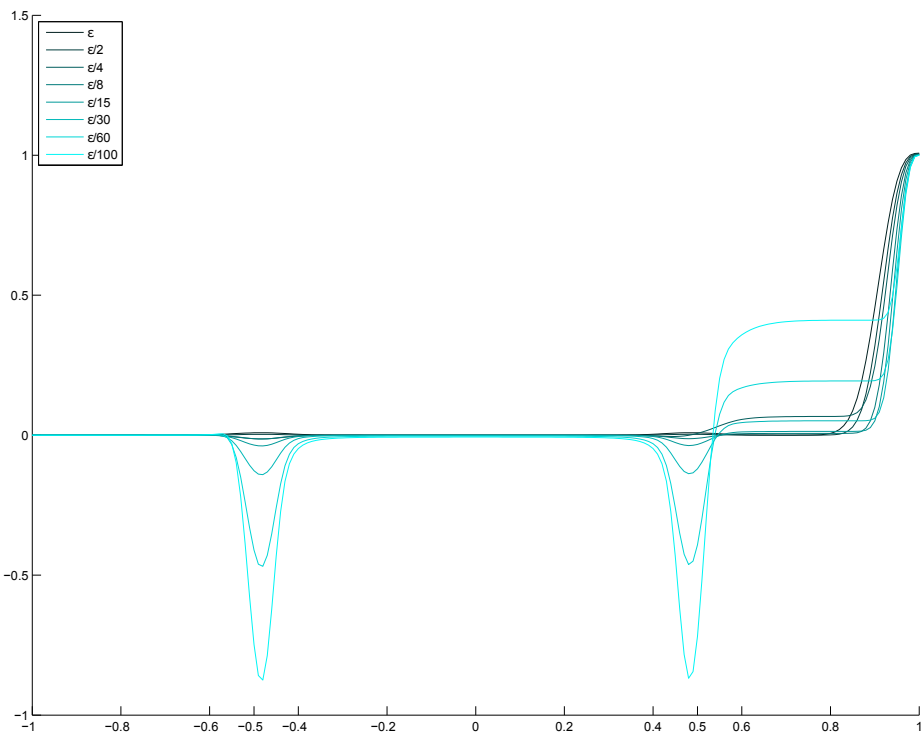
Figure 223: Solution component w_1 for ε varying between $1e-5$ and $1e-7$.
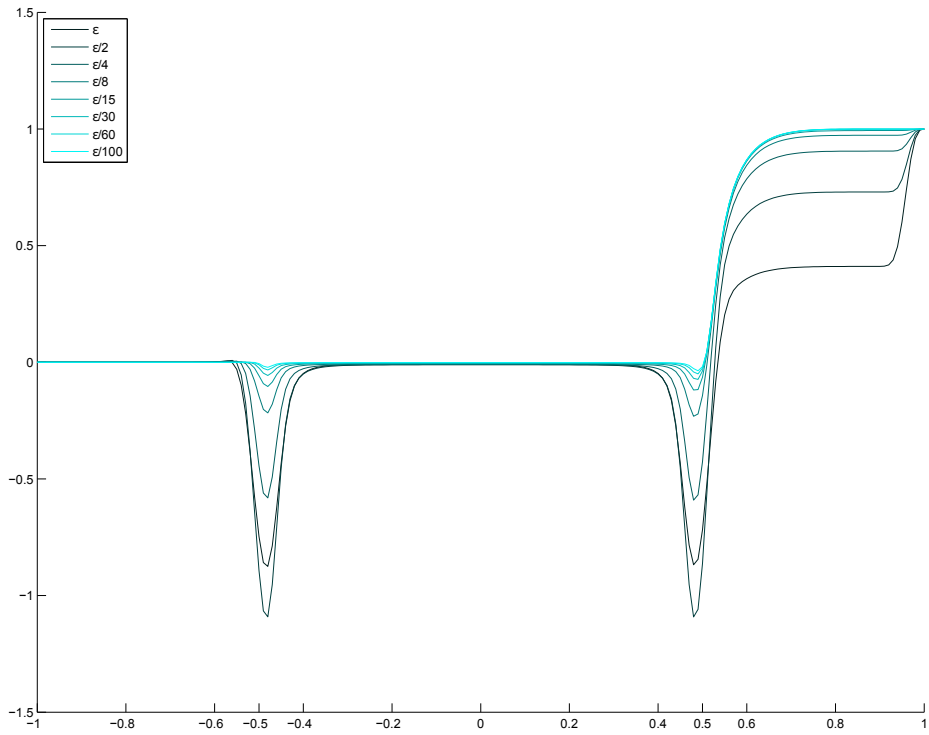
Figure 224: Solution component w_1 for ε varying between $1e - 7$ and $1e - 9$.
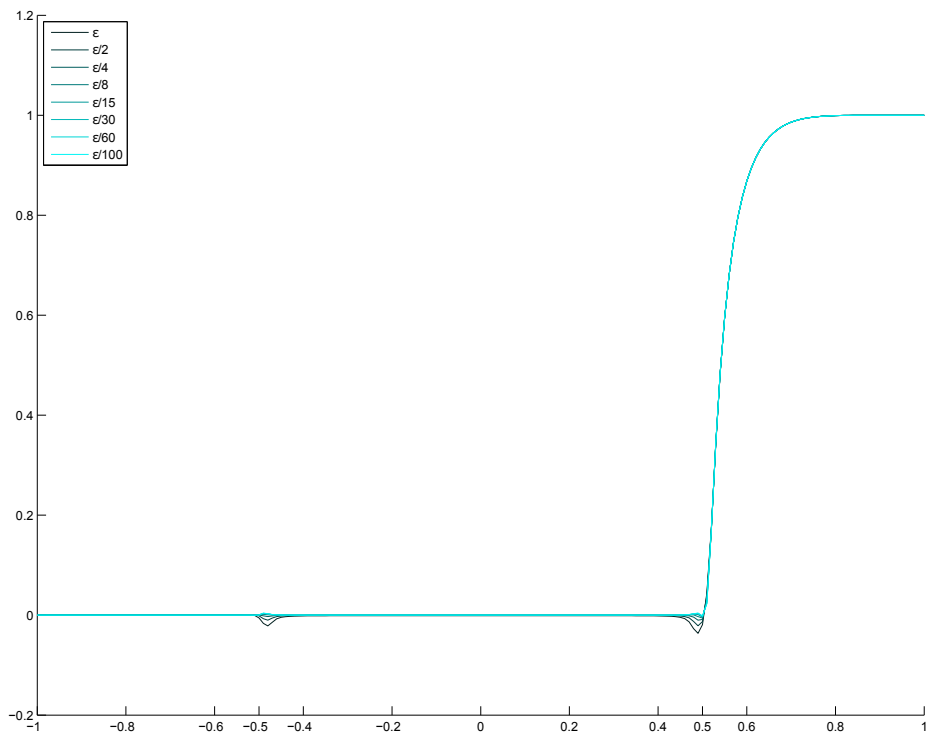
Figure 225: Solution component w_1 for ε varying between $1e - 9$ and $1e - 11$.
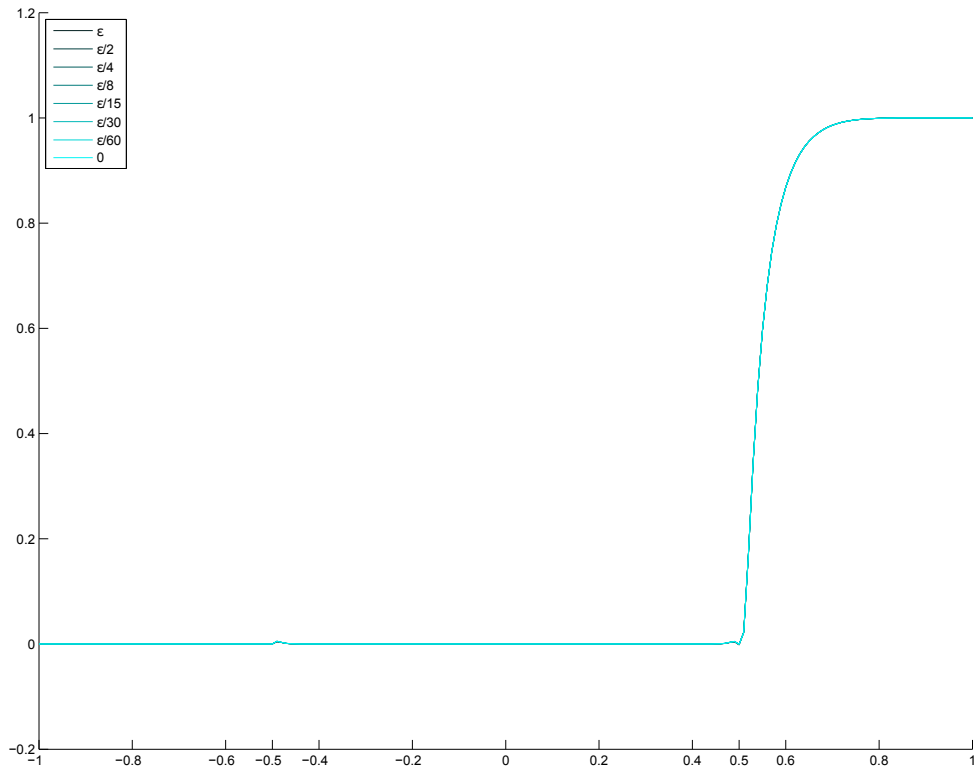
Figure 226: Solution component w_1 for ε varying between $1e - 11$ and 0.

3.4.2.4 Solution component w_2
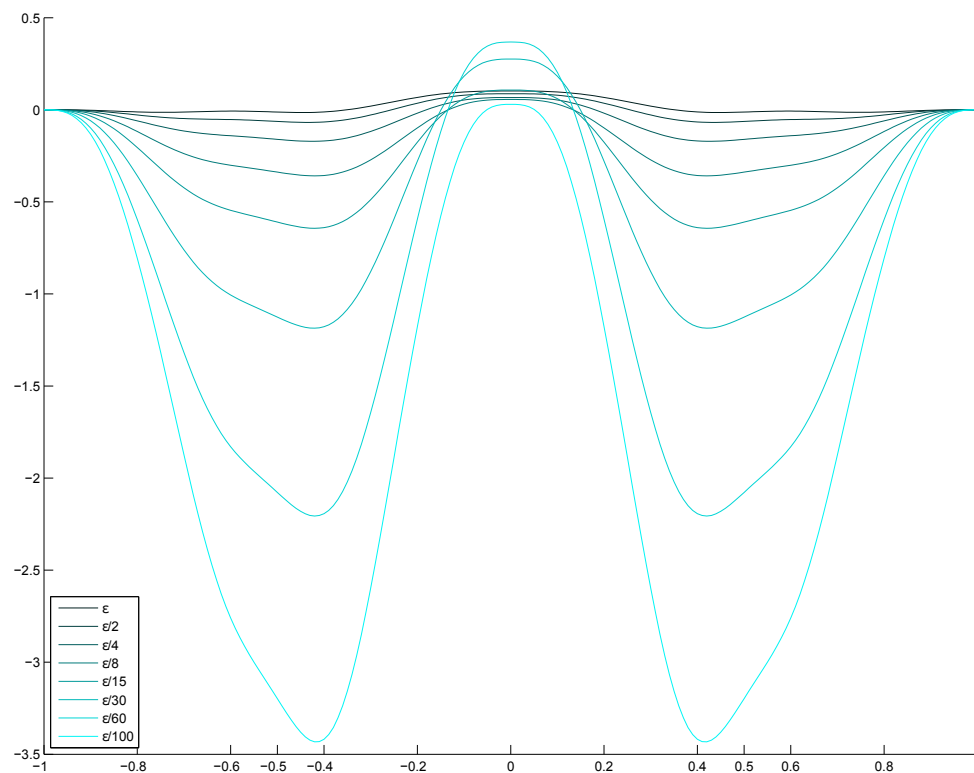
Figure 227: Solution component w_2 for ε varying between $1e-1$ and $1e-3$.
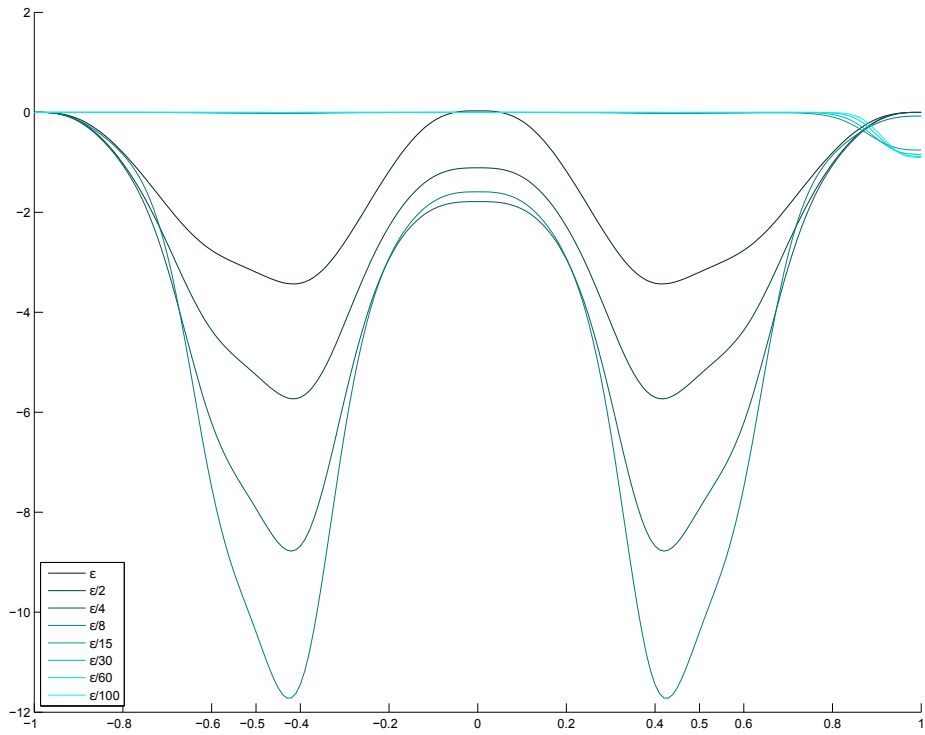
Figure 228: Solution component w_2 for ε varying between $1e-3$ and $1e-5$.
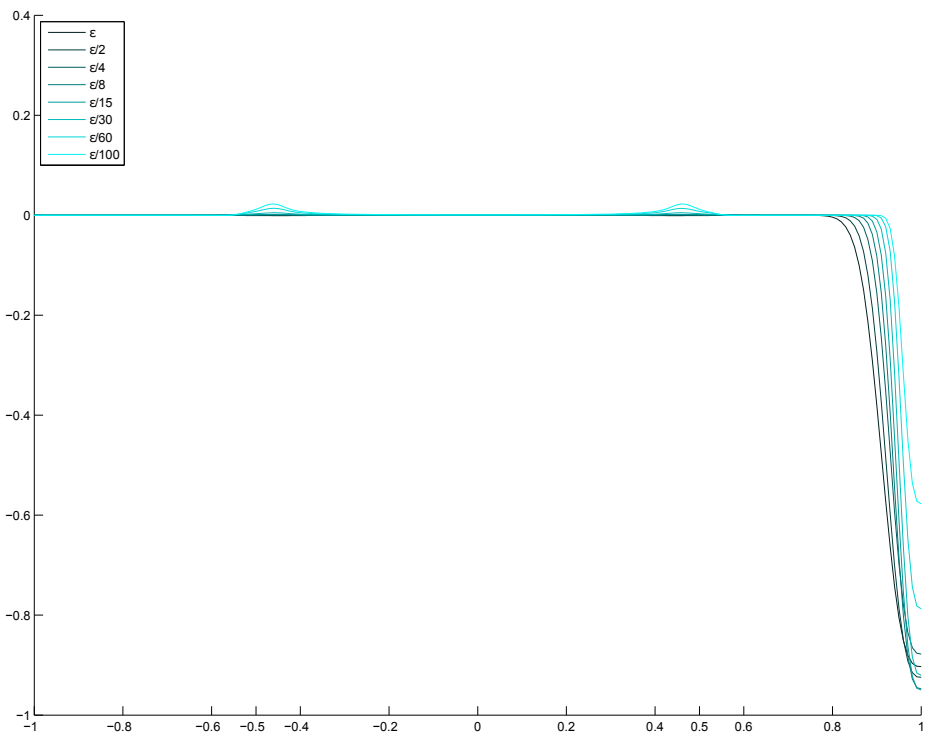
Figure 229: Solution component w_2 for ε varying between $1e-5$ and $1e-7$.

144
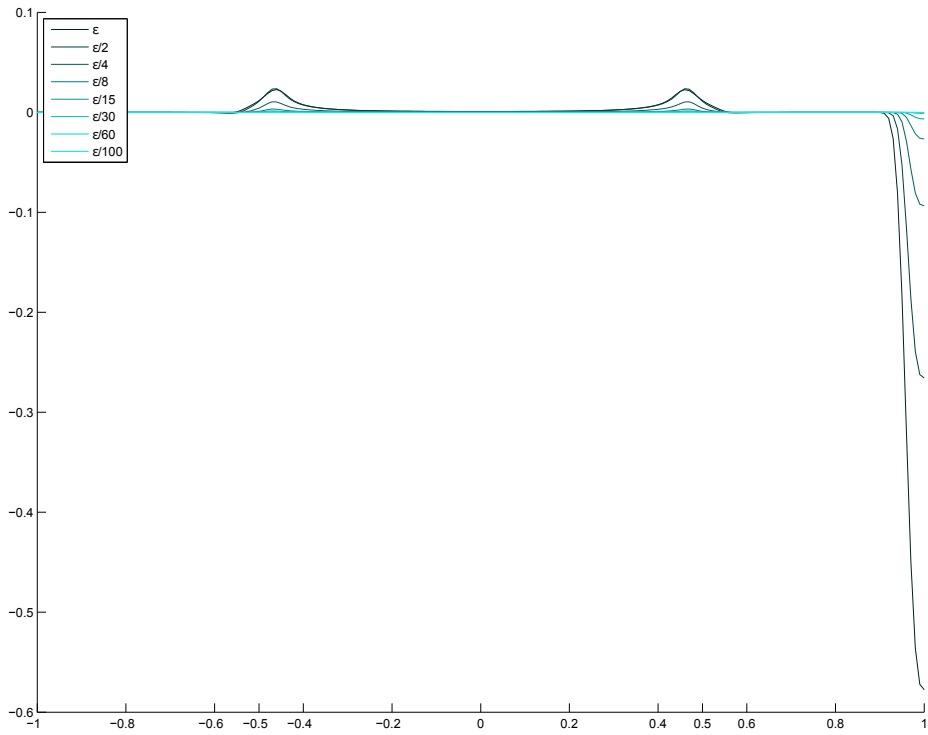
Figure 230: Solution component w_2 for ε varying between $1e-7$ and $1e-9$.
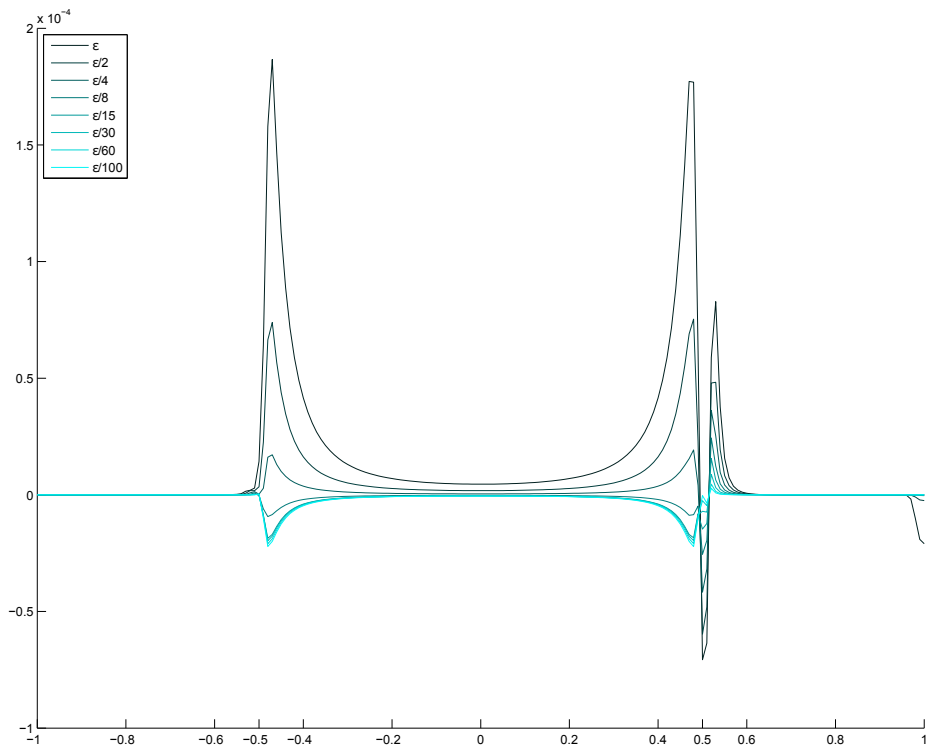
Figure 231: Solution component w_2 for ε varying between $1e-9$ and $1e-11$.
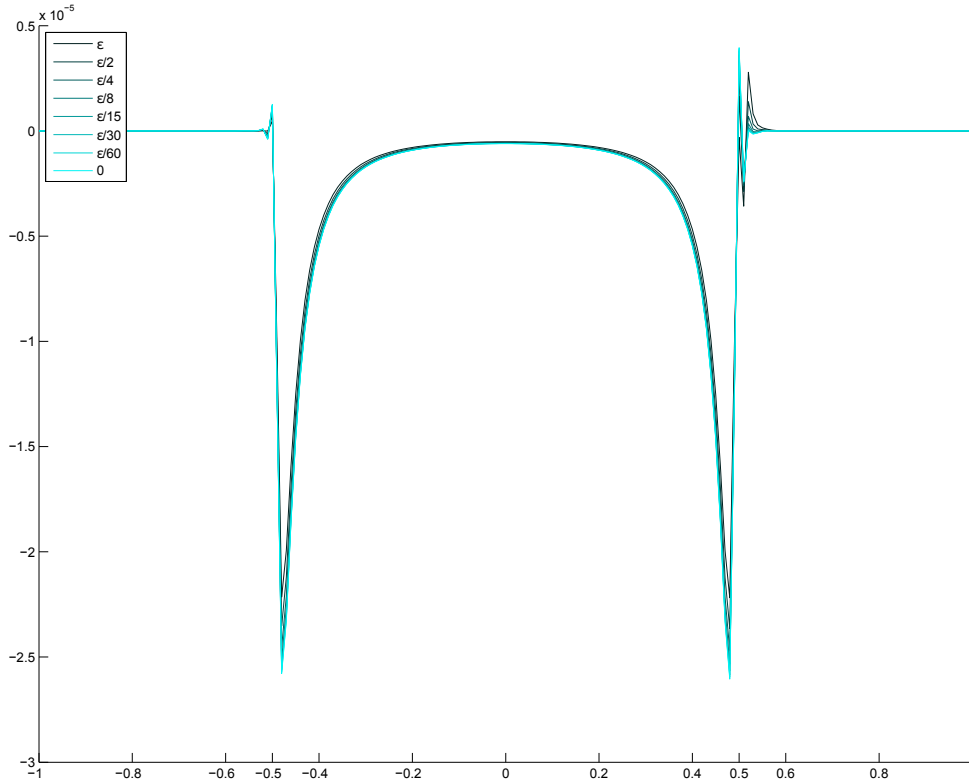
Figure 232: Solution component w_2 for ε varying between $1e - 11$ and 0.

3.5 First observations

Generally, we see that the solution behavior as a function of ε is kind of chaotic. First, when ε becomes very small, we observe continuous changes in the solution behavior, cf. the respective figures.

For these tiny values of ε, we are also able to observe that $w_{-j} = w_j$ which is supported by the theory. However, the more relevant solution property are the peaks which are clearly visible in all plots for ε very close to zero. Interestingly, these peaks occur at somewhat fixed x-values.

- For $J = \{-2, -1, 0, 1, 2, 3\}$, they occur at $x = -\frac{2}{3}$, $-\frac{1}{3}$, $\frac{1}{3}$, and $\frac{2}{3}$;

- For $J = \{-1, 0, 1, 2\}$, they occur at $x = -\frac{1}{2}$ and $\frac{1}{2}$.

To more precisely investigate and possibly explain this solution behavior, we design another series of tests, see following chapter.

3.6 Analytical results

Let us again consider the system (4),

$$Tw_x(x, v) - A(x)w(x, v) = 0, \quad 0 < x < L,$$

where $w(x, v) = (w_j(x, v), j \in J)^\top$. For the analytical background see Chapter 4 [24]. The DAE system (4) is called *tractable* or *solvable* if the determinant

$$\det(\lambda T - A)$$

does not vanish identically in $\lambda \in \mathbb{C}$. Whether this condition holds, crucially depends on J and on the potential V. Concerning solvability, two situations can occur:

(a) If the DAE is not *tractable/solvable*, its solutions are not unique.

(b) If the DAE is *tractable/solvable*, we still have a difficult situation. This is due to too many boundary conditions, which makes the BVP not solvable, in general.

Let us assume that the DAE is tractable. The problem with too many boundary conditions does *formally* not constitute any difficulty, since the algorithm which we apply is solving the resulting discrete system in the least square sense.

We now calculate $\det(\lambda T - A)$ for $J = \{-1, 0, 1, 2\}$ to find out when it is not vanishing,

$$\det(\lambda T - A) = \begin{vmatrix} \lambda v_{-1} & a_1(x) & a_2(x) & a_3(x) \\ -a_1(x) & 0 & a_1(x) & a_2(x) \\ -a_2(x) & -a_1(x) & \lambda v_1 & a_1(x) \\ -a_3(x) & -a_2(x) & -a_1(x) & \lambda v_2 \end{vmatrix}.$$

After some simplifications, we obtain

$$\begin{aligned} \det(\lambda T - A) = &- \lambda^2 a_2(x)^2 v_1^2 + a_1(x)^4 + a_2(x)^4 - 2a_1(x)^2 a_2(x)^2 \\ &+ a_1(x)^2 a_3(x)^2 + 2a_1(x)^3 a_3(x) - 2a_1(x)a_2(x)^2 a_3(x). \end{aligned}$$

For $a_2(x) \neq 0$, the above expression does not vanish identically in $\lambda \in \mathbb{C}$.

Let us also try a different approach – find out index of the problem. This is done by differentiating the algebraic constraint as long as necessary to obtain an explicit expression for w_0. The algebraic constraint reads:

$$0 = a_2(x)w_2(x) + a_1(x)w_1(x) - a_1(x)w_{-1}(x)$$

and after one differentiation, we have

$$0 = a_2'(x)w_2(x) + a_2(x)w_2'(x) + a_1'(x)w_1(x) + a_1(x)w_1'(x) - a_1'(x)w_{-1}(x) - a_1(x)w_{-1}'(x). \tag{5}$$

Now, we rewrite the other equations,

$$\begin{array}{llllll} 2w_2'(x) & & + a_1(x)w_1(x) & + a_2(x)w_0(x) & + a_3(x)w_{-1}(x) & = 0, & \left| \cdot(-\frac{a_2(x)}{2}) \right. \\ w_1'(x) & - a_1(x)w_2(x) & & + a_1(x)w_0(x) & + a_2(x)w_{-1}(x) & = 0, & \left| \cdot(-a_1(x)) \right. \\ -w_{-1}'(x) & - a_3(x)w_2(x) & - a_2(x)w_1(x) & - a_1(x)w_0(x) & & = 0, & \left| \cdot(-a_1(x)) \right. \end{array}$$

and use them to simplify (5),

$$\frac{a_2(x)^2 w_0(x)}{2} = (a_2'(x) + a_1(x)a_3(x) + a_1(x)^2)w_2(x) + \left(a_1'(x) + \frac{a_1(x)a_2(x)}{2}\right)w_1(x)$$

$$- \left(a_1'(x) + a_1(x)a_2(x) + \frac{a_2(x)a_3(x)}{2}\right)w_{-1}(x).$$

Since this is an explicit form for $w_0(x)$, the DAE system is an Index-2 problem (we have differentiated one time). Note, that this only holds for $a_2(x) \neq 0$

These considerations motivate to closer investigate the properties of $a_2(x)$. Let us begin by plotting this function, cf. Figure 233.
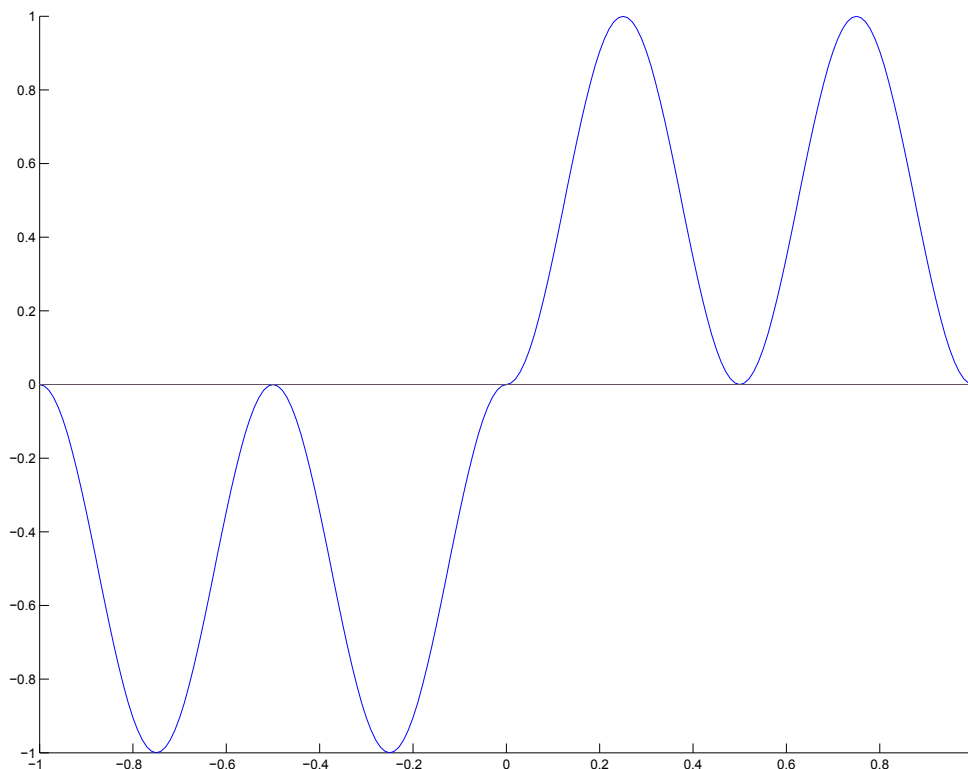

Figure 233: Plot of the fuction $a_2(x)$.

First, we note that $a_2(x)$ is zero at exactly those points where we observed peaks in the first series of results. This observation motivated the design of the second series of test runs, see next section.

3.7 Second results

Our aim was to eliminate the solution peaks, by manually removing the zeros of $a_2(x)$. This can be easily done by introducing a new parameter, μ, which we use to modify the

function $a_2(x)$:

$$a_2^\mu(x) = a_2(x) + \mu x.$$

As we can see in the following plot, where $\mu = 1$, function a_2^μ has no zeros, except the one at $x = 0$.
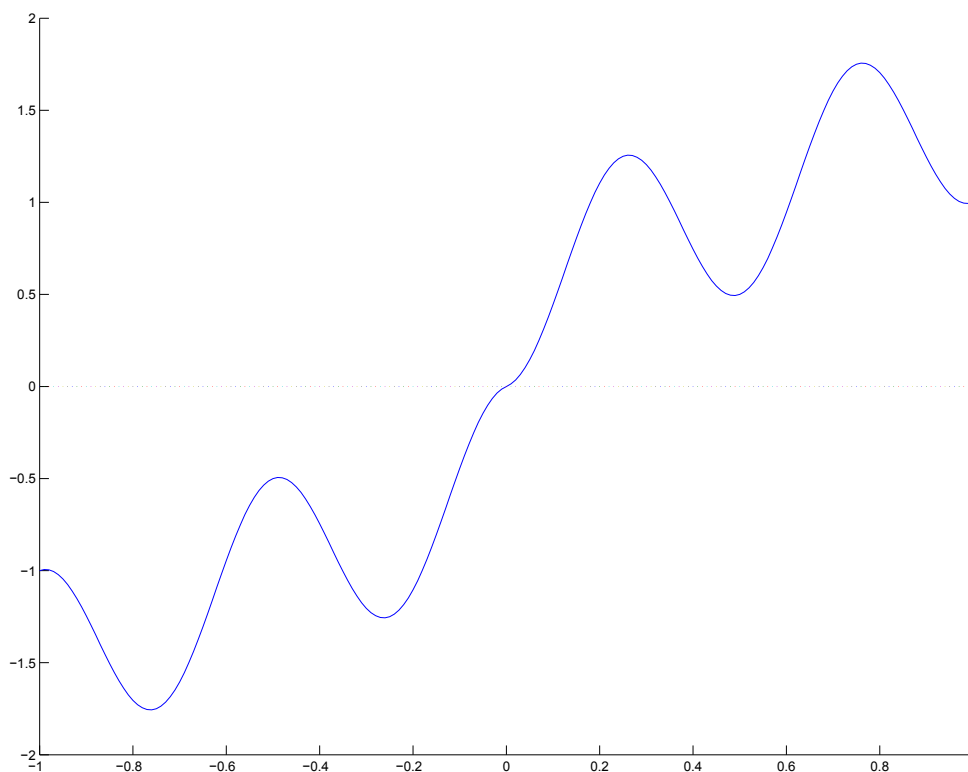

Figure 234: Plot of the function $a_2^\mu(x)$, $\mu = 1$.

Clearly, for $\mu = 1$ we can see a large change in $a_2(x)$, but as before for ε, we will consider $\mu \to 0$. The values for μ were chosen as $\mu = 1$, 0.1, 0.01, 0.001, 0.0001, and ε were varying between $1e - 9$ and 0.

3.7.1 Solution for $\mu = 1$
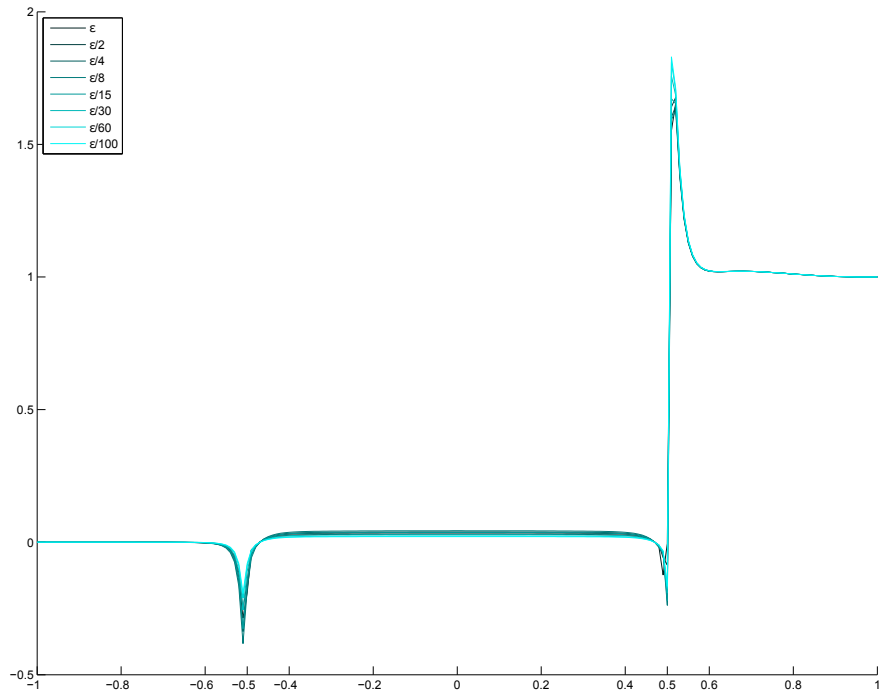
Figure 235: $\mu = 1$: Solution component w_{-1} for ε varying from $1e - 9$ and $1e - 11$.
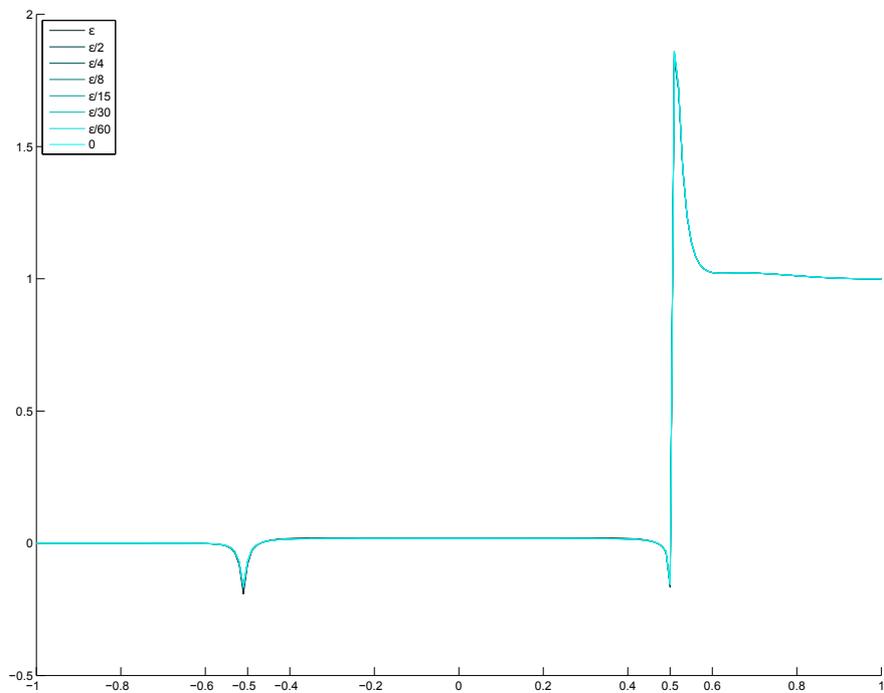

Figure 236: $\mu = 1$: Solution component w_{-1} for ε varying from $1e - 11$ to 0.
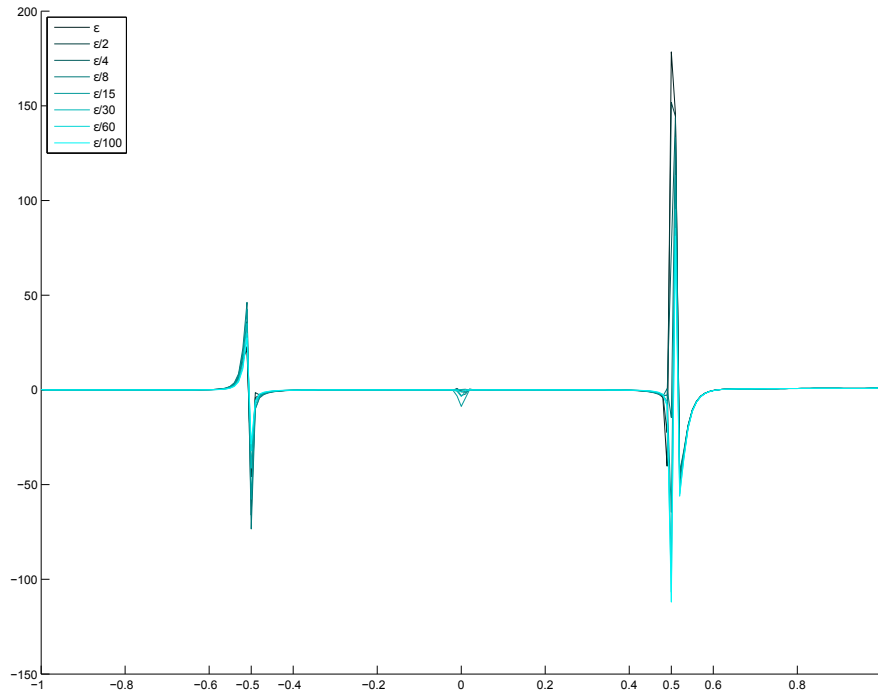
Figure 237: $\mu = 1$: Solution component w_0 for ε varying from $1e - 9$ to $1e - 11$.
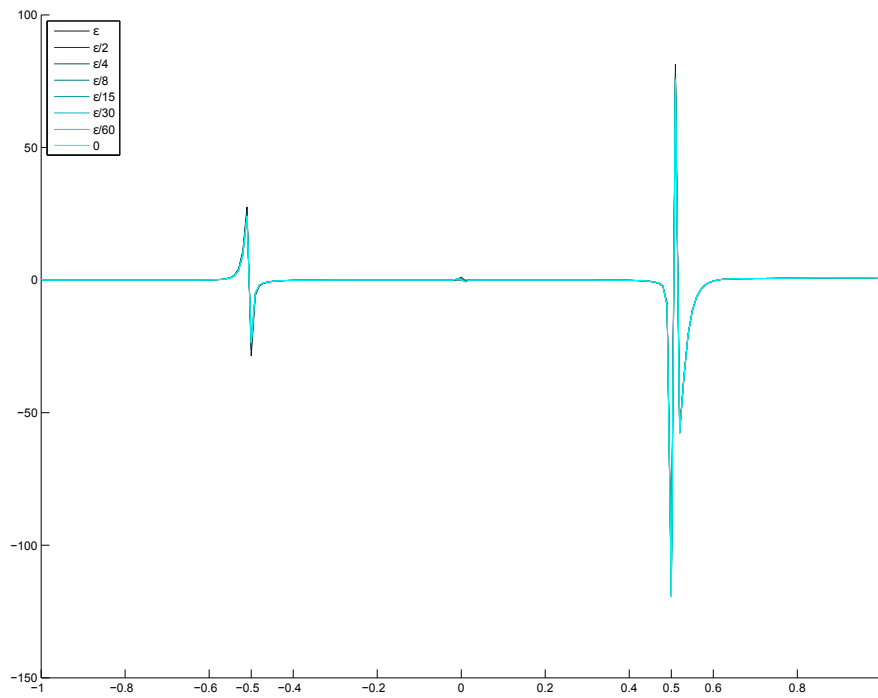
Figure 238: $\mu = 1$: Solution component w_0 for ε varying from $1e - 11$ to 0.
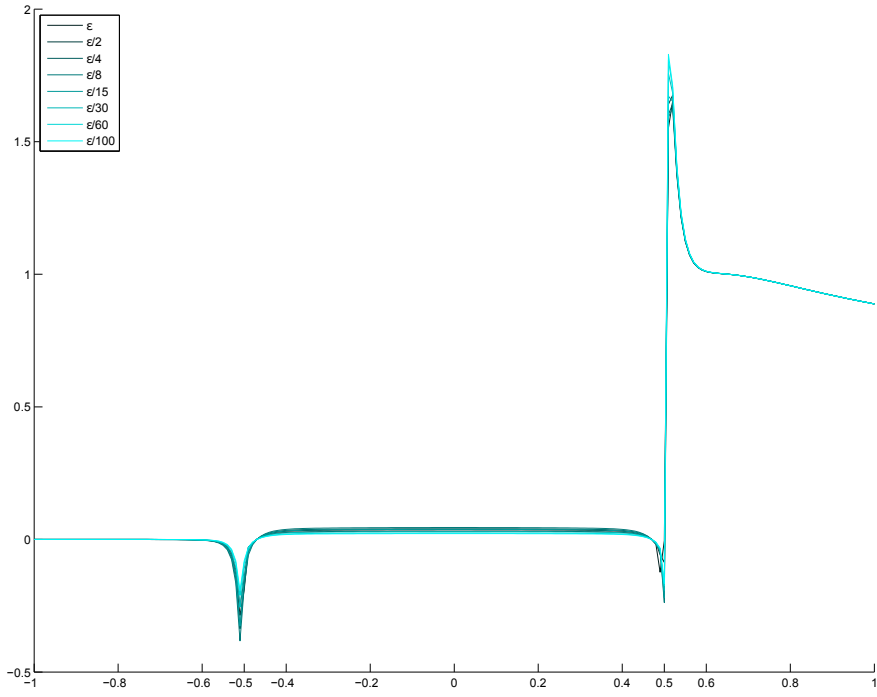
Figure 239: $\mu = 1$: Solution component w_1 for ε varying from $1e-9$ to $1e-11$.
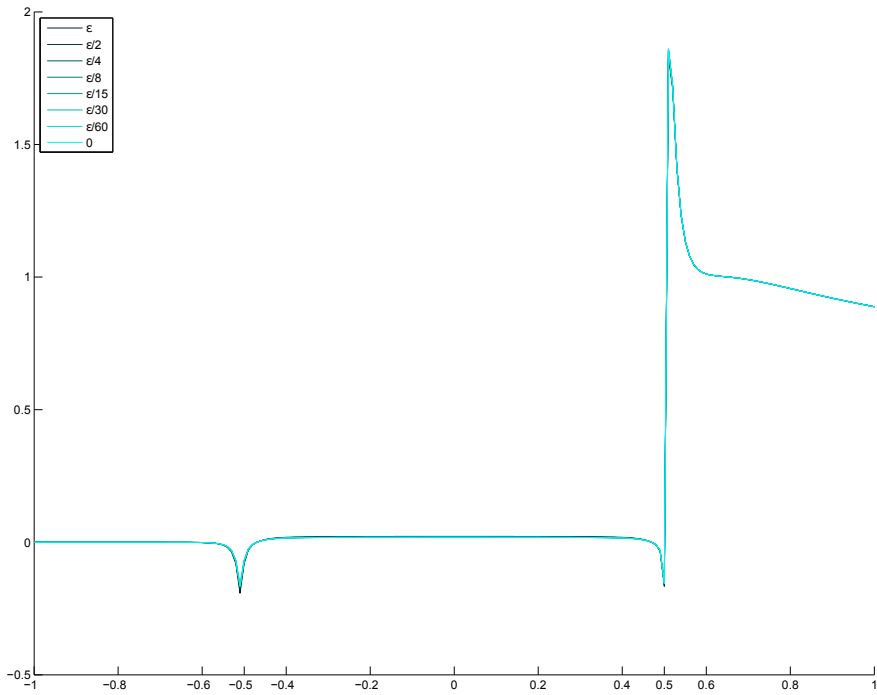
Figure 240: $\mu = 1$: Solution component w_1 for ε varying from $1e-11$ to 0.
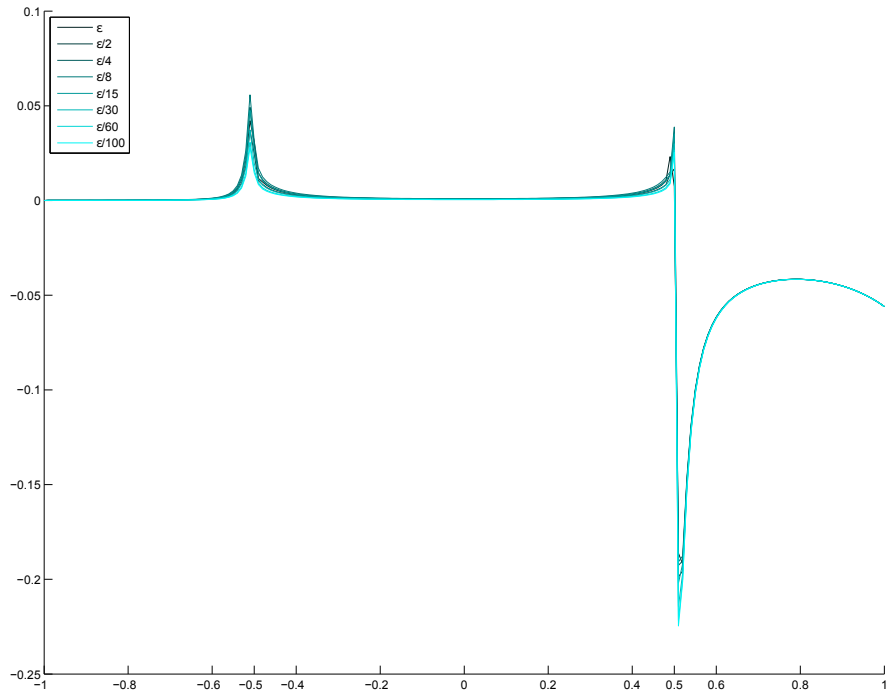
Figure 241: $\mu = 1$: Solution component w_2 for ε varying from $1e - 9$ to $1e - 11$.
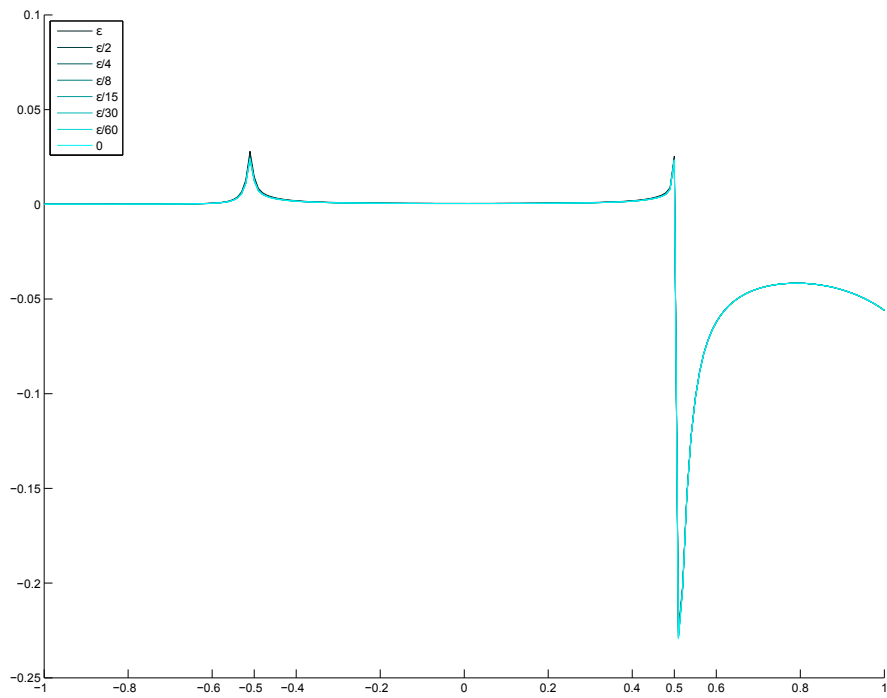
Figure 242: $\mu = 1$: Solution component w_2 for ε varying from $1e - 11$ to 0.

3.7.2 Solution for $\mu = 0.1$
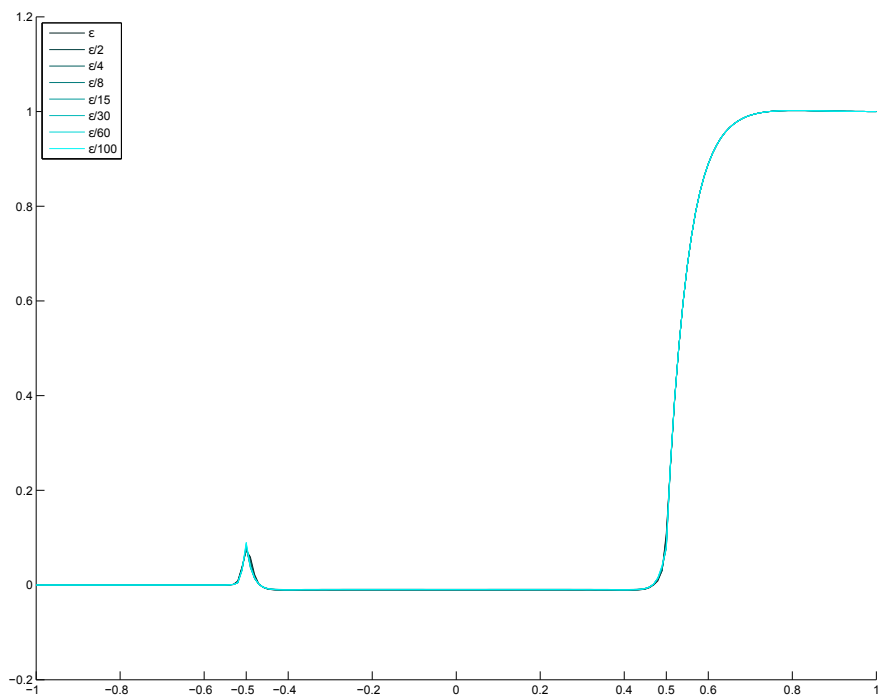
Figure 243: $\mu = 0.1$: Solution component w_{-1} for ε varying from $1e-9$ to $1e-11$.
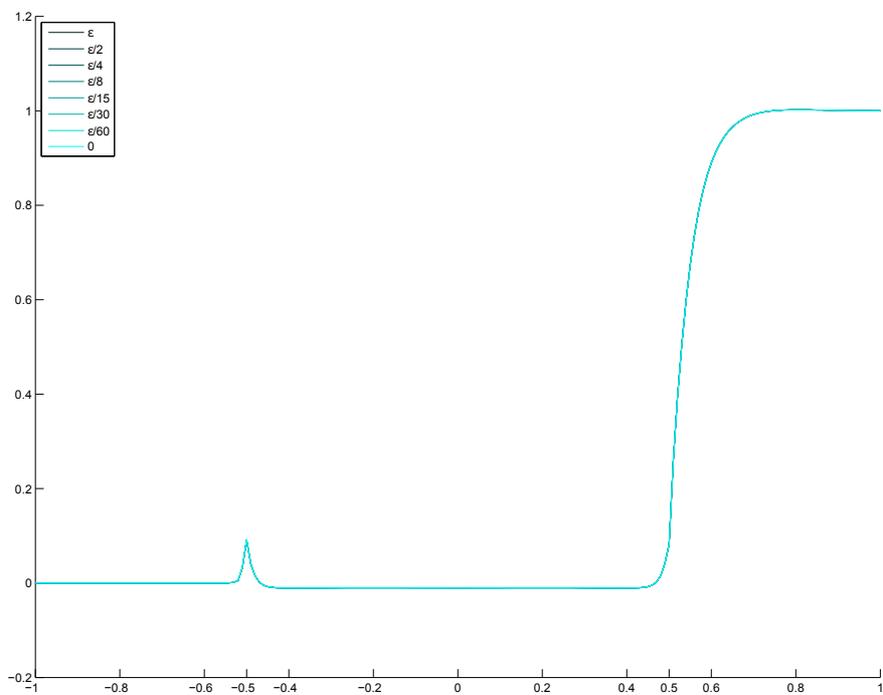
Figure 244: $\mu = 0.1$: Solution component w_{-1} for ε varying from $1e-11$ to 0.

154
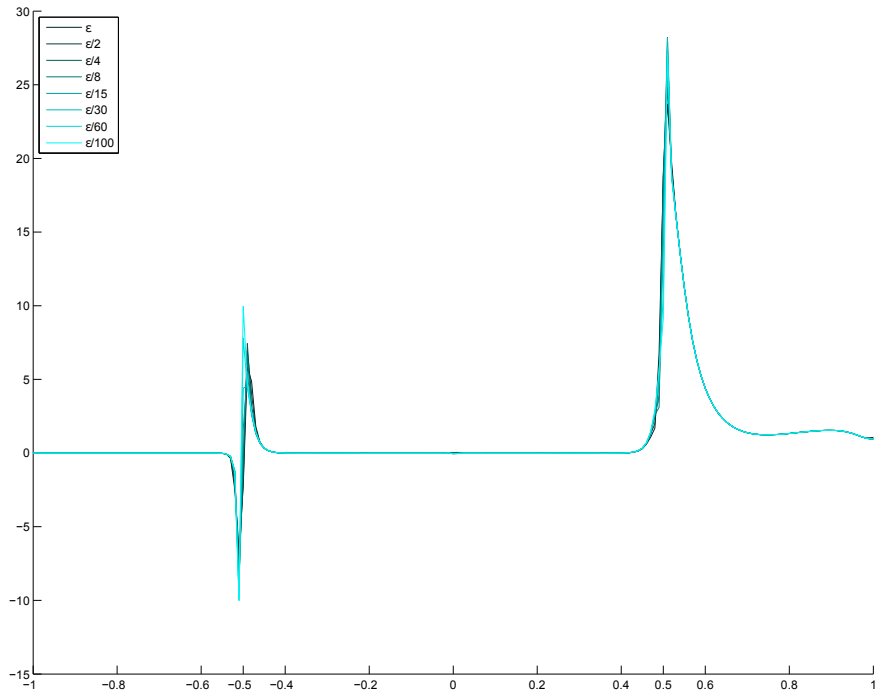
Figure 245: $\mu = 0.1$: Solution component w_0 for ε varying from $1e-9$ to $1e-11$.
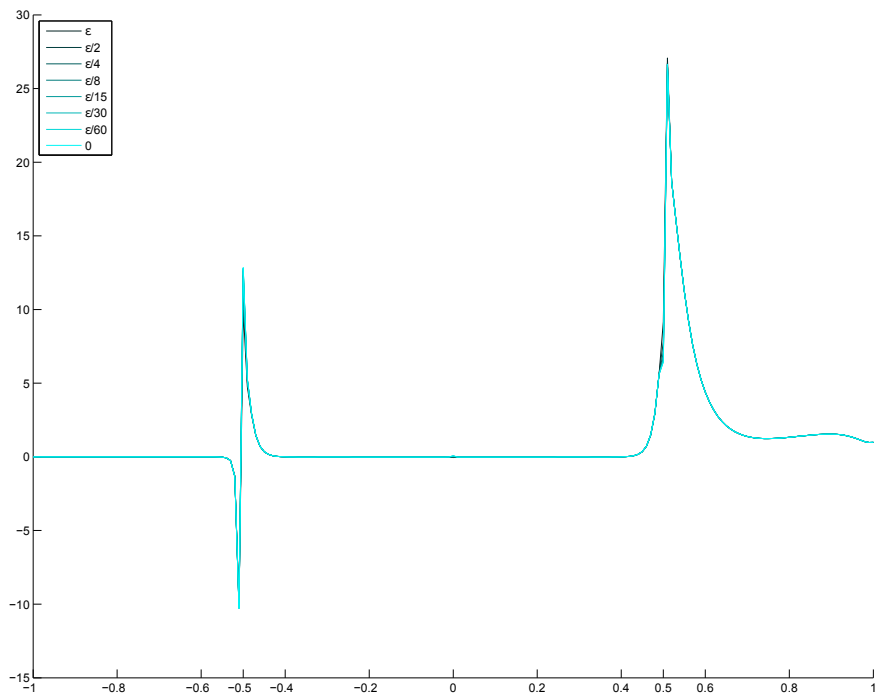
Figure 246: $\mu = 0.1$: Solution component w_0 for ε varying from $1e-11$ to 0.
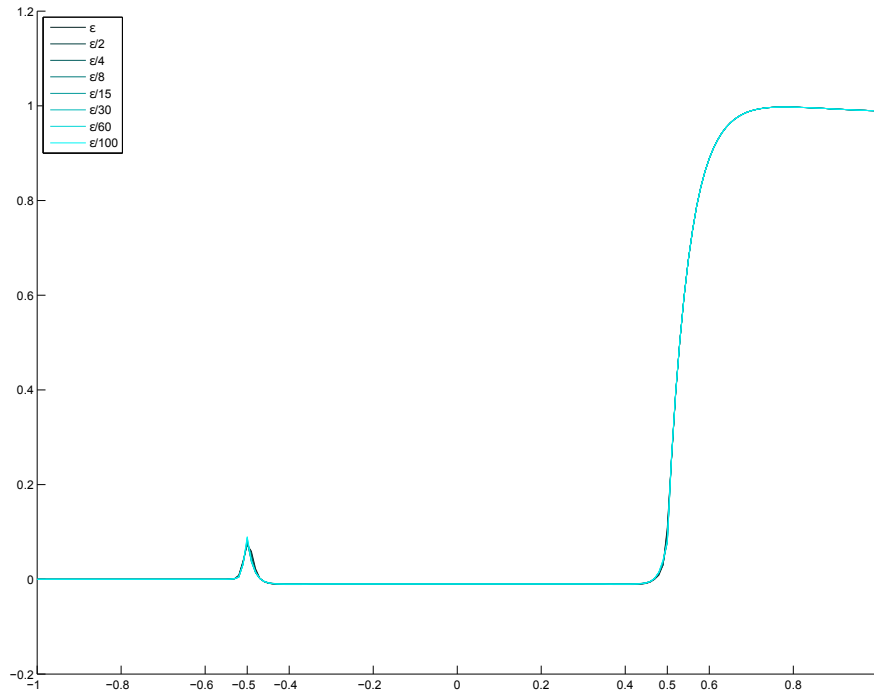
Figure 247: $\mu = 0.1$: Solution component w_1 for ε varying from $1e - 9$ to $1e - 11$.
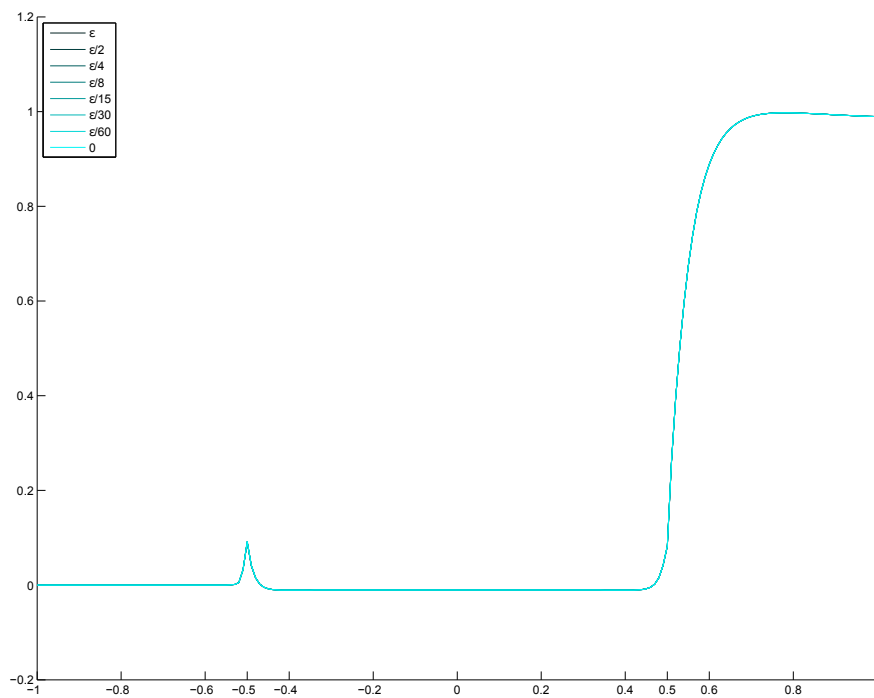
Figure 248: $\mu = 0.1$: Solution component w_1 for ε varying from $1e - 11$ to 0.
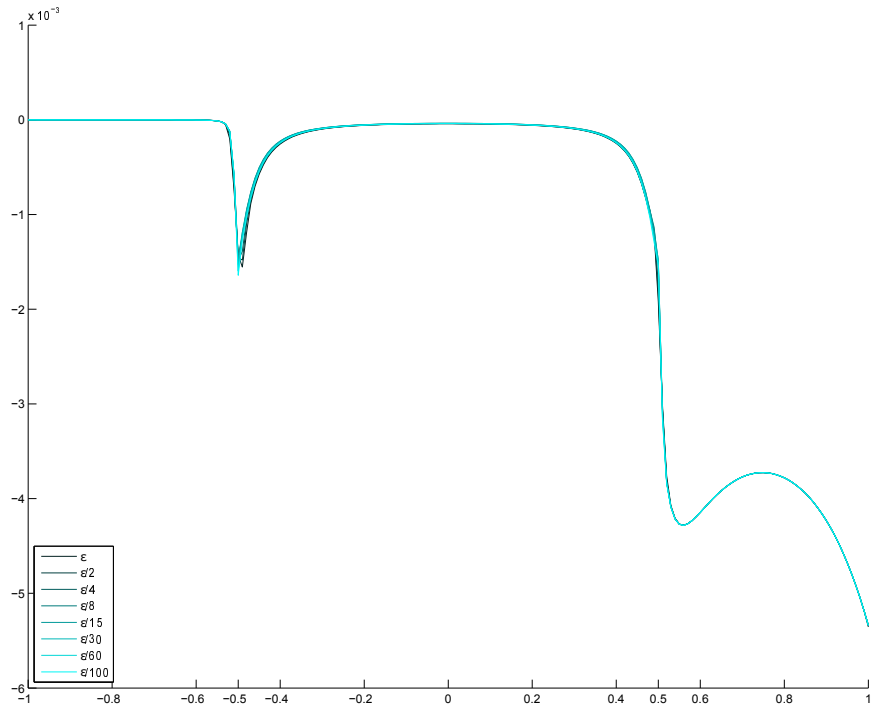
Figure 249: $\mu = 0.1$: Solution component w_2 for ε varying from $1e-9$ to $1e-11$.
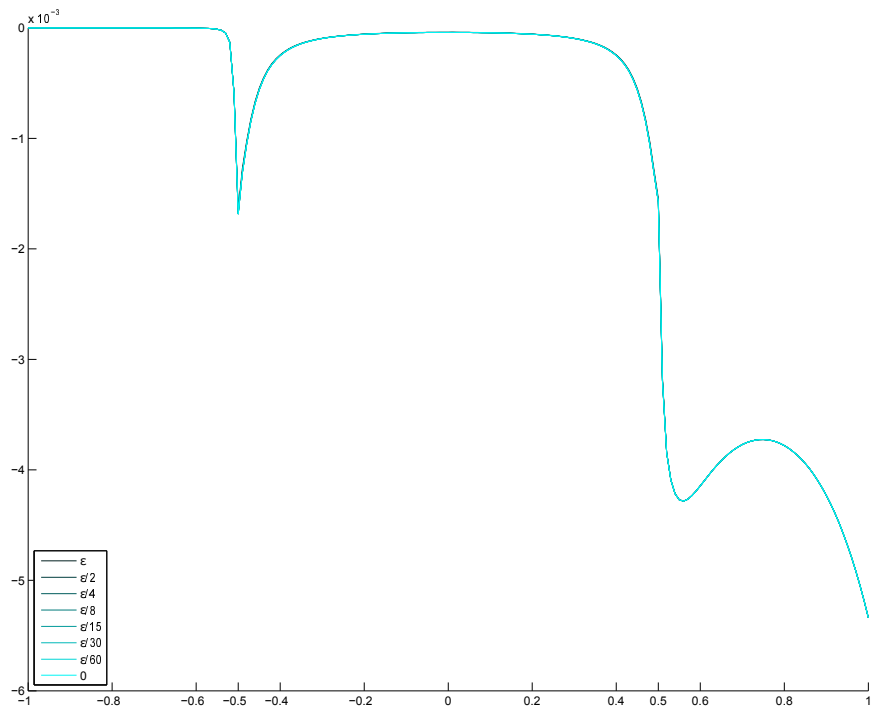
Figure 250: $\mu = 0.1$: Solution component w_2 for ε varying from $1e-11$ to 0.

157

3.7.3 Solution for $\mu = 0.01$
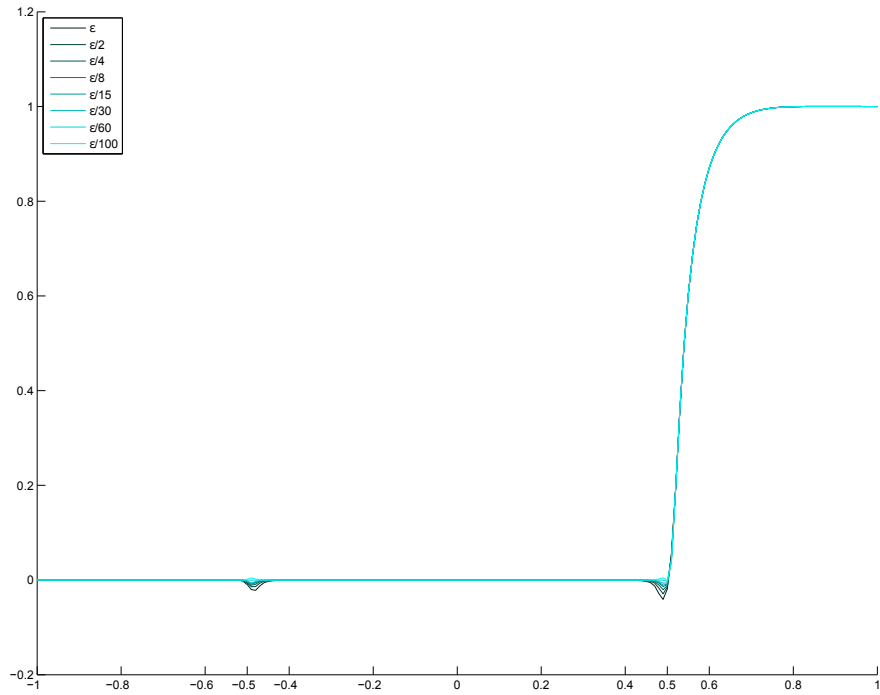
Figure 251: $\mu = 0.01$: Solution component w_{-1} for ε varying from $1e - 9$ to $1e - 11$.
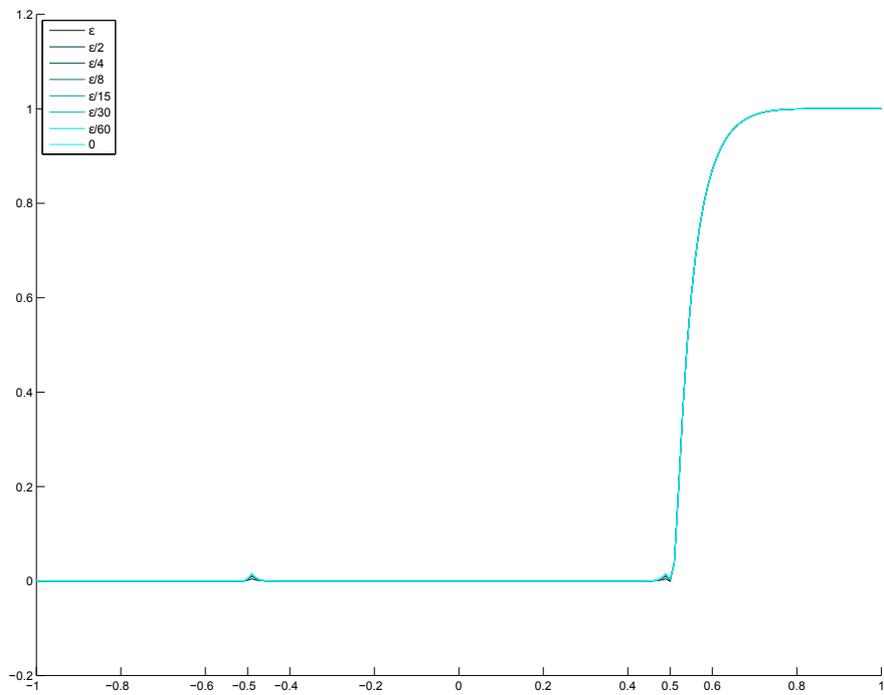
Figure 252: $\mu = 0.01$: Solution component w_{-1} for ε varying from $1e - 11$ to 0.
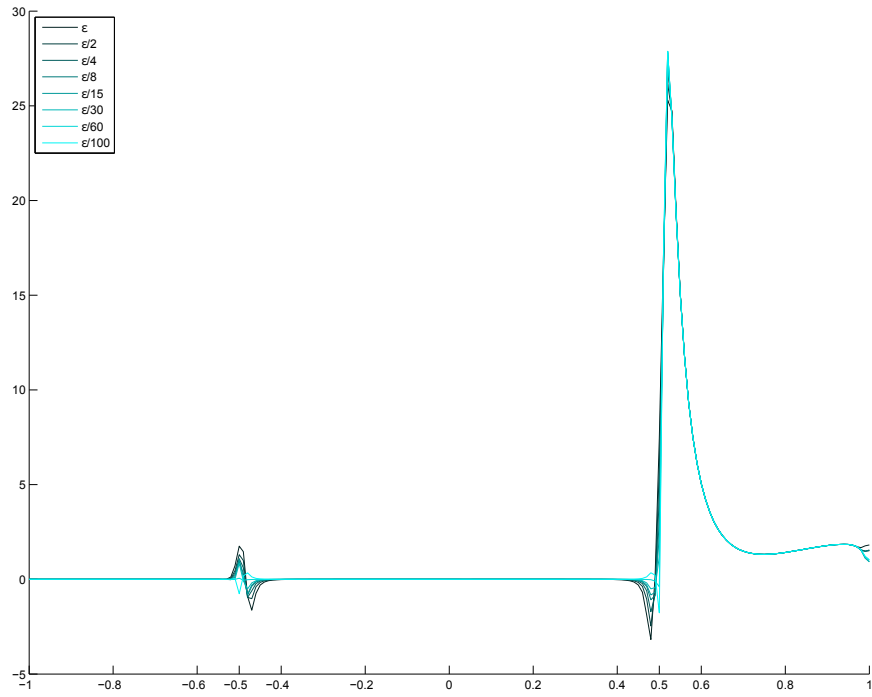
Figure 253: $\mu = 0.01$: Solution component w_0 for ε varying from $1e-9$ to $1e-11$.
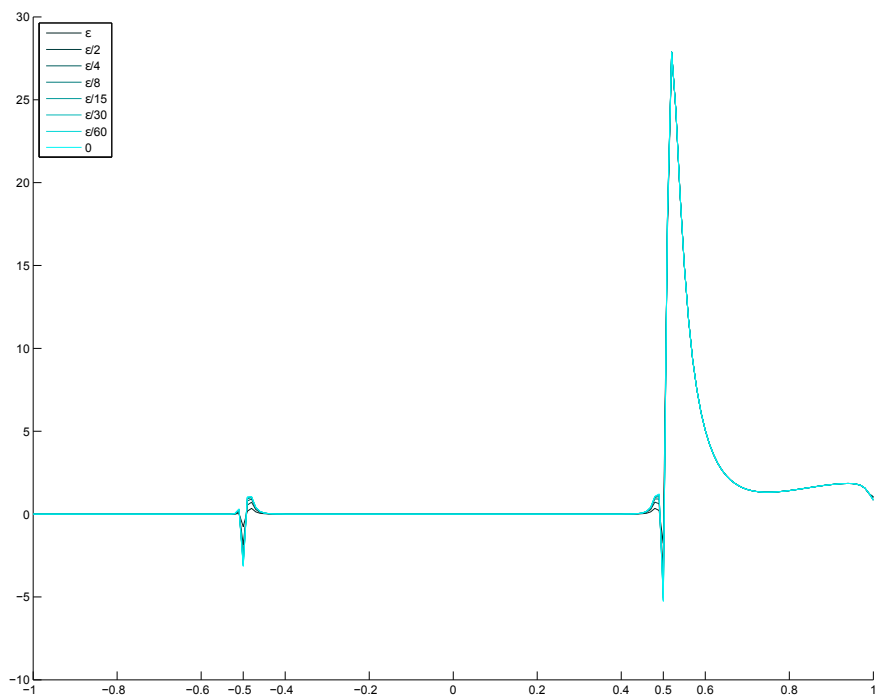
Figure 254: $\mu = 0.01$: Solution component w_0 for ε varying from $1e-11$ to 0.
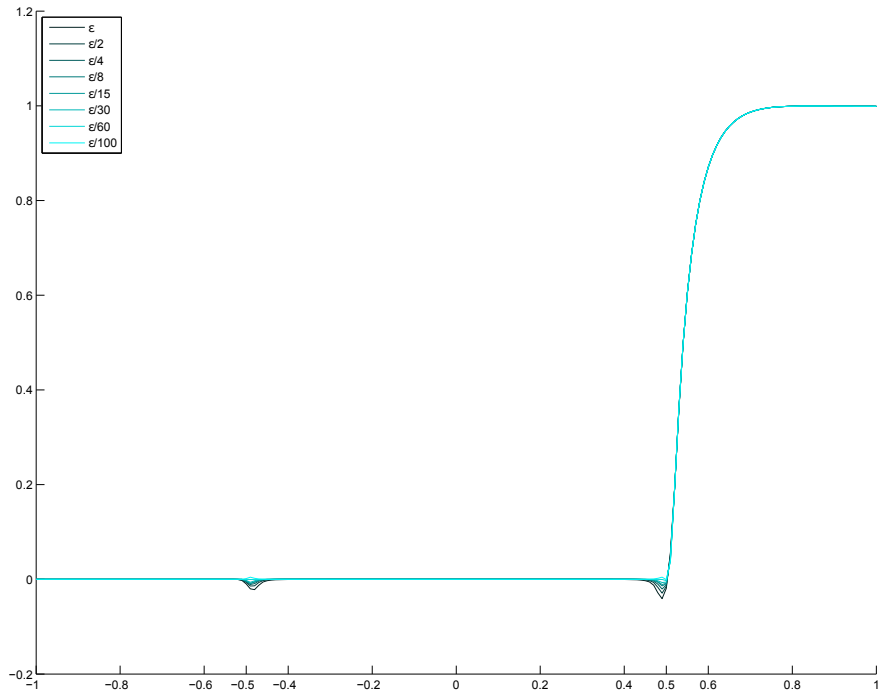
Figure 255: $\mu = 0.01$: Solution component w_1 for ε varying from $1e - 9$ to $1e - 11$.
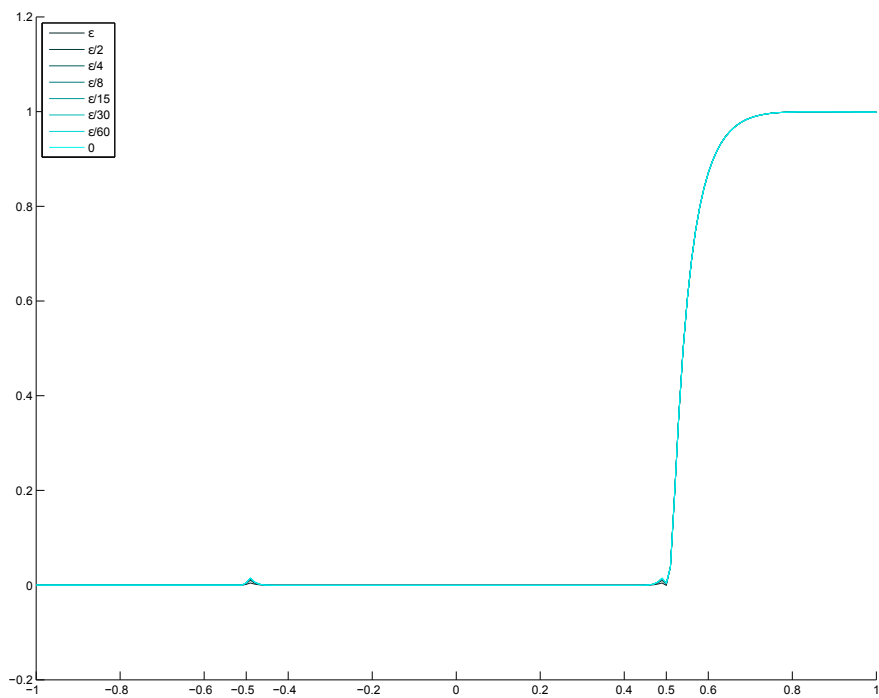
Figure 256: $\mu = 0.01$: Solution component w_1 for ε varying from $1e - 11$ to 0.
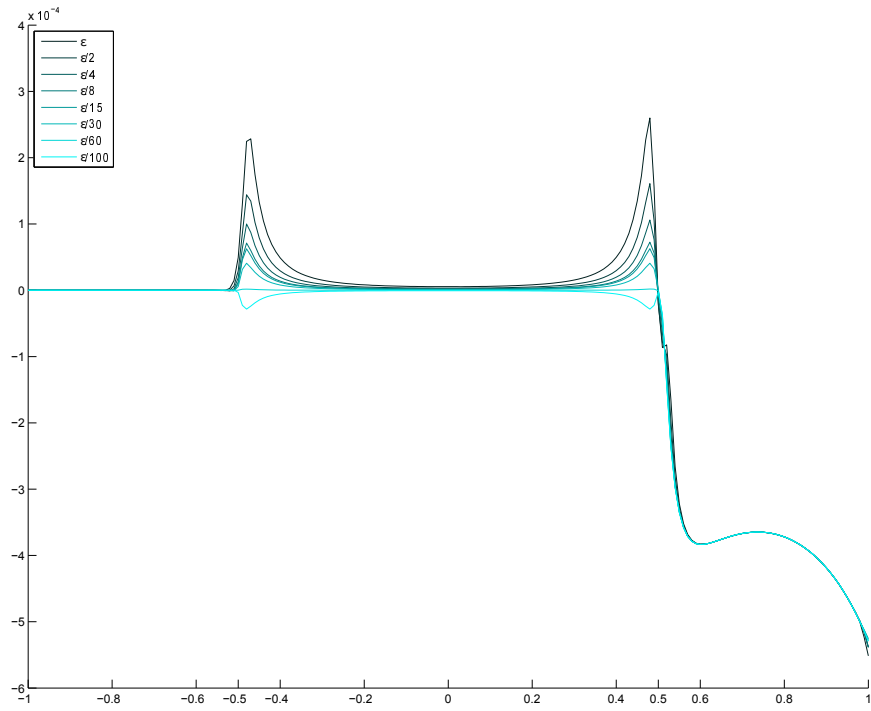
Figure 257: $\mu = 0.01$: Solution component w_2 for ε varying from $1e - 9$ to $1e - 11$.
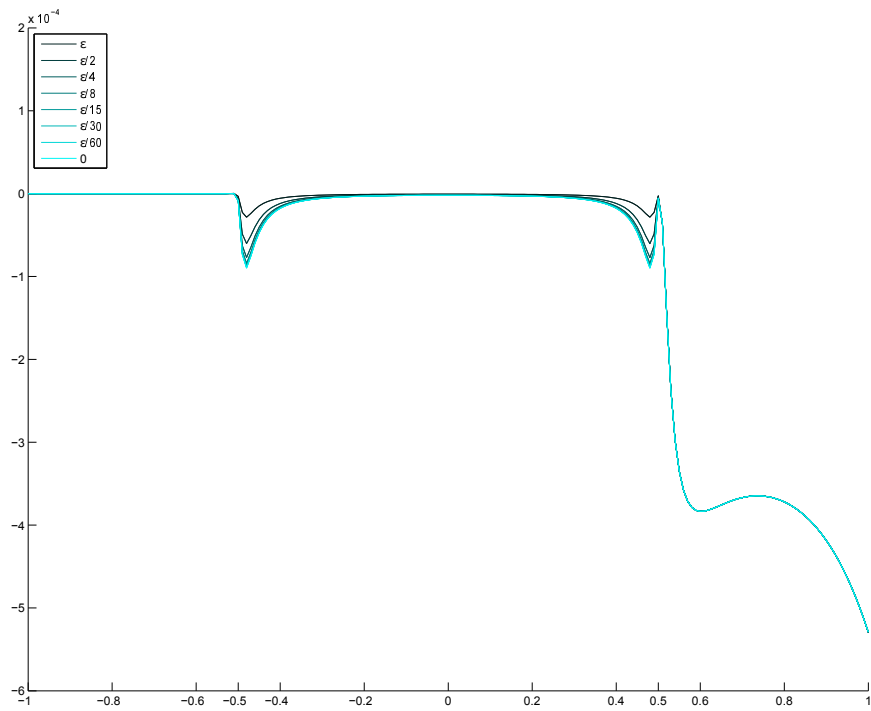
Figure 258: $\mu = 0.01$: Solution component w_2 for ε varying from $1e - 11$ to 0.

161

3.7.4 Solution for $\mu = 0.001$
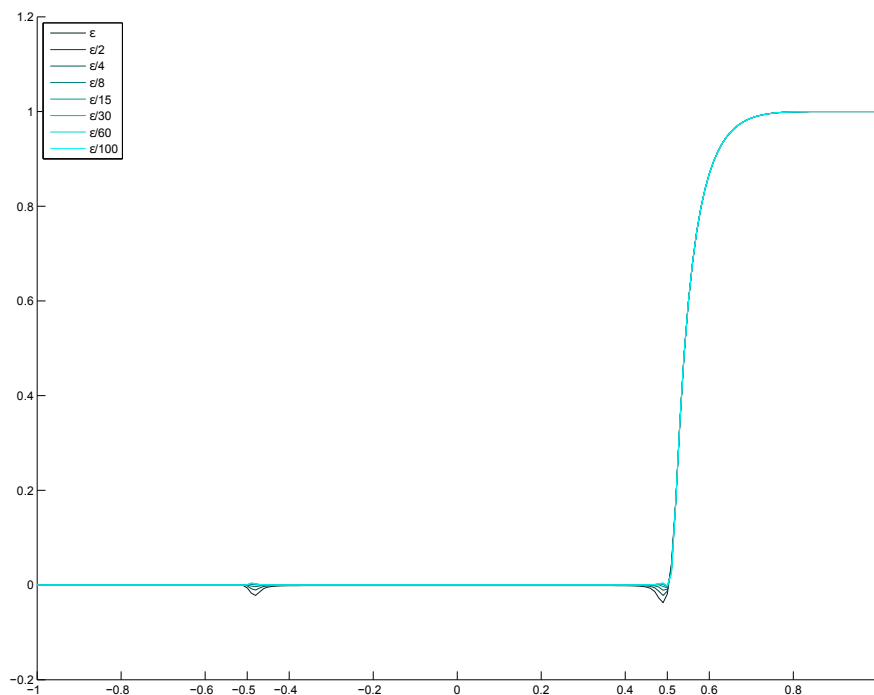
Figure 259: $\mu = 0.001$: Solution component w_{-1} for ε varying from $1e - 9$ to $1e - 11$.
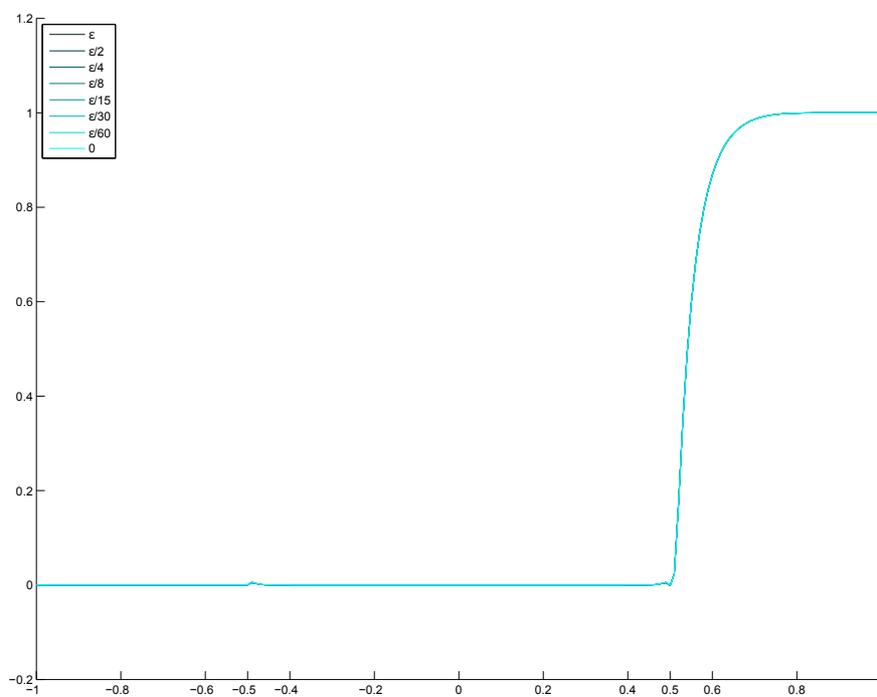
Figure 260: $\mu = 0.001$: Solution component w_{-1} for ε varying from $1e - 11$ to 0.
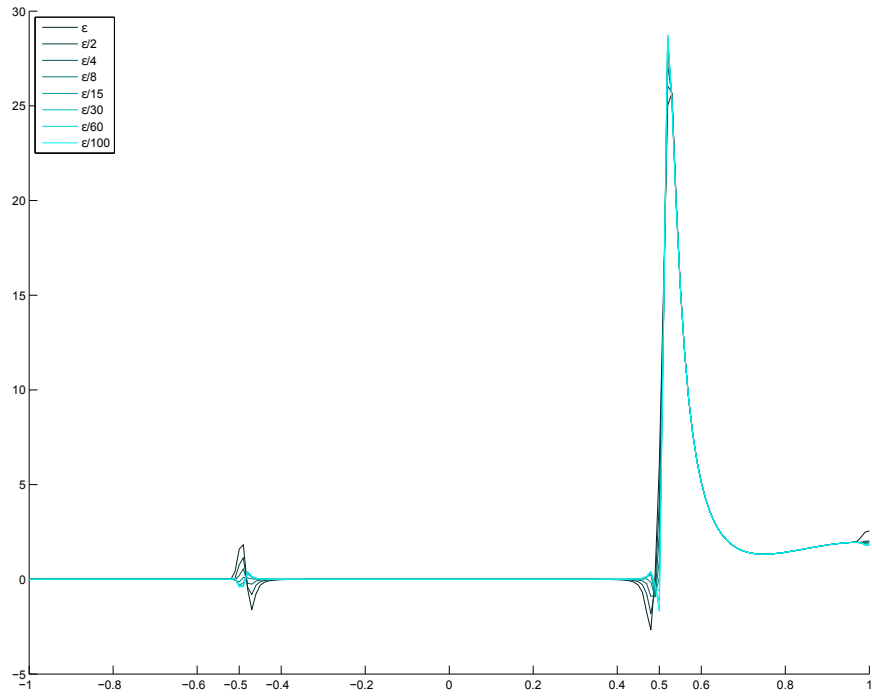
Figure 261: $\mu = 0.001$: Solution component w_0 for ε varying from $1e - 9$ to $1e - 11$.
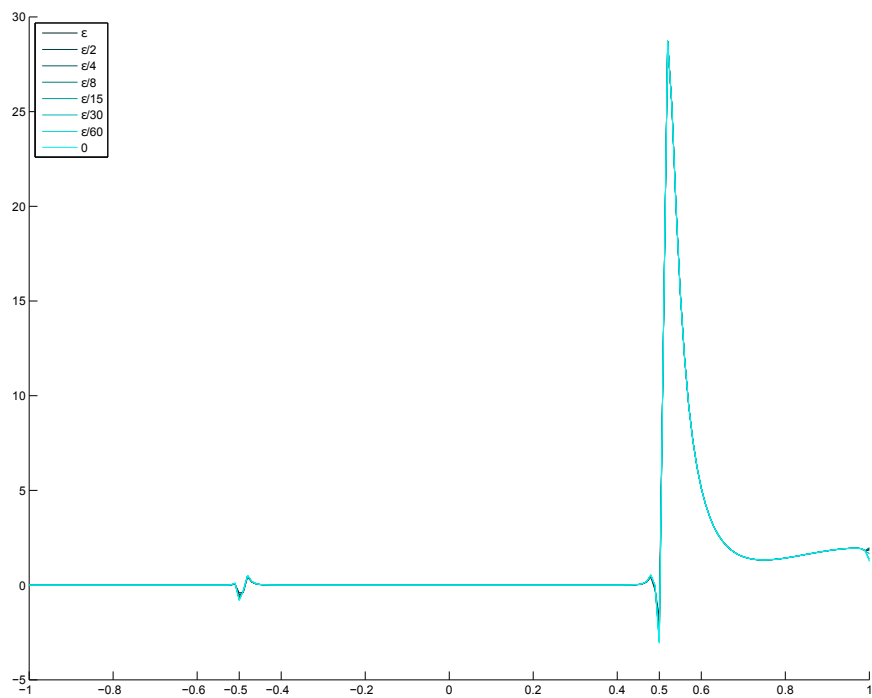
Figure 262: $\mu = 0.001$: Solution component w_0 for ε varying from $1e - 11$ to 0.
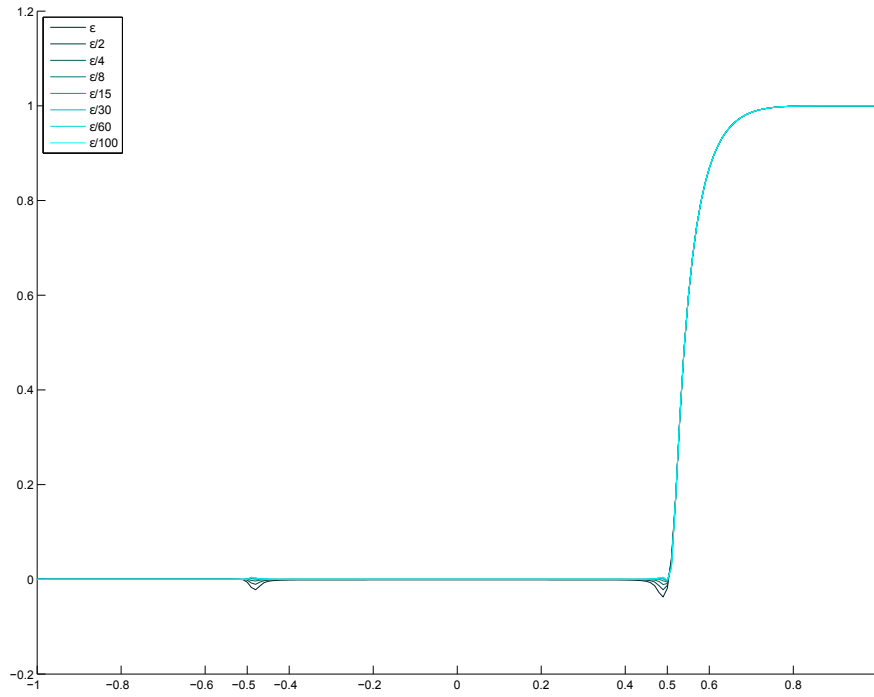
Figure 263: $\mu = 0.001$: Solution component w_1 for ε varying from $1e - 9$ to $1e - 11$.
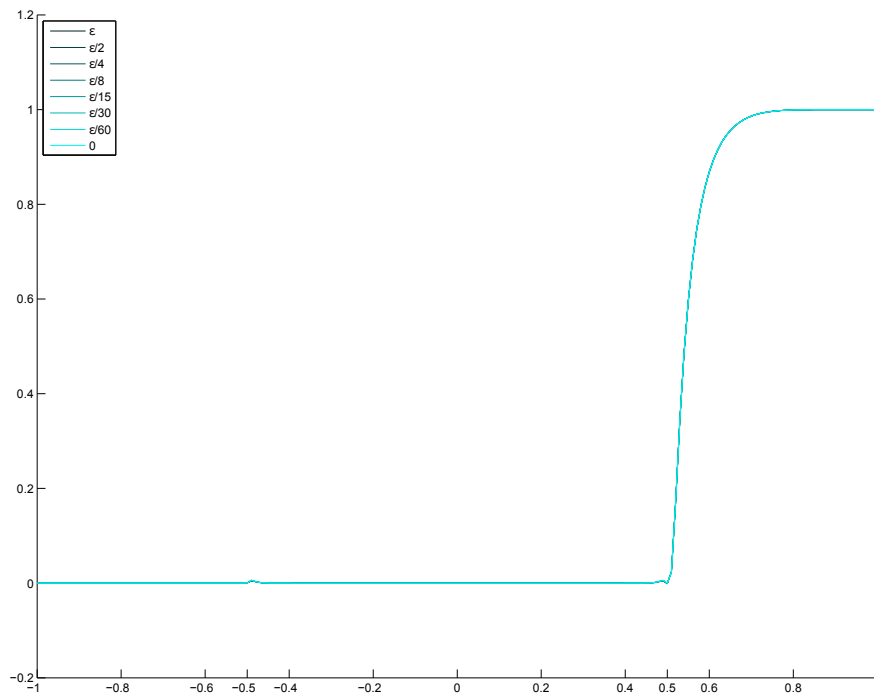
Figure 264: $\mu = 0.001$: Solution component w_1 for ε varying from $1e - 11$ to 0.
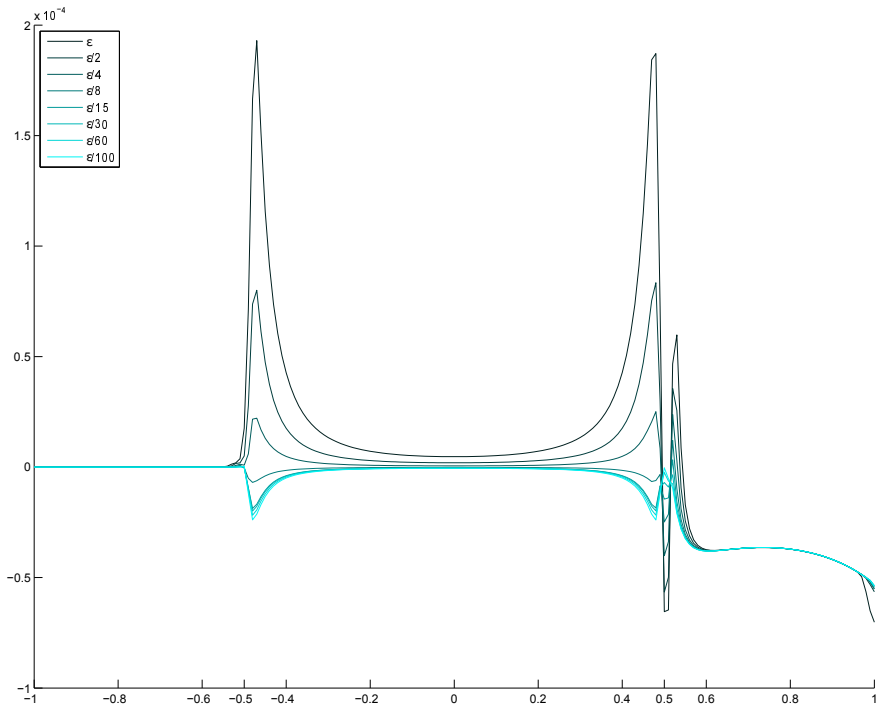
Figure 265: $\mu = 0.001$: Solution component w_2 for ε varying from $1e - 9$ to $1e - 11$.
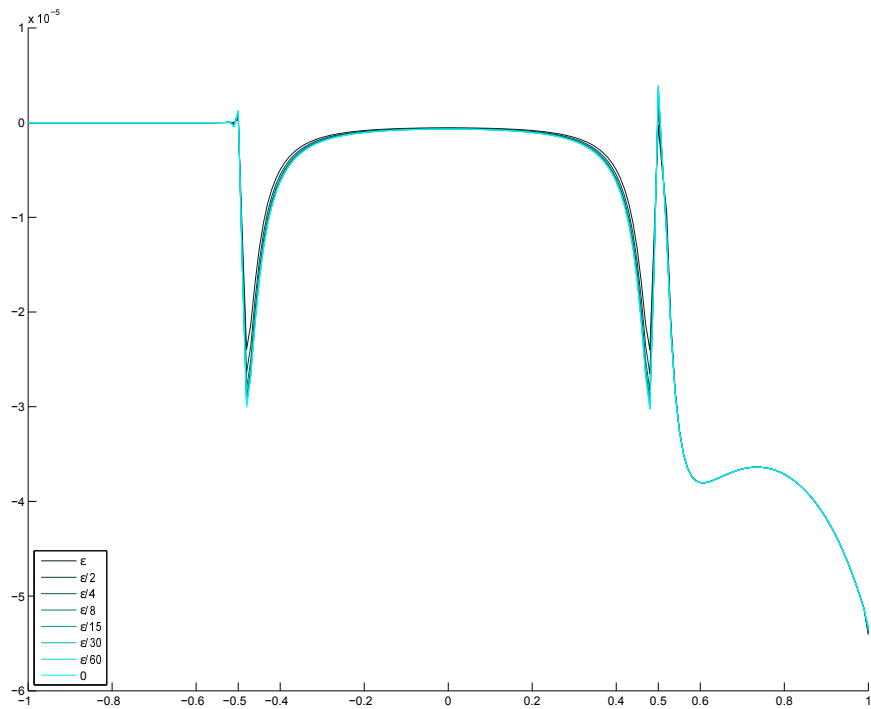
Figure 266: $\mu = 0.001$: Solution component w_2 for ε varying from $1e - 11$ to 0.

3.7.5 Solution for $\mu = 0.0001$
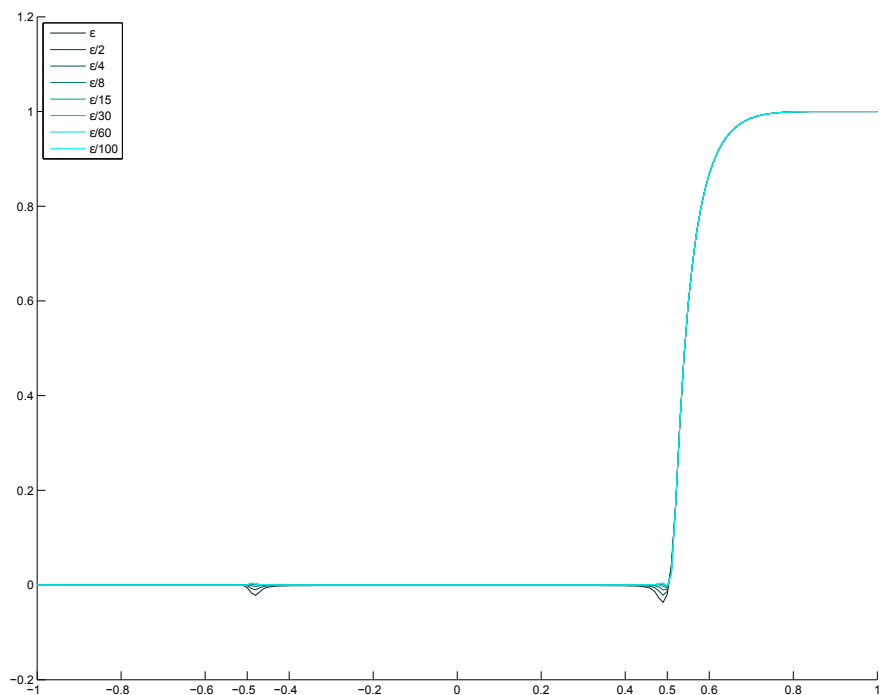
Figure 267: $\mu = 0.0001$: Solution component w_{-1} for ε varying from $1e - 9$ to $1e - 11$.
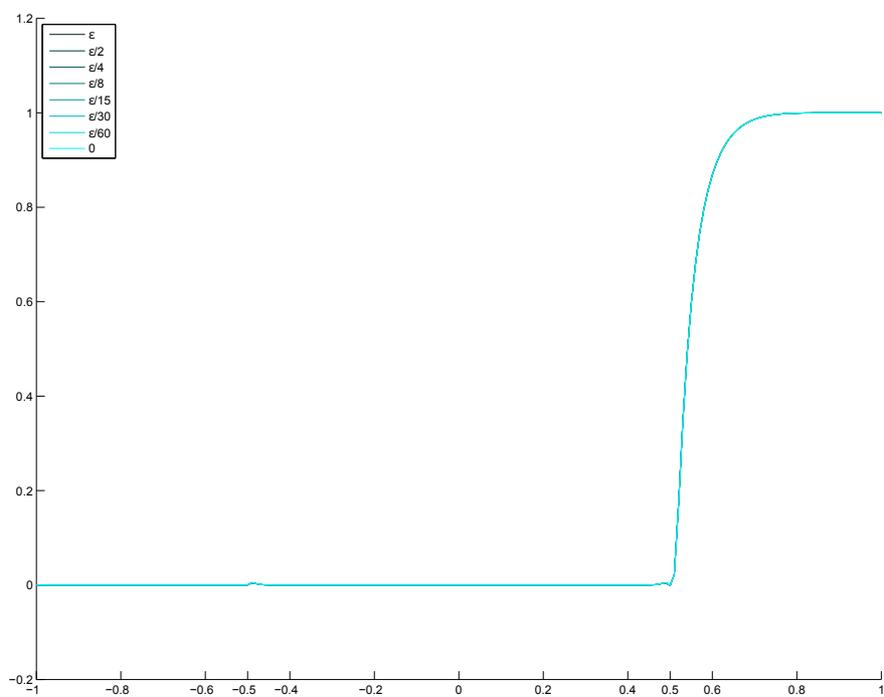
Figure 268: $\mu = 0.0001$: Solution component w_{-1} for ε varying from $1e - 11$ to 0.
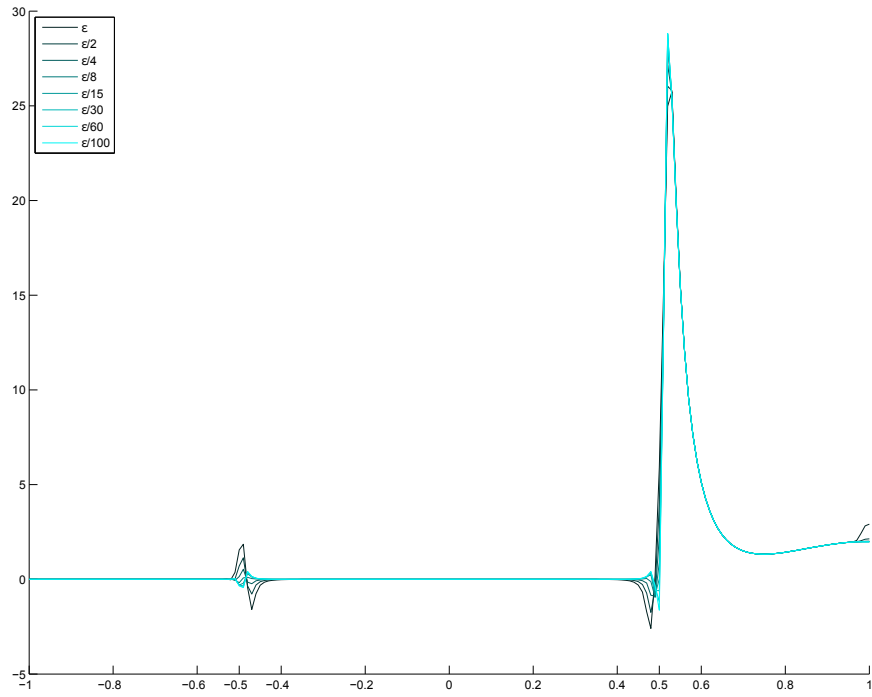
Figure 269: $\mu = 0.0001$: Solution component w_0 for ε varying from $1e-9$ to $1e-11$.
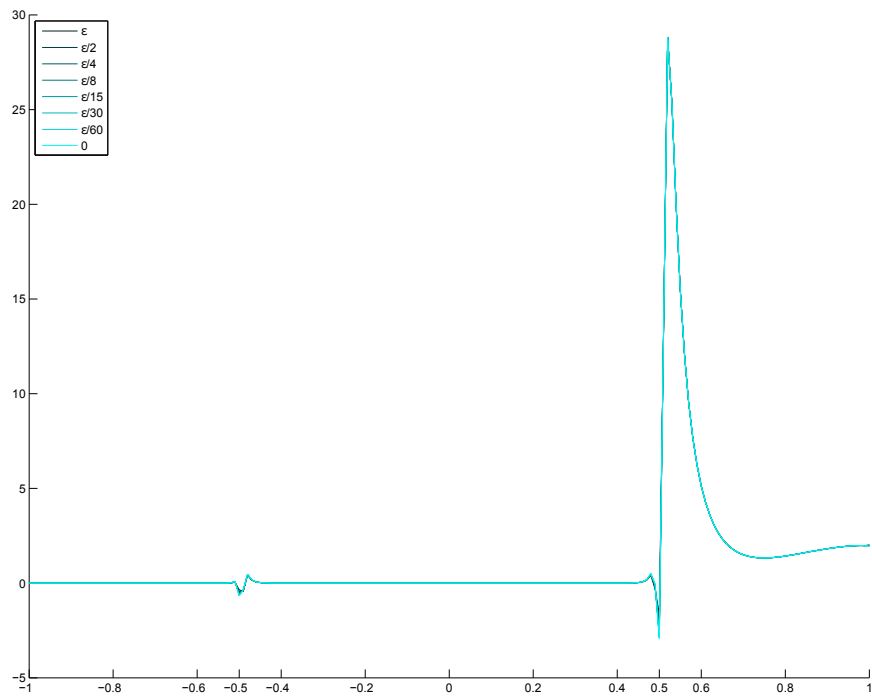
Figure 270: $\mu = 0.0001$: Solution component w_0 for ε varying from $1e-11$ to 0.
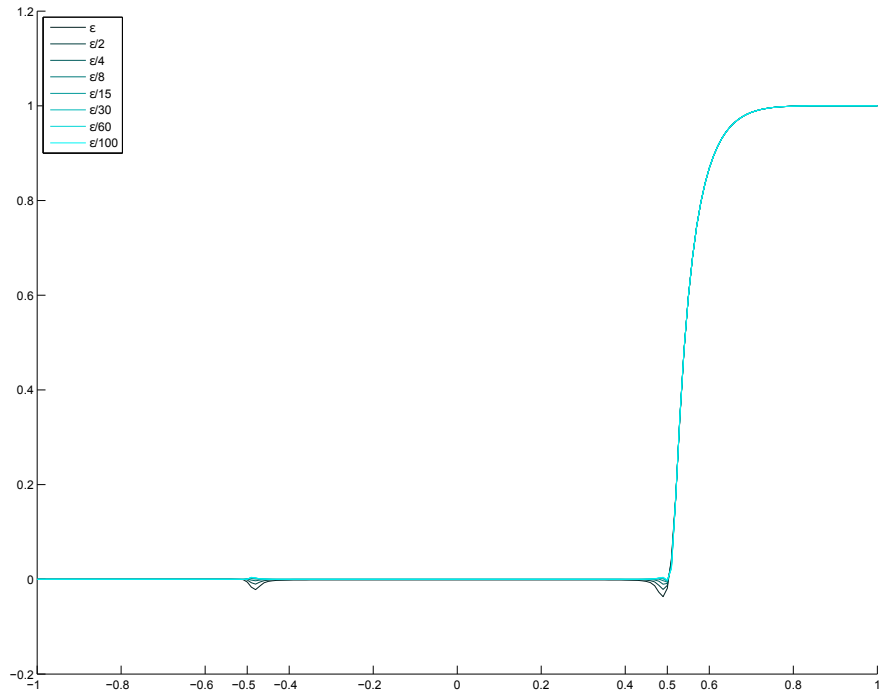
Figure 271: $\mu = 0.0001$: Solution component w_1 for ε varying from $1e - 9$ to $1e - 11$.
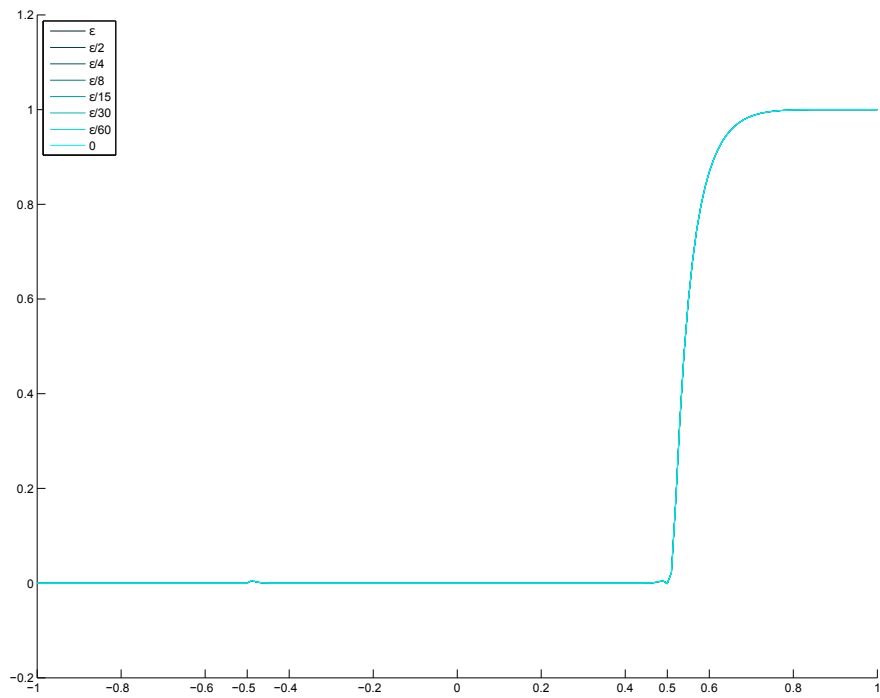
Figure 272: $\mu = 0.0001$: Solution component w_1 for ε varying from $1e - 11$ to 0.
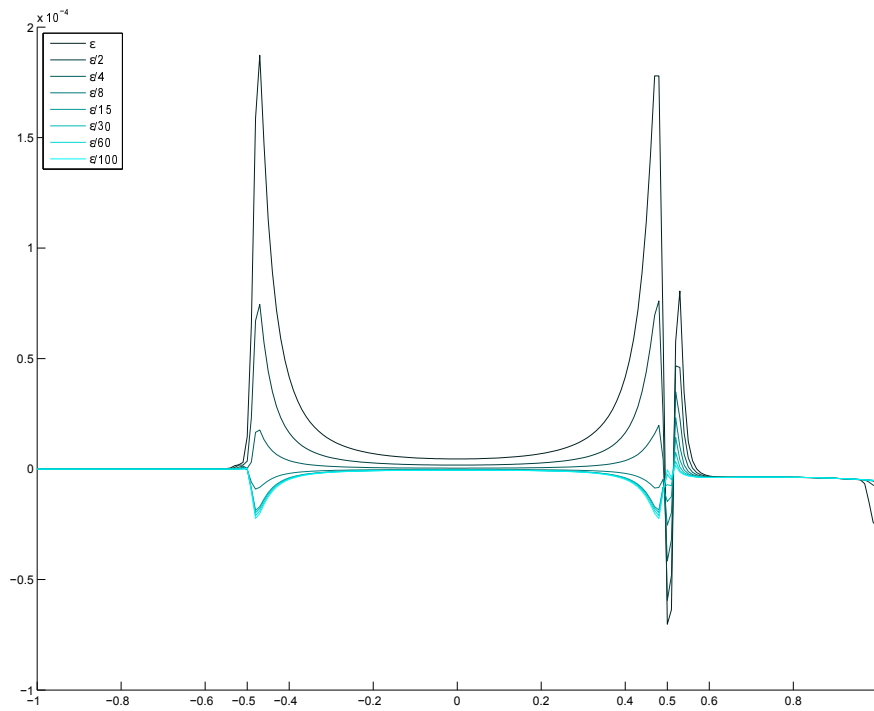
Figure 273: $\mu = 0.0001$: Solution component w_2 for ε varying from $1e-9$ to $1e-11$.
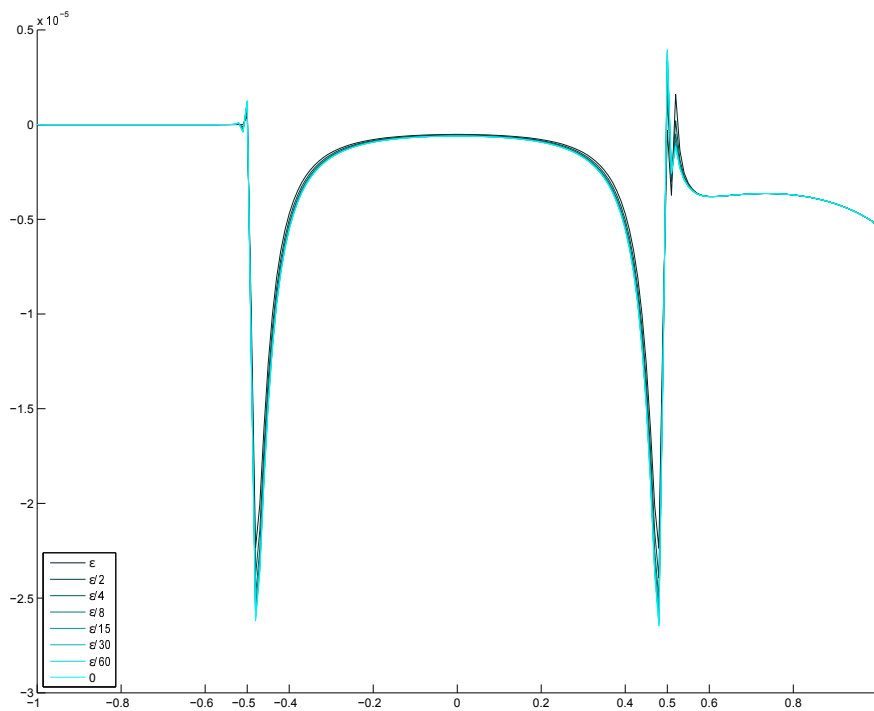
Figure 274: $\mu = 0.0001$: Solution component w_2 for ε varying from $1e-11$ to 0.

169

3.8   Conclusions

Obviously, although the behaviour of the solutions slightly changed after introducing the μ parameter, their fundamental structure, especially the peaks, did not alter much. Since the analytical insights are still being developed, we have to refer to future studies aiming at explaining the observations made in the experimental preliminary phase documented here.

References

[1] M. Guelma, A. Kogan, A. Kazarian, A. Livne, M. Orenstain, H. Michalik and S. Arnold, *Acquisition and Pointing Control for Inter-Satellite Laser Communications*, IEEE Trans. Aerospace and Electronic Systems, Vol. 40, No 4, pp.1239-1248, 2004.

[2] T. Norton, K.Conner, R. Covington, H. Ngo and C. Rink, *Development of Reprogrammable High Frame-Rate Detector Devises for Laser Communication Pointing, Acquisition and Tracking*, 2008 IEEE Aerospace Conference paper No. 1414. DOI 10.1109/AERO.2008.4526342.

[3] K. Harding, *Handbook of Optical Dimensional Metrology*, ed., CRC Press, Boca Raton FL, London, New York, 2013.

[4] S. Shuangyan, J. Xing and C. Hao, *Cleaning Space Debris with a Space-based Laser System*, Chinese Journal of Aeronautics, Vol. 24, No 4, pp. 805-811, 2014.

[5] M. Schmitz, S. Fasoulas and J. Utzmann, *Performance Model for Space-based Laser Dedris Sweepers*, Acta Astronautica, Vol. 115, pp. 376-386, 2015.

[6] M. E. Rogers, *Lasers in Space: Technological Options for Enhancing US Military Capabilities*, Center for Strategy and Technology, Air Univ., Maxwell Air Force Base, Alabama 36112, 1997.

[7] K. R. Nambiar, *Lasers: Principles, Types and Applications*. New Age International Pvt. Ltd. Pub., 2009.

[8] T. B. Bahder, *Navigation in Curved Space-time*, Am. J. Phys. 69, pp. 315-321, 2001.

[9] N. Ashby, *Relativity in the Global Positioning System*, Living Rev. Relativity, 6, 1, 2003.

[10] T. B. Bahder, *Clock Synchronization and Navigation in the Vicinity of the Earh*, Nova Science Pub. Inc., 2009.

[11] I. Ciufolini, A. Paolozzi, E. C. Pavlis, J. Ries, R. Koenig, R. Matzen, G. Sindoni and H. Neumayer, *Testing gravitational physics with Satellite laser ranging*, Eur. Phys. J. Plus, 126:72, 2011.

[12] J.M. Gambi and M.L. Garcia del Pino, *A Satellite-to-Satellite Laser Tracking Solution Within the Post-Newtonian Model of the Earth Outer Space*, Progress in Industrial Mathematics at ECMI 2012. Mathematics in Industry 19. Springer, Heidelberg, Dordrecht, London, New York, pp. 347-352, 2014.

[13] J.M. Gambi, M.C. Rodriguez-Teijeiro, M.L. Garcia del Pino and M. Salas, *Shapiro time-delay within the Geolocation Problem by TDOA*, IEEE Trans. Aerospace and Electronic Systems, Vol. 47, No 3, pp.1948-1962, 2011.

[14] J.M. Gambi, M.C. Rodriguez-Teijeiro and M.L. Garcia del Pino, *The post-Newtonian Geolocation Problem by TDOA*, Progress in Industrial Mathematics at ECMI 2010. Mathematics in Industry 17. Springer, Heidelberg, Dordrecht, London, New York, pp. 489-495, 2012.

[15] J.M. Gambi, J. Clares and M.L. Garcia del Pino, *FDOA post-Newtonian Equations for the Location of Passive Emitters Placed in the Vicinity of the Earth*, Aerospace Science and Technology, Vol. 46, pp.137-145, 2015.

[16] J.M. Gambi, M. M. Tung, J. Clares and M.L. Garcia del Pino, *Post-Newtonian Effects in Geolocation by FDOA*, Progress in Industrial Mathematics at ECMI 2014. To appear in: Mathematics in Industry 21. Springer, Heidelberg, Dordrecht, London, New York, 2016.

[17] J.M. Gambi, J. Clares and M.C. Rodriguez-Teijeiro, *Post-Newtonian Geolocation of Passive Radio transmitters by TDOA and FDOA*, Progress in Industrial Mathematics at ECMI 2014. To appear in: Mathematics in Industry 21. Springer, Heidelberg, Dordrecht, London, New York, 2016.

[18] J.M. Gambi, M. C. Rodriguez-Teijeiro and M.L. Garcia del Pino, *Newtonian and post-Newtonian Passive Geolocation by TDOA*, Accepted in Aerospace Science and Technology, January 2016.

[19] W. R. Leeb, *Laser Space Communications: Systems, Technologies, and Applications*, Rev. of Laser Engineering, 28, 12, pp. 804-808, 2000, and `http://publik.tuwien.ac.at/files/pub-et_4235.pdf`.

[20] J. W. Campbell, *Using Lasers in Space: Laser Orbital Debris Removal and Asteriod Deflection*. Center for Strategy and Technology, Air Univ., Maxwell Air Force Base, Alabama 36112, 2000.

[21] J.M. Gambi, M.L. Garcia del Pino and M. M. Tung, *Post-Newtonian Orbital Equations for Fermi Frames in the Vicinity the Earth*, Progress in Industrial Mathematics at ECMI 2014. To appear in: Mathematics in Industry 21. Springer, Heidelberg, Dordrecht, London, New York, 2016.

[22] J.M. Gambi and M.L. Garcia del Pino, *Post-Newtonian Equations of Motion for Inertial Guided Space APT Systems*, WSEAS Trans. on Mathematics, Vol. 14, pp. 256-264, 2015.

[23] J. L. Synge, *Relativity: The General Theory.* North-Holland, New York, 1960, Ch. 2.

[24] A. Arnold, H. Lange and P. F. Zweifel, *A discrete-velocity, stationary Wigner equation*, Journal of Mathematical Physics, Volume 41, Issue 11, pp. 7167-7180 (2000).

[25] A. Ilchmann and T. Reis, *Surveys in Differential-Algebraic Equations III*, Springer, Heidelberg, Dordrecht, London, New York, 2015.

[26] M. Hanke, R. März, C. Tischendorf, E. Weinmüller and S. Wurm, working title: *Least-Squares Collocation for Higher–Index Differential–Algebraic Equations*, in preperation.